Advanced Virgo Preliminary Design

VIR–089A–08

Issue 3

The Virgo Collaboration

written by
The Advanced Virgo Team*

October 28, 2008

* Contact person: G.Losurdo, Advanced Virgo Coordinator - e-mail: *losurdo@fi.infn.it*

F.Acernese [ac,5], **M.Alshourbagy**[ab,10], **F.Antonucci**[a,11], **S.Aoudia**[6], **K.G.Arun**[7], **P.Astone**[a,11], **G.Ballardin**[2], **F.Barone**[ac,5], **L.Barsotti**[ab,10], **M.Barsuglia**[14], **Th.S.Bauer**[a,12], **S.Bigotta**[ab,10], **S.Birindelli**[6], **M.A.Bizouard**[7], **C.Boccara**[8], **F.Bondu**[6], **L.Bonelli**[ab,10], **L.Bosi**[a,9], **S.Braccini** [a,10], **C.Bradaschia**[a,10], **A.Brillet**[6], **V.Brisson**[7], **H.J.Bulten**[ab,12], **D.Buskulic**[1], **G.Cagnoli**[a,3], **E.Calloni**[ab,5], **E.Campagna**[ac,3], **B.Canuel**[2], **F.Carbognani**[2], **L.Carbone**[a,9], **F.Cavalier**[7], **R.Cavalieri**[2], **G.Cella**[a,10], **E.Cesarini**[ab,3], **E.Chassande-Mottin**[14], **S.Chatterji**[a,11], **A.Chincarini**[16], **F.Cleva**[6], **E.Coccia**[ab,13], **C.Corda**[ab,10], **A.Corsi**[a,11], **F.Cottone**[ab,9], **J.-P.Coulon**[6], **E.Cuoco**[2], **S.D'Antonio**[a,13], **A.Dari**[ab,9], **V.Dattilo**[2], **M.Davier**[7], **R.De Rosa**[ab,5], **M.Del Prete** [ac,10], **L.Di Fiore**[a,5], **A.Di Lieto**[ab,10], **M.Di Paolo Emilio**[ad,13], **A.Di Virgilio**[a,10], **M.Drago**[c,15], **V.Fafone**[ab,13], **I.Ferrante**[ab,10], **F.Fidecaro**[ab,10], **I.Fiori**[2], **R.Flaminio**[4], **J.-D.Fournier**[6], **S.Frasca**[ab,11], **F.Frasconi**[a,10], **A.Freise**[*], **L.Gammaitoni**[ab,9], **F.Garufi** [ab,5], **G.Gemme**[16], **E.Genin**[2], **A.Gennai**[a,10], **A.Giazotto**[a,10,2], **M.Granata**[14] **V.Granata**[1], **C.Greverie**[6], **G.Guidi**[ac,3], **H.Heitmann**[6], **P.Hello**[7], **S.Hild**[*], **D.Huet**[2], **P.La Penna**[2], **M.Laval**[6], **N.Leroy**[7], **N.Letendre**[1], **V.Loriette**[8], **G.Losurdo**[a,3], **J.M.Mackowski**[4], **E.Majorana**[a,11], **N.Man**[6], **M.Mantovani**[2], **F.Marchesoni**[a,9], **F.Marion**[1], **J.Marque**[2], **F.Martelli**[ac,3], **A.Masserot**[1], **F.Menzinger**[2], **W.Michal**[7], **C.Michel**[4], **L.Milano**[ab,5], **Y.Minenkov**[a,13], **S.Mitra**[6], **N.Morgado**[4], **M.Mohan**[2], **A.Morgia**[ab,13], **S.Mosca**[ab,5], **B.Mours**[1], **I.Neri**[ab,9], **F.Nocera**[2], **G.Pagliaroli**[ad,13], **C.Palomba**[a,11], **F.Paoletti**[a,10,2], **S.Pardi**[ab,5], **A.Pasqualetti**[2], **R.Passaquieti**[ab,10], **D.Passuello**[a,10], **G.Persichetti**[ab,5], **F.Piergiovanni**[ac,3], **L.Pinard**[4], **R.Poggiani**[ab,10], **G.A.Prodi**[ab,15], **M.Punturo**[a,9], **P.Puppo**[a,11], **O.Rabaste**[14], **P.Rapagnani**[ab,11], **V. Re**[ab,15], **T.Regimbau**[6], **F.Ricci** [ab,11], **A.Rocchi**[a,13], **L.Rolland**[1], **R.Romano**[ac,5], **P.Ruggi**[2], **F. Salemi**[ab,15], **B. Sassolas**[4], **D.Sentenac**[2], **B.L.Swinkels**[2], **R.Terenzi**[ac,13], **A.Toncelli**[ab,10], **M.Tonelli**[ab,10], **E.Tournefier**[1], **F.Travasso**[ab,9], **G.Vajente**[ab,10], **J.F.J. van den Brand**[ab,12], **S. van der Putten**[a,12], **G. Vedovato**[c,15], **D.Verkindt**[1], **F.Vetrano**[ac,3], **A.Viceré**[ac,3], **J.-Y.Vinet**[6], **H.Vocca**[a,9], **M.Yvert**[1]

[1] *Laboratoire d'Annecy-le-Vieux de Physique des Particules (LAPP), IN2P3/CNRS, Université de Savoie, F-74941 Annecy-le-Vieux, France*

[2] *European Gravitational Observatory (EGO), I-56021 Cascina (Pi), Italia*

[3] *INFN, Sezione di Firenze, I-50019 Sesto Fiorentino[a]; Università degli Studi di Firenze, I-50121[b], Firenze; Università degli Studi di Urbino "Carlo Bo", I-61029 Urbino[c], Italia*

[4] *Laboratoire des Matériaux Avancés LMA, IN2P3/CNRS, F-69622 Villeurbanne, Lyon, France*

[5] *INFN, sezione di Napoli [a]; Università di Napoli "Federico II"[b] Complesso Universitario di Monte S.Angelo, I-80126 Napoli; Università di Salerno, Fisciano, I-84084 Salerno[c], Italia*

[6] *Departement Artemis, Observatoire de la Côte d'Azur, CNRS, F-06304 Nice, France.*

[7] *LAL, Université Paris-Sud, IN2P3/CNRS, F-91898 Orsay, France*

[8] *ESPCI, CNRS, F-75005 Paris, France*

[9] *INFN, Sezione di Perugia[a]; Università di Perugia[b], I-6123 Perugia,Italia*

[10] *INFN, Sezione di Pisa[a]; Università di Pisa[b]; I-56127 Pisa; Università di Siena, I-53100 Siena[c], Italia*

[11] *INFN, Sezione di Roma[a]; Università "La Sapienza"[b], I-00185 Roma, Italia*

[12] *National institute for subatomic physics, NL-1009 DB[a]; Vrije Universiteit, NL-1081 HV [b], Amsterdam, The Netherlands*

[13] *INFN, Sezione di Roma Tor Vergata[a]; Università di Roma Tor Vergata[b], Istituto di Fisica dello Spazio Interplanetario (IFSI) INAF[c], I-00133 Roma; Università dell'Aquila, I-67100 L'Aquila[d], Italia*

[14] *AstroParticule et Cosmologie (APC), CNRS: UMR7164-IN2P3-Observatoire de Paris-Université Denis Diderot-Paris VII - CEA : DSM/IRFU*

[15] *Gruppo Collegato di Trento[a] and Dipartimento di Fisica, Università di Trento[b], I-38050 Povo, Trento, Italia; INFN, Sezione di Padova[c] and Dipartimento di Fisica, Università di Padova[d], I-35131 Padova, Italia*

[16] *INFN, Sezione di Genova; I-16146 Genova, Italia*

[*] *Permanent address: School of Physics & Astronomy, University of Birmingham, B15 2TT, UK*

Contents

Advanced Virgo Preliminary Design:
PART 1:

Design overview, sensitivity, science case

1 Introduction

This document describes the preliminary design of the Advanced Virgo gravitational wave detector. Advanced Virgo (AdV) is the project to upgrade the Virgo detector to a second generation instrument.

Interferometric gravitational wave (GW) detectors of the first generation have successfully completed their first long-duration data taking runs. Upgrades that exploits available technology and allow to enhance the accessible volume of universe by about a factor 10 (Virgo+, Enhanced LIGO) are currently performed. However, it will be the second generation of gravitational wave detectors, that will give us the chance to open an exciting new window on the universe. AdV will be able to scan a 1000 times larger volume of the Universe than initial Virgo. Even though it will be hosted in the same infrastructures as Virgo, the AdV sensitivity (see sec. 3) will be better by one order of magnitude over most of the detection band.

The effort of the Virgo Collaboration towards the design of a second generation detector started in 2005 with the *Advanced Virgo White Paper* [1]. In fall 2007 an *Advanced Virgo Conceptual Design* was proposed [2] and submitted to the funding agencies together with a *Preliminary project execution plan and cost plan* [3]. The recent approval of Advanced LIGO [4] by the NSF represents an important step forward towards the creation of a world wide network of gravitational wave interferometers sensitive enough to start the epoch of gravitational wave observations.

This *Advanced Virgo Preliminary Design* summarizes the technical knowledge acquired so far on the different detector subsystems and represents an intermediate step between the Conceptual Design and the Final Design:

- in the first part the concept of AdV is introduced, with an overview of the main design features and the expected achievable sensitivity. The science case for AdV is discussed, describing the scenarios for the expected detection rates, the benefits of a network of GW detectors and the opportunities from multi-messenger observations;
- in the second part the design of the interferometer is described: optical configuration, laser, injection system, mirrors, thermal compensation, detection system and interferometer sensing and control. A chapter is dedicated to the parasitic noises that can spoil the sensitivity: this provides inputs to the chapter dedicated to the needed infrastructure modifications;
- part three is dedicated to the vibration isolation system. It describes the planned changes on the Virgo superattenuator, especially on the payload, that has to be compliant with a bigger mirror and fused silica suspension fibers. An important section is dedicated to the work done on the monolithic suspensions for Virgo+ and the related plans for AdV;
- though AdV will be host in the same Virgo facilities important upgrades of the vacuum system and of some infrastructures are needed. These are discussed in the fourth part. An overview of the envisaged upgrades of the electronics is also provided.

2 Advanced Virgo Design

The scope of this section is to give a summary of the central design features of AdV. Upgrades necessary to convert the initial Virgo instrument to the AdV detector, are briefly introduced here, while comprehensive and more detailed descriptions can be found in the Section 5 to 18.

Since AdV aims for a sensitivity about a factor 10 better than initial Virgo, most of the detector subsystems have to deliver a largely improved performance to be compatible with the AdV targets. The actual design choices of the AdV preliminary design were made taking into account the relevant knowledge achieved and some constraints:

- the knowledge and experience gained from the commissioning of first generation gravitational wave detectors;
- the constraints from the existing infrastructure and costs;
- the results of the vast R&D programs carried out within the GW community;
- the time constraints from the fact that AdV will join Advanced LIGO in the network of the second generation GW detectors.

At this stage of the design process, we present a set of consistent design parameters that will be iterated and settled towards final design. In the rest of this section we will briefly describe the AdV reference configuration by listing the main features of the AdV design (see also Fig. 1). At the end of this section a summary of the relevant design parameters for AdV is given in the Tables 1,2.

Interferometer optical configuration (Sec. 5)

- AdV will be a dual recycled interferometer. Beside the standard power recycling, a signal recycling (SR) cavity will be present. The tuning of the SR parameter allows to change the shape of the sensitivity curve, optimizing the detector for a given astrophysical source (fig. 3).
- The recycling cavities are designed to be non-degenerate for higher order optical modes (non degenerate recycling cavities, NDRC). This design is expected to greatly reduce the interferometer sensitivity to misalignments and thermal effects.
- The coating thermal noise limits the AdV sensitivity in the mid-frequency range. One way to lower its level is to enlarge the spot size on the test masses. Therefore, unlike Virgo, the beam waist will be placed closed to the center of the 3 km Fabry-Perot cavities, resulting in beam radii of 56 mm and 65 mm for the input and end mirrors, respectively.

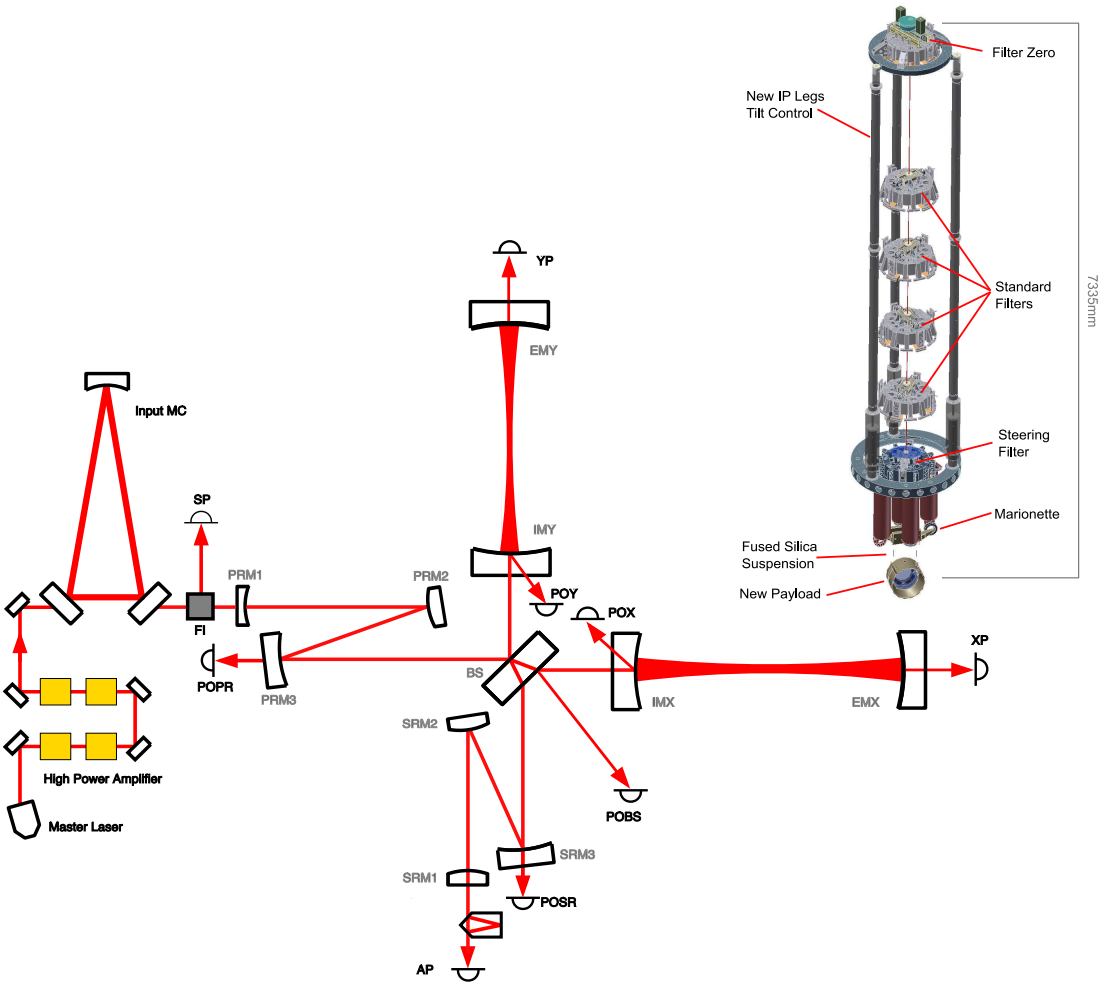

Figure 1: AdV Reference Design. Optical scheme, following the beam from the laser to the dark port: high power laser, triangular input mode cleaner, Faraday Isolator (FI), folded power recycling cavity (the mirrors PRM1/3 are on the injection bench, PRM2 is suspended from the PR SA), beam splitter, 3 km Fabry-Perot cavities, SR cavity (the mirrors SRM1/3 are on the suspended detection bench, SRM2 is suspended from the SR SA), output mode cleaner, dark fringe photodiode. An image of the Virgo superattenuator is shown.

Laser (Sec. 6)

- More laser power is needed to improve the sensitivity at high frequency, where it is shot noise limited. The AdV laser will provide a power of about 200 W. The design of the high power stage is based on the one developed at LZH for Advanced LIGO.

Injection system (Sec. 7)

- The input optics for AdV must be compliant with the 10 times increased optical power. Proper electo-optic modulators and Faraday isolators are being developed.
- The Virgo configuration for the input mode cleaner (144m long triangular cavity) will be kept.
- The use of non-degenerate power recycling cavity, makes the matching telescope currently hosted on the suspended injection bench obsolete. Instead the bench will host two mirrors of the power recycling cavity. It is therefore being redesigned accordingly.

Mirrors (Sec. 8)

- Given the much larger optical power in the cavities, radiation pressure noise becomes a limit in the low frequency range and heavier test masses are needed to reduce it. The mirrors designed for AdV have the same diameter as the Virgo ones (35 cm) but are twice as thick (20 cm) and heavy (42 kg).
- A large R&D effort is being carried out in the GW community to produce coatings with lower mechanical losses (an thus less thermal noise). The coating of the AdV mirrors is expected to start in mid 2010: new results from thr R&D might lead to a further improvement of the AdV sensitivity (see sec. 3).

Thermal compensation (Sec. 9)

- Thermal effects (originating from light absorption) create wavefront distortion that can spoil the interferometer dynamics. Such effects, visible even in Virgo and LIGO, might become dramatic in AdV and must be compensated for.
- The AdV Thermal Compensation System (TCS) consists of a combination of CO_2 laser projectors acting on dedicated compensation plates and ring heaters acting directly onto the test masses.

Detection (Sec. 10)

- AdV will use a DC detection scheme, which improves the quantum noise and eliminates some technical noises (such as RF phase noise) which would be (close to) limiting the detector sensitivity in case of heterodyne readout.

- The main photodiodes will be placed on the suspended detection bench (in vacuum) to improve the rejection of seismic and acoustic noise.
- The detection bench will host the Signal Recycling mirror and one of the folding mirrors of the non-degenerate Signal Recycling cavity.

Interferometer sensing and control (sec. 11)

- An extended *Variable Finesse Technique*, successfully tested in Virgo, will be used to achieve the full lock. The reference solution for the lock of the high finesse Fabry-Perot cavities foresees an auxiliary laser for which the arm cavity finesse is much reduced. Possible sets of modulation frequencies and cavity lengths have been defined (requiring to move the towers in the central building).

Vibration isolation and mirror suspensions (Sec. 13,14,15)

- The seismic attenuation provided by the Virgo superattenuator (SA) is compliant with the AdV sensitivity. The only important upgrade planned is the implementation of a tilt control at the base of the inverted pendulum: this will allow us to control the inertial platform in 6 degrees of freedom, increasing the detector robustness in windy days.
- The lower part of the SA will be modified to be compliant with the thicker and heavier mirrors.
- To reduce the pendulum thermal noise, the AdV test masses will be suspended by fused silica fibers.

Vacuum (Sec. 17)

- The current Virgo vacuum level needs to be improved by a factor of about 100 in order to be compliant with the AdV sensitivity. Such improvement requires to bake out the pipes. In the current configuration this can be done only if the towers are baked as well, which has several drawbacks. Therefore, cryotraps separating the 3 km tubes from the towers are proposed for AdV.
- Vacuum links with a larger diameter are needed in the central area, to allow for the larger size of laser beam and for the folded path in the non-degenerate recycling cavities. The links will have also different lengths to meet the new requirements on the position of the towers set by the interferometric sensing and control subsystem.

Infrastructure (Sec. 18)

- To reduce the influence of anthropogenic noise some noisy machines will be either replaced with more silent ones, seismically and acoustically isolated or moved out of the experimental halls.

AdV Overview, Part I		
Subsystem and Parameters	**AdV Preliminary Design**	**Initial Virgo Implementation**
Sensitivity		
Binary Neutron Star Inspiral Range	150 Mpc	11 Mpc
Anticipated Strain Sensitivity	$3.5 \cdot 10^{-24}/\sqrt{\text{Hz}}$	$4 \cdot 10^{-23}/\sqrt{\text{Hz}}$
Displacement Sensitivity	$1 \cdot 10^{-20}\,\text{m}/\sqrt{\text{Hz}}$	$1 \cdot 10^{-19}\,\text{m}/\sqrt{\text{Hz}}$
Instrument Topology		
Interferometer	Michelson	Michelson
Power Enhancement	Armcavities and Power Recycling	Armcavities and Power Recycling
Signal Enhancement	Signal Recycling	n.a.
Laser and Optical Powers		
Laser Wavelength	1064 nm	1064 nm
Optical Power at Laser Output	200 W	20 W
Optical Power at Interferometer Input	125 W	7 W
Optical Power at Test Masses	760 kW	4 kW
Optical Power on Beam Splitter	2.7 kW	0.3 kW
Test Masses		
Mirror Material	Fused Silica	Fused Silica
Main Test Mass Diameter	35 cm	35 cm
Main Test Mass Weight	42 kg	21 kg
Test Mass Surfaces and Coatings		
Coating Material	Ti doped Ta_2O_5	Ta_2O_5
Roughness	< 1 Angstrom	< 0.5 Angstrom
Flatness	0.5 nm RMS	< 8 nm RMS
Losses per Surface	37.5 ppm	250 ppm (measured)
Test Mass ROC	Input Mirror = 1416 m End Mirror = 1646 m	Input Mirror = flat End Mirror = 3600 m
Beam Radius at Input Mirror	56 mm	21 mm
Thermal Compensation		
Thermal Actuators	CO_2-Lasers and Ring Heater	CO_2-Lasers
Actuation Points	Compensation Plates and directly at Mirrors	Directly at Mirrors

Table 1: Main parameters of the AdV Preliminary Design (PART 1):

AdV Overview, Part II		
Subsystem and Parameters	**AdV Preliminary Design**	**Initial Virgo Implementation**
Suspension		
Seismic Isolation System	Superattenuator	Superattenuator
Degrees of Freedom of Inverted Pendulum Inertial Control	6	4
Suspension Fibres	Fused Silica Fibres (tapered)	Steel Wires
Vacuum System		
Pressure	$1 \cdot 10^{-9}$ mbar	$2 \cdot 10^{-7}$ mbar
Detection System		
GW Signal Readout	DC-Readout	Heterodyne (RF)
Output Mode Cleaner Suppression	RF Sidebands and Higher Order Modes	Higher Order Modes
Main Photo Diode Environment	in Vacuum	in Air
Lengths		
Arm Cavity Length	3 km	3 km
Input Mode Cleaner	144 m	144 m
Power Recycling Cavity	24 m	10 m
Signal Recycling Cavity	TBD	n.a.
Interferometric Sensing and Control		
Lock Acquisition Strategy	Auxiliary Lasers (different wavelength)	Main Laser
Number of RF Modulations	3	2
Schnupp Asymmetry	4 cm	85 cm
Recycling Cavity Design	Non-degenerate	Marginally stable
Signal Recycling Parameter		
Signal Recycling Mirror Transmittance	11 %	n.a.
Signal Recycling Tuning	0.15 rad	n.a.

Table 2: Main parameters of the AdV Preliminary Design (PART 2).

3 Sensitivity

3.1 The AdV reference sensitivity

The AdV reference sensitivity[1] as well as the main noise contributions are shown in fig. 2. The curve is calculated using the parameters in tables 1,2. The SR parameters have been chosen in order to maximize the sight distance for Binary Neutron Stars (BNS) [130]. The corresponding inspiral ranges are 149 Mpc for BNS and 753 Mpc for Binary Black Holes (BBH).

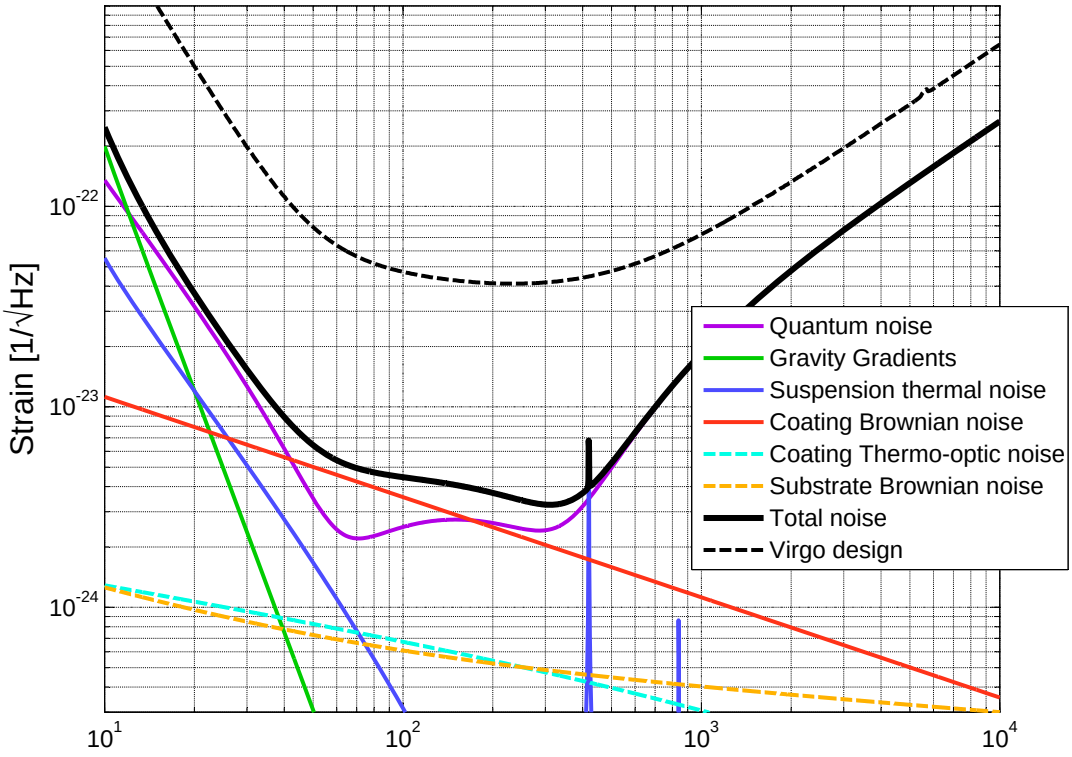

Figure 2: Reference AdV sensitivity and expected noise contributions. It has been calculated with SR mirror transmittance of 11% and SR phase of 0.15 rad, 125 W of laser power entering the interferometer, cavity finesse of 888, PR factor of 21.5. The chosen SR tuning optimizes the inspiral range for coalescing binary neutron stars. The Virgo design sensitivity is shown for the sake of comparison.

As already mentioned, the presence of the SR cavity allows to think of AdV as a tuneable detector: the sensitivity curve can be shaped in order to optimize it for targeting different astrophysical sources. The SR mirror transmittance influences the detector bandwidth, while the microscopic lenght of the SR cavity changes the frequency of the maximal sensitivity.

Fig. 3 shows some examples of sensitivity curves obtained with different tunings. With

[1] The sensitivity curves shown in this section have been plotted using the MATLAB *GWINC* code developed within the LSC [5] and adapted to AdV [6].

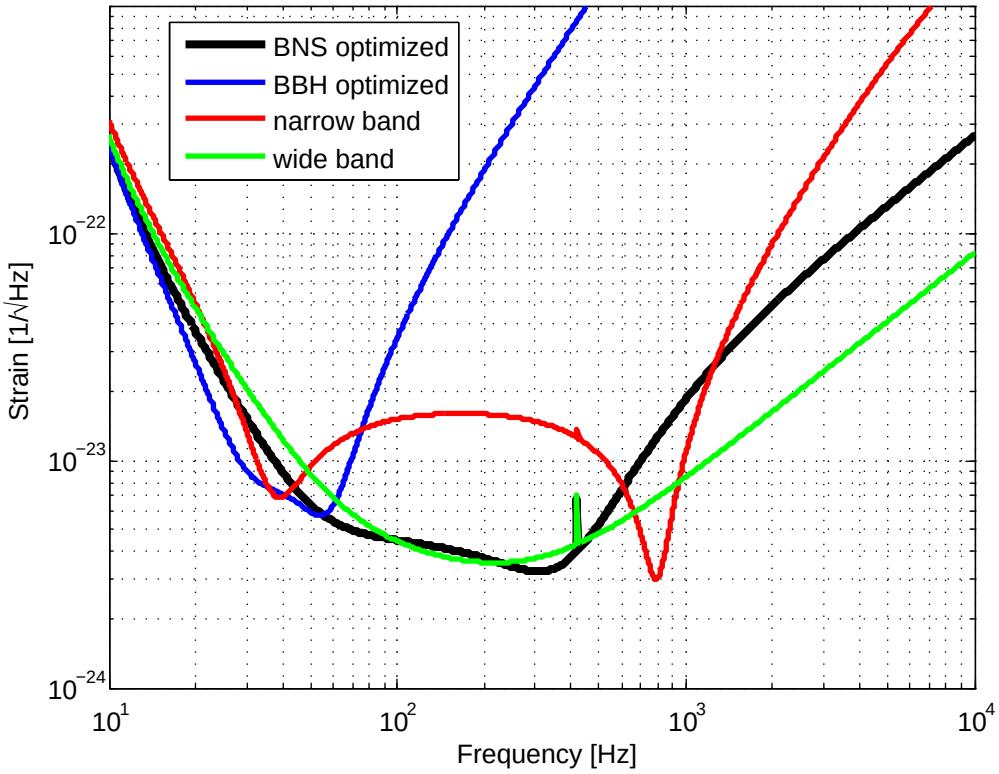

Figure 3: Tuning the AdV sensitivity by changing the SR parameters. The black curve corresponds to the reference sensitivity of fig. 2 and maximizes the inspiral range for BNS. The blue curve is optimized for BBH detection (BH of 10 $M_\odot$ are considered) and is obtained with a low input power (5 W). The red curve shows a narrow band tuning, useful to target a monochromatic source.

respect to the reference sensitivity (optimized for BNS) one can:

- enhance the low frequency response in order to increase the detectability of large mass BBH (blue curve in fig. 3). This also requires lowering the input power;
- enhance the sensitivity in a certain frequency range, *narrow banding* the response (magenta curve in fig. 3). This is indicated to target young pulsars;
- widen the detector response and increase the high frequency sensitivity for burst search (green curve in fig. 3).

3.2 Commissioning steps

Reaching the AdV design sensitivity will require several progress steps. The presence of the SR cavity and the tenfold laser power increase are features that require the commissioning team to face new problems. The commissioning will certainly start in a low power

configuration and the power will be then increased gradually, as the understanding of the detector improves and the control becomes more robust. It is also possible to start the commissioning without the SR mirror, in a configuration more similar to Virgo/Virgo+, though such choice will require to use a different control scheme and seems therefore less favourable.

Independent of the commissioning strategy, it is remarkable that, even in a preliminary configuration (in low power with SR or in high power without SR) AdV can reach a sensitivity allowing to take interesting science data. Fig. 4 compares the sensitivity curves achievable in the different commissioning scenarios, while in table 3 we list the inspiral range for BNS and BBH and the sensitivity at 1 kHz achievable in the various configurations described so far. It is remarkable that with 30 W of laser power in the interferometer (more or less the Virgo+ input power) one can achieve target BNS at about the same distance as the reference sensitivity, with much better sensitivity for BBH, at the cost of a bad response in the high frequency range. This suggests that AdV can be thought as a flexible detector with a high science potential even in a non complete configuration.

FIGURES of MERIT	**BNS insp.**	**BBH insp.**	**1 kHz sens.**
Virgo (design)	11	58	7.2e-23
AdV BNS opt. (reference, fig. 2)	149	753	1.8e-23
AdV BBH opt. (blue in fig. 3)	115	1412	4.0e-21
AdV dual rec. 5W in (green in fig. 4)	118	1325	1.8e-21
AdV dual rec. 30W in (magenta in fig. 4)	140	1325	1.6e-22
AdV no SR. 125W in (cyan in fig. 4)	107	311	2.2e-23

Table 3: The inspiral range for BNS and BBH and the strain sensitivity at 1 kHz for Virgo and some possible AdV configurations.

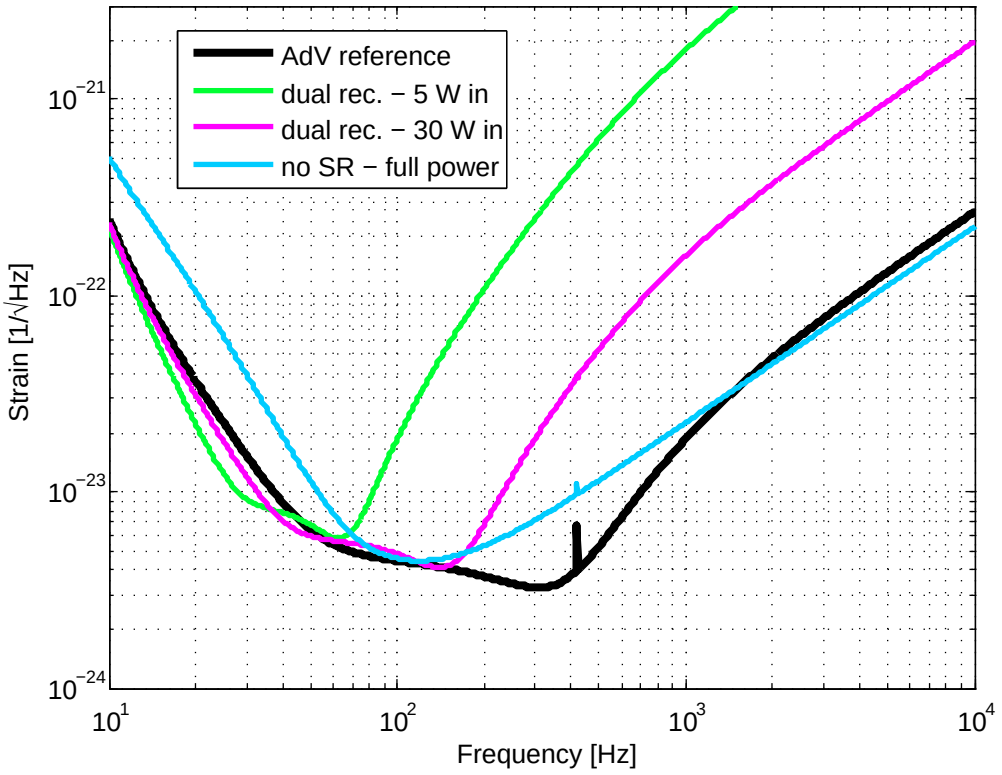

Figure 4: The AdV reference sensitivity (black) is compared with the ones achievable in the following cases: dual recycled 5W power in (green), dual recycled 30W power in (magenta), power recycled 125 W power in (cyan).

4 Advanced Virgo science case

This section addresses some of the scientific motivations for the realization of AdV, listing its main astrophysical targets, the potentialities for discovery and science, and the opportunities for collaborative work with other GW detectors, as well as with other observatories of e.m. and ν radiation.

4.1 Generalities

The AdV detector has the goal to contribute bringing the gravitational waves into maturity, by achieving an improvement in sensitivity of about a factor of 10 or better with respect to the initial Virgo design sensitivity.

AdV will harvest its scientific potential thanks to the close collaboration with the Advanced LIGO detectors, constituting a long baseline network of observatories, capable to coherently exploit the time, amplitude and phase information coming from the different sites, thus reconstructing the source position, the polarization of the impinging waves, ultimately giving access to the physics of the sources.

In Sec. 4.2 we will translate the AdV sensitivities into scientific potential for the different sources; these estimates are illustrative of the instrument capabilities. Then in Sec. 4.3 we discuss how these capabilities contribute to the AdV - AdvancedLIGO network as a whole. Finally in Sec. 4.4 we will address the importance and the potentialities of a multi-messenger approach to astrophysical phenomena, in collaboration with other instruments, sensitive to e.m. and neutrino signals.

Sensitivities: a choice We show in Fig. 5 a comparison of the AdV sensitivity (in two version, the "conceptual design" one and the "BNS optimized"), of the Virgo sensitivity, and of two possible sensitivity curves for the intermediate step, Virgo+, which is currently being commissioned. As discussed in Sec. 3 the AdV sensitivity is tunable, to optimize the detection probability for different sources. We will make the simplification of considering only a "BNS optimized" curve as the basis for quantitative considerations.

In the following, for some of the interesting GW sources, we try to list the scientific motivation and the chances of detecting or placing interesting upper limits. We fail to be exhaustive, though, leaving aside several interesting sources; we hope to address this shortcoming in future releases of this document.

4.2 Scientific potential

We list here briefly the sources which can be of interest for AdV, and provide when possible estimates of the source strength or the rate.

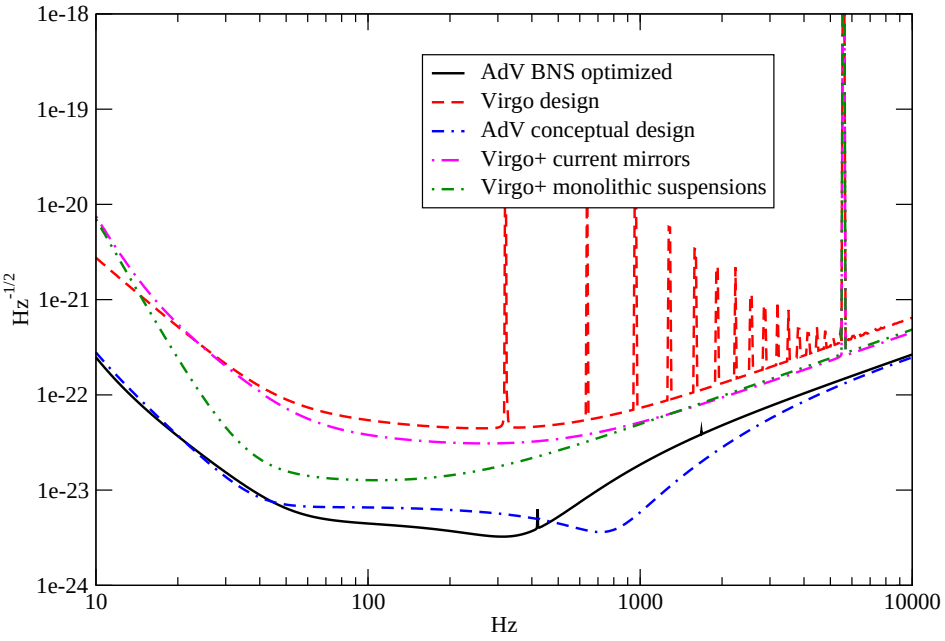

Figure 5: Comparison of AdV sensitivities with the design sensitivity of Virgo and Virgo+. The "BNS optimized" and the "conceptual design" AdV curves are representative, but not exhaustive, of the range of possible sensitivity tunings. We show Virgo+ curves in two different configurations, which include or not a subset of AdV technical solutions.

4.2.1 Binary neutron stars

The coalescence of a pair of compact objects is the best known event leading to copious production of gravitational waves.

A binary coalescence is conventionally divided in three phases:

inspiral during which the orbit shrinks adiabatically and the signal is believed to be well modeled with a post-newtonian expansion

merger which marks the collision of the compact objects

ringdown characterized by oscillating, decaying signals emitted by the resulting object

A coalescence is a very effective source; during the inspiral phase alone, it emits in GW an energy

$$\Delta E_{rad} \simeq 4.2 \times 10^{-2} M_{\odot} c^2 \left(\frac{\mathcal{M}}{1.21 M_{\odot}}\right)^{5/3} \left(\frac{f_{max}}{1\mathrm{kHz}}\right)^{2/3} \quad (1)$$

where the chirp mass $\mathcal{M}$ is defined as

$$\mathcal{M} = \mu^{3/5} M^{2/5} \quad (2)$$

in terms of the total mass $M \equiv m_1 + m_2$ and the reduced mass $\mu \equiv \frac{m_1 m_2}{M}$ of the binary

system, and f_{max} is the GW frequency at the end of the inspiral phase.

The existence of binary neutron stars is well attested by the observation of pulsars; moreover, the existence of binary pulsar signals allowed to extract the mass parameters of some pulsar pairs, for which values close to $1.4\mathcal{M}_{\odot}$ are found, the typical mass scale for these compact objects.

Scientific payoff of BNS detections A number of consequences would stem from a direct BNS detection;

- we already know, thanks to the observation of the Hulse-Taylor binary pulsar, that GW emissions explain the rate of orbital period variation. However, the direct detection of GW waves from the inspiral phase would be a very clean, direct confirmation of GR;
- with a network of detectors it is possible to reconstruct the waveform amplitude, which is a known function of source distance and binary mass parameters; the latters however can also be extracted by the time evolution of the waveform. It follows that a BNS event distance can be reconstructed, and if the event can be associated with an astrophysical object, it will serve as distance calibration, and potentially compete with other methods to determine the Hubble constant.
- the merger phase is also expected to emit GWs, whose shape is certainly dependent on the details of the NS structure, including the Equation of State (EoS) of the nuclear matter in the neutron star. Given the complexity of the system though, and the expected weakness of the merger signal in BNS, it is likely that more can be learned about the NS EoS in BH-NS collisions (see below).
- the ringdown phase of the resulting BH, characterized by the emission of waves corresponding to the quasi-normal-modes of the system, will give direct access to mass and spin parameters of the BH.

We will see later that a non-detection of BNS events would not violate strongly the astrophysical expectations, although a non-detection by the LSC-Virgo network over several years of observation would strain the models quite.

Expected rate of events There are basically two ways by which astrophysicists can predict the number of BNS events; an empirical one, based on the observation of the few compact binary systems which will coalesce on a timescale comparable with the age of the Universe, and a theoretical one, based on models of binary star formation and evolution.

For a recent account of the results of the empirical method, the reader is referred to [13], which on the basis of the observations, corrected for selection factors linked to the fact that we only see binary systems in which at least one component is a pulsar, quotes a rate range $\mathcal{R}_{emp} \in 3-190\mathrm{Myr}^{-1}\times\mathrm{MWEG}^{-1}$, where MWEG stands for Milky-Way Equivalent Galaxy.

The theoretical models display different cases, depending on assumptions about the dominant channel by which a pair of massive stars evolves into a pair of close compact objects, surviving two supernova explosions without being disrupted, and whether during a common envelope phase the binary system undergoes instead a premature merger as a result of friction. It is worth underlining that these theoretical models are crucial because they represent the only means to draw predictions about rates of mixed NS-BH and BH-BH systems, for which an empirical estimate is impossible, since such systems have not been directly observed.

The reader is referred to [14] for a recent re-estimate of the rates; the authors introduce several models, two of which (A and B) are more pessimistic, since they assume that binaries in a common envelope phase are more likely to undergo a premature merger; the third model (C) instead allows for survival of stars in the Hertzsprung gap (HG) through the CE phase and leads to larger estimates.

For BNS systems, model A predicts galactic merger rates $\mathrm{R}_A \in [12-19]\mathrm{Myr}^{-1}$; model B is slightly more pessimistic, with rates in $\mathcal{R}_B[7.6-12]\mathrm{Myr}^{-1}$, while model C is markedly more optimistic, with rates $\mathcal{R}_C \in [68-101]\mathrm{Myr}^{-1}$.

The range of variability of the results within each theoretical model depends also on the way they are calibrated, either by means of assumptions about the star formation rate, or by means of the rate of supernova events in a Milky Way type galaxy; low rates are obtained with star formation calibration, high rates with supernova calibration.

It should be underlined that the models A,B,C also predict a mass distribution for the BNS pairs, which is generally centered on $1.4-1.4M_{\odot}$pairs, but with some spread; the authors account for this spread by computing correction factors, that for BNS are close to 1 and that we omit in the following because given the large uncertainty they appear a rather unnecessary nuisance.

Another point to notice is that all model rates, not surprisingly, are compatible with the empirical rate.

The other ingredient for estimating the rate of detectable events is the density of MWEG, which can be assumed to be

$$\rho_{gal} \simeq 0.01\mathrm{Mpc}^{-3}. \tag{3}$$

For BNS events, the detection range is sufficiently close not to require correcting this density to take into account cosmological effects.

Finally, we need to estimate the distance up to which AdV can be expected to detect BNS signals; to this end, we will rely only on the accurate knowledge of the BNS waveform in the inspiral phase.

It is well known that the signal to noise ratio (SNR) of a signal in the inspiral phase can be written as

$$\mathrm{SNR} = \sqrt{4\int_0^{f_{Nyquist}} \frac{\left|\tilde{s}\left(f\right)\right|^2}{S_n\left(f\right)}df} = \frac{G_N\mathcal{M}^{5/6}}{r\left(c\,\pi\right)^{2/3}}\left(\frac{5}{6}\right)^{1/2}\sqrt{\int \frac{f^{-\frac{7}{3}}}{S_n\left(f\right)}df}$$

$$= \quad 1.56 \times 10^{-19} \left[\frac{\mathcal{M}}{M_\odot}\right]^{5/6} \left[\frac{\mathrm{Mpc}}{r}\right] \sqrt{\int_0^{f_{upper}} \frac{f^{-\frac{7}{3}}}{S_n\left(f\right)} df}\,, \tag{4}$$

The actual value of the f_{upper} beyond which the merger begins is somewhat model dependent; a conservative value is given by the so called "innermost stable circular orbit", ISCO, which at the lowest order in the PN expansion can be written as

$$f_{ISCO} \simeq \frac{4.4\mathrm{kHz}}{(M/M_\odot)} \tag{5}$$

and results therefore in a value of $f_{ISCO} \simeq 1600$Hz for a BNS pair.

Given the SNR expression, we can define a sight distance d_{sight} as the distance at which AdV will detecting, exploiting solely the inspiral phase, an event with an SNR=8. This value was conventially assumed as safe for a detection, but experience has shown that actual detectors may yield spuria well above this limit, depending on the quality of the detector noise.

It should be made clear though, that significant GW signal is expected also in the merger phase and the subsequent ringdown of the formed object; targeting these signals is foreseen in data analysis, and should increase the detectability of the event. We omit this effect because we are unable to size it quantitatively at the same level of accuracy possible for the inspiral phase.

The sight distance results to be

$$\frac{d_{sight}}{1Mpc} = \frac{2}{5} \times 1.95 \times 10^{-20} \left[\frac{\mathcal{M}}{M_\odot}\right]^{5/6} \sqrt{\int_0^{f_{ISCO}} \frac{f^{-\frac{7}{3}}}{S_n\left(f\right)} df}\,, \tag{6}$$

where the factor $\frac{2}{5}$ accounts for an average over source location and source polarization, which leads to a reduction of the SNR value as compared with the optimal case of a source emitting at the zenith of the detector. For a BNS, one has $\mathcal{M} \simeq 1.219 M_\odot$, and we show in Fig.6 a comparison of the BNS sight distances, as a function of the solar mass, up to 1kHz; even in case the upper frequency limit, which is $f_{ISCO} \sim 1.4$kHz, were to turn inaccurate, the sight distance is robust against variations of its value, and we can safely assume that AdV would have a sight distance of 148Mpc for the values considered.

The resulting volume observable by AdV alone is therefore $V_{BNS} \simeq 13.5 \times 10^6 \mathrm{Mpc}^3$; in Tab. we report for the different models the expected detection rates, on the basis of the simple formula

$$\rho = V_{BNS} \times \mathcal{R}_{MW} \times \rho_{gal} \tag{7}$$

where $\mathcal{R}_{MW}$ is the merger rate in a "Milky Way equivalent galaxy", as in Tab.4. It should be noticed that the authors [14] quote about 8 times larger rates for AdLIGO; the reason is that they assume a detection range of Advanced LIGO of $\sim$ 300 Mpc, which results by using coherently the three AdLIGO detectors, each having a sight distance of about 170Mpc.

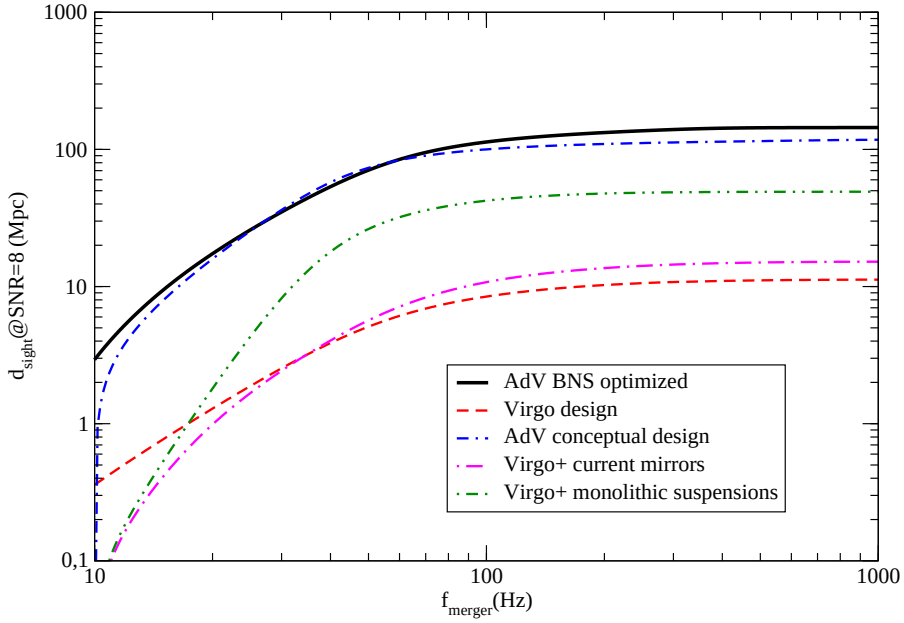

Figure 6: The sight distance, averaged over source location and polarization, assuming an SNR≥ 8, for binary neutron stars, as a function of the upper frequency cutoff. The different curves correspond to the sensitivities shown in Fig.5.

model	merger rate ($\mathrm{Myr}^{-1}\mathrm{MWEG}^{-1}$)	detection rate (yr^{-1})	comments
empirical	3 - 190	0.4 - 26	empirical model
A	12 - 19	1.6 - 2.6	reference model
B	7.6 - 12	1 - 1.6	full CE accretion
C	68 - 101	9.2 - 14	CE for HG stars

Table 4: Expected rate of BNS events for Advanced Virgo, in the different empirical and theoretical scenarios for the coalescence rates.

Let us anticipate here what we will discuss in Sec. 4.3; adding coherently AdV to the Advanced LIGO network leads of course to even larger detection range, and rates increased by about 20%, but more importantly allows to solve the inverse problem, locate the source position and reconstruct its polarization.

4.2.2 Binary black holes, and mixed systems

Differently from BNS, no BH-BH or BH-NS system has been observed yet; consequently, the assumptions about the coalescence rate of such systems is somewhat less firm. However, since the SNR scales roughly as $M^{5/6}$, larger mass systems are potentially visible to greater distances and their interest is quite substantial.

Scientific payoff Some of the considerations made for BNS events apply also to BBH and BH-NS events, in particular the possibility to measure the event distance, and actually to much larger distances.

The BH-BH collisions will be a unique laboratory; each BH is solely characterized by its mass and spin, which completely determine the dynamic of the event horizon, and a BH-BH collision can be studied by methods of Numerical Relativity, and yield accurate predictions about the waveforms. This program has met in the past enormous difficulties, which have been in large part overcome ingenuosly [16, 17] and start to yield complete predictions about the waveforms: see for instance [18].

A direct BBH observation would be a clean test of GR in a regime of strong fields, thus allowing for instance to discriminate alternative formulations of GR.

The BH-NS collisions have instead a good potential to shed light on the EoS of the NS; for a wide range of mass parameters, the latter will be disrupted by the tidal forces due to the BH, and the resulting GWs will be within the frequency range of GW detectors, thus allowing a direct probe of the NS structure [19].

It should also be noticed that BH-NS coalescences are one of the proposed mechanisms for producing the violent shocks that would generate Gamma Ray Burst events; the importance of collaborating with GRB detectors is paramount.

We will see that a non detection of BH-NS events would generally be compatible with current models of stellar evolution. Instead, a non detection of massive BBH events would challenge the theoretical expectations, and lead to revise substantially the models.

Expected rate of events There are essentially two ways by which a population of BBH or BH-NS systems can be inferred. First, it is possible to use the same population synthesis models applied to the BNS systems, and partially calibrated by the observation of binary pulsars, to infer the population of more massive stars [14].

Second, it is possible to exploit an unique observation, the one of a single binary system formed by a Wolf-Rayet massive star and a black hole, the IC10 X1, to infer the rate of

Model	$\mathcal{M}/M_{-}\odot$ range	$d_{eff-sight}$Mpc	merger rates Myr^{-1}	AdV detection rate yr^{-1}
A	$2.5-3$	300	$0.07-0.11$	$0.08-0.12$
C	$1.5-4$	286	$3.2-4.8$	$3.1-4.7$

Table 5: BH-NS results from population synthesis models

Model	$\mathcal{M}/M_{-}\odot$ range	$d_{eff-sight}$Mpc	merger rates Myr^{-1}	AdV detection rate yr^{-1}
A	$5-8$	613	$0.02-0.03$	$0.2-0.3$
C	$2.5-8.5$	545	$7.7-11$	$52-75$

Table 6: BBH results based on population synthesis models

BBH production, on the basis of the assumption that the WR star will soon evolve into a BH[15].

Rate based on population synthesis models The population synthesis models discussed in [14] display for BBH the same variation of the results, internal within each model and across models, that we have discussed for the BNS sources.

The more pessimistic model A predicts for pairs BH-NS galactic merger rates of $0.07-0.11\mathrm{Myr}^{-1}$, while for BBH systems it predicts chirp masses in the range $[4,\,8]M_{\odot}$and galactic merger rates in $[0.02-0.03]\mathrm{Myr}^{-1}$.

These values are to be compared with those resulting from the more optimistic model C, which assumes a more favorable evolution of the binary system through the common-envelope phase: for BH-NS sytems, galactic merger rates in $[3.2-4.8]\mathrm{Myr}^{-1}$, and for BBH systems galactic merger rates in $[7.7-11]\mathrm{Myr}^{-1}$ result.

In order to turn the galactic merger rates into predictions for AdV detection rates, the following crude formula can be adopted

$$R = \rho_{gal} \times \frac{4\pi}{3} d^3_{eff.sight} \times \mathcal{R}_{MW} \tag{8}$$

where the $d^3_{eff.sight}$ is an effective volume scale, reminiscent of a sight distance but which takes into account a population averaging. The authors of [14] scale the sight distance d_{BNS} by the factor $(\mathcal{M}/M_{\odot})^{5/6}$ in Eq.6, then average the volume factor d^3 over the synthetic mass population. This scaling can be roughly carried over on the AdV estimation, and we report the resulting effective sight distance in Tabb. 5, 6.

Please note that this estimate does not take into account the upper frequency cutoff at f_{ISCO}, see Eq.5; to gauge its importance, let us check again in Fig.7, for a BBH of $10-10M_{\odot}$, the behaviour of the sight distance as a function of the frequency cutoff. For these masses, which lie *above* the range simulated by the authors, the $f_{ISCO} \sim 200$Hz and the reduction of d_{sight} over a more naive estimate is rather negligible, an assumption therefore valid over the entire mass range.

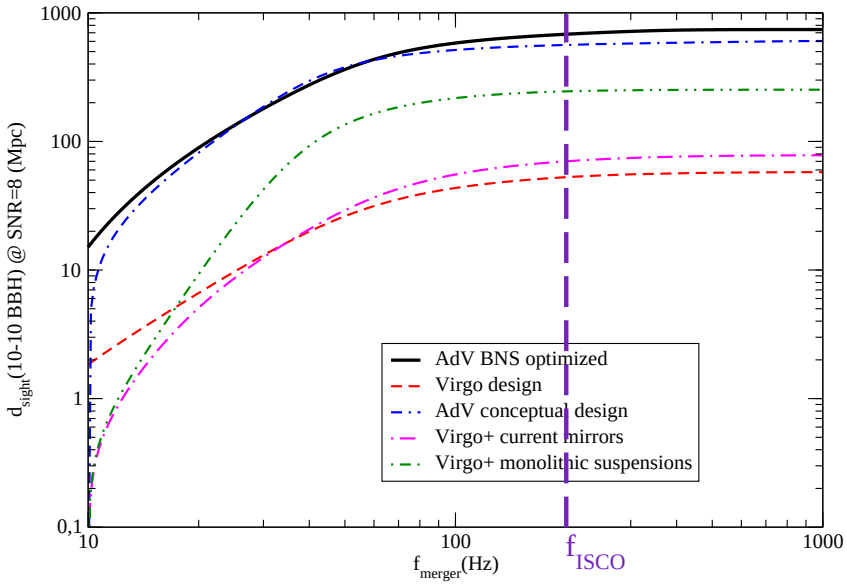

Figure 7: Sight distance, as a function of the upper frequency cutoff, for a double BH binary with components of $10M_{\odot}$each. Note that the $f_{ISCO} \sim 200$Hz , frequency up to which the curves should be considered valid.

To compute the last column of Tabb. 5, 6 we again assume $\rho_{gal} \sim 0.01\text{Mpc}^{-3}$, neglecting cosmological effects which start to be relevant for BBH systems. Again, the results we obtain are, not surprisingly, about 8 times smaller than the AdLIGO network, which we should remind comprises three equal detectors located at two sites, each with a sensitivity for BNS $d_{sight}(BNS) \sim 174$ Mpc. This scale alone boosts the observable volume, over AdV, by a factor $\sim (174/148)^3 = 1.6$. The estimates in [14] assume coherent analysis over the LIGO detectors, which scales up the sight distance by about a factor $\sqrt{3}$, and therefore boosts the observable volume by another factor ~ 5; together the two effects fully justify the factor 8 in the rates.

Besides the large variability of the models, which calls for caution by itself, another potential pitfall of population synthesis models is that they are not extended easily to higher masses, essentially because very large mass stars have a tremendously complex evolution, marked by explosive events and very large mass losses over short periods. However, as we will shortly see, larger mass systems might be a very interesting target.

Rate based on empirical observations Besides the systems simulated by binary evolution codes, there exist a very few but tremendously important observations of very massive binary systems, which lead to believe that high mass BH pairs are actually formed and are detectable by Advanced GW detectors.

In particular, the IC10 X-1 X-ray source is a binary tight system comprising a $24M_{\odot}$ BH (the largest known stellar BH) and a $35M_{\odot}$ Wolf-Rayet star, whose future evolution has been studied in depth in [15]. The authors predict that the system will evolve in a BH

pair with a chirp mass $\mathcal{M} \sim 14 M_{\odot}$; systems with such a mass are detectable by AdV up to about 1.1 Gpc.

The other important prediction in [15] is that the system will remain tight enough to coalescence in a few billion years. The authors are able to estimate the abundance of such systems and predict a rate of detection, for the three combined Advanced LIGO detectors, of 2300 events / year. Even AdV alone would see about 250/year events of this kind.

4.2.3 Rotating neutron stars

A rotating compact object, like a NS, distorted so as to possess a variable mass quadruple moment, would emit essentially monochromatic GW radiation, with a stability comparable to the one of the rate of pulsar electro-magnetic pulses.

The strength of the GW signal is essentially parametrized by the degree of asymmetry of the star, the so called "ellipticity" parameter ε; a typical estimate for the gravitational strain at Earth could be

$$h \sim 10^{-26} \frac{I}{10^{38} Kgm^2} \frac{10kpc}{d} \left(\frac{\nu}{100Hz} \right)^2 \frac{\varepsilon}{10^{-6}}. \quad (9)$$

where 10^{-6} is at the upper range of what is believed plausible for a neutron star, while "strange stars" might sustain higher asymmetries, even as large as 10^{-4}.

The weakness of the signal, and the need to integrate it over O(1yr) periods, lead to data analysis complications, due to the Doppler effect and the resulting line widening; however, the signal remains conceptually relatively simple and provides a clean laboratory for GW study.

Scientific payoff The detection of continuous GW signals from galactic pulsars would be a tremendously clean test of GR.

The strength of the signal is proportional to the ellipticity parameter ε, and this in turn to the rigidity of the NS crust.

For pulsars, the relationship between the GW emission frequency and the rate of e.m. pulses would help discriminating among competing mechanisms generating this asymmetry.

Moreover, it is well known that pulsar rotation may undergo sudden phase discontinuities, believed to be related to "starquakes", or rearrangements of the NS crust stresses. If such events could be related with analogous losses of phase coherence in the GW signals, this observation could shed light on the nature of the deformation and ultimately on the rich physics of these stars, which possess huge magnetic fields and are believed to contain a superfluid core.

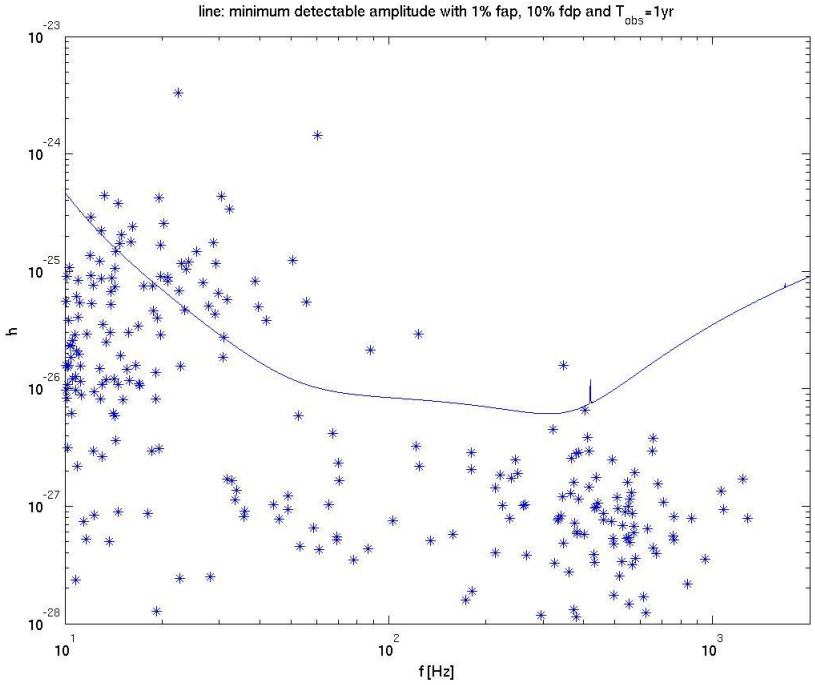

Figure 8: The curve shows the minimum value of h detectable by AdV, assuming a 1% false alarm rate, a 10% false dismissal rate, and an observation time (integrated) of 1 year. The dots represent the h value corresponding to the hypothesis that all the pulsar braking is due to GW emission.

Known pulsars The Doppler effect due to Earth rotation and revolution can be fully corrected for known pulsars, for which position and frequency are sufficiently known; for these sources, it is possible to estimate the chances for AdV of detection.

In Fig. 8 we show the minimum value of h that AdV can detect with 1 year of integrated observation, and the assumption of 1% false alarm and 10% false dismissal probabilities. The dots represent the upper limits to the h values that individual known pulsars can emit, assuming that their loss of rotational energy is entirely due to the GW emission. This is the so called "spin-down limit". The figure shows that even in a configuration optimized for BNS, AdV will be able to beat by orders of magnitude the spin-down limit for about 40 of the pulsars presently known, mostly at low frequencies.

In Fig. 9 we show the upper limits that it is possible to place on the ellipticity ε by exploiting 1 year of AdV observation time, under the same assumptions leading to reach the h_{min} limit discussed. If we believe that the realm of plausible ε values is rather $\leq 10^{-6}$, this clearly reduces somewhat the interest of the low frequency upper limits. However, it is also clear that at higher frequencies it is possible to reach plausible ε values, although it would be necessary operating the detector in SR mode optimized around 1kHz in order to also beat the spin-down limit for some millisecond pulsars.

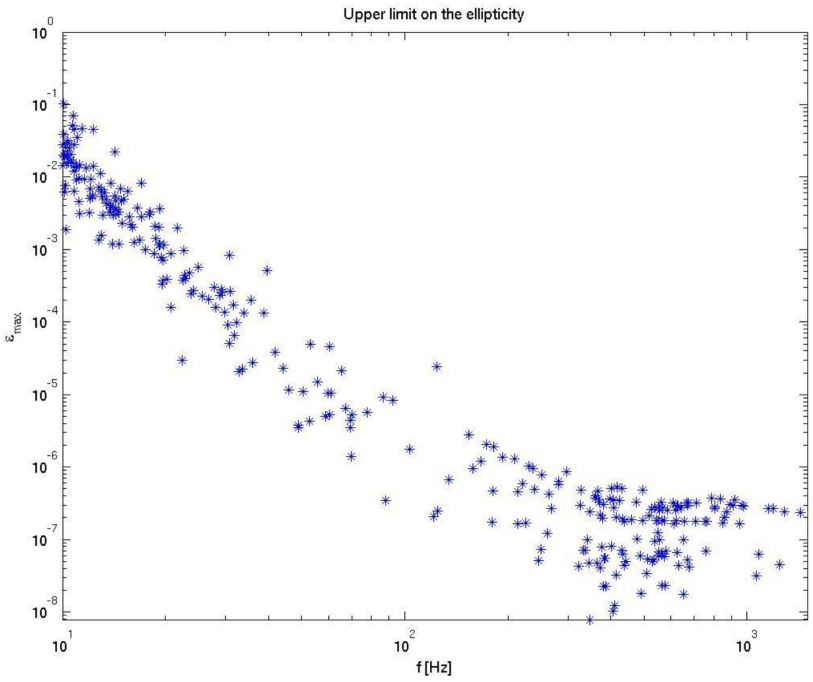

Figure 9: The plot shows the upper limits placed on the ε ellipticity of known galactic pulsars on the basis of 1 year of AdV observation time.

Unknown rotating neutron stars We detect as pulsars only a tiny fraction of the galaxy NS's; in fact, on the basis of the neutron star birthrate [20] it is possible to estimate that there exist $O(10^5 - 10^6)$ electromagnetically quiet NS in a radius of 1kpc; it makes therefore sense to perform non-targeted searches, at a reduced sensitivity, which may allow to discover close enough NS. The LIGO Scientific Collaboration has recently published a search [21] which uses part of the LIGO S5 run data which has been able to constrain $\varepsilon \leq 10^{-6}$ for the NS in a 500pc radius around Earth. Advanced detectors will improve over these limits: in Fig. 10 we show the distance, as a function of the frequency, at which a rotating compact object could be detected with one year of AdV operation, assuming $\frac{f}{\dot{f}} > 10^4$yr and under the assumption of having 10^9 candidates selected after an uncoherent search, to be followed coherently.

We actually plot a family of curves, corresponding to different values of the "ellipticity" ε, from $\varepsilon = 10^{-8}$ (lower curve) up to $\varepsilon = 10^{-5}$ (top curve). It is on one hand clear that even in advanced detectors the uncoherent search will be unable to cover the entire galaxy (distance scales $O(10kpc)$), still the chances of detection will be increased by 2 - 3 orders of magnitude.

Low Mass X-ray binaries We should mention another potentially interesting class of spinning neutron stars; the Low Mass X-ray Binaries, constituted by a NS which is spun-up by the infall of material through an accretion disk. The evidence is that the spin of this

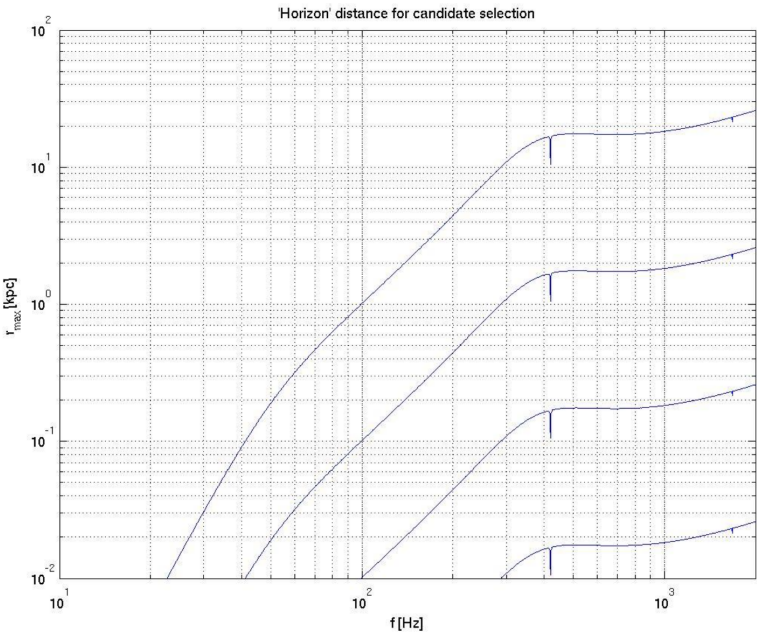

Figure 10: The plot shows the maximum distance at which a distorted, rotating NS could be detected during a non-targeted search, for given values of the ε ellipticity, from 10^{-8} (lower curve) to 10^{-5} (upper curve), on the basis of 1 year of AdV observation time.

systems results from the equilibrium between the torque due to the accretion mechanism and some braking mechanism, the most likely being the GW emission. The resulting GW frequencies are stabilized by this feedback mechanism and are expected in the range 600 - 1200 Hz; these sources could be targeted especially well operating AdV in narrow band mode, except Scorpius X-1 on which interesting limits (or a detection) can be placed also operating in wide-band mode.

4.2.4 Core collapse Supernovae

The collapse of the core of a massive stars, the so called Supernova Type II events, has long been considered one of the most interesting sources of GW emission, with optimistic values for the energy emitted in GWs, of the order of $10^{-2}M_{\odot}$, quite comparable to the energy emitted by a BNS coalescence.

More recent estimates of the energy emitted in GWs have shown, though, that the GW energy emitted is likely to be $\leq 10^{-8}M_{\odot}$, and this fact, together with the limited knowledge of the waveform emitted, reduces the prospects of detection by first generation interferometric detectors to galactic events, at best.

Galactic events are known to be rare: the latest galactic supernova observed has been the explosion of the blue star Sanduleak, which led to the famous 1987a event. The estimates of less than 1 event per two decades in the Milky Way and in the local group of galaxies

is supported by indirect evidence, provided by the Integral experiment. Integral has detected γ rays emitted in the radioactive decay of the ^{26}Al isotope, copiously produced in Supernova explosions; the galactic abundance of this Al isotope, about $3M_{\odot}$, is consistent with the supernova rate quoted above [22].

A recent review [23] recalls however that there may be 1 SN occurring about every other year between 3 - 5 Mpc from Earth.

The recent SN 2008bk, which exploded roughly 3.9 Mpc away, is an example SN from this region of space. Initial LIGO and Virgo class detectors had no chances, though, of detecting GWs from SN 2008bk.

Advanced detectors, however, could put some constraints on the GW emission strength, but still would probably not allow detailed GW observations. It is argued that the GW signatures of the neutrino, magneto-hydro-dynamic, and acoustic SN mechanisms may be mutually exclusive and that the mere detection, or, in fact non-detection, of GWs from a nearby SN can constrain significantly the core-collapse explosion mechanism.

It should be added that the standard model for SN core collapse indicates that the burst of neutrinos from the inverse β-decay, leading to the core neutronization and collapse, and the emission of GW radiation, are separated by a very small delay, of a few ms. This opens the way to very tight coincidences between neutrino and GW detectors, that would increase the detection confidence enormously.

An additional time delay between the GW signal and the neutrino flash is introduced during the propagation because of a non-null neutrino mass: this delay can be expressed as [28]

$$\delta t_{prop} = 5.2ms \frac{d}{10kpc} \left(\frac{m_\nu}{1eV}\right)^2 \left(\frac{10MeV}{E_\nu}\right)^2 \tag{10}$$

which means that a 1ms accuracy would constrain neutrino masses $< 1eV$.

The newly formed proto-neutron-star (or black-hole actually, depending on the starting mass) will be in an excited mechanical state, with oscillations that will gradually damp by internal friction and by the emission of GW as well. Some of these oscillations, like those of the so called $r-$modes, can last for months, thus being in principle detectable as a transient source of essentially monochromatic GW radiation.

4.2.5 Soft γ-ray repeaters

Soft gamma repeaters ("SGRs") are X-ray stars that emit bright, repeating flashes of soft (i.e. low-energy) gamma rays. While four SGRs have been identified in our galaxy so far, many other millions almost certainly exist, and a similar number probably exist in every other galaxy. According to the "magnetar" model, SGR are associated to neutron stars (NS) with very intense magnetic fields. The intensity is such that the star crust breaks under accumulated magnetic stress. A hot fireball forms which cools down through the emission of bursts of electromagnetic (EM) radiation. During the crust quake, the

star's nonradial seismic modes can be excited, thus leading to emission of a GW burst. Theoretical estimates predict comparable EM and GW energy release (within few orders of magnitude). The best upper-limit on the strength of the GW emission placed with current LIGO data is 10^{45} erg, which is within the range 10^{44}–10^{46} erg for the observed EM emission. With a sensitivity improvement by a factor of 10, it is possible to cover this entire range. SGR are thus detectable sources by advanced detectors and if they are not observed, stringent constraints on the underlying model will result from the upper-limits.

At times (though rarely), SGRs undergo "giant flares" during which the emission is dramatically increased with a total energy about a thousand times higher than in a typical burst. This has been the case the 27 December 2004 for SGR 1806-20. Quasi periodic oscillations (QPO) in the tails of the giant flares have been observed. QPO are thought to be driven by the star's seismic modes, the same that are expectedly sources of GW. This information can be used to narrow down the search in the GW spectrum to the observed QPO frequencies, leading to an improvement in sensitivity. For hyperflare events occurring at the time of advanced detector operation, the observable GW energetics at 100 Hz would lie in the range 10^{43} erg, leading to stringent constraints on the magnetar model [26].

4.2.6 Gamma Ray Bursts

The gamma-ray bursts, detected by instrumentation on board satellites, might be originated by shocks in matter rapidly accreting onto newly formed black holes.

The events are divided in two broad classes, a minority of *short* bursts (lasting less than about 2 s) and a majority of *long* ones, lasting anywhere between 2s to several minutes, with an average of 30s duration.

There is mounting evidence (see for instance [25]) that long GRB, or at least those with a softer γ spectrum, are associated with a type of core-collapse supernovae; more precisely the collapse of massive, rapidly spinning Wolf-Rayet stars, which end up in massive Kerr black-holes with accretion disks. Instead, good arguments (see for instance [24]) exist to assert that short bursts are related with coalescing BNS or NS-BH. It has also been argued in the past that NS-BH coalescences could be an alternative mechanism for long γ-ray bursts, although the collapsar model is now favored.

The γ rays would be powered by the accretion disk orbiting around the newly formed Kerr black hole; a disk, for instance, formed by material resulting by the tidal disruption of part of the two colliding objects, in the case of short GRB's[2].

If the pictures for *short* and *long* gamma ray bursts are correct, GW observatories may be able to detect the GW signal from the inspiral and merger event, or by the supernova explosion respectively. Such events have already been searched for in the data of the first

[2] It is worth recalling that the infall of matter on a BH is about the most efficient mechanism for turning matter in energy, far more efficient than thermonuclear reactions.

generation detectors (see for instance [27] for a search triggered by a long γ-ray burst), finding no evidence of a correlation.

It should be underlined that for most of the short GRB one has observational evidence, by way of measuring faint X-ray afterglows, that they occur at cosmological distances (for which $z \geq 0.1$), which lowers the chances of detecting the progenitor BNS or BH-NS event by means of first generation detectors.

Advanced detectors will have greater chances, and a confirmed association of GRB and BNS events would have tremendous consequences:

- the GRB trigger could give a greater confidence in the GW event, thanks to the tight time association. The models show that it is necessary to allow only for about 2 minutes before and after the GRB maximum in order to over-cover the time windows where a GW event is expected. Considering a GRB rate ~ 1/day, false alarms can be abated by factors $O(10^6)$. At fixed FA rate, the coincidence with GRB's allows to lower the SNR thresholds applied to GW events, for instance from 7 to less than 6, thus gaining a 60% increase in GW event rate.
- The BNS (or NS-BH) GW event would allow reconstructing the mass parameters of the progenitors, through observation of the inspiral phase, and potentially also the mass and spin parameters of the formed Kerr BH, by observing its Quasi-Normal-Modes; this would serve input for modeling the GRB process and could help understanding the complex dynamics in the accretion disk.
- The GW event would also constrain the distance, thus allowing to precisely calibrate the energy emission.

4.2.7 Cosmological stochastic background

The vacuum fluctuations of the early universe are expected, in the inflationary models, to have been amplified during the inflationary era giving rise also to a stochastic background of gravitational waves.

The models in general foresee a spectral density for these perturbation in form of a power law

$$\Omega_{GW}(f) = \Omega_{f_0} \left(\frac{f}{f_0} \right)^n \tag{11}$$

Standard inflationary theory foresee a flat spectrum $n = 0$, while other models, including string models, foresee $n > 1$, and therefore spectra increasing with the frequency.

It is well known that detecting a stochastic background requires cross-correlating the output of at least two detectors. An upper limit may result in the form

$$h_{100}^2 \Omega_{f_0} < \beta \frac{10\pi^2}{3H_0^2} \frac{1}{\sqrt{T \int I(f) df}} \tag{12}$$

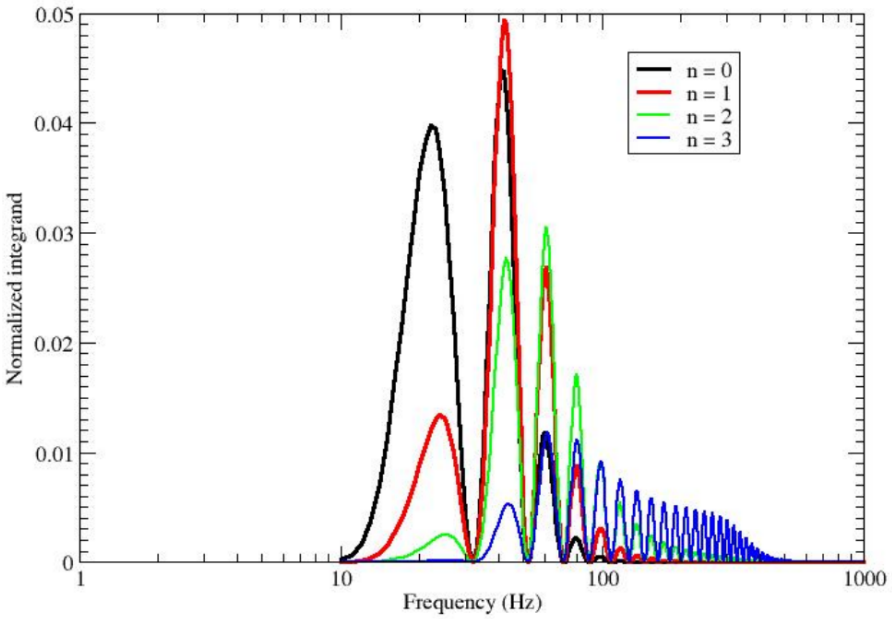

Figure 11: The plot shows, for different values of the power law index, the frequency dependency of the integrand $I(f)$, for AdV and the Hanford Advanced LIGO detector. It is evident how the relative weight of higher frequencies becomes more important for larger n values.

where h_{100} is just the Hubble constant in units of 100 km/s/Mpc. The factor β is a statistical factor related with the false alarm and false dismissal probabilities. The integrand $I(f)$ is in turn

$$I(f) \equiv \frac{\gamma^2(f)}{f^6 S_1(f) S_2(f)} \left(\frac{f}{f_0}\right)^{2n} \tag{13}$$

where $\gamma(f)$ expresses the coherence between GW background detected at different sites, where detectors having noise spectral density $S_i(f)$ are operated.

We show in Fig. 11 the function $I(f)$, normalized to unit integral, for different values of the exponent n. Since the upper limit in Eq. 12 depends upon the inverse of the integral of $I(f)$, the frequency regions where $I(f)$ is larger are also those most contributing to the integral, thus signaling portions of the frequency spectrum where more significant upper limits can be set.

For larger values of n, the integrand $I(f)$ is dominated by higher frequencies.

Limits on the spectra of background We show in Fig. 12 a comparison of the different models of stochastic background spectral dependence, as a function of frequency. The Ω_{f_0} scale is set as the upper limit which could be set by operating AdV and one of the Advanced LIGO detectors (the one at Hanford to be precise) for one year. The different

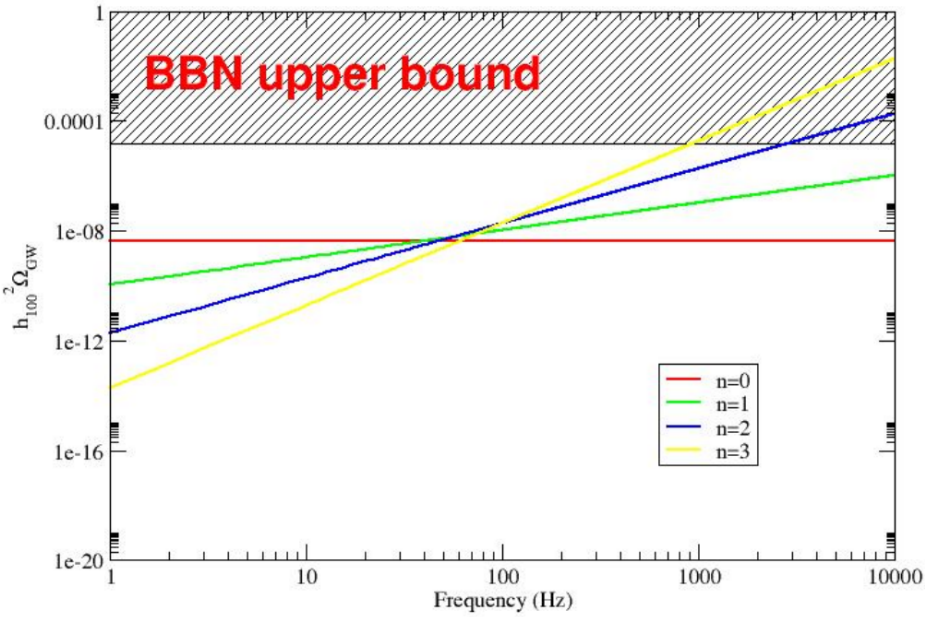

Figure 12: The plot shows, for different values of the power law index, the frequency dependency of the smallest spectral density limit that could be detected by integrating for one year data by AdV and one of the Advanced LIGO detectors.

curves show that for larger n the high frequencies become more important and so the role of AdV in an LSC-Virgo network.

However, note that the stochastic background is robustly bound by the big-bang nucleosynthesis limit: gravitational waves energy exceeding the bound would have led the Universe to evolve too quickly through the primordial nucleosynthesis phase and alter the observed balance of barionic matter.

Moreover, the LIGO S5 run should end up setting a limit shortly below the BBN bound.

4.3 AdV operation in a network of GW detectors

The AdV detector will harvest the best of its detection and GW science potential in cooperation with other GW detectors, and most notably with the Advanced LIGO detectors, which will be operating in a coordinated fashion with AdV, having a comparable sensitivity for most of the sources.

We have already discussed briefly how AdV would be exploited, in cooperation with Advanced LIGO detectors, to place upper limits or detect a stochastic background of gravitational radiation.

Another important role will be played in the detection and parameter estimation of signals emitted by point sources.

4.3.1 Coherent analysis

The reason why a network of GW detectors is on one hand a necessity, on the other hand a unique opportunity, lies in the simple nature of gravitational waves. As it is well known, in the theory of General Relativity the gravitational waves can be expressed as perturbations of the metric which are transverse and described by two polarization states $h_+, h_\times$, as appropriate for massless fields.

Now point sources of GW, like coalescing binaries or supernova explosion, have the property that this signal is fully coherent at any terrestrial site; each detector will be sensitive to a certain linear combination

$$h(t) = F_+(\theta, \phi)h_+(t) + F_\times(\theta, \phi)h_\times(t) \tag{14}$$

of the $h_+(t), h_\times(t)$ GW polarizations coming from the direction θ, ϕ, weighted by the antenna patterns $F_+, F_\times$.

While the antenna patterns depend upon location and orientation of each detector, the same h_+ (or $h_\times$) is received at any detector site, apart delays introduced by the finite speed of wave propagation, and small [3] Doppler effects due to Earth rotation.

It is possible to exploit this Earth-scale coherency to use a minimum of three detectors to reconstruct the two polarization components, as well as the source direction θ, ϕ, even without any knowledge of the waveform, as first shown in [12].

More in detail data generated by a network of n detectors reside in a n-dimensional space. Since GW have two polarizations and the detectors see a linear combination of them, the signal lies in a two-dimensional subspace. Therefore, the signature left by a GW in the data is zero when projected onto the complementary so-called "null" subspace (i.e., the $n-2$ remaining dimensions). This implies that when we have $n \geq 3$ (misaligned) GW detectors, the "null" subspace has at least one dimension: there exist at least one linear combination of the data such that the GW signal is canceled out. Those combinations are referred to as "null streams"; the larger the network, the greater the number of null streams.

Null streams are useful to veto false triggers due to instrumental artifacts, which do not obey this cancellation property. In a coherent search, it is required that the GW candidate has a large "coherent amplitude" (amplitude of the projection onto GW plane) as compared to its "null amplitude" (amplitude of the projection onto the null space).

In gaussian noise, a coherent operation of AdV and of the Advanced LIGO detectors achieves the maximum possible detection probability, at a fixed false alarm rate [29].

Adding AdV coherently to a network of Advanced LIGO detectors leads therefore to an increased detection rate. A quantitative estimate of the benefit is still under study, however previous analyses based on the initial LIGO and Virgo sensitivities were showing that the detection rate for BNS could be increased by about 20% [30]. Similar or greater benefits are possible for burst events [29].

[3] But significant for pulsar signals

It should be remarked, though, that the increased detection rate is of secondary importance with respect to the benefits resulting by having included a third site in a network of advanced GW detectors; this will make possible the solution of the inverse problem.

In particular, it will be possible by way of coherent analysis to reconstruct in an optimal way the source parameters, for instance for BNS signals [31].

4.3.2 Coincident analysis

The presence of non-gaussian noises may limit to some extent the applicability of coherent analysis techniques, even though the null streams requirements can help rejecting in large part the resulting extra false candidates.

However, much of the benefit of the detectors network can be harvested just on the basis of standard coincidence analysis, augmented by coherent follow-ups.

For instance, it can be shown that coincidence analysis using a LIGO-Virgo network can lead to pinpoint the source location of burst events, with an accuracy depending on the inverse SNR and generally smaller than 1^o already for moderate SNR values [34].

Analogously, it can be shown that a detection strategy of BNS based on a two-fold coincidence, followed by a coherent follow-up, is competitive with the coherent analysis starting at $SNR_{network} \geq 7$ [30].

In fact, detailed studies for burst [33] and BNS events [32] have demonstrated that a two-fold coincidence strategy in a three sites detector network is an efficient strategy, which allows to increase the chances of detection by about 25% over a LIGO network, and to reconstruct the source location as well.

The other advantage of coincidence analysis is the robust rejection of spuria, as well as the possibility to estimate the background noise by introducing relative time shifts among the data by the various detectors.

It is also possible to show that the bulk of information leading to the reconstruction of source direction is contained in the time delays across the detector network [35].

It is important to underline that a successful operation of AdV in a network of GW detectors requires that its sensitivity is comparable to its partners [29].

4.4 Multimessenger opportunities

In this section we would like to underline that a host of collaborative work with other observatories will be needed, in the Advanced Detectors era, to fully exploit the detector potentialities.

4.4.1 Radio observatories

We would want just to mention that radiotelescopes are instrumental for carrying out succesfully a detection program for continuous signals emitted by pulsars.

As discussed already, the targeted search of GW emitted by known pulsars relies on the assumption that the phase evolution is coherent over long time scales. If a "star quake" occurs, it can introduce a "glitch" both in the series of EM pulses and in the GW signal. Knowing whether a glitch has occurred is possible, if the radiotelescopes regularly check the count of pulses for slight variations in the expected arrival of the event.

The Advanced detectors will need this information at least for the most interesting pulsars, ensuring that sufficient coverage of the targets is in place throughout the observation phase.

Needless to say, a confirmed correlation between GW and EM glitches would tell us a lot about the structure of the NS crust and its dynamics.

4.4.2 Optical observatories

Ground based optical detectors remain the most important source of information in the e.m. spectrum for a variety of sources, including the light curve of supernova events.

Robotic detectors are sufficiently inexpensive to be dedicated to systematically follow-up a reasonable number of triple coincident triggers issued by LIGO and Virgo detectors, for which a source position could be reconstructed with sufficient accuracy.

We expect such a program to be potentially rewarding, while being affordable in terms of human and monetary resources.

4.4.3 X-ray observatories

A range of X-ray satellites, including Chandra [36] by NASA and X-MM Newton [37] by ESA, are operating in Earth orbit and provide data of interest also for the GW community.

Indeed, although γ-ray events have captured most of the interest, it is well known that also X-ray prompt bursts or longer tails have been observed in conjunction with core-collapse supernovae and GRB events.

While both Chandra and X-MM Newton missions can be expected to last until the beginning of the Advanced GW Detectors era, we can hope that the joint ESA-NASA X-Ray Evolving Universe Spectrometer (XEUS) [38] will be operating as a successor.

4.4.4 Gamma-ray observatories

Probably Gamma Ray Bursts constitute the most exciting recent discovery in astrophysics, and the most likely source of events correlated with GW signals.

The NASA's SWIFT [39] satellite, which is a veritable multi-messenger observatory, carrying also optical and X-ray telescopes, will carry on its mission during the Enhanced GW detectors era, but is not expected to be alive in the AdV era. It will be replaced by the recently launched international Fermi Gamma-ray Space Telescope (formely known as GLAST) [40], which retains the capability of "swift" pointing towards GRB sources, while providing greater sky coverage and sensitivity over a much wider range of energies, up to ~ 300 GeV.

We have already underlined the importance of γ-ray events as potentially correlated with coalescing binaries and core-collapse supernovae. It is expected that advanced detectors will both search for events at times triggered by GRB observatories, but also issue alerts for triple or quadruple coincident events that could be worth investigating by pointing satellite based instruments.

4.4.5 Low energy neutrino observatories

The so-called "thermal" neutrinos, having energies of a few tens of MeV, are produced in short bursts (a few seconds) in the core-collapse supernovae, through the inverse β-decay process of neutronization. They are copious and carry out some 99% of the gravitational energy released, so that the existing detectors, like Super-Kamiokande [41], LVD [42] and IceCube [46] can detect them within the Milky Way and beyond the magellanic clouds [4].

These detectors operate under the agreement [43], exchanging time information about events, and regularly searching for coincidences which could correspond to a real SNe [5]. Both Super-Kamiokande and IceCube are expected to be in operation in the AdV era.

A correlated detection of an event by neutrino detectors and by GW detectors would first of all strengthen the case of a real detection, which means that at fixed FA rate the detector thresholds could be lowered and events originating further out in space could pass the first trigger level and be detected. Further, such a coincident detection would provide information about the collapse mechanism, and the relative GW - neutrino timing would allow probing the neutrino masses.

4.4.6 High energy neutrino observatories

In the Advanced detectors era we expect to have at least two large scale neutrino observatories in operation; IceCube [46] at the south pole, which is under realization as a successor

[4] Even though IceCube is designed for high energy ν, it can detect SN neutrinos in the Large Magellanic Cloud with a 5σ significance

[5] The Sudbury Neutrino Observatory (SNO) [44] was also part of the agreement snews, and has been recently decommissioned. Plans are underway, though, to upgrade it to SNO+ [45]

to AMANDA [47], and the large scale KM3Net detector [48] in the Mediterranean sea, successor to the existing detector Antares [49] and to the R&D projects NEMO [50] and NESTOR [51].

These neutrino detectors use an array of photomultipliers, regularly spaced in a large volume of water, to collect and detect the Cerenkov light emitted by charged particles which result from the collision of the high-energy ν's with the nuclei in water. The simultaneous excitation of several photomultipliers allows to reconstruct the direction of the charged particles and to infer the one of the incoming ν. The angular resolution is expected to be of the order of 1^o, therefore comparable with the one expected for the LSC-Virgo network of advanced detectors.

There is a range of potential sources of joint ν - GW emission; among the most promising we just list

Short GRBs High Energy ν's might be emitted during the binary mergers [24].

Long GRBs HE νs are expected to be produced in the shocks by accelerated protons, with fluxes sufficient to be detected at cosmological distances by km^2 scale ν detectors like IceCube and KM3NeT.

Soft Gamma Repeaters giant flares the violent crustal reorganization occurring in magnetars is believed to emit both GW and ν's, with fluxes that might be detectable or at least allow to constrain the models.

As with other joint observation, the simultaneous detection of GWs and HE ν's would give enormous insight into the generation processes, and also increase the reach of both instrument classes to fainter, further out events.

Advanced Virgo Preliminary Design:

PART 2:

Interferometer

5 Advanced Virgo: interferometer configuration

5.1 Introduction

This section describes the optical parameters and configuration of the AdV interferometer. The optical layout and the main parameters of the design are briefly summarised first, followed by a more detailed description of the design process and the motivation for the selected design option.

The design of the AdV core interferometer falls within the scope of the *Optical Simulation and Design* (OSD) subsystem. The optical layout and the nomenclature of the core interferometer, including the Michelson interferometer, its arm cavities and the mirrors forming the Power- and Signal-Recycling cavities is shown in Figure 13. Compared to the optical layout of Virgo, the AdV design features three main changes: the inclusion of Signal Recycling, the change in the arm cavities' geometry from a flat-concave to near-symmetric design and the move from marginally stable recycling cavities to non-degenerate recycling cavities. These topics will be described in more details in the following sections. A further challenge for the OSD subsystem is to ensure that the optical layout of the core interferometer supports the envisaged tenfold increase in sensitivity. A number of improvements over the Virgo layout are deemed necessary to achieve this, most importantly the careful separation of *auxiliary* beams, originating at anti-reflex surfaces, from the main interferometer beam and a careful study of noise due to light scattering.

5.1.1 Optical layout

The optical layout of the main interferometer in the current AdV baseline design is shown in Figure 13, with the main or core interferometer being defined as the long-baseline Michelson interferometer formed by the central beam splitter (BS) with arm cavities (X-arm and Y-arm) and the so-called recycling mirrors (PRM, SRM) in the input and output ports of the Michelson interferometer. This optical layout is essentially the same as the Advanced LIGO design.

The laser light, after being filtered by the input mode-cleaner (IMC, not shown in this figure), is injected into the interferometer through the semi-transparent Power-Recycling mirror. Arm cavities as well as the Power-recycling mirror are used to enhance the light power circulating in the arm because the signal-to-shotnoise ratio of the optical readout scales with the square root of the circulating power. The main output port of the interferometer is the so-called *asymmetric port* (AP), with the Michelson set such that this port is on the dark fringe. Before being detected on a high-power photo diode the signal is optically enhanced and filtered in the Signal Recycling cavity (formed by SRM1 and the Michelson) and then spatially filtered by a small rigid mode-cleaner cavity (OMC). The other optical outputs depicted by photo-diodes in figure 13 are detection ports that can potentially be used for interferometer control or monitoring purposes.

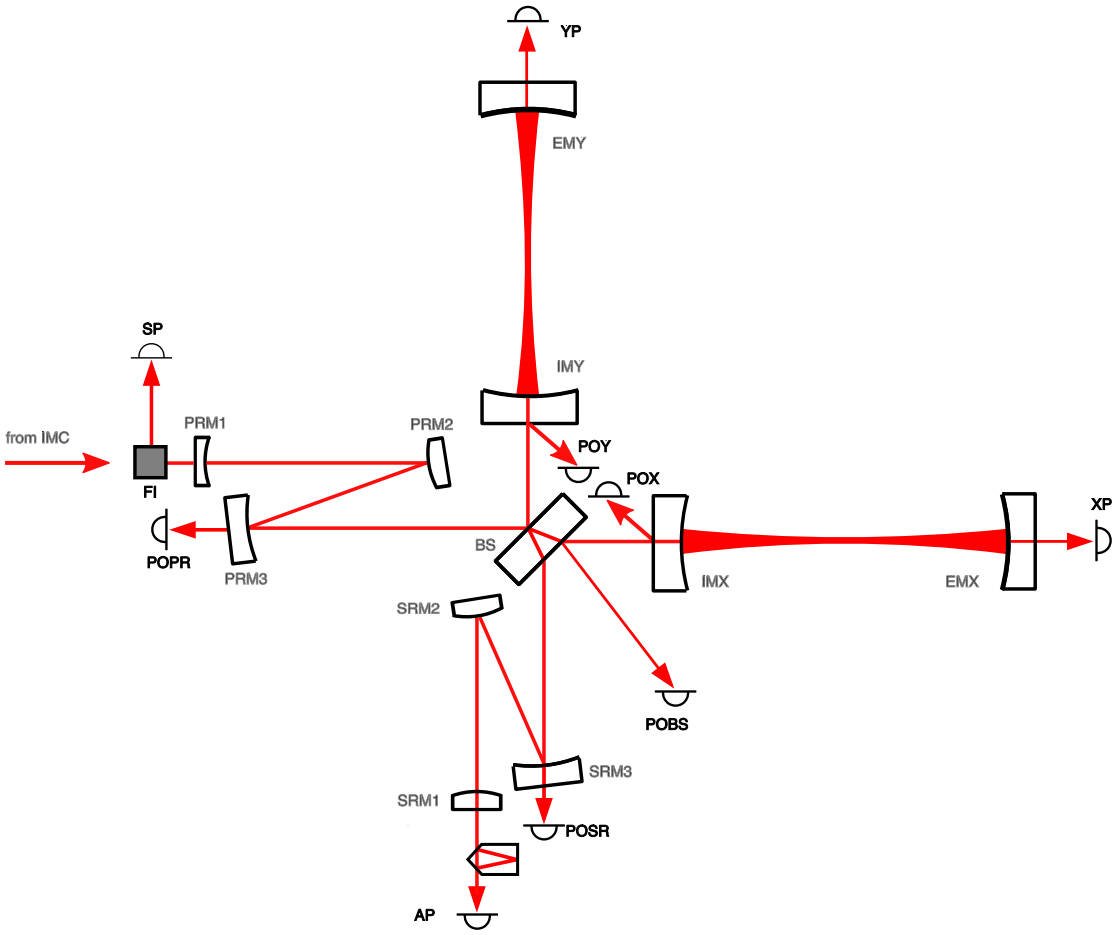

Figure 13: Optical layout of the AdV core interferometer: A new, clear nomenclature has been chosen [118] for Advanced VIRGO in order to avoid inconsistencies and possible confusion with the ongoing work on the Virgo interferometer: The interferometer arms will be identified by the letters *X* and *Y*, with the North arm, in-line with the input beam, being the X-arm. Cavity mirrors are called input mirror (IM) or end mirror (EM). Thus the North arm cavity (X arm) is formed by IMX and EMX. The recycling mirrors are called power recycling mirror (PRM) and signal recycling mirror (SRM). The dark fringe output port the Michelson interferometer is the *asymmetric port* (AP). The *symmetric port* (SP) denotes the back reflection from the Michelson (in-line with the X-Arm).Other readout ports are named after the optical component providing the beam: the light transmitted by the X-Arm cavity is called XP. So-called 'pick-off' beams will be labelled with *PO*, i.e. the reflection from the anti-reflective coating of the beam splitter will be detected in POBS. The folded optical path inside the Power- and Signal Recycling cavities increase the cavity lengths, which is required to achieve non-degeneracy for these cavities. The curvatures of the Recycling mirrors and of the folding mirrors are determined by cavity length and the required Gouy phase, see section 5.7.

5.1.2 Design summary

The current configuration of the main interferometer is defined by the parameters given in table 7. This section provides a brief explanation of the optical parameters, in the same order as following sections with a more detailed description.

Light power The light power circulating in the arms is maximised by increasing either the finesse of the arm cavity and/or the finesse of the Power Recycling cavity (see below) to reduce shotnoise.

Arm cavity geometry Both arm cavities have the same geometry, with the beam waist being close to the center of the cavity. This minimizes the thermal noise contribution. Care has been taken to reach a stable cavity suppressing higher-order modes.

Arm cavity finesse Both cavities have the same finesse. High-finesse cavities help to reduce shotnoise and have advantages with respect to noise suppression but are limited by losses in the cavity which are difficult to predict accurately. Currently we have based the finesse on the assumption of very low losses, this might be adjusted later, depending on results from an ongoing R+D program.

Geometry of mirror and beam splitter substrates The size of the mirrors should be as large as possible to minimise thermal noise and is limited by technical constraints. The thickness does not influence the optical design. So far, no decision has been taken regarding wedges in the substrate. In some configurations wedges can create extra pick-off beams or can help to separate such beams from the main beam.

Power Recycling cavity The Power Recycling mirror is used to further enhance the circulating light power and thus to reduce shotnoise. The finesse of the cavity is designed following the arm cavity finesse. The current design features a non-degenerate cavity with two turning mirrors and a folded path. This design should make the interferometer more robust against thermal deformations and misalignments.

Signal Recycling cavity The Signal Recycling mirrors allows to tune and shape the quantum noise limited sensitivity of the detector; the SRC finesse affects the detector bandwidth and the SRM tuning the frequency of the peak sensitivity. The only drawback of Signal Recycling is a more complex control system. The current design envisages also this cavity to be non-degenerate but a complete design has not been provided.

AdV Optical Configuration			
Light Power			
arm cavity power	760 kW	power on BS	2.7 kW
Arm cavity geometry			
cavity length L	3000 m		
IM R_C	1416 m	EM R_C	1646 m
Beam size IM w	56 mm	Beam size EM w	65 mm
waist size w_0	8.5 mm	waist position z	1385 m
Arm cavity finesse			
finesse	900	round-trip losses	75 ppm
transmission IM T	0.7%	transmission EM T	5 ppm
Power recycling			
transmission PRM T	4.6%	finesse	70
PRC length	24 m	Beam size on PRM1	1.8 mm
Signal recycling			
transmission SRM T	11%	finesse	40
SRC length	TBD	SRM tuning	0.15 rad
Mirrors			
IM diameter	35 cm	EM diameter	35 cm
IM thickness	20 cm	EM thickness	20 cm
IM wedge	TBD	EM wedge	TBD

Table 7: Parameters of the AdV interferometer. Some parameters cannot be given yet (TBD) but will be determined at a later stage, see text. Throughout the text we quote numerical values for several optical parameters. These numerical values provide consistent sets in the context of the respective subsections. However, at this stage they represent approximate values to be adjusted more accurately during the design process rather than precise and final settings. Therefore the values given in this table have been rounded to a few significant digits.

5.2 Design strategy

The goal of the optical design is to find and provide a consistent set of parameters and specifications for the core optical components, such as the size and geometry of the mirrors, their positions as well as their optical properties. The foremost design driver is the detector sensitivity, while care should be taken to reduce the envisaged commissioning time for the interferometer when possible. AdV will make use of the same facility as the Virgo detector; this puts some constraints on the interferometer design. In particular the vacuum enclosure can only be changed slightly, see Section 17.

One aim of the AdV project is to be able to take data together with the Advanced LIGO detectors. The R+D process within the LSC towards Advanced LIGO has been very successful over the last years, so that a very detailed design for the Advanced LIGO detectors exists and most technical issues are well understood. In order to make the best possible use of this existing knowledge we have decided to adapt the technical designs from Advanced LIGO whenever possible. This should not only cut short the path towards the final AdV optical design but will allow us to share and exchange valuable commissioning experience with the Advanced LIGO detectors later on.

5.2.1 Evolution of core interferometer optics parameters

Creating a technical design for a complex instrument like a gravitational wave detector is a long and iterative process. The main work stream of the OSD subsystem is to continually advance the technical details of the core interferometer. However, every design change has an impact on the connected subsystems, most importantly the input optics, the detection subsystem and also the length sensing and control subsystem. The impacts need to be evaluated and taken into account even during the initial phase of the designing the key features of the main interferometer. The OSD strategy for optimizing this process is based on slowly reducing the parameter space: if several options for a particular part of the design exists, these should be evaluated and compared thus a baseline solution can be chosen, which will then be studied in more detail. However, a final decision for a particular option and the corresponding definition of specification should only be performed when orders need to be places. For example, the size and geometry for the interferometer mirrors must be chosen for ordering the mirror substrates, while the details of the coatings can still be changed - until the substrates have been polished. This method allows to adapt to the most recent results from R+D projects while providing a clearly defined and consistent baseline at all times. In this the core interferometer plays a central role because it represents the dominant link between various other subsystems. It is therefore important to provide clear interfaces to other subsystems. The OSD subsystem has taken care always to provide a consistent and well documented layout for the core interferometer at the various stages of the development, starting by defining original draft design and a new nomenclature in [118], to the recent draft design for a non-degenerate Power-Recycling cavity [135].

5.2.2 Optical simulation tools

The optical design of high precision laser interferometers relies heavily on numerical simulations. In addition to commercially available optical design tools like Zemax, the gravitational wave community has over the years developed a rich suite of software tools aimed at the particular needs of the design and commissioning of long-baseline interferometers with complex, coupled sensing and control systems.

At the current stage of the design of the AdV detector many design options and parameters are not yet fixed. In most cases the parameters have been constrained but in some cases several very different options are still possible, for example in the case of certain RF modulations, for which the actual frequency can be defined at a later stage. Therefore, it is at the moment not possible to define *the one* (optimal) parameter set for a full numeric simulation. We instead expect a constant change and adaptation of the parameter set, for which a large number of numerical analyses should be repeatedly undertaken. For this reason a MATLAB-based set of tools (OSD_Tools) has been developed and provided to the community, which allows us to simplify the automation of numerical simulations based on text input files. This tool set has been demonstrated in [128].

5.3 Beam size and waist position in the arm cavities

The size and shape of the laser beam inside the interferometer is defined by the surface shape of the cavity mirrors; the beam sizes at the IM and EM as well as the position of the cavity waist are determined by only two parameters, the radii of curvature (ROC) of IM and EM. Since inside the two Fabry-Perot cavities of the Michelson interferometer the GW interacts with the laser light, creating signal sidebands, the two arm cavities can be seen as the heart of the AdV detector. The characteristics of the arm cavities have not only a high impact on the detector sensitivity and bandwidth, but also on the overall detector performance. Therefore a thorough design of the ROCs, taking all relevant aspects into account, is of high importance.

In order to find the optimal ROC values a trade off analysis needs to be performed taking into account the following aspects:

- Coating Brownian noise
- Clipping losses of the mirrors
- Mode-Non-Degeneracy

5.3.1 Coating Brownian noise

The power spectral density, $S_x(f)$, of the coating Brownian noise can be expressed as [126]:

$$S_x(f) = \frac{4k_B T}{\pi^2 f Y} \frac{d}{r_0^2} \left(\frac{Y'}{Y} \phi_{\parallel} + \frac{Y}{Y'} \phi_{\perp} \right) \tag{15}$$

where f is the frequency, d the total thickness of the coating, r_0 describes the beam radius, Y and Y' are the Young's Modulus values for the substrate and coating respectively. $\phi_{\parallel}$ and $\phi_{\perp}$ are the mechanical loss values for the coating for strains parallel and perpendicular to the coating surface.

As indicated by Equation 15 the amplitude spectral density of the coating Brownian noise decreases proportional to the beam radius, r_0, at the mirror. Since the contribution from the coating Brownian noise (together with the quantum noise) directly limits the AdV sensitivity in the mid-frequency range (see Figure 2), the overall detector sensitivity increases with larger beam size at the IM and EM. That is the reason for moving the cavity waist from the IM (where it is placed in initial Virgo) towards the center of the arm cavity, resulting in roughly equal beam sizes at the IM and EM.

In addition one can see from Equation 15 that the amplitude spectral density of the coating Brownian noise of a mirror is proportional to the square root of the coating thickness. Due to the fact that for the very high reflectance of the EM a thicker coating is required than for the IM, the coating noise contribution of the EM would be higher than the one of the IM (assuming identical beam sizes). However, the lowest overall coating thermal noise of all four IM and EM is obtained for equal coating noise contribution of all four mirrors. This can be achieved by positioning the cavity waist not directly in the center of the arm cavities, but slightly shifted towards the IM.

5.3.2 Clipping losses of the mirrors

As shown above the AdV sensitivity can be improved by increasing the beam size at the main test masses of the Fabry-Perot cavities. However, technical constraints, such as the actual size of the dielectric coatings or the free apertures of the reference masses limit the maximum beam size for a certain amount of tolerable clipping losses.

There are two problems connected to clipping losses: If the laser beam is too large for the mirror or its coating some light will be clipped, thus reducing the achievable power enhancement inside the interferometer. In addition if the clipped light is not properly destroyed or dumped, it might cause scattred light noise.

A detailed analysis of the maximal coating size to beam size ratio can be found in [127]. For the baseline mirror diameter of 35 cm clipping losses are going to limit the maximum beam radius at the test masses to about 5.0 to 6.5 cm.

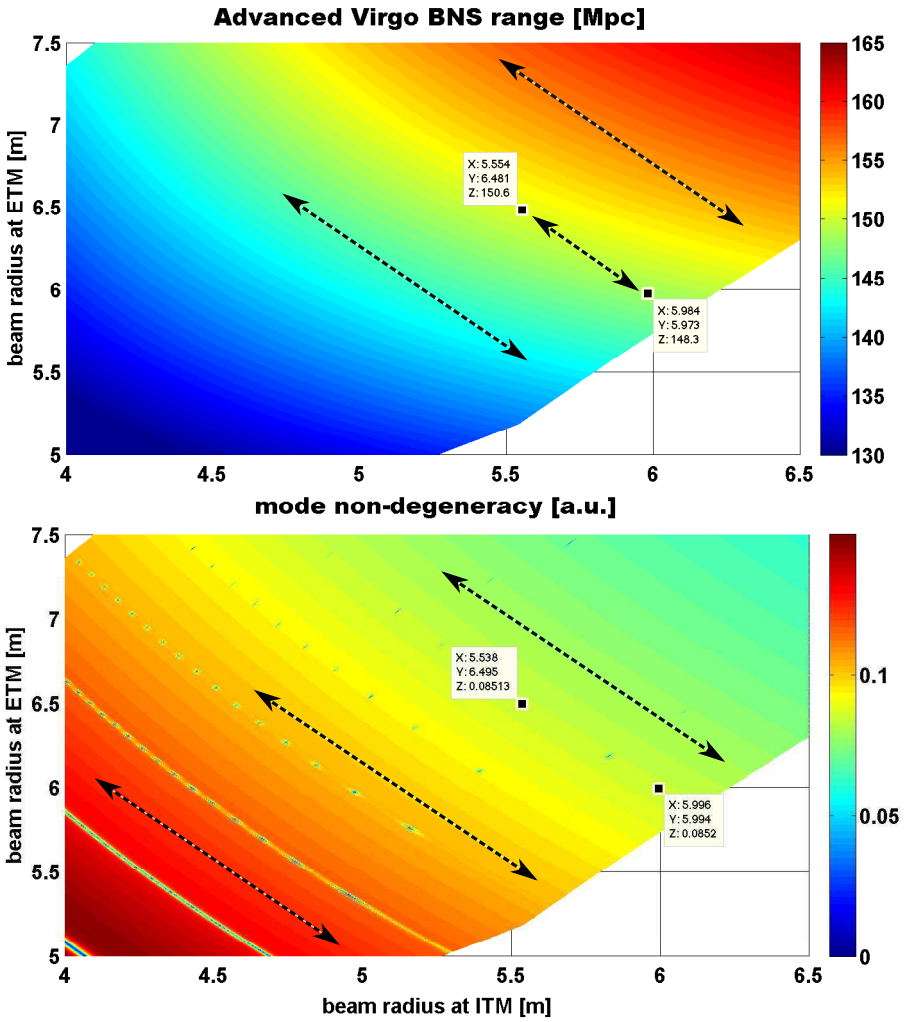

Figure 14: The lower subplot shows the mode-non-degeneracy in the arm cavities. Areas of the same color represent beam sizes combinations with identical cavity stability. As indicated by the dashed arrows one can move along a color boundary and keep the cavity stability at the same level. The upper subplot shows the achievable sensitivity, i.e. the BNS-range for AdV depending on the beam sizes. Again areas of same color indicate identical sensitivity. The orientation of the terraces for the non-degeneracy and the sensitivity is found to be different. This is why it is possible to improve the sensitivity, while keeping the cavity stability constant by following the black arrows in the upper subplot towards the upper left corner.

5.3.3 Mode-Non-Degeneracy

In order to prevent light to be scattered into higher order optical modes (HOM) it is important to choose the mirror ROCs in a way to ensure that no lower order HOM is resonant inside the arm cavities. Furthermore, considering inevitable manufacturing inaccuracies of the ROC, we have to find ROC values sufficiently separated from the resonances.

In the following we will define a figure of merit for the cavity non-degeneracy. The Gouy phase of the HOM of the order k is defined as [128]:

$$\phi_k = k\frac{1}{\pi}\arccos\sqrt{(1-\frac{L}{R_{c,i}})(1-\frac{L}{R_{c,e}})}. \tag{16}$$

with L being the length of the arm cavity and $R_{c,i}$ and $R_{c,e}$ being the radii of curvature of the input and the end mirrors, respectively. The mode-non-degeneracy for a single HOM of the order k, Ψ_k, can then be expressed as follows:

$$\Psi_k(L, R_{c,i}, R_{c,e}) = |\phi_k - \mathrm{round}(\phi_k)|. \tag{17}$$

In case Ψ_k equals zero any optical mode of the order k is degenerate with respect to the fundamental (TEM_{00}) mode. Finally in order tor provide a comprehensive figure of merit for the non-degeneracy of a cavity we have to combine the Ψ_k for all different HOM of interest. Taking into account all HOM up to the order N, we can now calculate the inverse quadratic sum of the individual $1/\Psi_k^2$ weighted by a factor $1/k!$:

$$\Theta_N(L, R_{c,i}, R_{c,e}) = \frac{1}{\sqrt{\sum_{k=1}^{N}\frac{1}{\Psi_k^2}\frac{1}{k!}}} \tag{18}$$

Θ_N can then be used as figure of merit for the non-degeneracy of the Advanced Virgo arm cavity design.

5.3.4 Trade-off of sensitivity and mode-non-degeneracy

Figure 14 shows an illustrative example of the trade off analysis required to choose the optimal beam sizes for advanced Virgo. In the upper subplot a scan of the figure of merit for the detector sensitivity, i.e. the binary neutron star inspiral (BNS) range versus the beam size at input and end mirrors is displayed. (This analysis uses the noise models described in [6] and the Signal-Recycling configuration optimized for maximum BNS range [130].) As already discussed in Equation 15 the sensitivity increases with the beam sizes. The lower subplot of Figure 14 shows a scan of the cavity non-degeneracy, Θ_{15}, including HOM of up to order 15. One can see a general tendency for decreased cavity non-degeneracy for larger beam sizes. In addition we see stripes diagonal stripes of very low non-degeneracy, especially for small beam sizes. These stripes indicate beam sizes for which one specific HOM is exactly resonant inside the arm cavities.

	input mirror	end mirror
beam radius [mm]	56	65
ROC [m]	1416	1646

Table 8: Design parameter of the AdV arm cavity geometry.

The polishing accuracy of the mirror ROC sets a lower limit to the favourable mode-non-degeneracy: We require the arm cavities to be still stable, even in the case of a relative ROC deviation of 2 %, leading to the requirement: $\Theta_{15} > 0.085$. Therefore, in terms of non-degeneracy of the arm cavities it would be optimal to go for a beam size combination indicated by the colour range from orange over yellow to light green in the lower subplot of Figure 14. For smaller beam sizes the risk of accidentally hitting the resonance of one of the lower order optical modes is too high, while for larger beam sizes the cavity is too close to instability.

However, for a specific mode-non-degeneracy it is possible to maximize the sensitivity by introducing asymmetric beam sizes at the input and end mirrors as mentioned in Section 5.3.1. Along each black dashed arrows in the lower subplot of Figure 14 the cavity non-degeneracy stays constant. Drawing arrows with identical slope into the upper subplot of Figure 14, one can see that it is possible to increase the sensitivity by moving towards the upper left corner, while keeping the mode-degeneracy at a constant level.

Using the two boundaries described above, $\Theta_{15} > 0.085$, and a maximum beam size of 6.5 cm (see Section 5.3.2) we can derive the optimal beam sizes and ROC values listed in Table 5.3.4. For these set of parameters the lowest order HOM close to resonance inside the arm cavity is of order 11 [129].

5.4 Substrate geometry of core optics

For each of the AdV core optic elements the actual substrate geometry has to be chosen. The shape of the optics rear surface and its relative alignment in respect to the front surface determines important characteristics of the optical layout. In case of parallel front and rear surfaces an etalon is formed, which can be used to tune the overall reflectance of this particular mirror. Introducing a macroscopic misalignment of the two substrate surfaces, creates a wedge, which destroys any potentially undesired etalon effect and provides secondary beams from the reflection at the rear surface.

We developed and evaluated designs for AdV using various combinations of etalons and wedges [121], which will be briefly summarized in the following sections. Recently we found, that for the design of non-degenerate recycling cavities it might be beneficial to introduce lenses into the input mirrors. The compatibility of such lenses with wedged optics is currently under investigation. The actual decision whether to use macroscopic wedges needs to be taken before ordering the mirror substrates, while the use of lenses might only need to be decided when the mirror substrates will be send to the polishing.

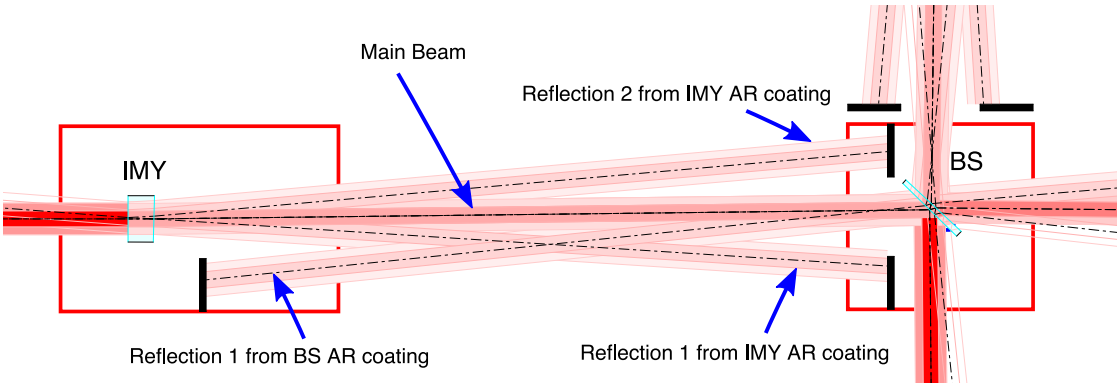

Figure 15: This CAD drawing illustrates how extra beams are generated if 'macroscopic' wedges are present in the mirror substrates. Please note that this picture shows an example layout, not the current design for AdV.

5.4.1 Wedges

There are, essentially, two motivations to have wedges on the input mirrors and the beam splitter. First of all, it is desirable to create additional pick off beams for optimization of the interferometric sensing and control scheme (see Section 11). In addition it is necessary to separate the main beam from the unavoidable secondary beams originating from the beam splitter AR coating.

Figure 15 shows an illustration of the use of macroscopic wedges in a potential AdV layout. In this configuration, wedges of 1.5 degree have been implemented into the input mirrors as well as into the beam splitter. All beams have a preserved clear aperture of 5.5 times the beam size, thus all pick-off beams can be either extracted from the tanks or properly dumped to avoid undesired interference and scattered light problems. Details of a design, requiring vacuum links of 1 m diameter between the towers of the central area (see Section 17.6.2), are available in [119].

It has to be noted that if microscopic wedges are used in the input mirrors, lateral and vertical movement of these test masses causes differential arm length noise. This noise coupling imposes a strict requirement for the seismic isolation performance for any mirror featuring a macroscopic wedge. As shown in [120] the attenuation provided by a standard Virgo superattenuator is found to be sufficient for the envisaged AdV wedge sizes.

5.4.2 Using the etalon effect

State-of-the-art coating technology produces accurate coating refelectivities, very close to the design values. However, experience from commissioning of the currently operating laser-interferometric gravitational wave detectors revealed the presence of unexpected losses inside the arm cavities, which are object of intensive investigations. Such losses, if not distributed equally, can potentially cause an imbalance of the arm cavities.

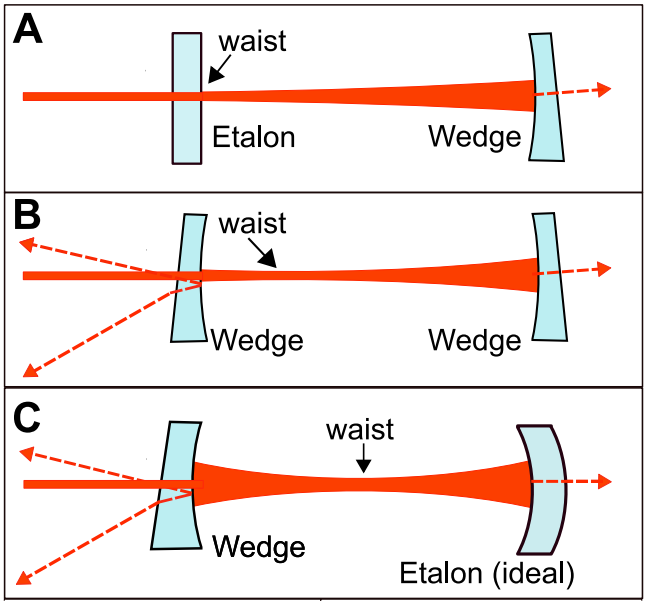

Figure 16: Arm cavity design with different combinations of wedges and etalons. A: Initial Virgo design. B: Initial LIGO configuration. C: Potential AdV design. This concept offers maximum flexibility by featuring wedges at the input mirrors and using the etalon effect in the end mirrors.

Unbalanced arm cavities (arm cavities with differing finesse and/or losses) are undesirable for the following reasons:

- Due to the different light storage times inside two arm cavities, the common mode rejection for several technical noise sources is reduced resulting in a stronger noise coupling into the gravitational wave channel [123, 124]. In particular the coupling of radiation pressure noise originating from laser intensity noise into the main interferometer output is increased.
- The dark fringe contrast is reduced resulting in an increased waste light level at the detection port and a reduced power recycling gain.

Hence, it is considered to utilise the etalon effect in one or both of the cavity mirrors in order to provide the possibility of in-situ balancing of the two arm cavities. This might significantly reduce the technical problems listed above and therefore speed up the commissioning of AdV.

A potential AdV arm cavity design was developed, providing pick-off beams from the wedged input mirrors and using the etalon effect in the end mirrors to provide the possibility of balancing the arm cavities (see Figure 16C). A full evaluation of the influence of etalon imperfections onto the overall AdV performance, as well as of potential noise couplings has been carried out [121]. Numerical simulations were used to derive requirements for the manufacturing accuracy of an end mirror etalon for AdV. Furthermore, analytical approximations have been derived for the achievable tuning range of an imperfect etalon

depending on the curvature and orientation mismatch of the two etalon surfaces. It was found that displacement noise originating from temperature driven optical phase noise of the etalon will not be limiting the AdV sensitivity [122]. In addition the influence of the etalon effect onto the AdV alignment sensing and control system has been analysed and was found to be negligible [125].

Therefore the use of the etalon effect for in-situ balancing of the arm cavities can be considered as a fully evaluated option for AdV.

5.5 Arm cavity finesse

The power enhancement inside the arm cavities is determined by their finesse, i.e. the refelctivities of the cavity mirrors and the round-trip losses inside the arm cavity. The advantage of using a high finesse for the AdV arm cavities is a reduced coupling of several noise sources, originating from within the small Michelson interferometer, to the GW channel. On the other hand, high finesse arm cavities require extremely low round-trip losses.

The current baseline value for the AdV arm cavity finesse is 885, assuming scattering losses of 37.5 ppm per mirror surface. At the moment it is not guaranteed that such low scattering losses can be achieved in a reliable and reproducible way (see Section 5.8.1). However, the fact that the final arm cavity finesse only needs to be decided when the polished mirrors are send to be coated, gives us the chance to reevaluate the optimal arm cavity finesse for AdV, taking into account the most recent results of mirror roughness analyses from within the Virgo and also LIGO collaboration.

5.6 Signal Recycling

The term Signal Recycling [138] (SR) refers generally to a Michelson interferometer with a semi-transparent mirror in the asymmetric port. It has been developed and demonstrated over more then ten years from table-top experiments, via implementations on prototypes [137] to being used routinely in the GEO 600 detector today [136]. The main aim of Signal-Recycling is to increase the signal-to-quantum-noise ratio of the detector. Depending on the arm cavity finesse, Signal Recycling comes in two different flavours. If the arm cavities have a low finesse, Signal Recycling can be used to further *decrease* the detector bandwidth to increase the peak sensitivity. This represents to ordinal Signal Recycling configuration. Instead the arm cavities can be designed to have a very high finesse and then the Signal Recycling cavity can be tuned differently in order to *increase* the detector bandwidth again. The latter configuration is often called *resonant sideband extraction* (RSE) and represent the setup chosen for Advanced Virgo.

Figure 17 shows the effect of the Signal Recycling mirror (SRM) on the quantum-noise limited sensitivity of Advanced Virgo for various parameter options. The top plot illustrates how a low transmittance of the SRM can be used to increase the peak sensitivity

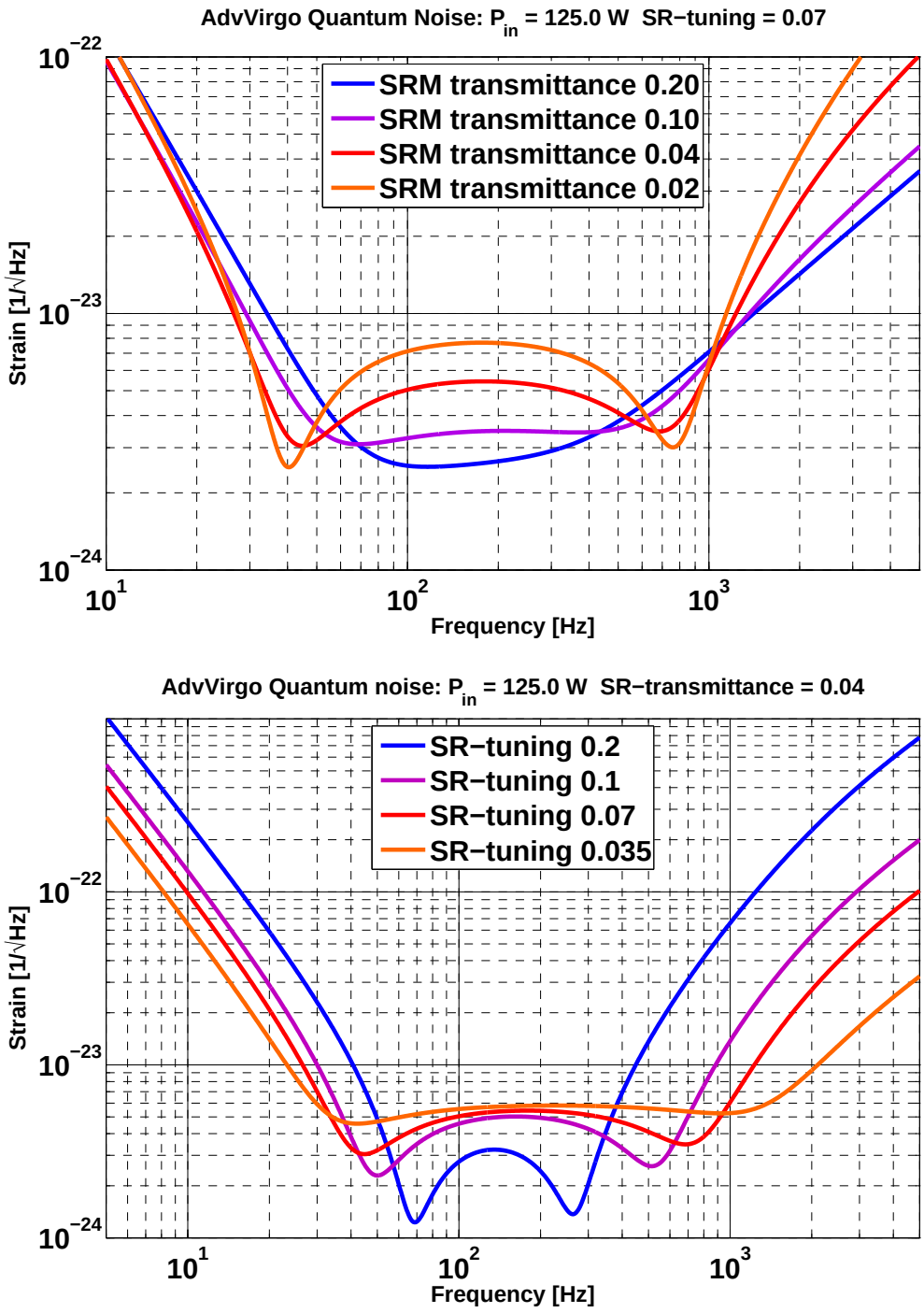

Figure 17: The two plots illustrate the impact of the two Signal-Recycling parameters, *transmittance* and *tuning* of the Signal-Recycling mirror, on the Advanced Virgo quantum noise. This shows that the exact change of the quantum noise is complex, mostly due to the optical-spring effect. However, the first order effects are that the transmittance changes the finesse of the SRC and thus the bandwidth of the detector, whereas the tuning changes the center frequency of the SRC and thus the frequency of the peak sensitivity of the detector.

by reducing the bandwidth. The lower plot shows, how the quantum-noise limited sensitivity changes shape when the SRM tuning is changed. The tuning can be easily changed during operation.

The Virgo vacuum system already includes a vacuum tank for the Signal Recycling mirror. The main challenge of Signal Recycling is the more complex control system (see Section 11). Not only does it add three new degrees of freedom (1 longitudinal and 2 alignment) but it forms a very complex split, coupled four-mirror cavity with the Power-Recycling mirror and the arm cavity input mirrors and in consequence the control signals for these mirrors can become more strongly coupled.

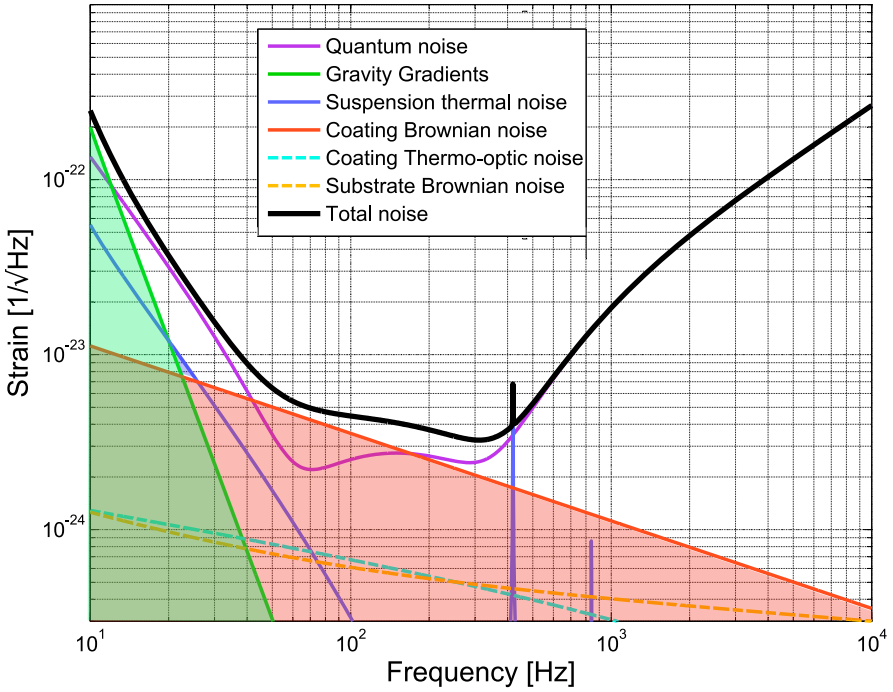

Figure 18: Fundamental noise contributions to the Advanced Virgo sensitivity. The pink trace indicates the quantum noise for one specific set of Signal Recycling parameters. It is possible to optimise the Advanced Virgo sensitivity for different figures of merit (such as BNS range), by changing the Signal Recycling detuning and the Signal Recycling mirror transmittance. The coloured areas indicate regions which are not accessible via any Signal Recycling optimisation because they are buried by other fundamental noise sources.

5.6.1 Optimisation of the Signal Recycling parameter

As shown in Figure 17, the shape as well as the level of the quantum noise varies strongly with the actual Signal Recycling parameter. Therefore, the variation of the two Signal Recycling parameter (together with the circulating optical power) offers the possibility to

optimise the Advanced Virgo sensitivity for different figures of merit, such as the binary neutron star (BNS) inspiral range.

The sensitivity range available by such an optimisation is shown in Figure 18. At low frequencies the boundary is given by the level of gravity gradient noise, while in the mid and high frequency range coating Brownian noise restricts the achievable sensitivity.

Automated optimisation routines have been developed, basing on OSD-tools [128], [131] and a GWINC model of Advanced Virgo [6]. These software routines can be used for multi-parameter optimisation (Signal Recycling tuning, Signal Recycling mirror transmittance and circulating optical power) of the Advanced Virgo sensitivity for any desired figure of merit. The detector configuration optimised for binary neutron star inspiral range [130] was chosen to be the Advanced Virgo reference configuration (see Figure 2) featuring a Signal Recycling detuning of 0.15 rad and a Signal Recycling mirror transmittance of 11 %.

5.7 Non-degenerate recycling cavities

One of the major evolutionary step during the development of the optical layout of AdV was the inclusion of non-degenerate (or stable) recycling cavities. This is also a major difference with respect to initial Virgo and initial LIGO, which have a marginally stable (or degenerate) power recycling cavity.

A Fabry-Perot cavity is stable when the transversal mode spacing is much larger than the linewidth of the cavity itself. In these kind of cavities the high-order modes cannot simultaneously build-up when the fundamental mode is resonant. On the contrary, in a degenerate cavity, the optical power is easily transferred from the fundamental mode to the higher-order modes in presence of misalignments, thermal deformation of the mirrors or any other defects in the mirror geometry.

Deformations of the RF sidebands inside the power recycling cavity have been widely observed in initial Virgo and LIGO [133] and this has been one of the main problems encountered during the commissioning of the two detectors. Due to these deformations, the LIGO wavefront sensors, used for the global alignment of the interferometer, were not correctly working without a thermal compensation system. Furthermore, a reduction of the RF sidebands recycling gain was observed. A similar decrease of the recycling gain and an unbalancing between the upper and lower sidebands have been observed in Virgo. The impact on the interferometer sensitivity was in this case very limited due to the presence of the output mode-cleaner, but the establishment of a robust lock acquisition procedure and of a global alignment strategy took very long.

Even though the AdV baseline features a DC-detection scheme for the gravitational wave readout (or the differential mode of the arms), the RF sidebands are still necessary for both the control of the four longitudinal auxiliary degrees of freedom, and for the angular control.

During the Virgo commissioning big difficulties were experienced also in tuning the longitudinal control, even with a 'cold' interferometer, i.e. while the thermal effects in the optics could be neglected. A strong sensitivity of the longitudinal error signals to the alignment conditions of the interferometer was observed as well as offsets, change in the demodulation phases and a general mismatch of the measured sensing matrix with analytical or numerical models. Even today these effects are not completely understood, however, the negative impact of the marginally stable geometry of the recycling cavity seems very likely. Simulations are on-going to fit the experienced problems during the Virgo commissioning to numerical models.

The necessity to have an 'easy' and fast way to simulate the interferometer behaviour and the control systems in the presence of small defects is another point in favour of the non-degenerate cavities. In fact the simulation of a beam resonating in a marginally stable cavity needs more complex tools (modal expansion with many modes or a Fast Fourier Transform code) with respect to a stable cavity. Rapid progress during commissioning or fault mitigation relies heavily on a fast responses from the simulation group. Modelling of the full detector has so far only been achieved with models using modal expansions with only a few modes.

The arguments presented above ordinate from the experience with the Power-Recycling of the Virgo detector and apply directly to a design of a Power-Recycling cavity in AdV. In addition, D'Ambrosio [93] and successively Pan [94] have shown that a marginally-stable Signal recycling cavity can cause a significant signal loss. For example, if the signal to noise ratio of Advanced LIGO should not be reduced by more than the 1 percent due to mode mixing, the peak-to-valley surface distortion of the mirrors (in their central region) in the SRC must be less then 1 to 2 nm. This would translate into very stringent requirements for the optical surfaces and the thermal compensation system.

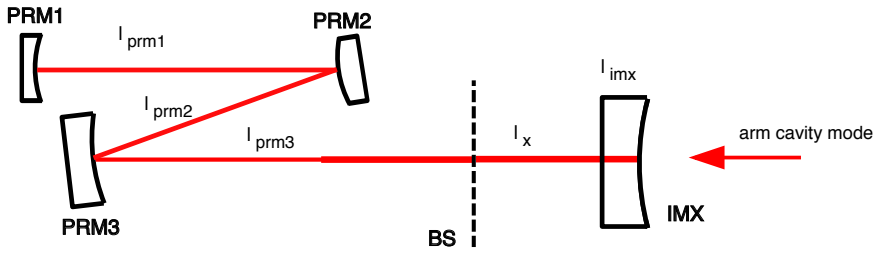

Figure 19: Simplified layout for a non-degenerate power recycling cavity, following the Advanced LIGO design. IMX represents the X-arm cavity input mirror, PRM1 is the power recycling mirror and PRM2 and PRM3 are turning mirrors that act as a kind of mode-matching telescope. PRM1 and PRM3 would be located inside the injection tower, PRM3 in the power recycling tank. The front face of IMX is shown to be flat in this picture, for the solution including a lens in the input test masses, this surface would be curved to create the lens effect.

Design Procedure We have prepared the first draft design for a non-degenerate Power-Recycling cavity. The design closely follows the concept from Advanced LIGO [134] which results in an optical layout which can be easily adapted for changes in specifications by small changes to the recycling mirrors. Therefore in adapting the Advanced LIGO concept for AdV we have established a well-understood design process which can now universally applied during the down-selection of possible options.

In the following we describe the draft optical layout for the Advanced Virgo Power-Recycling cavity (PRC). The main aim of the non-degenerate cavity design is to have a specific non-zero Gouy phase. Typically this can be obtained if the length of the cavity is larger than the Rayleigh length. Since the Rayleigh range of the beam inside the arm cavities is several hundred metres, while the lengths of the recycling cavities is only several metres, any optical design for a non-degenerate cavities should try to increase the length of the respective cavity as much as possible and use focusing elements to reduce the Rayleigh length of the beam. Figure 19 shows a simplified layout of a non-degenerate PRC. We have performed the analysis with the X-arm only, ignoring the presence of the beam splitter substrate. In practice then IMX represents both input test masses and lx is the common small Michelson length $(lx + ly)/2$. The design should recreate the following features of the Advanced LIGO design:

1. the PRC should have a single trip Gouy phase of 160 deg
2. a beam waist is located between PRM1 and PRM2
3. the beam size at PRM1 is reasonably large

The distances between the PRM mirrors are largely defined by the location of the vacuum tanks. Therefore the length of the PRC cannot be increased except for folding them beam. Nevertheless, the Rayleigh range of the beam must be reduced to less than the typical distance between the cavity optics (≈ 5 m). The Rayleigh range is defined as:

$$z_{\mathrm{R}} = \frac{\pi w_0^2}{\lambda} \tag{19}$$

With $\lambda = 1064$ nm we require a beam waist, w_0, of about 1 millimeter size (or smaller), which in turn demands at least one strong focusing element in the PRC.

The second requirement from the list above, then leads to the layout as shown in Figure 19: PRM3 is used as the main focusing element and PRM2 is used as a defocussing element which can be utilized to fine tune the parameters of the waist in between PRM2 and PRM1 (i.e. to fulfil requirement number three from the list above). If the curvatures of IMX, PRM3 and PRM2 are set, the curvature of PRM1 follows automatically from the fact that the cavity must have a stable eigenmode.

The main difference between the AdV setup and the current Advanced LIGO design is that Advanced LIGO features a PRC of approximately 50 m length (single trip) whereas the Virgo vacuum system limits the length for AdV to 25 m. To compensate for that, the design presented here features lenses in the input test masses (i.e. curved AR coated surfaces). Figure 20 explores the parameter space of radii of curvature of PRM2 and

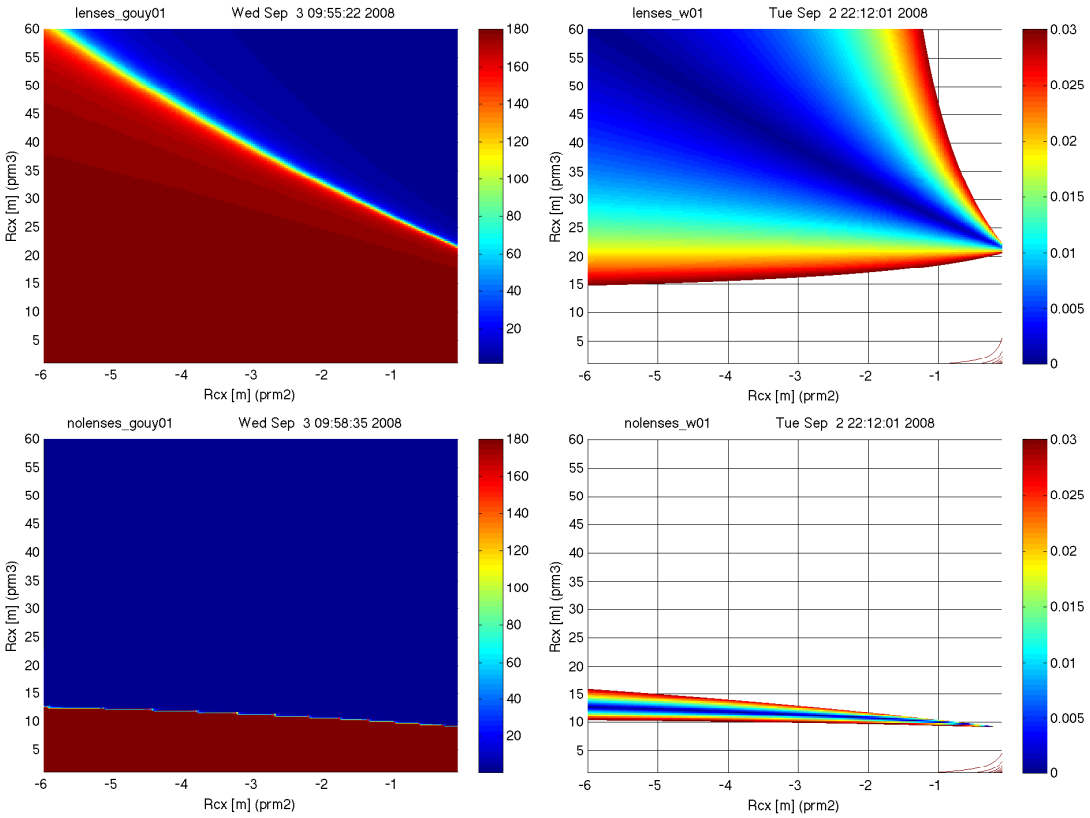

Figure 20: The two upper plots depict two parameters of a non-degenerate PRC when the input test masses feature a lens of $R_{\mathrm{C,IMXAR}} = 10.5\,\mathrm{m}$. The left plot shows the single trip Gouy phase as the function of the radius of curvature of PRM2 and PRM3. The right plot shows the beam size on PRM1 in the same parameter space (the color scale is in meters). The two lower plots show the same data for a design in which the input test masses have a flat secondary surface.

PRM3. The two lower plots refer to a design without lenses in the input test masses and one can see that the useful parameter space is confined to a very narrow, almost one-dimensional region. The purpose of a lens inside the input mirror substrates would be to reduce the beam size on PRM3 and thus loosen the requirements for the curvatures of PRM3 and PRM2. This effect can observed in the upper plots of Figure 20.

However this option features several disadvantages, most notably a larger astigmatism of the laser beam in the recycling cavities and more stronger constraints on the use of wedges in the core optics (see Section 5.4).

Draft design and further steps Following the Advanced LIGO design concept we have developed a set of tools to adapt this concept to AdV recycling cavities. We further have provided a draft design for the Power-Recycling cavity [135]. For the calculations an arm

cavity mode with Gaussian beam parameter $q = 1400 + i275.838$ was used. The core parameters of this design are the radii of curvatures of the mirrors:

component	IMX (AR)	PRM3	PRM2	PRM1
R_c [m]	10.5	30	-1.849	2.118

The corresponding beam parameters inside the Power-Recycling cavity are:

	IMX (AR)	BS	PRM3	PRM2	PRM1
w [mm]:	50	38.5	16.5	2.17	1.77
w_0 [mm]:	0.162	0.162	0.106	0.395	0.395
z [m]:	-23.9	-18.4	-5.18	-2.49	-2.01
R_c [m]:	-23.9	-18.4	-5.18	-2.57	-2.12

The columns refer to optical surfaces inside the PRC and the rows to parameters of the beam, with w refers beam size on the respective component; w_0 and z give the beam parameters for each beam segment in the form of waist size and position; R_c is the radius of curvature of the beam's phase front. These parameters refer to the beam *leaving* the respective component. This design provides a single-trip Gouy phase of 160 degrees. The relative distances between the objects are:

	l_{prm1}	l_{prm2}	l_{prm3}	l_{x}	l_{imx}
length [m]	4.5	4.5	10.5	5.5	0.1

This results in a cavity length[6] of $L_{\mathrm{prc}} = 25.2\,\mathrm{m}$. The lengths used in this design put the optics into the existing vacuum enclosure but require a major redesign of the injection and detection bench because each of these would now need to accommodate two mirrors from the respective recycling cavity.

The draft design further includes lenses in the input test masses and thus manages to gives values for the beam sizes and curvatures very similar to the Advanced LIGO case. Further development of this design will focus on the feasibility of lenses in the input test masses, possible astigmatism in the off-axis telescopes and on finding the optimal Gouy phase for the Power- and Signal-Recycling cavities. Particular emphasis will be given to the interfaces of the core interferometer to the injection subsystem (see Section 7) and the detection subsystem (see Section 10).

5.8 R+D programs related to the optical design

5.8.1 Optical losses due to surface defects

Mirror losses (see also Section 8) are dominated by the scattering of the optical beam from the TEM_{00} mode towards higher order modes. The analysis of available polished surfaces shows that the spectral density of the surface defects is usually regular and decreases

[6] Please note that for compatibility with RF modulation frequencies the power recycling length must be adjusted to be close to 24 m. However, this has only a small influence on the cavity parameters presented here. The exact cavity length and the exact radii of curvatures will be determined at a later stage.

towards high spatial frequencies. Typically, the surface roughness is of the order of a few nanometers at the 10 cm scale, and of an Angstrom or less at the scale of 100 μm (superpolish).

The simulations with DarkF show that the simple classical formula

$$l = \left(\frac{2\pi\delta x}{\lambda}\right)^2, \tag{20}$$

which expresses the loss, l, as a function of the RMS surface roughness (integrated over the beam area), δx, and of the wavelength λ, is roughly valid in that case. The requirement that the loss per mirror be less than 37 ppm (for the AdV IM and EM) implies that the RMS polishing error should be less than 1 nm ($\lambda/1000$), over a diameter of 20 cm. This is at the extreme limit of the capacity of classical polishing techniques. The surface metrology itself is not always available at this level of precision: on a small area, the sensitivity of the interferometers is sufficient, but the precision of the measurements is limited by the 'stiching' technique used to reconstruct the full mirror surface, and by the precision of the reference 'flats'. To reach the goal, there are different complementary possibilities, but some R+D remains necessary.

- After the classical steps of polishing, some of the advanced polishing companies are now able to improve the mirror flatness by removing excess material from the surface with an ion beam. We would have to check that this does not degrade too much the subsurface, does not create local defects or surface pollution, and maintains the superpolish.
- Another possibility, already demonstrated at LMA, consists in 'filling the holes' by depositing silica, instead of erasing the bumps. We call this technique 'corrective coating'. The present R+D on that subject consists in designing an appropriate robot, able to handle heavy mirrors (up to 42 kg) with enough speed and accuracy. This study is realized in collaboration with LAPP.
- Up to now, corrective coating has been performed only on relatively small areas (a few cm in diameter). The RMS deviation of the corrected surface is good enough, but its spectral density shows a slight pixelisation related to the geometry and the motion of the robot. To evaluate its effect and specify the new robot, it is useful to run optical simulations with larger 'synthetic' mirror maps, obtained by extrapolation of the existing small ones. This effort has started in Lyon and Nice.
- The metrology and particularly the stitching technique also need to be improved in Lyon: since the precision of the stitching seems to be presently limited by the mirror vibrations, the main efforts will consist in improving the mirror supports and their seismic and acoustic isolation.

5.8.2 Higher-Order Laguerre Modes

The intensity profile of the beam in the arm cavities determines how much of the thermal noise of the optics is coupled into optical phase noise, i.e. differential arm length noise.

It has been shown [139] that using higher-order Laguerre-Gauss modes could reduce the effects of thermal noise (and other thermal phenomena) in comparison to the standard interferometer using a lowest-order Gaussian beam. R+D programs in Birmingham, Artemis Nice and APC Paris have been started to investigate the possibility to use higher-order Laguerre-Gauss modes (HOLMs) in AdV after a certain period of running in the baseline configuration using the TEM_{00} mode. This section describes the status of the respective R+D program related.

Flat beams or higher-order Laguerre-Gauss modes The motivation for using alternative beam shapes is to lower the limiting thermal noise in the region around 100 Hz due to a wider intensity distribution over the mirror surface. The thermal noise can be significantly reduced using flat top beams or HOLMs compared to the currently used fundamental TEM_{00} mode. The thermal noise reduction factors for different mode shapes are given in Table 9. The advantage of the HOLMs is that they offer larger improvements of the coating thermal and substrate thermal noise compared to the flat top beams. Furthermore the HOLMs are fully compatible with spherical mirror curvatures as they are currently used in all detectors, whereas flat top beams need specially shaped so called *mexican hat* mirrors [140].

Thermal noise reduction factors	TEM_{00}	LG_{33}	LG_{55}	Flat top beam
Coating thermal noise	1	2.2	2.3	1.5
Substrate thermal noise	1	2.7	2.7	1.8
Thermo elastic noise	1	0.6	0.4	1.8

Table 9: Comparison of the expected thermal noise reduction factors for different modes [141].

Length and Alignment sensing Laguerre-Gauss modes can be used with standard spherical optics and thus are compatible with traditional interferometer designs. However, little work had been published regarding the performance of HOLMs in high precision length sensing and control systems. The length and alignment sensing using HOLMs has been analysed theoretically and compared to the performance of a TEM_{00} mode in [142]. The outcome of this analysis shows that HOLMs perform even better than the fundamental TEM_{00} mode. For example, the coupling of a differential misalignment of the arm cavities into dark port power is suppressed by a factor of approximately two by using a LG_{33} mode compared to the TEM_{00}.

Beam parameter comparison Higher-order Laguerre-Gauss modes of a given beam parameter have a larger intensity distribution than the fundamental TEM_{00} mode of the parameter. In practise the beam size is limited by clipping losses at the mirror edge. Typically we chose the beam parameters so as to keep the clipping losses at constant level of e.g. 1 ppm (see figure 21). Therefore, in order to change an optical layout from

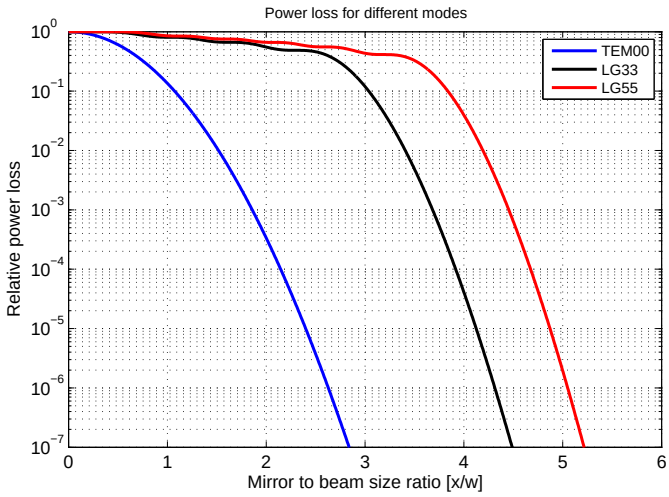

Figure 21: Power loss occurring on a mirror for different modes of the same beam parameter. This plot can be used to determine the scaling factor for the mirror or the beam size when changing the design from one mode to the other.

the fundamental mode to higher-order modes the beam parameter has to be reduced or the mirror must be enlarged. The corresponding scaling factors for the LG_{33} and LG_{55} in comparison to the TEM_{00} mode are given in Table 10. Hence, instead of using a TEM_{00} mode with a beam width of $w = w_{00}$ in the detector, we have to use a smaller beam size of $w = 0.64\, w_{00}$ in case of a LG_{33} instead. Please note that the beam parameter of the cavity mode is defined by the radii of curvature of the mirrors. Thus, if the beam parameters are changed in the design, mirrors of the same size but with a different radius of curvature are required.

Scaling factors	TEM_{00}	LG_{33}	LG_{55}
Mirror size	1	1.64	1.92
Beam size	1	0.61	0.52

Table 10: Scaling factors for mirror size and beam size for different mode shapes to keep the clipping loss constant.

Expected improvements in Inspiral ranges Because of the lower thermal noise contribution by using HOLMs we can expect an increased sensitivity which is reflected e.g. in increased inspiral rages. In [141] three different scenarios have been presented. Each scenario compares an interferometer configuration using a TEM_{00} mode with one using LG_{33} mode. The scenarios investigate the performance for the two modes, when a) the same mirrors are used, b) optimised mirrors are used for each mode and c) when thermal compensation is used to 'optimise' the mirrors for the respective mode. For each configuration the existing BENCH/GWINC model of AdV was used to calculate the expected sensitivity from which the inspiral ranges are derived automatically. In summary the

inspiral ranges of the configurations using the LG_{33} mode was always better, providing improvements (depending on the actual type of the binary) of 17%–32%.

Thermal distortion The temperature gradients due to absorption of laser light cause distortions of the substrate changing the radius of curvature of the reflecting surface. The calculations have been made in [102]. This effect directly affects the field inside the cavity (also the RF sidebands circulating in the central interferometer). Using flat beams or HOLMs significantly reduces this effect. For comparison, in initial Virgo the effect changes the radius of curvature of the input mirrors by 22 km·W, while we the corresponding numbers for flat beams (324 km·W) and for example the LG55 mode (937 km·W) are much better.

Mode generation Exotic modes are used in various different areas of physics. The favoured HOLMs are e.g. often used in cold atom optics as light guides or in optical traps. There exists different techniques to transform a TEM_{00} into a HOLM e.g. holograms [143], diffractive gratings [144] or a combination of phase plates and a cylindrical lens converter [145]. Currently the Virgo R&D program has a pending project which proposes to generate HOLMs with high efficiency but moreover high quality. The intention of the project is to perform the needed development of a mode converter for the generation of HOLMs and to verify the theoretical analyses experimentally to enable the later application of HOLMs in AdV and future projects.

Conclusion and consequences The theoretical analyses performed till this day conclude that HOLMs are extremely appealing. Their property to be fully compatible with spherical mirrors and commonly used auxiliary optical components makes their implementation relatively simple. Furthermore the reduced thermal noise and thermal distortions result in much better sensitivity of the detector. The expected increase in the inspiral ranges by 17%–32% is highly attractive. Future work must focus on the experimental verification of the results obtained from the theoretical analyses.

6 Pre-stabilized laser

6.1 Overview

The Pre-Stabilized Laser (PSL) system will deliver 200 W. It will be pre-stabilized in frequency and amplitude to bring down the noise of the laser to the level required at the entrance of the suspended Input Mode Cleaner (IMC), and should respect a set of requirements concerning beam geometry and beam jitter.

The system consists of the following elements:

- the high power laser including the power supplies for pumping diodes, the cooling system and the injection locking optics and electronics;
- the frequency pre-stabilization loop locking the laser frequency on the suspended input mode cleaner (IMC), and the fast photodiode utilized in that loop;
- a triangular pre-mode-cleaner (PMC) for spatial and frequency filtering of the beam, housed in a vacuum vessel to avoid acoustic noise and mirrors contamination, and its control optics and electronics;
- the power stabilization of the laser with a control loop utilizing a special photodiode (100mA standing current and good uniformity) mounted after the input mode cleaner and on a seismically isolated table under vacuum;
- the positioning of the electro-optics modulators (EOM) and Faraday isolators (FI) used between the Master laser and the high power amplifiers or injection-locked lasers;
- the design of the External Input Bench (EIB) will be shared with INJ system, for matching and steering optics used by both systems.

The PSL system does not include the optics and mechanics of the IMC.

6.1.1 PSL location

As with the initial Virgo, the PSL will be located in the Laser Lab that houses the laser bench and the EIB shared with the Input Optics system. The Laser Lab needs to be a class 1000 clean room to ensure dust free and clean conditions with a temperature regulated to better than 0.5 °C for stable environment. The external detectors table will be arranged and specified once the layout of the Injection bench (and the Input Mode Cleaner) will be done. The high power laser will be enclosed in a sound proof enclosure as it has been done for the initial Virgo, because the laser frequency and the beam jitter have been found to be very sensitive to local acoustic noise. The electronics racks will be placed inside the Laser Lab following the requirements of noise and bandwidth of the lasers controls. The chillers of the laser system which are noisy will be located in a separate room behind the Laser Lab.

6.1.2 Interface with the other subsystems

The PSL subsystem will interface with other systems for:

- the high power (HP) standing EOM and FI tested by the INJ subsystem and the position of power stab photodiode on injection bench;
- the monitoring issues, by DAQ subsystem;
- the sound proof enclosure and the maintenance of laser Lab cleanliness, by IME subsystem;
- the HP standing mirrors realization, by MIR subystem;
- the vacuum tests of PMC, by VAC subsystem.

6.2 Baseline optical layout

The optical layout of the PSL has the following major components: the HP laser, a frequency stabilization path taking the reflected signal from the suspended IMC, the power stabilization loop including the special photodiode sitting under vacuum, the PMC to filter out high order modes of the HP stage. The HP laser will consist of the master 2W NPRO laser and two injection-locked stages of 20W and 200W. An EOM is placed downstream of the master laser to provide a set of modulation sidebands required to produce error signals for control loops of injection locking and PMC length stabilization.

6.2.1 The AdV laser

To reach 200W output power in single frequency operation, the HP laser consists of a stable low power master laser which transfers its stability to one or two higher power laser by amplification or injection locking. A choice between one case or the other could be made for each couple master-HP lasers. The HP stages baseline solution will consist of two Nd:YVO4 oscillators, a medium stage of 20W and a HP stage of 200 W. In the case of injection locking, the stability requirements of the resonator are given by the locking range of the oscillator which is function of the ratio of resonator internal power and the power injected into the laser oscillator:

$$\Delta\nu_{\mathrm{inj}} = \frac{\gamma_{\mathrm{osc}}}{\pi}\sqrt{\frac{P_m}{P_s}} \tag{21}$$

where γ_{osc} is the cavity decay rate, P_m is the injected master power and P_s in the HP oscillator power. To increase the locking range, the ratio of the HP to the master powers should be kept low, requiring then a double-stage injected lasers while Pound-Drever-Hall locking scheme help stabilizing the oscillator resonator for each stage by increasing the gain of the injection process. The frequency noise of the slave laser is then governed by the master laser well below the locking range and dominated by the slave noise at frequencies higher than the locking range. Another possibility is to use a scheme with

only one stage of injection locked oscillator of 180-200 W with a power ratio of the order of 100 between the slave and the master. A trade-off between the laser noise and the number of HP stages has to be found. HP Fiber amplifiers have encountered a dramatic progress recently, and a possible option would be their use for the HP stage as amplifiers.

6.2.2 The Master laser

The master laser is a monolithic stable structure which reliability and reproducibility have been largely demonstrated in the initial Virgo or LIGO. It is a commercial NPRO laser produced by Innolight, Hannover, the maintenance and follow-up of this laser are definitely ensured. The output power we need for AdV is 800 mW, the same as initial Virgo, in the case we keep the 20W Nd:YVO4 as intermediate medium power stage. In this case, there is no additional work for its study. In the alternate solution where we can simplify to keep only one HP stage, the output power needs to be around 2W, and we need to perform some measurements on it or rely on the tests done by the LSC collaboration.

6.2.3 The Medium power stage

The medium stage for the AdV Laser (fig. 22) is based on the 20W laser used for the initial Virgo (LZH design). It is a ring resonator in bow-tie configuration and involves two conductively cooled Nd:YVO4 crystals, each being longitudinally pumped by a fiber coupled laser diode at a rate of $< 60\%$ output power . Temperature stabilization of the laser crystals and the pump diodes is performed by computer-based PID controllers. The employment of a low thermal expansion steel for the resonator block in combination with the negation of adjustable resonator components results in a high intrinsic stability and a reduced acoustic sensitivity of the slave oscillator. The resonator is equipped with three transducers to control its length: one piezo-electric transducer (PZT) with large dynamic, one fast PZT with small dynamical range and one thermally controlled mounting). It is injection-locked to the output radiation of the 800 mW power of the Master laser and a Pound-Drever-Hall control loop acts on these three transducers to increase the gain of the injection locking process in the servo-loop bandwidth.

6.2.4 High power stage

The 200W HP stage is based on the (proven) design adopted for Advanced LIGO; it is a ring resonator with four pumped Nd:YVO4 heads combined in a birefringence compensation scheme. This configuration (see fig. 23) is different from the 60W amplifier provided by LZH for Virgo+ but the thermal management of the crystals are the same. Thermally induced mechanical stress results in stress induced birefringence and causes depolarization, bifocusing: this stress can be compensated by involving two identically pumped rod's and a 90° quartz rotator. A relay optic consisting of two identical lenses images the principal planes of the rods onto each other while keeping the laser field unmodified. Therefore a nearly perfect birefringence compensation can be achieved. In the

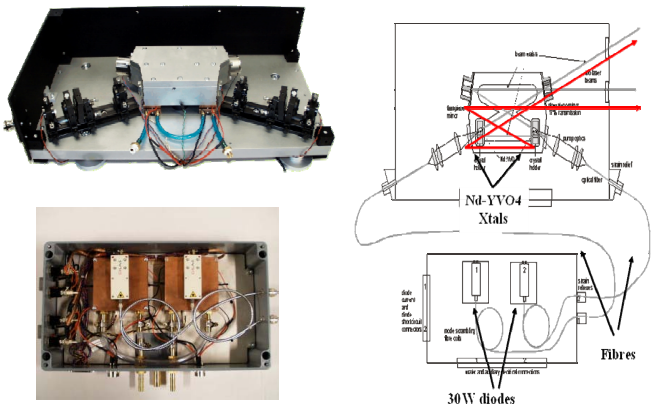

Figure 22: Medium power stage of 20W in bow-tie configuration.

laser tested so far by LIGO, two birefringence compensated pairs are formed to a ring square resonator design.

A three lens optic images the end surface of the homogenizer into the laser crystal (see fig. 23). The laser crystal consists of a 3 mm diameter multi-segmented Nd:YAG rod with two 7 mm long undoped segments at both ends and a 40 mm long low-doped center segment. The undoped end caps reduce the thermally induced mechanical stress on the end surfaces of the rod and eliminate any mechanical deformation of the ends. Further on, the complete doped region of the rod can be effectively cooled, which is essential for the end-pumped geometry in connection with direct water cooling. During propagation, the pump light is mixed and guided by total internal reflection at the rod surface. The crystal involves a double pass for the pump light in order to reduce the longitudinal thermal gradient and reduce the overall mechanical length.

6.3 Control strategy

Fig. 24 shows the control scheme for the AdV PSL. The set of requirements given below is based on our experience of Virgo extrapolated to the goal sensitivity of AdV as well as the data taken from the documents of Advanced LIGO, since the design and performances of both detectors will be comparable. The definition of the final requirements will need more calculations and modeling studies, taking into account the design changes. For instance, the following numbers assume the same filtering of the IMC as for Virgo and the same prestabilization scheme (i.e. a laser prestabilized on the IMC and a power stabilization

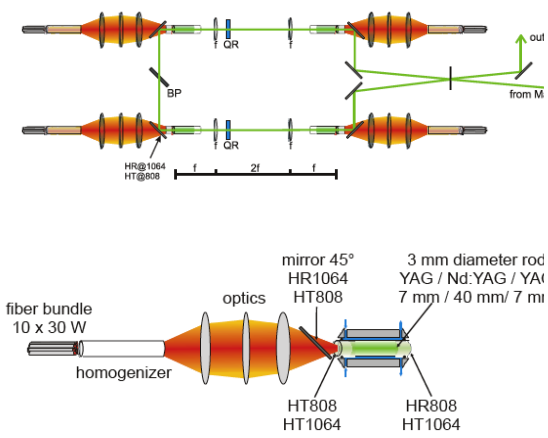

Figure 23: TOP: schematic layout of the Advanced LIGO HP stage. BOTTOM: schematic layout of an end-pumped laser head designed by GEO-LZH

performed after the IMC). They also assume that the contrast and asymmetries of the interferometer, and the precision of alignment and longitudinal controls, will remain the same as they are in Virgo, and that the OMC (output mode cleaner) is unchanged. The possible change to the DC detection might relax some constraints in RF range compared to Virgo while needing some relevant effort in the low frequency range.

6.4 Requirements

Requirement	**Value**
Power	200 W
Frequency noise	$LSD(f) < 10/f$ Hz/$\sqrt{\text{Hz}}$ above 10 Hz
Power noise	$RIN(f) < -170$ dB/$\sqrt{\text{Hz}}$ (for 10 Hz$< f <$10 kHz)
Beam jitter	$< 10^{-6}$ rad/$\sqrt{\text{Hz}}$
Beam geometry	$M^2 < 1.05$ (h.o.m. content $< 5\%$)

Notice that:

- the frequency noise figure referes to the prestabilized laser at the entrance of IMC and will be refined as part of the first deliverable of the Interferometer Sensing Control system (ISC);
- since AdV will use a DC detection scheme, the laser power noise at RF frequency will not be significant. Instead, if RF detection is used, the requirement will be $RIN(f_{\text{mod}}) < -185$ dB/$\sqrt{\text{Hz}}$ (shot noise for 1W detected power);

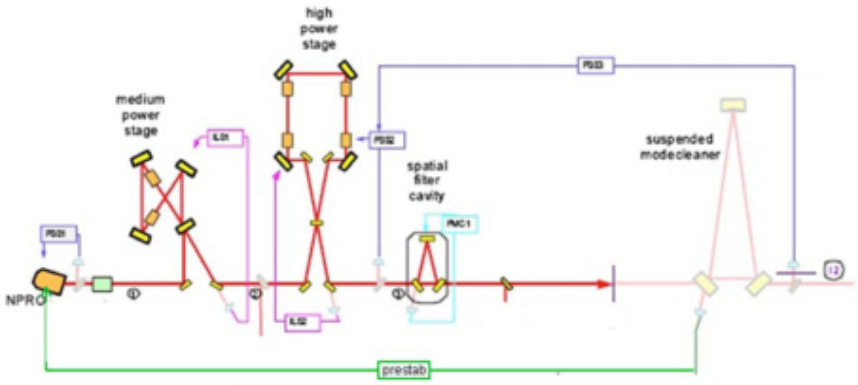

Figure 24: A schematic of the optical layout and control strategy for the AdV PSL.

6.4.1 Frequency pre-stabilization

For frequencies around some tens of Hz, the only reference for frequency stabilization is the common mode of the two Michelson arms. A short rigid cavity would have an important thermal noise and would not fit the requirements. The frequency stabilization scheme for AdV is likely similar to the one used for the initial Virgo, The global interferometer stabilization scheme utilizes nested loops incorporating error signals from the arms Fabry-Perot cavities, the recycling cavity, the common-mode of the long arms. The equivalent filter of this composite cavity is a first order pole of 10 Hz for the frequency fluctuations of the laser. This loop is not sufficient because its unity gain is limited to 20 kHz (50 kHz is the free spectral range of the cavities) and would not fit a very large loop gain in the detection band up to 10 kHz. A first stage of stabilization is needed, the so called prestabilization stage, which locks the laser frequency to the IMC length, controlled itself by the long baseline cavity. This strategy is detailed by the ISC system and the first delivery of this system will be to specify the requirements for the prestabilization of the laser at the input of the IMC. An EOM at the output of the Master laser serves to impinge modulation sidebands on the laser to lock the medium power and HP cavities as well as the PMC length with a Pound-Drever-Hall loop. The prestabilization locks the laser frequency on the IMC length and the feedback loop will act on the master laser transducers: the fast actuator, a piezo-bonded to the crystal, the slow actuator which is the temperature control of the crystal. Then its stability will be transferred to the HP stages by injection locking and Pound-Drever-Hall loops described above. Another possibility to avoid sidebands HP laser is to use the technique of tilt-locking [60] to control the injected stages and the PMC cavities. This method requires no more R&D and could save extra sidebands on the laser beam.

6.4.2 Power stabilization

The damping of relaxation oscillations is implemented on the Innolight master laser (Noise Eater); it uses a photodiode just at the output of the master laser. Though this loop seems to be enough performant for initial Vigo, in collaboration with Innolight, we have improved this loop by adding more gain between 0-20 kHz range and it can be implemented on the AdV Master laser if needed. To reach the -170 dB required, the laser needs to be stabilized via a photodiode capable of detecting more than 35 mA (shot noise limit for a noise of $3\,10^{-9}/\sqrt{\mathrm{Hz}}$). The sensitivity of beam jitter on the photodiode and the effects of acoustics and of dust particles in the optical path have been highlighted many times in table-top experiments, and consequently this photodiode has to be inserted under vacuum at the point where beam jitter is minimized. The location after the IMC has been proven convenient in initial Virgo this position is taking as the baseline solution. Since the power stability is more demanding for AdV, the real power noise has to be checked out on the second out-of-loop photodiode and need further investigations.

6.5 The pre-mode cleaner

The pre-mode cleaner (PMC) is used to filter out the high order modes inherent to the HP stage. Depending on the main modulation frequency (fmod) value, the PMC could be used also to filter the power noise around this fmod. Following the measurements done on a GEO 180W prototype [59], the laser is shot noise limited above 10 MHz, then a Fmod below 9 MHz will encounter some technical noise of the laser. Consequently the PMC should be designed to act as a low pass filter for fmod in the range of 5 to 10 MHz if necessary. The PMC is a three mirror ring-cavity (two-plane and one curved) inserted into the main beam path and has a high transmission for the fraction of the light in the TEM00 mode. A length control system based on a pzt-mounted-curved mirror is needed to keep the cavity resonant with the incoming beam and to compensate for large drifts over long periods of time. A Pound-Drever-Hall loop or a Tilt locking loop will be used to pick up the signal reflected by the PMC. Following the amount of power distributed on high order modes, the finesse of the PMC will be designed by a trade-off between spatial filtering, noise filtering and circulating power. Today the PMC of Virgo+ (fig. 25) stands a power of about 60W without mirror damage thanks to high quality coated mirrors by LMA-Lyon and a vacuum enclosure to keep it air-free and dust-free. The pzt mounting sits behind the curved high reflectivity mirror and will encounter serious heating unless a careful design of negative/positive expansion type could be designed for it.

6.6 Possible option: fiber amplifier

There will be multiple advantages in using a partially or totally fibered laser system, once it will have been proven that it meets specifications: permanent alignment, stable mode structure, easy evolution towards higher powers, and lots of new possibilities for adding auxiliary beams or sidebands, in addition to low cost, better efficiency and minimal

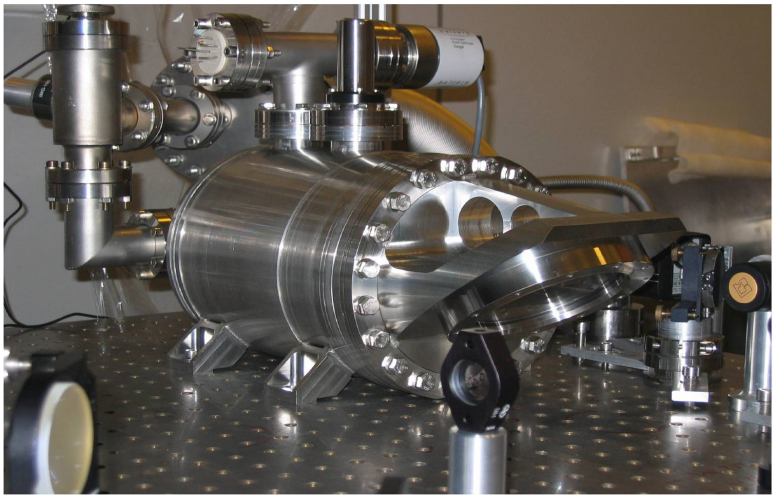

Figure 25: AdV PMC will look like the Virgo+ pre-mode-cleaner, here in the vacuum housing and sitting on the laser table.

maintenance. A high gain, high power (G=2000, P> 150W) prototype amplifier will soon be tested in Nice, and techniques are being developed for controlling its parameters (frequency/phase, power, polarisation). Once the noise performances are satisfying, this will be interchangeable with the Nd-YVO4 amplifying chain described above. A further step will consist in bringing the beam directly inside vacuum to the suspended input bench with a single mode fibre. The fibre technology is not yet ready for that second step, but there is a strong motivation, for commercial and military reasons.

7 Injection system

7.1 General requirements

The Injection system (INJ) of AdV takes care of the optics downstream of the high power laser, and of the interface of these optics and the laser itself. The whole system must deliver a beam with the required power, geometrical shape, frequency and angular stability. Given the 180-200 W power delivered by the High Power AdV laser, it is required:

Requirement	**Value**
Transmission to the ITF	$> 70\%$ (125 W)
Non-TEM_{00} power	$< 5\%$
Intensity noise	$2 \times 10^{-9}/\sqrt{\text{Hz}}$ at 10 Hz
Beam Jitter	$< 10^{-9}$ rad$/\sqrt{\text{Hz}}$ ($f >$100 Hz)

An Electro-Optic Modulation (EOM) system will provide the needed RF phase modulation (for control and sensing purposes). A power adjustment system, probably consisting of a half waveplate and a polarizer (as it is done for Virgo+ power adjustment) will be used in order to tune ITF input power(important for ITF lock acquisition). A matching and steering system in air will be used to couple the beam into the in-vacuum suspended input mode cleaner (IMC). The IMC will geometrically clean the beam and reduce its amplitude and lateral fluctuation. The resonant IMC of which the length is locked on the reference cavity (RFC) will also serve as first stage of frequency pre-stabilization. After the IMC an intensity stabilization section will provide the signal for stabilizing the laser RIN and reach the requirements. An in-vacuum Faraday isolator will prevent interaction of the ITF (interferometer) reflected light with the IMC and laser system. Finally, an ITF mode matching telescope will give to the beam the correct dimension for matching with the interferometer.

7.2 Schematics

The schematic layout will include an in-air (outside vacuum) part and an in-vacuum part, namely:

- In-air
  - EOM for RF modulation
  - Faraday isolator
  - Power adjustment system
  - Collimation and steering optics
- In-vacuum

- Input Mode Cleaner
- Reference Cavity
- Faraday isolator
- Matching telescope
- Steering optics
- Power stabilization photodiode

At present, there is only one option still considered as possible for the final configuration of the INJ layout: this is the Reference Solution (see Fig.26). This solution is close to the one adopted by Advanced LIGO, and can benefit from the R&D activity carried out by LIGO and Virgo.

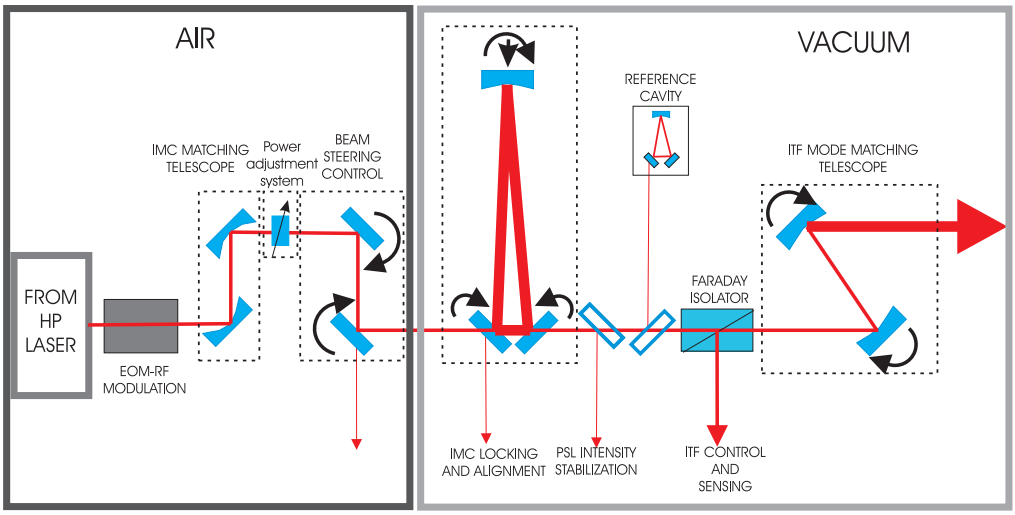

Figure 26: Schematic of the AdV Reference INJ subsystem solution: the laser will be a SSL (solid state laser). The IMC (input mode cleaner) will be a suspended resonant triangular cavity.

An other solution (Fibre Solution) is considering the possibility to replace the input mode cleaner with a fiber component (this could eventually be considered as an upgrade of AdV IMC). An innovative R&D activity, which has no counterpart in LIGO, is going on about this subject, and in the next years a decision about the feasibility of this solution has to be taken. A possible path would plan starting with the Reference Solution and provide in INJ optical design the possibility to shift to the Fibre Solution. This solution will include also an alternative system for the laser frequency pre-stabilization.

- Reference Solution (with solid state laser (SSL) source):
  - High power optical components
  - Suspended resonant input mode cleaner (IMC)

  - Suspended bench(es) supporting Faraday isolator, reference cavity (RFC), and matching telescope

- Fibre Solution:
  - High power optical components
  - Fibre IMC
  - Suspended bench(es) supporting Faraday isolator and matching telescope

7.3 IMC

The laser light must be frequency and spatially stabilized before it can be used in the interferometer. The input mode cleaner (IMC) provides active frequency stabilization through feedback to the laser, passive frequency noise suppression above its cavity pole frequency, and passive spatial stabilization at all frequencies. The input mode cleaner also reduces higher order modal content of the laser light, suppressing beam jitter. For the AdV IMC, we have selected 2 possible configurations that are presented in this document. The first one is the traditional triangular mode cleaner which is currently used in all the interferometric gravitational waves detectors. The reference solution for AdV is with a 144 m triangular resonant suspended IMC.
The second solution should consist in an optical fiber that should spatially filter the laser beam before entering the interferometer (see sec. 7.5). The fiber IMC could be implemented as an upgrade of the resonant IMC if the related R&D is successful.

7.4 Resonant suspended IMC for AdV

The present Virgo IMC is a Fabry-Perot triangular cavity with a high finesse (about 1,000). The cavity configuration is flat-flat-curved. Two flat suspended mirrors define the base and act as the input and output couplers. The third mirror (curved one) is suspended in the Mode-Cleaner tower 143.5 meter far from the injection tower.

Two solutions have been considered for a suspended IMC for AdV in the conceptual design document [2]: the first one consisted in keeping the same Virgo IMC length, using the current infrastructures. The second consisted in reducing the IMC length to reduce scattered light problems we are currently struggling against in Virgo.

The shorter IMC has been discarded since it involved a huge modification of the current infrastructure (build and install a new tower that will be at least 20 meters far from the current injection tower). This was a huge and expensive work since the present building may be too small to accommodate a vacuum tank. It seemed not conceivable for AdV.
The advantage of keeping the current infrastructures resides in its low cost and easy implementation. However, a lot of work has to be performed in order to reduce the light

scattered inside the IMC (see sec. 7.4.1). In particular, we have to work on coating and surface roughness specifications together with LMA lab and the substrate provider. As mentioned in sec. 7.11.2, the possibility to use a larger clear aperture FI (at least 25 mm since the beam waist at the output of the IMC is about 5 mm with the 144-m-long IMC and 180 m radius of curvature end mirror) should be kept open.

7.4.1 Scattered light in the IMC

The incoming light impinging on the mode cleaner end mirror is scattered by the mirror surface, which is not perfect. Thus, due to the small angle of the mode cleaner (about $3\,10^{-4}$ rad), a part of the scattered light can propagate in the opposite direction and be sent back to the laser. The biggest problem is that this light can interfere with the light reflected by the ITF and create some fringes at the level of the IMC alignment photodiodes. These interferences can spoil the performances of the IMC control and add some noise to the laser beam sent in the ITF [65]. A solution to reduce the scattering from the IMC end mirror is to decrease the IMC length but as it has already been discussed in the previous section this configuration seems too expensive. Another possibility consists in improving the surface quality of the IMC end mirror in order to reduce back-scattered light coming from this mirror. It seems reasonable that with this kind of mirror and a 40 dB isolation FI we can get rid of the fringes visible in the IMC alignment signals. We have also to study the effect of IMC end mirror of radius of curvature and cavity waist size on the amount of scattered light.

7.4.2 Jitter suppression

Beam pointing noise specifications for AdV are 10^{-9} rad/$\sqrt{\text{Hz}}$ after the input mode cleaner [66], considering that the input mode-cleaner controls are enough stable not to reintroduce beam jitter noise due to suspended Mode-cleaner motion. Because higher-order modes are suppressed by the input mode cleaner, beam jitter is also decreased. The filtering efficiency depends on two things: the finesse F has to be as high as possible and the IMC has to be non-degenerate (higher-order modes should not be resonant in the IMC). The main concern about beam jitter is IMC control. We have to deeply study this point in order not to reintroduce jitter noise due to IMC motion.

Most often the beam pointing noise is dominated by acoustic and thermal effects induced noise on components in free-space propagation (EOM, FI, etc...). The R&D program that aims to study thermal effects in those components will probably help a lot improving beam pointing noise.

7.4.3 IMC instabilities

- **Radiation pressure and IMC motion**: The IMC and ITF mirrors will be subjected to incremental radiation pressure changes as the input power is changed.

Nevertheless, it has been shown [67] that it should be possible to lock the IMC with an incident power of 180 watts increasing the IMC end mirror mass to 900 g. Further studies are needed to define how heavy should be the IMC end mirror in order to minimize the radiation pressure phenomenon.

- **IMC thermal effects**: Substrate and coating absorption of the IMC mirrors will lead to change in the radius of curvature of the three IMC mirrors [68]. Evaluation of the output beam characteristics has to be given in order to foresee a compensation of this thermal effect if necessary and define mirror coating absorption specifications. Since we are already experiencing this kind of effect in Virgo+ IMC cavity flat mirrors, we can take benefit of this experience to define requirements on substrate and coating absorption.
- **IMC frequency noise**: The frequency stability of the laser beam at the output of the IMC is known to be strongly dependent on the IMC length. The frequency stabilization loop has to be reviewed in order to minimize this noise and to reach the specifications on frequency noise that are required by the interferometer (see Interferometer Sensing Control for frequency noise requirements).

7.4.4 IMC suspension strategy

In case of a triangular IMC, we have to define how the 3 mirrors have to be suspended. We have 2 possibilities:

- The IMC end mirror has its own suspension and the 2 flat mirrors are fixed on a dihedron which is put on a suspended bench (Virgo current configuration).
- The 3 mirrors are suspended individually, this solution can be interesting to remove the dihedron resonances that are visible in the dark fringe for Virgo but in this case radiation pressure can be an issue also for flat mirrors.

This item has to be deeply investigated to determine the strategy to choose.

7.4.5 Resonant IMC: summary

For the AdV resonant IMC, two possible configurations have been discussed in the conceptual design document[2]

- The one using the current infrastructure: 144-m-long IMC.
- A shorter IMC, to reduce scattered light coming from the IMC end mirror. This solution would require a new building to host the IMC end mirror.

The second configuration seems not feasible for AdV since it requires a huge work on infrastructures and a non-negligible extra-cost for AdV project. The 144-m-long triangular resonant IMC seems to be compliant with the requirements of AdV but thermal effects, radiation pressure and scattering, in particular, have to be deeply studied to design a

system as insensitive as possible to those effects. Moreover IMC control scheme and the suspension itself of the new suspended mode-cleaner have to be upgraded to fulfill the requirements in term of frequency and beam jitter noise foreseen for AdV. The reference solution for AdV IMC would be:

- 144-m-long triangular resonant IMC

We have to keep the possibility to integrate the fiber IMC later on if this device fulfills AdV requirements.

7.5 Fiber IMC option for AdV

As already suggested above, a fibre optic can be used to clean the output beam of the laser or even to convert this beam to a desired high order mode. The main advantages over a resonant mode cleaner would be the absence of maintenance, the simplification of the controls (all alignment controls suppressed except the positioning of the fibre end), and the simplification of the optical scheme. No more frequency pulling by the mode cleaner motion, no more need to adjust precisely the modulation frequency, etc ... The only drawback would be the need for more active control of the frequency and power fluctuations, since we would loose the filtering effect of the long IMC above 500 Hz.

7.5.1 Status of the related R&D

This study started three years ago, with the initial goal to replace the mode-cleaner by a singlemode fibre, using the new technology of hollow photonic crystal fibres (PCF). The potential advantages, which have been confirmed, are a higher transmission and the absence of frequency selectivity, which permits the transmission of sidebands (or even of auxiliary laser beams). This R&D today is the continuation of the previous work, where the hollow PCF will be replaced by a solid silica LMA (large mode area) Bragg fibre. This mainly requires the manufacturing of an adequate LMA single-mode fibre, preferably with a polarization maintaining structure. The first prototype has been delivered , it is under test for coupling efficiency, beam geometry, phase, power, and polarization noises, at different power levels, depending on the highest power available at the time of the test.

7.6 Mode Matching Telescope (MMT)

The MMT should deliver the light from the Faraday Isolator to the ITF with the proper mode content. The coupling efficiency of light into the main interferometer shall be 0.95 or greater in TEM_{00}. Actually, it should be about 0.99 as already demonstrated with the current parabolic MMT. The mount of the mirrors will be equipped with closed-loop picomotors to be able to remotely fine adjust the mode-matching and eventually align the beam in the ITF.

7.6.1 Reference solution : Non-degenerate recycling cavity

The MMT in the non-degenerate recycling cavity case will be rather simple. The design specifications for a non-degenerate recycling cavity have not been completely finalized yet. Design study activity is still required on this item. However, it is expected that the requirements on the MMT will be less stringent than in the case of Marginally stable recycling cavity.

7.6.2 Marginally stable recycling cavity

In this case, the design of the MMT should be close to the Virgo one: it should be an off-axis parabolic telescope, consisting in 2 parabolic mirrors longitudinally separated by around 700 mm. Current telescope is confocal because the manufacturers claimed they couldn't provide parabolic mirrors with the needed characteristics to build an afocal telescope. This may not be true anymore. An afocal telescope design should relax in a significant way the tuning tolerances and the requirements for the mirrors. Both options are under study. The major issue is actually to meet the constraints imposed by the diameter of the optical free aperture at the output of the telescope (around 300 mm) and the physical dimensions of the Suspended Injection Bench. A detailed design and a study to recover any error within the range of the mirrors' specifications by repositioning the 2 parabolic mirrors are under progress.

7.7 Reference cavity (RFC)

The low-frequency stability will be achieved by an additional control system that stabilizes the input mode cleaner length below 15 Hz to the length of a so-called reference cavity (RFC), a 30 cm-long rigid triangular cavity. In the case of the baseline where we consider the non-degenerate power recycling cavity, the RFC can be put below the suspended injection bench as in Virgo. This will ensure a good isolation of the reference respect to acoustic and seismic noise. This cavity is part of the laser frequency pre-stabilization loop. For AdV, we should be able to keep the Virgo RFC (see figure 27) (requirements about frequency noise will be given by ISC and laser frequency prestabilization will be carried out by PSL subsystem (see sec.sec:laser).

7.8 Power control and stabilization

Power amplitude fluctuation can generate noise in the ITF both through a fringe offset and differential radiation pressure, owing to cavity reflectivity asymmetries. At the AdV power (> 100 W input power) the differential radiation pressure is expected to dominate. Functional requirements, computed in the assumption of 1% asymmetry and 50 ± 1 beam splitter reflectivity, give limits on the amplitude fluctuations at the level of $10^{-9}/\sqrt{\text{Hz}}$ at 10 Hz at the output of the IMC cavity (see PSL section for more details).

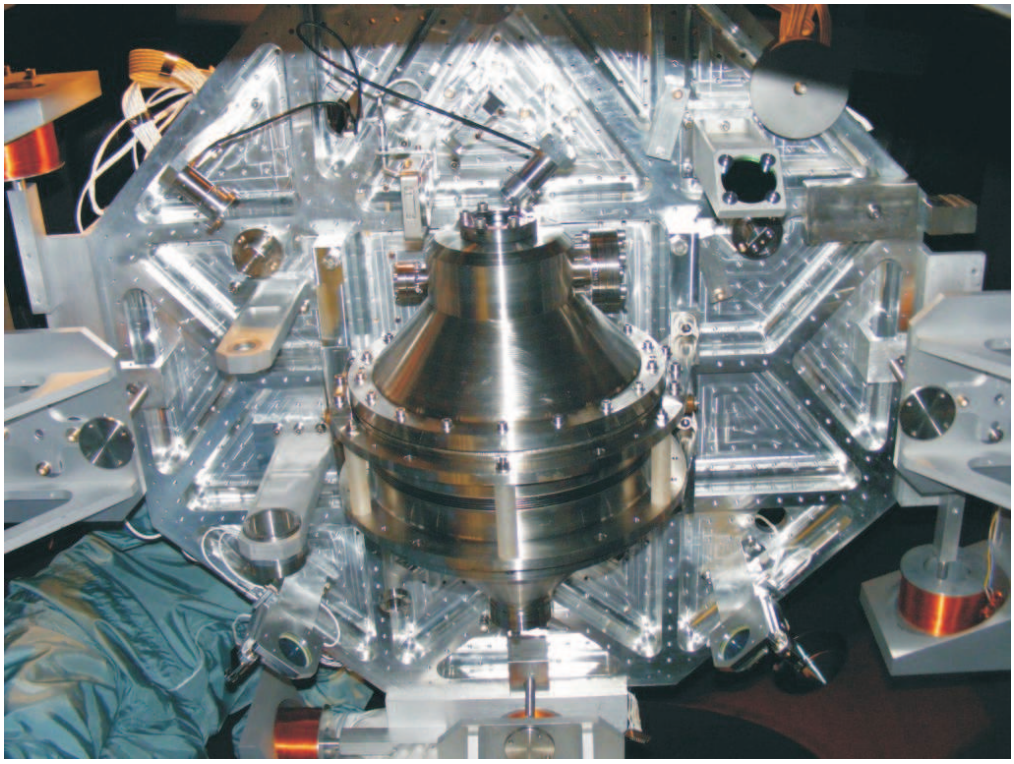

Figure 27: Picture of Virgo RFC attached to the lower part of the Suspended Injection Bench : in AdV reference solution, the RFC should remain the same and should be put under vacuum and suspended as for Virgo.

The power stabilization loop will be an extension of the system used by present Virgo. The signal for the power stabilization is picked up in vacuum after the IMC and fed back to the laser source. A place where to put this photodiode will be foreseen in the design of the suspended injection bench (SIB). A further stabilization stage could use as error signal the power in the power recycling cavity if needed.

7.9 SIB reference solution layout

For the reference solution a 3D drawing of the AdV Injection Bench in the case of non-degenerate power recycling is shown in Fig.28. In this configuration, we have to accommodate the IMC input mirrors, the Faraday isolator and two mirrors of the power recycling cavity (PRM1 and PRM3) and the Reference Cavity (RFC) that can be kept under the SIB as in Virgo. This release also the constraints about SIB faraday isolator clear aperture since in this case a 20mm-diameter clear aperture should be enough to avoid any clipping. In this scheme, we are not considering the way we are fixing PRM1 and PRM3 mirrors (if we need to suspend these mirrors or add an attenuation stage to the Injection bench suspension). The requirement on the displacement of these optics

will be given by ISC.

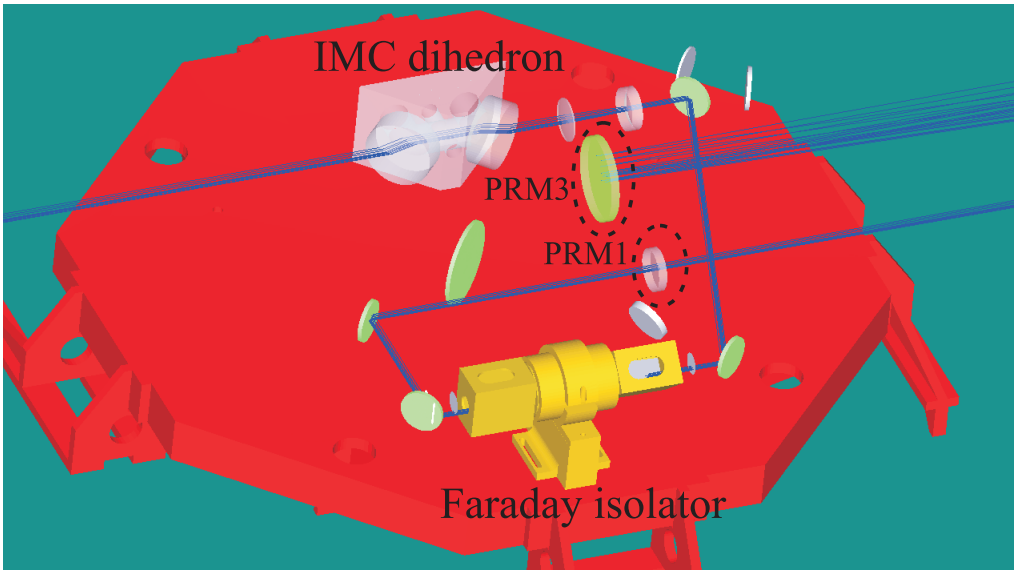

Figure 28: AdV suspended injection bench 3D view in the case of a non-degenerate power recycling cavity

7.10 EOM and RF Modulation

DC modulation is baseline. Nevertheless, RF modulation will be used for the control of the interferometer, both for longitudinal locking and alignment. The main difference between the EOM to be used in AdV and Virgo resides in that the power that the first EOM will have to withstand will be almost 10 times higher (180-200 W instead of 20 W). Thermal effects will become more significant ([52]), and the choice of RTP (or $RbTiOPO_4$, rubidium titanyl phosphate), a less absorbing material than presently used KTP, would be recommended ([53]). Also wedged cut RTP (and AR coated) crystals would represent an improvement ([54]). Requirements in AdV for EO modulation will also be different: many of these parameters will affect the driving electronics and signal generator choice. Indicative numbers for the single sideband noise requirements (modulation phase noise) can be found in [55], and for modulation index noise (amplitude noise) in [56]. More than one modulation frequency will likely be used in AdV (probably three for ITF control and one for IMC lock), either for control and for monitoring. The increased sensitivity and complexity of the interferometer will make important addressing the problems of sidebands on sidebands generation. The solution of this problem could imply novel EOM topology (see for example [57]) or new modulation generation technique (see for example [58]), which have still to be fully tested and assessed .

7.11 Faraday isolator

7.11.1 High power Faraday isolator

Light back reflected by the ITF towards the IMC has already been an issue in Virgo. This problem will be more significant with the higher power of AdV. The solution for this problem has been the use of an in-vacuum Faraday isolator placed between the IMC and the ITF. Either in the case in which a suspended IMC or a fiber IMC will be used, an in-vacuum Faraday isolator between the interferometer and the IMC will be necessary. With the higher AdV laser power (180-200 W input power), standard Faraday isolator will exhibit loss of optical isolation, owing to thermally induced birefringence, and very high thermal lensing. In order to reach a good level of optical isolation ($\approx$ 40 dB) a specifically designed Faraday isolator has to be used, including depolarization compensation and a passive correction of its thermal lensing. A design developed in many years of extensive experimentation has already been adopted by LIGO, and should fit also to AdV needs.

The main questions to be addressed, as far as the in vacuum Faraday isolator is concerned, could be summarized as:

- withstand high average power (300 W) on long periods;
- provide enough optical isolation;
- compensate depolarization and thermal lensing;
- provide good transmission and reflection;
- not to be too big and heavy.

At present there is no precise requirement about how much optical isolation is to be obtained by the in-vacuum optical isolator. There is a general agreement that, in presently operating interferometer, an isolation of about 30 dB is satisfactory. Virgo experience shows that a lack of optical isolation (less than 20 dB) makes the locking acquisition of the recycling cavity difficult or impossible, and some visible effects on the low frequency ITF alignment start to be visible. The present setup makes it not possible to modify remotely the isolation, in order to perform tests on effects on sensitivity. No experience in this direction is available either in LIGO. It is generally agreed that in the next interferometers an isolation better than 40 dB should be provided, even in view of the fact that experienced degradation of the isolation with the change of power and when going from air to vacuum have been observed. The prototype for high power operation in LIGO, which will be used already in Enhanced LIGO, exhibits an optimal optical isolation exceeding 49 dB at more than 100 W input laser power. However, simulations of thermo-optical effects in TGG show that the isolation ratio changes when going from air to vacuum, depending on the laser power going through the Faraday crystal. These simulations have been confirmed both in Virgo experience [64] and in LIGO bench tests. In order to optimize the optical isolation, a remote tuning will be necessary (analogous to that planned for Virgo+).

Optical isolation performances, according to LIGO experience (which has been carried on in collaboration with Novgorod IAP group), strongly depends, at laser power level typically exceeding 50 W, on thermal depolarization effects in TGG crystal. Depolarization has to be ascribed mainly to the temperature dependence of the Verdet constant and to photoelastic effect [61]. Many years of extensive experience in the Novgorod group [62] have lead to an optical design of a Faraday isolator which compensate thermal depolarization effects. The optical isolation provided by the prototypes reaches 49 dB with more than 100 W laser input power.

The schematics of the candidate Faraday isolator for AdV is described in detail in [62]: it comprises an input polarizer, a $\Lambda/2$ waveplate, two TGG crystals rotating the polarization by 22.5°, separated by a $-67.5°$ polarization rotating Quartz Rotator, and an end polarizer. A difference, with respect to LIGO, could be the use of a larger free aperture TGG crystal: the LIGO isolator has a free aperture of 20 mm. In AdV, if the beam coming out from the IMC will have a diameter of 1 cm, a 25-30 mm aperture Faraday isolator should be more convenient, in order to avoid beam size reduction.
The candidate polarizers are Calcite Wedged polarizers (about 4.3° wedge) or Brewster Thin Film polarizers (tests are foreseen to be done within High power input optics R&D program see sec. 7.12.3 for the first experimental results).

Further improvements to the Faraday isolator will be the possibility to remotely compensate a loss of optical isolation in vacuum and a compensation of the thermal lensing. In Virgo it has already been experienced a drop of optical isolation of the Faraday isolator when going form air to vacuum: after tuning the isolator for optimal isolation in air, a loss of about 10 dB of isolation has been measured. This results have been confirmed by the experience in LIGO performed with the prototype isolator (see also [63]). In order to correct this effect, already in Virgo+ a system is planned, which entails the insertion of a $\Lambda/2$ waveplate, mounted on a motorized mount, between one polarizer and the TGG crystal. By remotely rotating the waveplate by less than one degree it should be possible to correct this effect. Thermal lensing in the in-vacuum Faraday isolator has also already been experienced in Virgo. The induced thermal lensing results in a mismatching of the beam with respect of the ITF. The thermally induced focal length in Virgo, with 10 W input power in the Faraday isolator (almost 20 W considering the reflection of the unlocked ITF) was of the order of 100 m. In this case, the induced mismatching is of the order of 1%, thus not affecting the ITF performances. Scaling the present Virgo situation to the AdV higher power (200 W), the computed resulting induced focal length is of about 13 m, thus yielding an unacceptable mismatch of 37%. Passive compensation will use DKDP (deuterated potassium dihydrogen phosphate, KD_2PO_4) calibrated bar mounted after the Faraday isolator. The thickness of the bar is critical for exact lensing compensation, the exact dimensions depending on DKPD and TGG parameters. These parameters are not exactly known a priori, this making it difficult to cut exactly the slice with the right length. The effect of the DKDP slice could be changed by changing the crystal temperature: a remote temperature modification should be implemented. The DKDP should be contacted to a heater/cooler (e.g. a Peltier placed below the thermally conductive mount of the DKDP), thus allowing to tune the lens compensation.

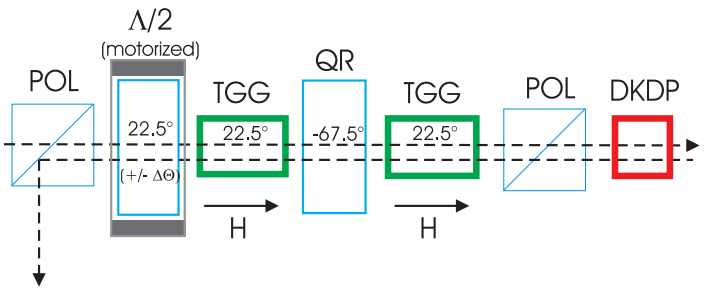

Figure 29: High Power in-vacuum Faraday isolator

The dimensions of the Novgorod-IAP Faraday isolator are quite big: $60.5cm \times 12.7cm \times 26.5cm$. The weight is about 14 kg. The clear aperture is 20 mm. In order to accommodate the beam coming out of the IMC (5 mm waist at present) a larger clear aperture would be desirable (25-30 mm). The rotator crystals are TGG, polarizers still to be decided (Calcite or Brewster thin film). All materials have to be vacuum compatible. The accommodation of this large device in the input bench vacuum vessel of Virgo could be an issue. A solution for the available space has to be found.

7.11.2 Larger clear aperture Faraday isolator

A possibility to use a larger clear aperture Faraday isolator has been considered: at the state of the art, it would be possible to have efficient Faraday isolators with a clear aperture up to 25-30 mm: this apertures would accommodate a 5 mm semidiameter beam without any clipping problem. The development of a larger aperture Faraday would require some R&D, since it has never been made up to now, and would probably lead to larger dimensions and weight (however, likely less than 700 mm and 20 kg). This possibility has to be kept open, since it would allow to use the beam of the 144 m IMC (5 mm semidiameter) without reducing its size with a telescope: a reducing telescope could introduce astigmatism and produce parasitic reflections. Moreover, reducing the size of the IMC beam, means that the mode matching telescope should have a larger magnification power (need of a faster mode matching telescope). Therefore, the possibility of having a larger Faraday isolator would yield several significant advantages. The problem would be mainly in its dimensions. On this purpose, a design study carried out by IAP has started in september 2008 in the frame of a collaboration between IAP and EGO. The design study should give dimensioning of vacuum compatible faraday isolators enabling to work up to 300 W with a clear aperture going from 23 mm up to 30 mm.

7.12 Status of the related R&D

Laser and Injection optics of AdV can benefit of the many years of R&D already performed by LIGO in investigating high power components like electro-optical modulators and Faraday isolator. The results obtained by LIGO are available. In consideration of the state of advancement of the R&D of LIGO, Virgo has opted for relying as much as possible on LIGO research, and concentrate his effort mainly on alternative solutions, like the fiber IMC. Hence, the AdV reference solution, will be largely based on the results obtained in LIGO.
On the other hand, starting from the results of LIGO, further investigations in collaboration with LIGO are being performed also in Virgo. One R&D program has been started on fiber IMC (see sec. 7.5). Another three years R&D program is about high power optical components for AdV has already started, with the purpose to define some important elements for AdV. The scope of this R&D is to test the compliance of all optical components of the injection system with the 200 W high power laser that will be used for AdV and choose the optical components that can fulfill AdV requirements and should be installed for AdV. This includes the Faraday Isolator and the electro optical modulators (EOM) already mentioned in sections 7.10 and 7.11 but also polarisers and retarding wave-plates that will be used on the laser and injection systems. In all these components, thermal effects will likely introduce additional thermally induced lensing, and/or birefringence effects, together with other potential unexpected problems. All these effects have to be measured and understood. Then some strategies of compensation have to be elaborated. In LIGO the tests on input optics components have not been performed with input power larger than 100 W, so the measurements to be performed in Virgo will give additional information. The tests actually going on are taking advantage of LIGO experience in order to design components for the specific needs of AdV. Relying on this expertise, some alternative solutions could also be tested in a second time. The material and configuration selection deriving from this study should lead to a full scale system to be used in Advanced Virgo

In order to perform these tests a high power laser facility was set-up in EGO optics lab. It relies on a commercial 200W ytterbium laser from IPG photonics. As cleanliness is a very important issues at this power, a specific enclosure has been designed and placed in a dedicated laboratory (see [71] for more details).

We take a special care to the characterisation of this laser source which is spatially single mode (M^2=1.2), polarized but not longitudinally single-mode. The power, beam profile and M^2 were checked before designing the bench where the high power components have to be tested.

7.12.1 High power isolator tests

First of all, we focused on the understanding of the thermal effects happening in faraday isolators. When heated up, the thermal effects created in a TGG crystal (magneto-optic material used in faraday isolators) are responsible for thermal lensing, modification of the

polarisation rotation and depolarization. All these effects are spoiling the performances of the isolator and can be different if the isolator is placed in air or in vacuum, since it changes significantly the thermal conditions.

To study the thermal lensing effects, we set up the test bench that can be seen in figure 30. We use the 200W pump laser to heat up some faraday components located in a test area. The lensing effects are evaluated looking at the modifications of a low power single mode laser (JDS Uniphase 100mW NPRO laser) used as a probe beam. This laser is sent on the element to be tested in opposite direction and polarisation with respect to the pump beam. The probe laser is then analysed with a Shack Hartmann wave front analyser.

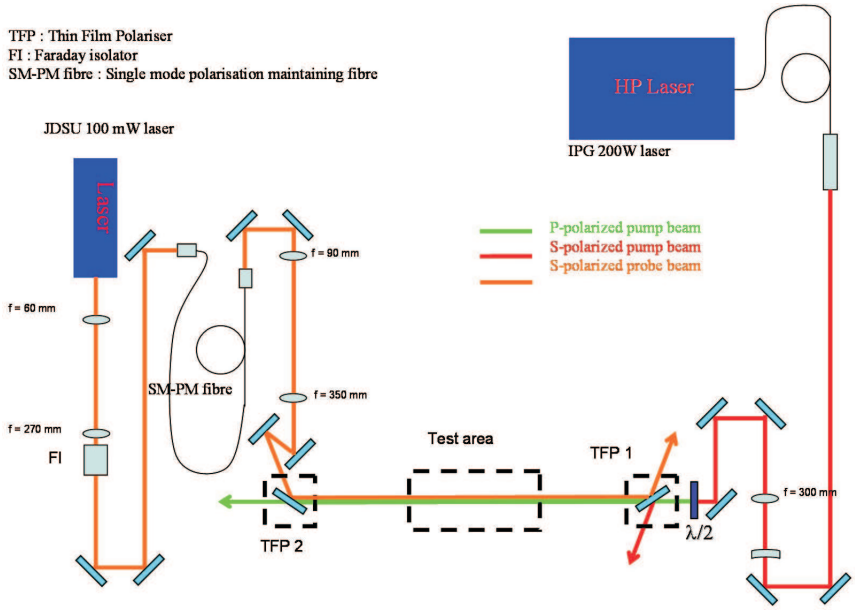

Figure 30: High power input optics test bench scheme.

Figure 31 gives the results of these measurements for different laser power from 10 to 85 W for two different TGG crystal rods from the same manufacturer (Northrop Grumann). These samples are actually of the same kind that the one installed in the current Virgo SIB faraday. In order to understand the measured effects, we developed a finite element model analysis code to compute the thermal heating of the TGG samples. Figure 31 also shows the simulated focal length for different values of absorption of the crystal. The simulations are in good agreement with the measurements, with absorption values close to the manufacturer's one (about 1500 ppm).

All these measurements have been carried out in air. In a vacuum, as only the radiation is cooling down the samples, the heating of the crystal is much different. Nevertheless we could show with the simulation that the thermal lensing is quite the same, due to the fact that this is depending quite only on the radial temperature gradient inside the crystal and not on its the average temperature. In-vacuum measurements are planned to

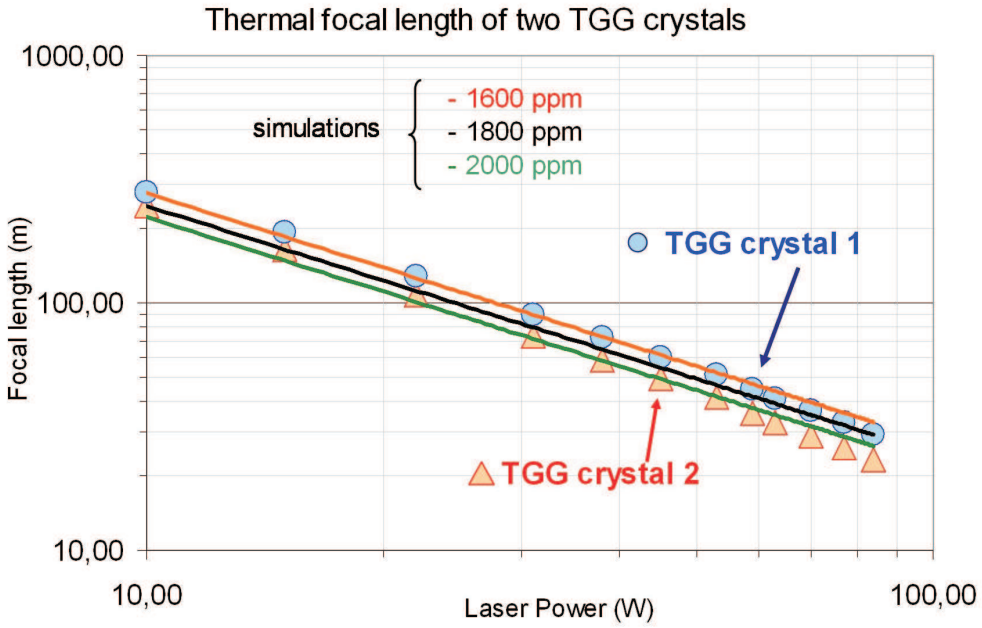

Figure 31: Thermally induced lensing in TGG. Triangles and circles are experimental results. Lines correspond to results obtained with the finite element model code.

confirm the simulations results.

We can see in these measurements that already at average power, we are experiencing significant lensing effect (23m is reached at 84 W for TGG crystal 2) in TGG crystals. It is clear that the current design of faraday isolators has to be modified in order to reduce this effect when going to high power. One possibility is to include in the rotator a element realizing a passive compensation of these geometrical distortions. For example it is possible to include a crystal of DKDP which exhibits a large negative dn/dT values (dn/dT_{DKDP}=-4.4.10^{-5} K^{-1} to compare with dn/dT_{TGG} = 1.9.10^{-5} K^{-1}). With the same setup, we performed some tests at different laser power with a 10 mm z-cut DKDP provided by MolTech GmbH. With the measured values, we could compute the length of DKDP necessary to correct for the TGG distortions. As an example a TGG of 1600 ppm losses heated by 40 W can be corrected using a length of DKDP of about 4 to 6 mm.

The second spurious thermal effect impacting faraday isolators is the depolarization inside the TGG crystal. This effect was characterized with the 200 W pump laser by placing a TGG crystal between two crossed polarizers. By measuring the small fraction of light transmitted (P_{tran}) by the second polarizer, it is possible to evaluate the depolarization defined by : $\gamma = P_{tran}/P_{tot}$ for different laser power (P_{tot}) (cf. figure 32).

We can see from these results that for power higher than about 70 W, γ is proportional to P^2 (see [62]). This depolarization inside the TGG crystal cannot be compensated and directly affects the isolation factor of the Faraday. One strategy can be to tune the

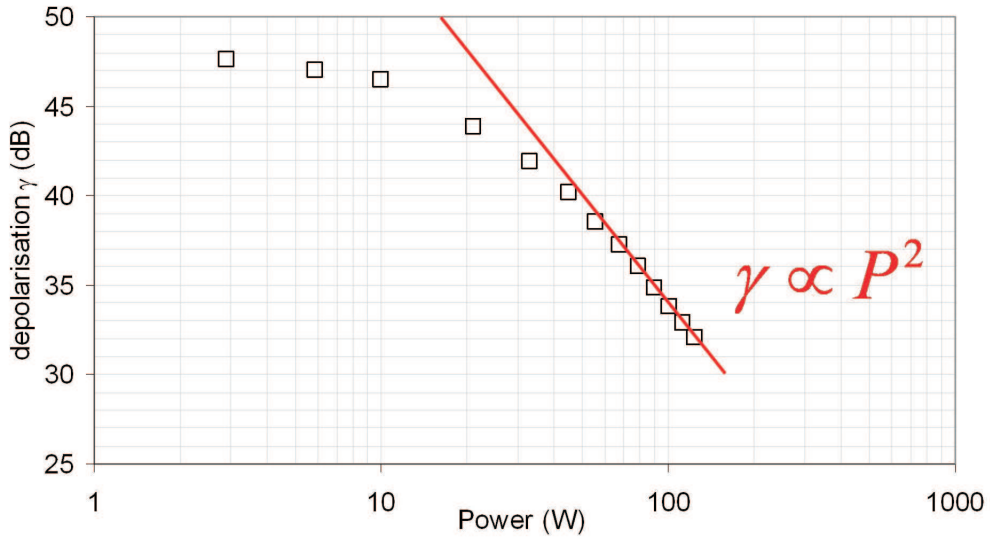

Figure 32: Depolarization (dB) in a TGG crystal as a function of the incident laser power (W).

way the TGG is cut with respect to its crystallographic axes. According to Khazanov [72] this parameter has a big importance on the amount of depolarization. Taking into account this property, it seems more convenient to design faraday isolators with depolarization compensation[61] [72] as described in section 7.11 which are by design less depolarizing and also less sensitive to TGG crystallographic orientation. In order to design such an isolator that fulfills AdV requirements, a collaboration recently started with the Novgorod-IAP (Khazanov group).

The third thermal effect spoiling isolators properties is the modification of the rotation angle of the faraday isolator when the TGG crystal is heated. This is due to the temperature dependence of the Verdet constant (V) and can be derived from:

$$\delta\theta = \frac{1}{V}\frac{dV}{dT}dT\theta \tag{22}$$

where dT is the temperature change of the Faraday crystal due to laser heating and $\theta = nLVB$ (n is the TGG refractive index, L, the crystal length and B, the magnetic field). This effect results in a loss of isolation observed when ramping up power inside a faraday isolator. We could measure this loss of isolation using the 200 W pump laser heating a spare of the actual Virgo SIB faraday. By retro reflecting a small amount of the power transmitted by the faraday (about 4%), we could measure the isolation, shown in figure 33, for power going from 2 to 48 W. These tests were done by tuning the isolation at low power (2W) and by measuring the ratio between back transmitted light and total light sent back into the isolator when the power is increased. As we can see, the isolation change is much different in air and in vacuum, due to the different thermal conditions.

In order to check these measurements, we measured for a power of 37W the temperature change of the crystal and used this value to compute the isolation change using equation 22. We found isolations of about 34 dB and 37 dB in vacuum and in air respectively, which is quite in good agreement with the measurements.

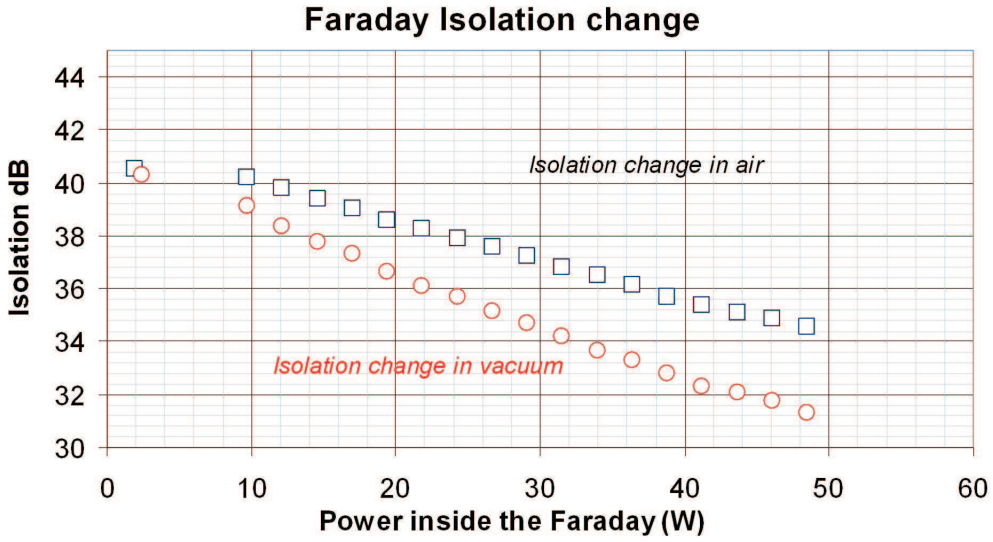

Figure 33: Experimental measurement : Faraday isolation change vs laser pumping power (W). in air (squares), in a vacuum (circles).

In order to compensate for this effect, it is possible to introduce a half wave plate inside the isolator (between the faraday rotator and a polarizer) to compensate for the rotation change due to the temperature. This solution has been tested under vacuum for a laser power of 38 W. By turning the wave plate of about 0.7°, the isolation can be improved from 32.8 to 36.4 dB. The limit of isolation is then probably due to depolarization inside the TGG. These measurements, in additions with the simulation tools that have been developed helped to understand thermal effects in the Faraday isolators. The next step will consist in designing and building (within 2009) a prototype that fulfills AdV requirements in collaboration with Novgorod-IAP group.

7.12.2 Electro-Optic Modulator studies.

The optical setup used to carry out Faraday isolator studies can be easily modified to study EOM materials by using a smaller beam waist. Some tests will be realized soon in order to identify a suitable crystal with a lower absorption than the one actually used in Virgo (KTP). A few components are already available and should be tested soon. We have two RTP crystals (from the Raicol company) which are known to be low absorption and high damage threshold electro optical material, 1 KTP crystal (Virgo EOM kind) and a MgO doped LiNb03 crystal. This component has already been characterized at

LMA, Lyon in mid-February 2008 (measured absorption is 110 +/- 10 ppm/cm). We also plan to design and test electronics able to drive these EOMs. With the aim to get a prototype compliant with AdV design sensitivity curve (frequency, modulation depth, noise).

7.12.3 Polarizers and wave plate studies.

Concerning wave plates, two different items suitable for high power were tested. They are optically contacted wave plates from lambda research (WPO-25.4CQ-0-2-1064) and CVI (QWPO-1064-10-2). The first one shows a polarization quality of only 30 dB at 10W and can therefore be rejected. The item from CVI is indeed very good and shows a quality better than 45 dB at 125 W. In the future we are planning to test true zero order wave plate, that are potentially the least sensitive to any thermal effect.

We also started to identify some polarizers suitable for high power use. A first set of Brewster angle thin film plate polarisers has already been tested. We could measure these items from four different manufacturers : CVI (ref TFP-1064-PW-2025-C), Thales (spares of the Virgo laser bench), coated substrates from the LMA (spares of the Virgo+ laser bench) and EO tech (spares of the actual Virgo SIB faraday polarizers). The measured polarization quality for a power of 10 W and a waist of about 1 mm are respectively 24, 36, 35 and 50 dB. All the three last items has also been tested up to a power of 125 W, showing only a few dB of difference in the polarization quality. In spite of these good polarization properties, these thin film plate polarizers have a few drawback. As they must be used at the Brewster angle they are introducing a beam displacement and they must be finely tuned at the right angle in order to achieve a correct polarization quality. As this tuning is quite sensitive, the polarization quality become sensible to be alignment. Besides, the incidence angle of 56° is not really convenient for designing a full optical bench. In order to overcome these problems we identified a few other high power polarizers that will be tested soon. From CVI we will try some thin film plate polarizers at 45° incidence (TFPN-1064-PW-1025-UV) and some optically contacted polarizing cube, working at 45° incidence (PBSO-1064-100) and 58° incidence (HPBS-1064-100) that seems to show even higher polarization quality. We are also planning to test some epoxy-free (chemically activated direct bonding) polarizing beam splitter cubes from Precision Photonics. The technology developed by this company is different from optical contacting and seems very promising for high power use.

8 Mirrors

As it is shown in fig. 2, mirrors play a crucial role in the sensitivity of AdV. On one side the mechanical losses in the coating determine the quality factor of the mirror and as a consequence the displacement of the mirror surface due to its thermal vibration. On the other side the optical losses in the coatings determine the amount of power which is lost in the Fabry-Perot cavity and as a consequence the power that is stored in the recycling cavity. This quantity determines the quantum noise which is expected to limit the sensitivity at the higher frequencies. R&D is ongoing at LMA to improve the mechanical performances of coating without degrading the optical performances. Titanium doped Ta_2O_5 coatings recently developed at LMA are the best solution known so far. The AdV baseline design foresees the use of mirrors, for the Fabry-Perot cavities, 35 cm in diameter and 20 cm thick i.e. mirrors having the same diameter as Virgo but twice as thick. An alternative option is to use 30 cm thick mirrors i.e. weighting 63 kg. A larger mass could be interesting if the gravity gradient noise is found to be smaller than foreseen by the present model adopted within Virgo. In this case, and supposing that ribbons were used to suspend the mirrors, a heavier mirror would allow to reduce the radiation pressure noise thus improving the sensitivity at low frequency. A larger substrate is likely to be required for the beam-splitter as this component lies at 45 degrees with respect to the beam axis. A substrate 55 cm in diameter and 6.5 cm thick has been considered (larger pieces are available if the specifications on the optical quality of the silica can be relaxed with respect to what is used in Virgo). In the AdV baseline, non degenerate cavities will be used for the power recycling and signal recycling. Instead of a large mirror (35 cm in diameter and 10 cm thick) like in Virgo, three smaller mirrors will be used to realize these two cavities (diameter between 5 and 15 cm). Although there are 6 mirrors instead of 2 for these cavities, the cost will be comparable: the cost increase of the polishing will be compensated by the decrease of the bulk silica cost. At last, due the thermal compensation implemented in AdV, two compensation plates (CP) will be necessary. They should be fixed on the back of the reference mass. Since the clear aperture due to the coil-magnet actuators on the back of the reference mass is 280mm, a maximum diameter of 280 mm for the CP is foreseen. The thickness will be of about 10 cm.

8.1 Substrates

The AdV baseline foresees the use of fused silica for the mirror substrates. Tests on sapphire were done at LMA in the context of the Advanced LIGO pathfinder. The results obtained favored the choice of fused silica [75]. No alternative material is being considered today by Virgo. On the other hand a new type of fused silica with smaller absorption is available today. According to the company producing it, the bulk absorption for this material is about 3 times smaller than the one used for Virgo and the other performances (Quality factor, index homogeneity, residual strain) are still the same. The cost of this new type of Silica is comparable to the one used for Virgo. Reducing the absorption in the substrates is certainly of interest as the power absorbed causes thermal lensing in all transmissive optics. The problems increases with the power stored in the interferometer

and with the thickness of the substrates. On the other hand one should remind that so far thermal effects are dominated by coating absorption, and this will be enhanced by the high finesse of AdV. From this point of view it is more important to improve the absorption of the coatings than to improve the losses of the silica. Both for the old type of silica used for Virgo as for the new one recently developed, it is possible to obtain pieces of the size requested by the AdV baseline. Recently, for the AdV baseline, it has been decided to use a high quality fused silica for the input mirror and the beam splitter (respectively Suprasil 3002 and Suprasil 3001) as these optics transmit a relatively large amount of power (of the order of 2 kW). Fused silica of a lower optical quality will be considered for the end mirrors as in this case the mirrors are reflecting most of the light (baseline Suprasil 312). The only constraint in this case is the substrate mechanical quality factor that has to be sufficiently high to avoid increasing the thermal noise above the level determined by the mechanical losses in the coating. Fused silica of lower mechanical and optical quality (baseline Herasil 102) can be used for the mirrors of the power recycling cavity as a relatively small power is transmitted trough this optic and the interferometer output is less sensitive to the thermal noise affecting these masses. The same material is considered for the signal recycling mirror even if in this case the sensitivity to its internal thermal noise as a function of the interferometer optical imperfection and asymmetries will have to be studied. This type of fused silica will be also used for the compensations plates.

8.2 Polishing

Traditionally the quality of polishing is characterized by two different parameters: the flatness and the micro-roughness. The first parameter gives the rms of the difference between the perfect surface (typically a sphere) and the actual surface as measured in by phase map interferometer (i.e. for spatial wavelengths going from about 1 mm, up to the radius of the mirror). For Virgo this parameter was measured to be in the range of a few nm [73, 74]. The second parameter gives a measurement of the mirror surface roughness at small scale lengths (from a few microns, up to about 1 mm). For the Virgo mirrors this parameter was found to be of the order of 0.05 nm. The distinction between these two different length scales originates in the fact that different instruments are used to measure them: both effects contribute to scatter the light from the fundamental mode to higher order modes. They generate losses and extra noise. These polishing losses will play an even more important role in AdV due to the higher finesse of the cavities. Depending on the difference in the losses between the two cavities they could be the source of finesse asymmetry and contrast defect thus modifying the constraints on other subsystems. According to the simulation of the Virgo interferometer recently done at Nice and ESPCI, using the real mirrors maps measured at LMA, the lack of flatness represents one of the main origin of losses in the cavity. The value deduced from the simulation amounts to 250 ppm per round trip. For comparison the measured losses per round trip, as deduced from the measurement of the recycling gain, amount to 500 ppm. The additional losses measured are thought to be due to the mirror contamination (this remains to be verified). Anyhow the losses foreseen by the simulation alone exceed

by a large fraction the losses assumed in the AdV baseline (∼75 ppm per round trip). For this reason it is necessary to improve the mirror flatness. Two paths are possible in this regard. For the first one, the classical steps of polishing will be done by external companies. Then, the second step will consist in improving the mirror surface figure by using the so-called corrective coating technique. This technique, originally developed at LMA, consists in measuring the mirror surface map and correcting it by adding an additional layer of silica wherever is necessary. An R&D program about corrective coating had been supported at LMA during the first R&D program launched by EGO back in 2002. The corrective coating technique was tested on a 150 mm diameter flat mirror with good performances (RMS wavefront: 0.9 nm, Wavefront PV: 9 nm). In order to reach the AdV specifications on the flatness, an additional investment will be required to develop a new robot for the Virgo large coater in Lyon. But this is an investment for the future as other mirrors upgrades can be done using this technique. The possibilities of the corrective coating need to be quickly characterized to understand its applicability to AdV. An effort of modeling will have to be done to understand if a given polished substrate can be used in AdV or if they should go through a corrective coating process.

For the second path, after the classical steps of polishing, some of the advanced polishing companies are now able to improve the mirror flatness by removing excess of material from the surface with an ion beam, but the consequence of that is the high cost of this type of component. The performance of this type of polishing has to be checked. The two solutions are roughly comparable in term of cost but the corrective coating one has the advantage that further mirrors upgrades can be realized at a later stage and in this case it will be cheaper.

8.3 Coating

The mirror coatings are certainly the most sensitive component of the mirrors and among the most important in the interferometer as they determine both the total mechanical losses of the mirrors and their optical losses. As mentioned above an R&D program is ongoing since several years at LMA and is still supported by EGO. At present the lower mechanical losses measured for Ta_2O_5 coating are those obtained with Ti doped Ta_2O_5 and amount to about 1.6 to 1.8 10^{-4} [9]. It is clear that a further decrease of the mechanical losses will directly benefit to the sensitivity of the detector. For this reason the search of new materials to be used for coatings having both low optical losses and low mechanical losses should remain one of the priorities of the R&D program. One of the main difficulties in this context is to find materials with lower mechanical losses without degrading the performances in terms of optical losses. Another option to reduce the mechanical losses consists in optimizing the thickness of the different coating layers (Ta_2O_5 and SiO_2). Since the Ta_2O_5 is the more lossy material, it is possible to reduce the mechanical losses of the multi-layer by reducing the amount of Ta_2O_5 and increasing the amount of SiO_2. For a given required reflectivity it is possible to find an optimum combination. Recently at LMA a mirror was coated using this technique and delivered to Caltech. The results obtained on the TNI experiment are positive. An evaluation of

	Input Mirror IM	End Mirror EM	Beam Splitter BS	Non degenerated Power and Signal recycling Cavities		
				PRM3/SRM3	PRM2/SRM2	PRM1/SRM1
Number of parts	4	4	2	3	3	3
Fused Silica Nature	Suprasil 3002	Suprasil 312	Suprasil 3001	Herasil 102	Herasil 102	Herasil 102
Diameter	350 mm	350 mm	550 mm	150 mm (TBC)	50 mm (TBC)	50 mm (TBC)
Thickness	200 mm	200 mm	65 mm	50 mm	50 mm	50 mm
Roughness Reflective side	<1 Å RMS	<1 Å RMS	<1 Å RMS	<1 Å RMS	<1 Å RMS	<1 Å RMS
RMS Flatness Reflective side	0.5 nm RMS (TBC) ∅ 150 mm	0.5 nm RMS (TBC) ∅ 200 mm	3 nm RMS (TBC) ∅ 250 mm	3 nm RMS (TBC) ∅ 100 mm	3 nm RMS (TBC) ∅ 20 mm	3 nm RMS (TBC) ∅ 20 mm
Transmission Reflective side	0.7 % (TBC)	# 10 ppm (TBC)	50 %	# 10 ppm (TBC)	# 10 ppm (TBC)	TBD

Figure 34: A summary of the main features of the AdV mirrors.

the inpact on the sensitivity curve is in progress. At the moment the reference solution for the coating design is the quarter wave stack as the AdV sensitivity curve is calculated with this assumption. Moreover, with a quarter wave design it is easier to adjust the reflectivity needed at the wavelength of the auxiliary laser used for lock acquisition.

The absorption losses of the coatings play also an important role as they determine the power absorbed in the test mass and thus the thermal lensing effect. The lower are the losses in the coating the lower is the required thermal compensation. Since the first generation of VIRGO mirrors the absorption in the coating has been reduced. An absorption level around 0.3-0.4 ppm is done currently on high reflectivity mirrors (IM, EM) thanks to the use of Ti doped Ta_2O_5. Nevertheless, due to the increase of the finesse, the absorption in the coating is likely to remain the main origin of the mirror heating. At the present time, we can not know if it is possible to decrease more this level of losses. R&D on coatings is needed to investigate possible paths to reduce them further. Due to the higher reflectivity of the input mirrors it will be important to check that the transmission of the two mirrors and, more critical, the losses in both arms are equal. Otherwise, the asymmetry in finesse and reflected power might be too large. Specifications for these parameters will have to be defined. In case the asymmetry is too large, then an imperfect AR coating on the other face of the substrate provides a way to improve the symmetry by tuning the reflectivity of the input mirrors. In case this is not required, 'perfect' AR and a wedge between the two faces of the substrates might be used. In both cases the specification for the AR coatings will have to be determined. In the second case the presence of larger wedges will have to be taken into account when designing the tools required both for the coating and for the metrology. The table in fig. 34 summarizes the main characteristics of the different type of mirrors for AdV.

8.4 Metrology

The metrology tools, necessary to completely characterize the Virgo mirrors, have already been developed for the first mirror generation (absorption, scattering, transmission, wavefront, radius of curvature, roughness, point defect detection). Since 2002, improvements of these benches have also been obtained. The size of the AdV mirrors will impose modifications of the several sample holders to be able to map the scattering and the absorption losses, because of the weight increase. But these changes will not be too expensive. Nevertheless, the new beam configuration in the AdV interferometer should also imply the use of a larger beam splitter (diameter greater than 400 mm). This dimension will induce considerably large and expensive modifications of the metrology mirror holders. Moreover, for the scatterometer for instance, we do not know at the moment if the manufacturer (SMS) will accept to do this modification. The beam splitter will be measured at 45° incidence (wavefront of each side and transmitted wavefront). The reproducibility and the reliability will be the same as the one for the measurements at 0° of incidence (RMS reproducibility of absolute measurement lower than 1 nm).

8.5 Cleaning

During the coating process the mirrors are cleaned several times. Due to safety reasons the cleaning procedures used for Virgo cannot be simply transposed to the larger mirrors that will be used in AdV. A different cleaning procedure will have to be developed. A new procedure has been identified by the team at LMA and its development had been already proposed and supported by EGO in the context of the 2nd R&D program. The implementation of this new cleaning procedure will require some investment at LMA. Before being sent to the site the mirrors will have to be protected against contamination and properly packed. Special boxes adapted to the larger size of the AdV mirrors will have to be procured.

8.6 Charge buildup

It is well known that the electrical charging of fused silica samples affects its mechanical losses. A degradation of Q is correlated with the charge on the surface. On the other side the random charges stopping inside the mirror induce a shot noise effect, which depends on the absolute value of the number of charges deposited (multiplied by the Z^2) and not on the net charge itself. Electric charges accumulating in the mirror generate in-fact spurious Coulomb forces between the masses and the surrounding apparata. This process may increment the noise level of the experiment. It is important that this effect could affect more the detector sensitivity in the case in which electrostatic actuators will be used.

8.6.1 Mirror Charge Control

The measurement of the net charge deposited on to the mirror can be performed by means of electrostatic driving electrodes facing the mirror surfaces. The charge can be measured by modulating the voltage of the electrode and measuring the coherent response at the modulation frequency of the mirror motion. Charge transfer can be then performed until the induced mirror displacement is minimized, yielding a neutralization of the charge. This charge measurement technique is conceptually easy to realize. A drawback is the difficulty in the determination of the overall mirror charge, because of the limitation of the measured charging electrodes size and distance from the mirror itself. The identification and selection of the most sensitive areas where to perform the charge measurement is a first task. Two parallel strategies can be followed to mitigate the charge accrual on the mirrors. On one side, UV light irradiation can be used to neutralize the total charge accumulated onto the mirror surfaces, when combined with a dedicated charge measurement technique. On the other side, making use of electrically conductive mirror coatings can ensure electrostatic homogeneity. Here we list characteristics, advantages and drawbacks of these two strategies.

UV light irradiation This is the technique currently used in LIGO, GEO600 and chosen for LISA. The charged mirrors are kept electrically neutral by irradiating with UV light the charged surfaces and/or the surrounding ones. Photoelectric emission produces electron currents from the illuminated surfaces, and the electrons can be then driven from one side to the other with appropriate biasing DC voltages, ensuring bipolar charge transfer. The conventional UV light sources are RF excited mercury vapour lamps and UV LEDs. UV lamps have been largely chosen in the past as the source for irradiation, they ensure a widespread spectrum of wavelengths (tens of nm), but they show several undesired characteristics, like fragility, power instability, sensitivity to temperature fluctuations, short lifetime (hundreds of hours) and, very important, they are sources of electromagnetic interference. UV LEDs have been recently identified as an alternative source and they have been successfully tested either for LIGO and LISA. The UV LED emission efficiency ensures photoelectric emission for several kind of materials and typical lifetime is in the order of 10^4 hours. UV LEDs allow the so called AC charge transfer technique, based on the On/Off fast modulation of the UV light combined with an in phase (or out of phase) square modulation of an electric bias voltage, which allows bipolar charge transfer.This technique has been successfully demonstrated and presents several advantages compared to the standard DC technique, first of all the possibility to modulate the UV light at frequencies far from the frequency band of the gravitational wave measurements avoiding low frequency drifts and instabilities. The only disadvantage of the UV LED is the narrow spectrum of wavelengths produced by a single diode. Selection of LEDs with the desired wavelength, based on the chosen mirror coating material, must be performed and the related properties must be investigated. The advantages and the efficiency of the implementation of a charge control system based on UV light are visible. A limitation of this charge transfer technique is the fact that, if the mirror surface is not electrically conductive, charge can be removed only from the irradiated surfaces, forcing to irradiate

with UV photons the whole mirror surface. Also, the role of surface reflectivity, which could limit the absorption of UV photons and thus the extraction of the electrons, must be considered as well as the geometry to be chosen for the illumination of the surfaces themselves. As an alternative, one could select the mirror areas most sensibly coupled, through the charge, to the surroundings, and focus the charge mitigation only on these areas. Finally, a possible drawback comes from the impact of UV light itself on the quality of the mirror surfaces and in particular on the mirror coatings, with related possible degradation.

Mitigation of the accumulated charge Conductive coatings can help to reduce the charge accumulation on the mirrors. The provided higher electrical homogeneity sensibly reduces the role of charge patches, that can be limited down to the level of few tens of mV in the case of metallic coating. It must be noted that, in case of a non-conductive mirror, the UV irradiation only ensures the neutralization of the total charge on to the mirror, but it does not cancel the presence of single charge patches localized in small portions of the mirror surface itself. Conductivity of the mirror surfaces makes more efficient the UV discharging scheme and it makes it simpler because the portion of the mirror surface to be illuminated is sensibly smaller. Drawbacks of such a coating are a possible degradation of the mirror mechanical quality factor and simultaneously the deterioration of its optical properties. For this reason the choice of the coating material is very important to find the best ratio between the gain introduced by the surface conductivity and the limitations introduced by its mechanical losses or the optical properties.

8.6.2 Status of R&D

A study on the charge buildup has still to be started within the Virgo project. For GEO600 and LIGO great work has been performed on the UV discharging and on the conductive coating strategy. An R&D activity in the Virgo frame has to start from these experiences. Two main tasks are to be investigated:

- **Simulation approach**
  A study is needed to take in account the interaction between a charged test mass with the surrounding apparata to estimate the level of the noise that can be introduced by the charge, and to try to find a strategy to minimize its effect. On the other side it is needed to estimate the noise induced by the charge shot noise on the electrostatic actuators in case they will be implemented for AdV.
- **Measurements**
  Few tasks are quite important to be investigated to have a complete overview of the charging effect on the detector and to minimize its effect. The followings are the most urgent:
  - *Effect of charge on Mirror Q degradation*
    It has been demonstrated that charge has a role in the mirror Q degradation, this effect induces a rubbing friction between the mirror and a piece of dust

attracted by the charged sample that appears as a Coulomb damping. A facility has to be developed to directly measure this effect and to better minimize it.

– *Charge measurement and control techniques*
The charging of the masses has to be monitored to be discharged and to decrease its noise level. The geometry of the measuring system has to be evaluated to reduce the "patch effect".

– *UV light-Mirror coating interactions*
There is an indication that the UV light could damage the coating surface changing its absorption and reflectivity. A direct measurement of it is important to chose the better strategy to be followed.

– *Effect of Mirror coatings on the Q factor*
The possibility to have a conductive coating to reduce the charge effect is an open question and one of the most discriminant between this and the UV light will be the effect of a coating with these characteristics on the mechanical Q of the optics.

9 Thermal compensation

The TCS will correct for a wide range of thermal effects in several optics. While R&Ds to reduce the coating and substrate absorptions are ongoing, TCS provides great flexibility for corrections in case some optics does not meet the specifications. In addition, TCS provides an online tool for correcting mirror radius errors, and can be used to suppress acoustic parametric instabilities [168]. For these reasons, TCS should be designed with as much flexibility as possible.

9.1 TCS design

In the test mass, the optical power is predominantly absorbed by the HR coating and converted into heat, producing a gradient of temperature inside the substrate. Two different effects originate from the heating of the test mass:

- nonuniform optical path length distortions (thermo-optic effect, also termed thermal lensing) mainly due to the temperature dependency of the index of refraction.
- change of the profile of the high reflective surface, due to thermal expansion (thermo-elastic deformation).

In the case of Virgo/Virgo+ the main thermal effect is the thermal lensing, affecting the Power Recycling Cavity (PRC): in presence of thermal lensing, which changes the cavity mode, the input laser no longer matches the PRC cavity, the coupling coefficient between the laser TEM_{00} and the cavity TEM_{00} is less than one. In the case of Advanced Virgo, the other thermal effect will also be relevant due to the much higher circulating power in the FP cavities. Thermal expansion will change the profile of the high reflective surface. A bump will raise in the center of the test mass faces, making their surface profile non-spherical. Given uniform absorption at the .5 ppm level expected in advanced detectors, this departure from sphericity will not make the arm cavity resonant modes significantly non-Gaussian. The cavity becomes less concentric, and the spot sizes at the mirrors will shrink. The resulting increase of thermal noise has been estimated to be of the order of 15% [76]. To maintain the arm cavity mode structure, it is necessary to control the radii of curvature of all test masses.

The thermal effects will then create distortions both in the recycling and in the Fabry-Perot cavities:

- wavefront distortions in the SRC and PRC cavities;
- HR surface elastic deformations in both ITMs and ETMs.

TCS needs to compensate for both effects.

A TCS has been installed in Virgo+, based on a pre-stabilized CO_2 laser projector, that shines a heating pattern onto the HR surface of both the input mirrors. The power stabilization level, necessary to be compliant with the Virgo+ sensitivity requirements, has been estimated to be of the order of $10^{-7}/\sqrt{\text{Hz}}$ @ 30 Hz [77].

It has been shown [78] that, in principle, it would be possible to act with a CO_2 laser on both faces of the ITM and correct both wavefront distortions and HR surface deformations. But, in order to keep the TCS noise below the sensitivity, it is necessary to reduce the RIN of the CO_2 laser at the level of $10^{-8}/\sqrt{\text{Hz}}$ @ 50 Hz. This level of RIN is one order of magnitude below what it is possible to achieve.

Thus the necessity to introduce a new transmissive optic (Compensation Plate), placed in the recycling cavity, which to act on with the CO_2 laser. Since CPs live entirely within the recycling cavity and have no HR surfaces, the effect of the actuator noise is much less important on a CP than on a test mass. The coupling of the carbon dioxide laser noise to the IFO noise is much lower. Calculations of the noise coupling of the CP have been performed [79] and show that the power stabilization level required would be of the order of $10^{-6}/\sqrt{\text{Hz}}$ @ 100 Hz, less stringent than the Virgo+ case.

The CP can effectively correct only the wavefront distortions in the recycling cavities. To control the radii of curvature of the test masses, a shielded ring heater (RH), placed around each TM, will be used.

Thermal effects can arise also in the beam splitter. If the BS contribution to thermal lensing in the recycling cavities is small, its effect could be compensated by the compensation plates. The need for a direct compensation of the BS must be further investigated.

The reasons to prefer a CO_2 laser projector instead of a heating ring to heat the CP are:

- CO_2 laser projector can compensate non-axysimmetric thermal lensing;
- most of the apparatus lives outside vacuum and can be easily upgraded as new understanding of the ITF is realized.

These considerations naturally lead to a TCS scheme that closely follows the concept from Advanced LIGO. Figure 35 shows the scheme of the AdV TCS using both CO_2 lasers and heating rings.

9.2 Compensation plate

The CP interacts directly with the interferometer beam. As such, it must satisfy requirements like those of a core optics with respect to displacement noise, absorption and scattering, index homogeneity, antireflection coatings, and the like. In order to minimize etalon effect in the CP, a wedge of about 10 arcminutes is foreseen. The noise injected by an individual CP is injected only into a single arm of the recycling cavities. Because the CP has no HR surfaces, the noise motion requirements for the CP are relatively modest. In particular, the IFO should exhibit no sensitivity to motion of the CP along the beam axis (see next section). Because the CP will be wedged, there will be sensitivity to transverse motion. The transverse noise requirement is shown in fig. 36. Since the CP is foreseen to be attached to the ITM reference mass, this requirement is expected to be easily met. The most feasible solution is to fix the CP on the back of the reference mass. Since the clear aperture due to the coil-magnet actuators on the back of the RM is 280

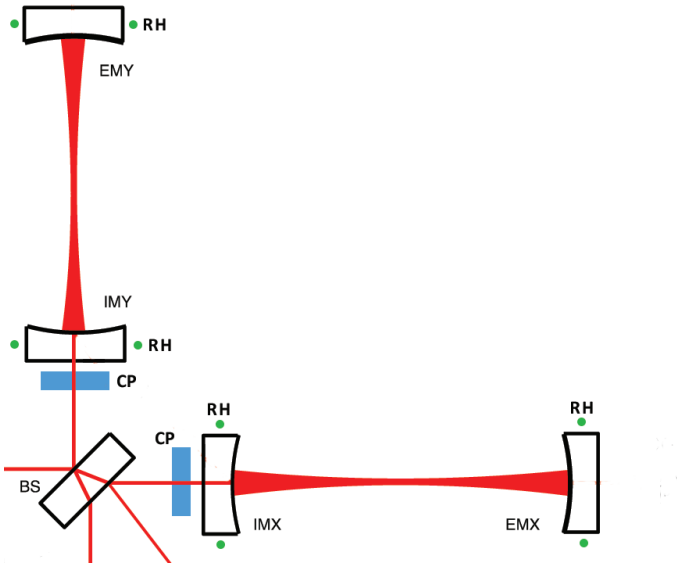

Figure 35: AdV TCS layout: the green dots represent the test masses shielded ring heaters, the blue rectamgles represent compensation plates.

mm, a maximum diameter of 280 mm for the CP is foreseen. The thickness will be of about 10 cm.

The internal thermal noise of the CP must satisfy the same requirement. The internal thermal noise of the CP is estimated to be more than an order of magnitude below the noise exiting the arm cavity [80].

9.2.1 Influence of the CP on Alignment and Longitudinal controls

Longitudinal controls

An Optickle [152] simulation has been set up with the same parameters used for the LSC design. The compensation plate is modeled by a simple mirror with 100 ppm reflection (to simulate the anti-reflection coating on the two surfaces), without any wedge (worst case), placed behind the IMX, inside the power recycling cavity. The compensation plate is free to move indipendently from the other optics. The simulation computes the transfer function (including radiation pressure effects) from CP motion to all longitudinal error signals and to the main gravitational channel.

The results show that the coupling to the auxiliary degree of freedom error signals is negligible. The transfer function from CP motion to the gravitational channel is shown in fig. 37.

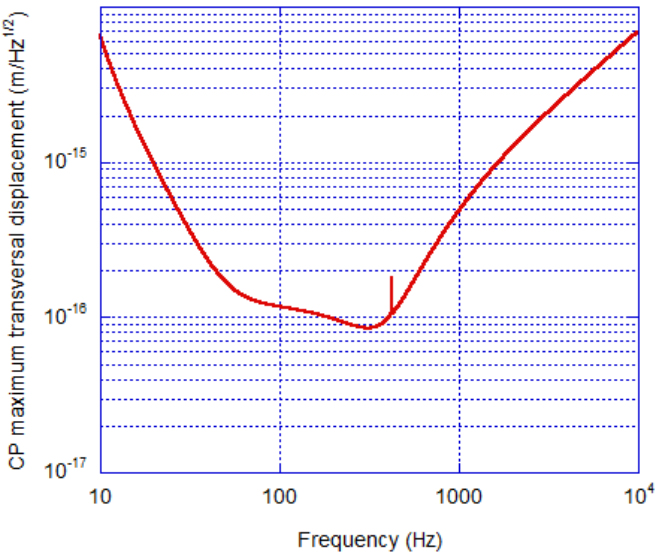

Figure 36: CP maximum seismic transversal displacement. Calculations have been performed considering a wedge of 10 arcminutes and a safety factor of 10 wrt the AdV sensitivity.

To estimate the amount of noise injected by CP, the following very conservative estimate of CP motion has been computed. The reference mass motion is dominated by the correction sent for the longitudinal control of the arm cavities. It is assumed that the arm locking will act also on the input mirror, using the same level of correction needed for Virgo. The correction is calibrated to compute the induced mirror motion, which is the same of the RM if the two have the same mass. The effect on the gravitational channel is again shown in fig. 37.

In addition, it has been noticed [81] that if a plate with faces perpendicular to the beam is moving longitudinally in a cavity, it induces power fringes; with 100 ppm AR coating, the relative power variations will be 4%, on a time scale of 1 s. These variations may fool the DC locking of DARM. The way to avoid this effect is to have a wedged or tilted CP.

In conclusion, CP motion coupling is small enough to give a contribution slighlty below the design sensitivity even if the CP motion is over-estimated as explained. Moreover, the use of wedges or tilt will further reduce the effect, since reflected beams will not completely recombine with the main beam.

Alignment

The effects of the presence of a CP on the Automatic Alignment control system have been simulated by modeling a single cavity with Finesse and introducing a 100 ppm mirror with a 1 deg wedge (worst case) behind the IMX mirror.

The first effect studied is the CP etalon effect, considering the worst case without wedge.

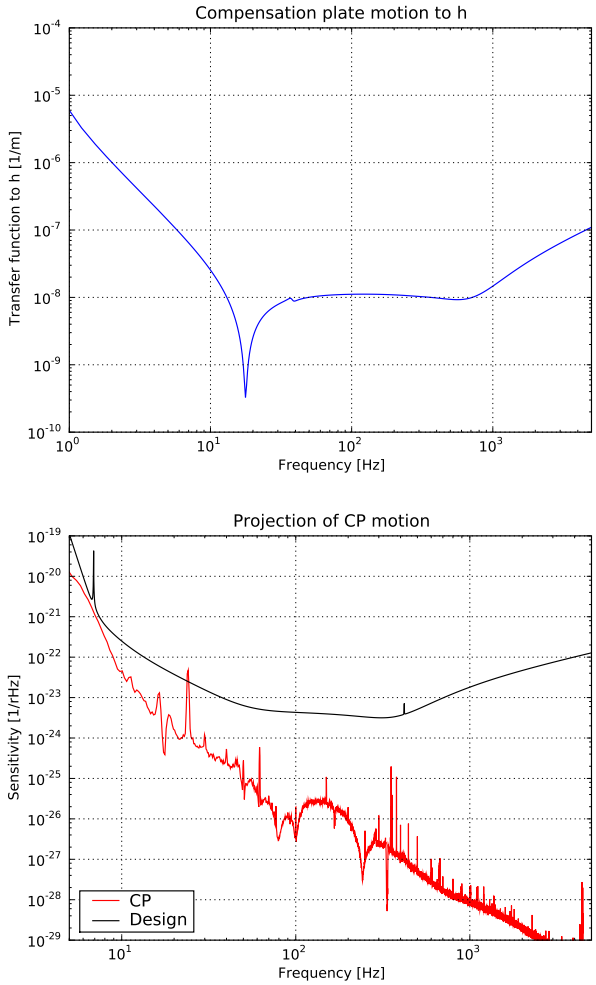

Figure 37: Results of simulation of CP motion coupling. The top plot shows the transfer function from CP motion to the gravitational channel. The bottom plot shows a projection of CP motion in h, using the conservative estimate explained in the text.

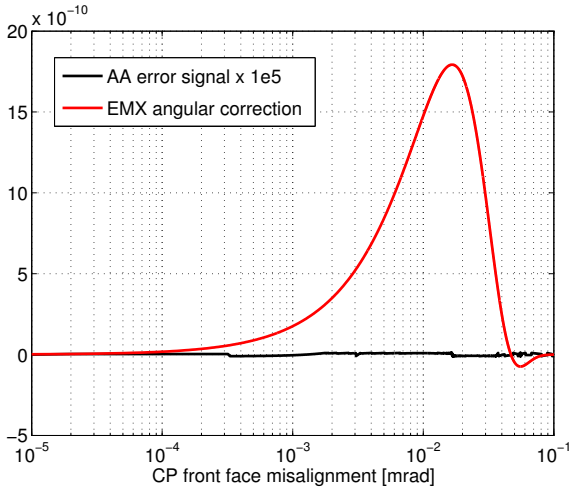

Figure 38: Effect of the CP front face misalignment on the automatic alignment error signal, which produce an equivalent cavity angular displacement up to nrad. The solution is to angularly displace the CP front face more than 1 mrad with respect to the IMX front face.

The etalon tuning produces a very small optical gain variation on the Automatic Alignment error signals, of the order of 1 per thousand.

The major consequence of using a wedged compensation plate arises when the face of the CP looking at the F-P cavity is slightly misaligned with respect the IMX HR face. The misalignment produces an amount of higher order modes which corresponds to a not minor cavity mirror misalignment. If we lock the cavity, longitudinally and angularly, a CP front face misalignment induces the Automatic Alignment control loop to misalign the cavity mirror, as it is shown in fig. 38, of about 1.5 nrad for a 10 μrad of CP misalignment. Moreover it has to be noticed that this effect disappears for CP misalignment larger than 0.1 mrad, thus in order to avoid it the CP front face should be misaligned, with respect the IMX front face, more than that.

The thermal effects on the CP mirror, which essentially modify the ROC of the CP to $\sim$ 2700 m, when the ITF is operated at full power, do not introduce strong variations on the previous results, see fig.39.

From the above considerations, a tilted CP must be used. Since the compatibility of highly wedged optics with non degenerate recycling cavities is under investigation, at present the new reference mass design takes into account a CP tilted of about 1 deg with respect to the ITM, with a small wedge (of the order of 5 arcminutes) to reduce etalon effect in the CP itself.

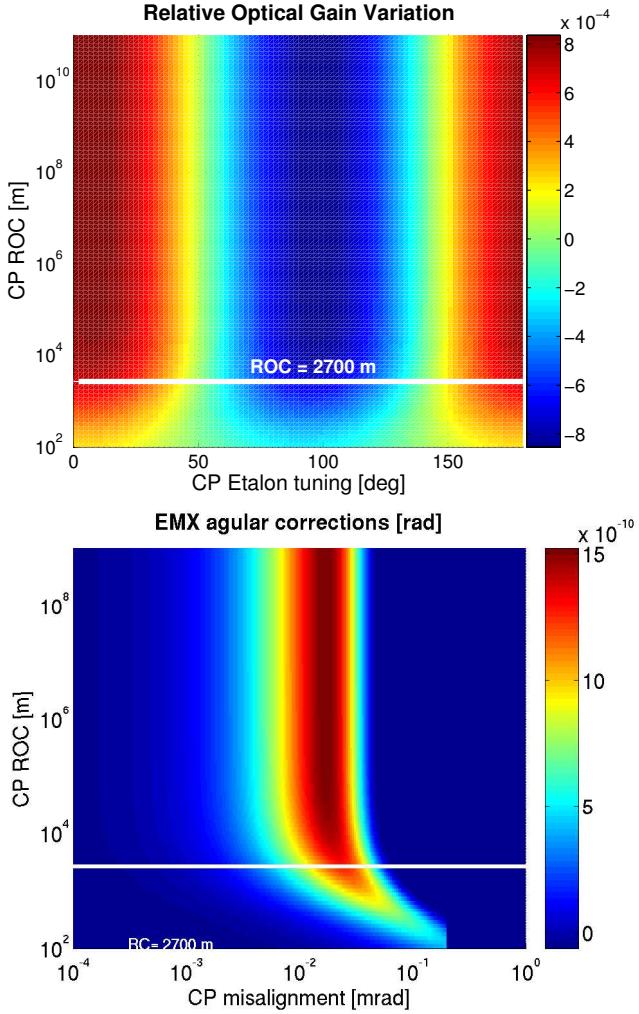

Figure 39: Consequences of the Etalon tuning and CP misalignment (top and bottom plot respectively) considering the thermal effects, which modify the CP radius of curvature. Increasing the thermal effects, thus decreasing the CP ROC, the aftermath on the alignment error signals are diminished due to the spoiling of the CP-IM cavity.

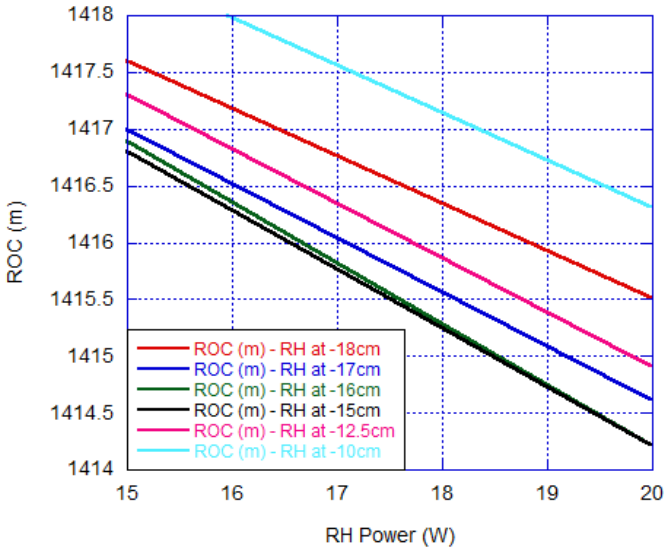

Figure 40: The plot shows the ROC of the TM as a function of the RH power for different positions along the TM side.

9.3 Test mass shielded ring heaters

While CP will only compensate thermal aberration effects in the recycling cavities, compensation and control of the test mass HR surfaces could be done by shielded ring heaters, embedded in the reference mass. There would be four of these: one around each test mass, toward the AR face. The test mass ring heaters would control the arm cavity mode shape. The input mirror ring heaters would also provide limited compensation of thermo-optic effect in the recycling cavities. The test mass ring heaters might also be used to temperature-tune away radiation-pressure parametric instabilities [168].

To study the effect of the ring heater, we first considered the case of a simple ring heather placed around the TM, heated by the YAG beam. As an example we show in fig. 40 the TM ROC as a function of the RH emitted power and of its position along the side of the TM. It is possible to notice that if the position of the RH is at about 15cm from the TM HR surface, the power required to recover the ROC of 1416m (ITM ROC, see Table 5.3.4) is minimized. This would minimize any heating of the reference mass. It must be underlined that the simple ring heater is a very unefficient solution, since only a small fraction of the emitted power reaches the TM. By putting the ring heater into the focus of a parabolic reflecting shield, the amount of emitted power reaching the TM would increase, thus decreasing the required total emitted power, and avoid unwanted heating of the reference mass.

The design with the RH around the TM is less sensitive to actuator noise fluctuations than designs that heat the HR surface, because the heating is entirely on the substrate far from the ITF beam, and the radiation pressure averages to zero over the test mass. However, there is a slight coupling of overall power fluctuations to HR surface displacement. A test

mass ring heater changes the radius of curvature of a test mass's HR surface by flexing the mirror. Since the position of the centre of the HR surface relative to the test mass centre of gravity varies with the flexure, any power fluctuation in the ring heater will create displacement noise [79]. The ring heater thermal inertia will passively smooth power fluctuations on its input supply, this should make easier to meet the noise requirements. Simulations to optimize the geometry, position and shielding of the RH are in progress.

The ring heater can in principle compensate for thermal aberrations in the recycling cavity, as demontrated by Ryan Lawrence [82], thus avoiding the use of CPs and CO_2 laser projectors. But it cannot compensate at the same time for both thermal lensing and thermal effects in the Fabry-Perot cavity. Moreover, it cannot compensate wavefront distortions in case of non-uniform absorptions.

9.4 TCS sensors

Each piece of optics with a significant thermal load should be independently monitored. The HR face of each test mass could be monitored in reflection for deformation. The TM/CP phase profile could be monitored on reflection on-axis from the recycling cavity side using a Hartmann sensor. On-axis sensing would require that the probe beam enters the recycling cavity through a pickoff port, such as the wedged AR face of the beamsplitter. The group led by Jasper Munch at the University of Adelaide, Australia, has been developing a Hartmann sensor for the Gingin experiment and as a potential wavefront sensor for Advanced LIGO. This latter device has been demonstrated to have adequate precision for Advanced LIGO. The University of Adelaide's Hartmann sensor [83] has been demonstrated to have a shot-to-shot reproducibility of $\lambda/580$ at 635 nm, which can be improved to $\lambda/16000$ with averaging, and with an overall accuracy of $\lambda/6800$. The use of the Adelaide Hartmann sensor in AdV is desirable.

9.5 Status of the related R&D

The definition of the TCS of AdV can benefit of the many years of R&D already performed by LIGO [82, 80]. The results obtained by LIGO are available. In consideration of the state of advancement of these R&D, Virgo has opted to rely as much as possible on LIGO research, and concentrate his effort to investigate those aspects of thermal lensing correction not yet fully studied.

Last spring, an R&D program has been proposed to EGO Stac [84, 85]. This R&D has been evaluated as necessary for AdV. The activity consists of development of Finite Element Analysis (FEA) and measurements of thermal effects induced in the optics and their compensation:

- **Finite Element Modeling**
  FEA is necessary to determine the amount of thermal effects both on the TM and in the CP and the compensator parameters (such as dimensions of the CP, profile and power of the CO_2 beam, dimensions and power of the heating ring).

The FEA modelling also serves as consistency check for the measurements results. This modeling effort is in a well advanced state and has already supplied useful indications to define the TCS parameters.

- **Measurements**
  The efficiency of a scaled down prototype compensator (CP heated by CO_2 laser and shielded heating ring on TM) in correcting at the same time both wavefront distortions and thermo-elastic deformations will be measured. The possibility to monitor both thermal effects will give information for the development of a closed loop control scheme. Other issues will be addressed with the proposed R&D program. For example, an ellipticity in the shielded ring heater can cause deviations in the phase profile of a compensated optic at large radii. The measurement will give information on the geometric tolerances of the system (ellipticity, centering). In the frame of this R&D we also plan to define a dedicated wavefront sensor to be implemented on Advanced Virgo. The University of Adelaide (Australia) is investigating the possibility to increase the performances of the present Hartmann sensor and improve some weakness of the previous design, such as drift due to temperature variations. A prototype is planned to be ready in a timescale of 1 year. We propose to characterize this sensor to verify the possibility to use it as a TCS dedicated sensor in Advanced Virgo.

The experimental activity will start as soon as the requested budget is delivered.

9.6 Directional Radiative Cooling

A possible alternative solution to thermal effects would be to eliminate the beam deposited heat at the source (the stored beam spot) before it has a chance to deform the mirror, rather than mitigating its effects with a counter-deformation. This could be done by directional radiative cooling of the beam spot [86]. Figure 41 shows a conceptual scheme of this compensation system. The trick is to image a sufficiently cold black body, like a liquid nitrogen cooled target, on the beam spot (but not on the rest of the mirror), from a sufficiently large solid angle. The total emispheric emitted power from a 6cm radius spot is around 4.4W at a wavelength of about 10μm. It has been calculated that a solid angle coverage of a quarter to one steradian is sufficient to collect the expected power absorbed by the TM ($\sim$0.5W). By placing parabolic collectors in front of the cold targets (see fig 42), their dimensions could be reduced to 5cm [87].

The efficiency of Directional Radiative Cooling (DRC) as a thermal compensation system has been analized with ANSYS thermal simulations [88]. A perfect cooling profile has been assumed:

- Gaussian profile exactly matching the heating profile;
- capable of extracting (from the HR surface) all the absorbed power from the test mass (0.4W in the coating plus 0.1W in the substrate).

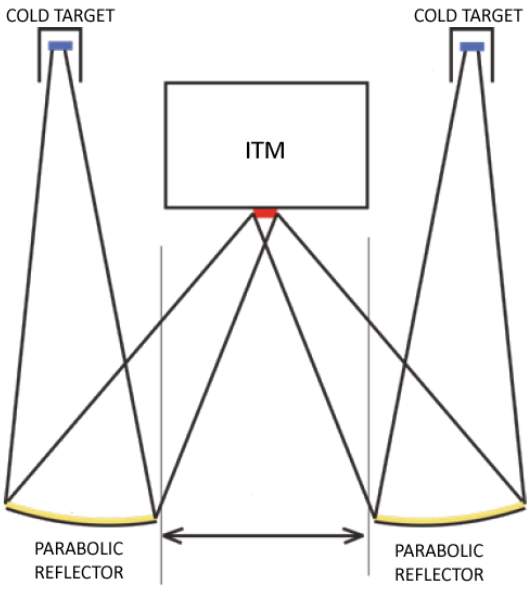

Figure 41: Conceptual scheme of the Directional Radiative Cooling.

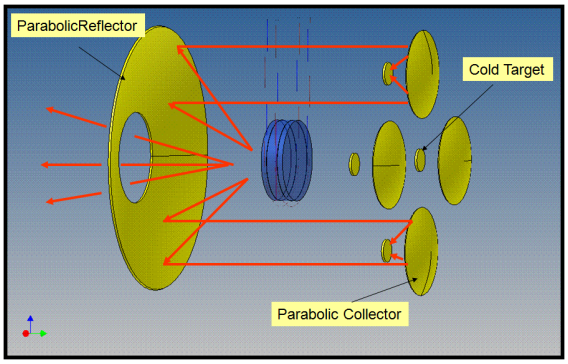

Figure 42: Conceptual scheme of the Directional Radiative Cooling that makes use of parabolic collectors to reduce the size of the cold spot.

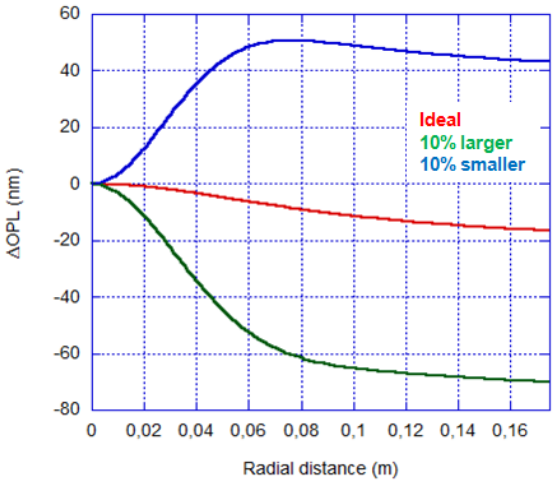

Figure 43: Optical path length increase for a perfectly matched profile (red curve) and mismatched by ±10% (green and blue lines).

The results are that the perfect DRC is efficient in correcting at the same time both wavefront distortions and changes in the radii of curvature of the TM. The performances have also been tested in the case of a non perfect match between the cooling and heating profiles, introducing a difference of ±10% in the waist. The result is shown in fig 43, where the optical path length difference is plotted for the three cases. The analysis shows that a 10% mismatch corresponds to an increase of the residual lensing of one order of magnitude.

DRC is a new idea (a proof-of-principle experiment has been performed [86]) and a simulation activity both optical (Zemax) and thermal (ANSYS) is ongoing. In the meanwhile, new measurements under vacuum with different setups are needed. These activities aim to give answers to some important issues:

- how to produce a Gaussian profile exactly matching the heating profile;
- what if the absorptions in TM are not uniform;
- how to efficiently tune the cooling power without introducing noise.

Most of all, it is necessary to investigate those issues directly related to the AdV requirements:

- scattered light: is the presence of large reflectors placed in front of the TM at small angle (∼20°) compatible with AdV specifications;
- since most of the apparatus lives in-vacuum, how to make it more flexible, to be easily upgraded as new understanding of the IFO is realized.

All these issues must have a positive answer before DRC can be taken into account as the TC System for AdV.

10 Detection system

This section starts by describing the AdV features which will have consequences on the detection system. Then it focuses on components of the detection system which should be modified.

This section focuses on the foreseen changes of the detection system. Unless specified, the current design applies.

10.1 AdV features impacting the detection system

The following subsections described the changes of the optical layout from Virgo/Virgo+ to Advanced Virgo will require modifications of the detection system

10.1.1 DC detection

The main motivation for selecting the DC readout scheme is a smaller (about 20%) shot noise with respect to the AC readout. There are also advantages for technical noises:

- There is no demodulation noise which is usually one of the dominant source of noise at high frequency for the AC readout.
- There is no frequency noise due the asymmetry of losses into the Fabry-Perot cavities which is one of the limitations for AC readout at high frequency. The frequency noise due to finesse asymmetry is the same as in the AC readout case.
- Larger photodiodes can be used since no demodulation is needed. They simplify the beam alignment and reduce the power density. They also make the detection much more insensitive to environmental noise coupling via beam jitter. Large photodiodes have the drawback of a large capacity which reduce the signal bandwidth and therefore when using a AC readout scheme, the size of the photodiode is limited. In the DC readout case this limitation is removed, at least for the photodiode sensing the dark fringe beam.
- The problem of reduced spatial overlap between the carrier and the sidebands is also not present with DC readout.

Switching to a DC readout scheme for the arm's differential control has several consequences on the detection system:

- The sidebands should be removed from the dark fringe by means of the Output Mode Cleaner (OMC) so that their contribution to the dark fringe is small enough (less than few %) and they do not increase the shot noise. This requirement is not compatible with the current OMC design which should transmit the sidebands and therefore the OMC must be changed.

- Since the power noise of the sidebands is not filtered by the double cavity even a small sideband contribution can be a limitation at high frequencies. Furthermore in Virgo the power is stabilized after the input mode cleaner using a photodiode located under vacuum. However the power noise observed in the interferometer (currently the B5 photodiode which will be the POBS beam in AdV) is relatively high at low frequencies (below 50 Hz) due to the noise introduced by the control loops (the power recycling longitudinal control in the Virgo case). It seems therefore necessary that the power stabilization uses as error signal a measurement of the power stored inside the recycling cavity for the low frequency part (below 50-100Hz). Using such a beam for the power stabilization will imply to seismically isolate these photodiodes and to put them under vacuum.

More details on technical noises in the case of AC or DC readout can be found in [89].

DARM offset: In the DC readout scheme a small offset is added to the dark fringe working point so that the DC channel of the dark fringe is sensitive to the gravitational wave signals. In first approximation the DC power on the dark fringe is given by:

$$P_{\mathrm{car}} = \frac{P_0 G}{2}\left[(1-C) + \frac{1}{2}\left(\frac{8\mathcal{F}}{\lambda}L_{\mathrm{off}}\right)^2\right] \tag{23}$$

where P_0 is the input power, G the effective recycling gain, C the contrast, $\mathcal{F}$the finesse, L_{off} the offset. The offset should be tuned so that the contribution of the contrast defect is small enough. Assuming a contrast defect as good as for Virgo (few 10^{-5}) and given the high finesse of AdV (~ 1000) an offset as small as $5 \cdot 10^{-12}$ m could be used. This offset also has to be kept well above the locking accuracy (it is of the order of 10^{-13} m in Virgo, see more in the interferometer sensing and control section). The offset should not be too high in order to keep the carrier power noise under control: the power noise increases quadratically with the offset while the optical gain only increases linearly. The baseline value for the DARM offset is 10^{-11} m (see table 12).

10.1.2 Signal Recycling

One additional longitudinal degree of freedom, the signal recycling cavity length, has to be controlled. This changes the length sensing and control scheme and additional modulation frequencies will be added (see the Interferometer sensing and control section). The modulation frequencies for the control signals are now going up into 80MHz range (see table 12), a factor 10 higher than the current value. This will have an impact on the photodiodes and associated electronic used for the controls.

10.1.3 High power

The input laser power will be increased but this does not translate to a direct increase of the power seen on the output ports of the interferometer thanks to the signal recycling scheme and the tuning of the optical parameters. Assuming the parameters of the table 12

the power expected on the dark fringe beam after the OMC, and therefore the suppression of the side bands and higher order modes, could be computed using the Finesse and Optickle simulations. The value found (see table 5 of [158]) is of the order of 100mW. Since the current photodiodes could stand up to 100mW per photodiode this indicate that we can still use just a couple of photodiodes for the main dark fringe beam ("AP").

For the other beams, there will be a power increase. However, we are usually not shot noise limited and therefore this is not really an issue.

During the locking procedure or unlock events, the power seen by the photodiodes change a lot. Fast shutters and systems to remotely adjust the maximum power impinging on the photodiodes are therefore required and the existing shutters may have to be upgraded.

10.1.4 Non Degenerated Recycling Cavities

With the non degenerated recycling cavities a folding mirror and the signal recycling mirror will have to be placed "on" the detection bench. These are sensitive objects which require a seismic isolation level better than the one needed just for the output mode cleaner (see [159]). This will impact the layout of the suspended detection bench and its seismic isolation. Space will be required, although space will be gained since the non degenerated recycling cavities solution provides at the same time part of the beam matching telescope.

A side effect of the use of folded Non Degenerated Recycling Cavities and the change of the BS wedge is the difficulty of sending the POBS beam on the suspended detection bench. This beam is currently used to check the alignment of the suspended bench and therefore the alignment of the OMC. This will have to be evaluated as part of the detailed optical design and alternate solution(s) based for instance on the POSR beam have to be investigated.

10.1.5 Back scattering mitigation

Due to the improvement of the sensitivity, additional care should be taken with the issue of the backscattering. A study [146] has shown that the main requirement is to put/keep the AP photodiodes under vacuum on the suspended detection bench. Improvements of the mechanical structures of the end benches and external bench are required too.

10.1.6 Long term maintenance

By extending the life of Virgo, AdVirgo requires a continuous effort to maintain the various components (hardware and software) up-to-date with enough spare parts. Experience has also indicated that more flexibility is appreciated and triggers redesigns. This is especially true for the photo-detectors and the associated electronic, as well as the software.

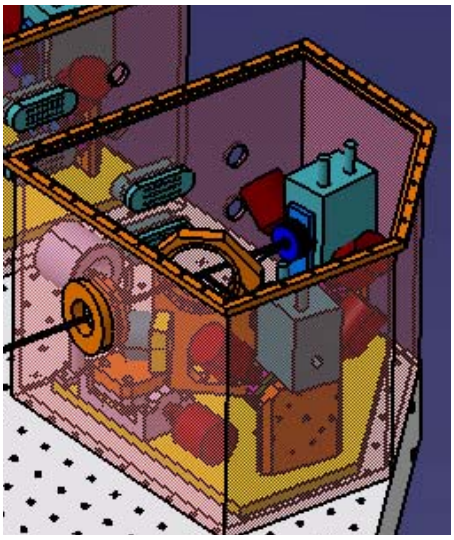

Figure 44: Drawing of the box hosting the B1 photodiodes for Virgo+ (AP photodiodes for AdV).

10.2 Photodiodes

The electronic of the photodiode will have to be redesigned in order to work with the new modulation frequencies and to provide all the needed demodulation signals.

As part of the Virgo+ effort to mitigate the seismic and acoustic noises, work is ongoing to put under vacuum the photodiodes reading the Virgo dark fringe beam ("B1" or AP in AdV labbelling) and recycling cavity beam ("B5" or POBS). Given the limited time/resources available for the Virgo+ preparation, the selected solution (see figure 44) was to build airtight tanks to host all the non vacuum compatible elements: the photodiodes themselves, their pre-amplifiers, the stepper motors used to fine positioned them, the shutters to protect them and the associated beam dump used during lock acquisition.

Such big boxes are nevertheless not very flexible and use space on the suspended bench. Therefore the development of vacuum compatible components (photodiode, preamplifiers, shutters) is needed for AdV. The use of airtight tanks will be the backup solution.

The monitoring and alignment system will have to be upgraded to support the operation of the photodiode under vacuum.

It has to be mentioned that since the number of existing photodiodes is limited and since they are no more produced it is foreseen to search for new photodiodes as part of the long term maintenance. These photodiodes will have either larger surface for the dark fringe beam after the output mode cleaner or larger bandwidth for the control signals.

	F_{OMC}	l_{opt} (cm)	l (cm)	ρ (cm)	w_0 (μm)	f_{sc}	$\theta_{i,max}$ (deg)
AdV baseline	100	21.4	7.4	60	220	0.6×10^{-6}	18
F=400	170	21.4	7.4	60	220	1.7×10^{-6}	18
$f_2 = 50$ MHz	160	21.4	7.4	150	280	0.9×10^{-6}	14
m=0.2	200	21.4	7.4	60	220	2×10^{-6}	18

Table 11: Characteristics of a monolithic cavity. F_{OMC} is the OMC finess, l_{opt} the optical length, l the geomtrical length, ρ the radius of curvature of the curvate surfaces, w_0 the waist, f_{sc} the fraction of light back-scattered by the OMC, $\theta_{i,max}$the angle of incidence on the mirrors. The first line is for the AdV baseline parameters, the second line with the arm cavity finesse reduced to 400, the third one corresponds to a reduce modulation frequency of about 50MHz instead of about 80MHz, the last one for a modulation index of 0.2 instead of 0.1.

10.3 The Output Mode Cleaner for AdV

Virgo is currently using an OMC which is a triangular monolithic cavity of 2.5 cm with a finesse of 50 which filters the high order geometrical modes but transmits the sidebands. As discussed previously, a new output mode cleaner has to be designed to get ride of the sidebands in the DC modulation scheme adopted for AdVirgo.

The parameters to be defined are: the finesse, the length, the waist, the geometry and the type of cavity (either a monolithic OMC as used in Virgo or an OMC consisting of individual mirrors rigidly connected by a spacer).

The main issues in the OMC design is first the finesse should be set so that the losses inside the cavity are not too high. Then, since DC readout will be used the output mode cleaner has to filter not only the carrier higher order modes but also the sidebands from the modulation frequencies and their higher order modes in order to keep a low shot noise. The light back-scattered by the cavity should be low enough in order to avoid to add any phase noise to the sensitivity. The use of a monolithic cavity will be decided on the basis of the needed length but also on the induced additional losses and thermal effects. It is also assumed that a four mirrors ring cavity will be used in order to be compliant with Higher Order Laguerre Modes.

The Virgo note [147] discusses the OMC design and presents different solutions. In all cases the cavity is small enough so that a monolithic cavity can be used. The baseline approach is therefore to select the OMC geometry by taking a geometrical length of 7.4 cm and then to adjust its finesse according to the final choice of AdV optical parameters and modulation frequencies. The table 11 present valid OMC solutions for various AdV options. With these solutions, the sidebands contribute to less than 1% of the shot noise and the losses in the OMC are expected to be less than 1%.

Let us add that an R&D program is ongoing to test a monolithic mode cleaner with the Virgo geometry but with a higher finesse. The result of this study will help us in the fine tuning of the OMC parameters design.

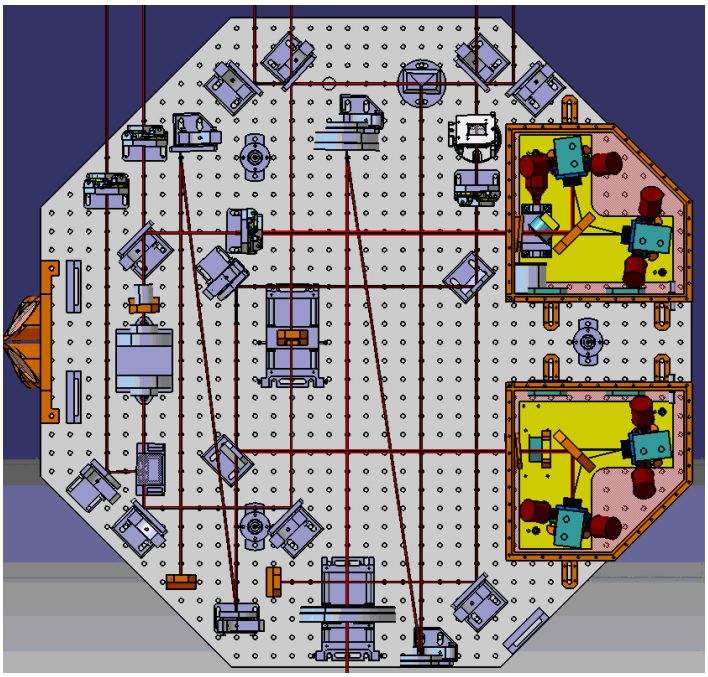

Figure 45: Layout of the Virgo+ suspended detection bench with the photodiode (right part). The OMC is in the lower left part of the bench. The central part is used for the input telescope.

10.4 Detection benches layout

The layout of the detection benches will have to be updated to accommodate the changes required for the AdV optical design.

10.4.1 Suspended detection bench

The most critical bench is the suspended detection bench which is under vacuum and has the prime task of providing the right environment for the output mode cleaner. The figure 45 presents the layout of this bench in the Virgo+ configuration once the photodiodes will be installed under vacuum. This layout has to be changed to accommodate at least:

- The folding mirror of the signal recycling cavity and the signal recycling mirror. These mirrors will have to be suspended, either from a structure attached on the

suspended bench or from the marionetta located above the bench. The design of these local suspensions will have to be carried out by the DET subsystem (together with INJ and PAY). This is in addition the required increase of seismic isolation which could be given by one or more filter stages (see the superattenuators section). The required controls elements will add complexity on the detection bench although we will recover some space from the current input telescope.

- The larger OMC. Even if its length is only 7cm long, its oven used to control will require a little more space than the current 2.5 cm long OMC.
- As part of the commissioning activities, baffles and beam dumps have been added to dump the secondary beams produced by the optical elements. Some baffles are directly put on the detection bench and other are just attached around the bench to the vacuum chamber. The upgrade for AdV is the opportunity to have a better design which integrates them onto the suspended bench to benefit of the seismic isolation.

All this will have to be accommodated on the detection bench. It is too early to state if the space available on the top of the bench will be enough or if additional space like the bottom part of the bench will have to be used. Nevertheless, this is a problem which could be solved once the elements to install on the suspended detection bench will be better known.

This reorganization is a good opportunity to apply to the suspended detection bench some of the improvements foreseen for the clean air distribution in the large mirror vacuum chambers.

10.4.2 External detection bench and other benches

The external detection bench will have to be reshuffled to accommodate the new layout of the suspended bench. The mechanical structure will have to be reinforced to avoid resonances at low frequency (below about 50 Hz) and to reduce the noise from the air conditioning system. This also the right time to revisit the cleanliness of the bench.

Similar work as to be made for the end benches.

Since new pick-off beams from the input mirror or beam splitter will be available, they will require small additional optical benches to host the required photodiodes, cameras or other devices.

11 Interferometer sensing and control

11.1 Sub-system scope

The role of the Interferometer Sensing and Control (ISC) system of AdV is to define the required techniques to maintain the correct resonant condition of fields corresponding to the five main lengths inside the interferometer, and define a technique to maintain the alignment of the eighteen angular degrees of freedom. The ISC sub-system also produces a lock acquisition technique, and defines a solution to mitigate the parametric instabilities.

The details on scope, tasks, quality assessment, partition of tasks between design requirements and preliminary design, inputs and outputs with other sub-systems are found in [148]. The design requirement phase is almost finished, and the preliminary design is well advanced.

11.2 Operating point

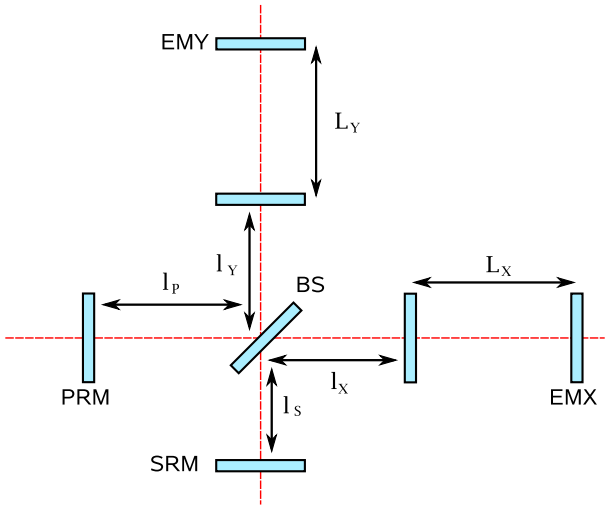

Figure 46: Definition of lengths in AdV. All lengths are considered between high-reflection coated surfaces, taking also into account the mirror substrates. For non degenerate recycling cavities, the lengths sum up the distance with folding mirrors.

Referring to fig. 46, the microscopic motion of all lengths around the operating point are combined to form the following physical degrees of freedom:

$$\begin{aligned} DARM &= L_X - L_Y \\ CARM &= \frac{L_X + L_Y}{2} \\ PRCL &= l_P + \frac{l_x + l_y}{2} \\ MICH &= l_x - l_y \end{aligned}$$

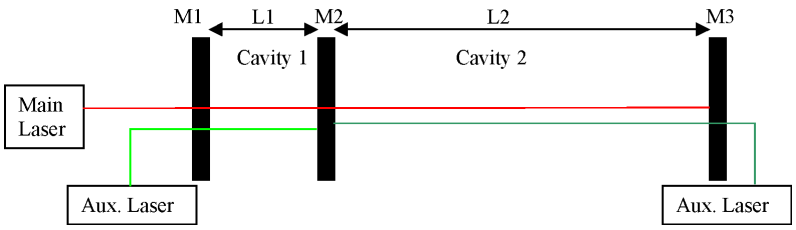

Figure 47: Optical configuration of the test facility. For clarity, the various beams have been vertically shifted. In real conditions, they should overlap in order to see the same cavity length.

$$SREC = l_S + \frac{l_x + l_y}{2}$$

The operating point in the linear state is defined as follows. CARM and PRCL are tuned to the resonant position and MICH to the minimum of power transmission to the dark fringe. DARM is slightly detuned from resonance for DC read-out [149]. SREC is also detuned by a static amount which is used to profit from the signal recycling shaping of the detector response [153]. This *signal recycling tuning* is of the order or 0.1 rad.

11.3 Longitudinal lock acquisition

The lock acquisition strategy deals with the actions needed to bring the interferometer from a un-controlled condition to the final science mode configuration. As a first step the two recycling mirrors are mis-aligned in order to avoid their reflection to interfere with the main beam entering the interferometer, and the arm cavities brought to resonance. Then the other degrees of freedom are brought into operation.

11.3.1 Double cavity lock acquisition experimental demonstration

At LAL, we investigate a new technique to make the lock acquisition of a complex optical system easier. Dedicated lasers control each degree of freedom of the system independently from the others. The auxiliary laser wavelengths are such that the finesses of the cavities are much reduced, so that their linear ranges are enhanced. Once each degree of freedom is under control, the interferometer is brought in a deterministic way to its working point where the error signals from the main laser can be used: an offset in the auxiliary laser error signals is introduced and a smooth transition is performed. If successful, this scheme could be used as guidance for the lock of any complex optical configurations. If the quality of the alignment is an issue (this point has to be investigated), we can envisage to use the auxiliary lasers to perform a pre-alignment sufficient to perform the locking with the main laser.

The principle of this lock acquisition has been successfully tested in simulation on a single cavity.

The CALVA experiment[172] aims at the locking and the alignment of two coupled cavities illuminated by a high power laser. The first cavity is a low finesse and short cavity while the second one is a high finesse and long cavity (fig. 47), mimicking the behavior of the power/signal recycling cavities versus arm cavities in AdV. The first cavity has been built at LAL and the injection of the lasers will occur in November 2008. The first semester of 2009 will be used to validate the principles on a single cavity while the construction of the second cavity will be done. The study of the coupled cavities will take place on the second semester of 2009.

This technique will probably be used in AdV only for the lock acquisition of the long arm cavities; it will have no effect on the sensitivity of the instrument, but will speed up its commissioning.

11.3.2 Arm cavity lock with auxiliary laser implementation

The auxiliary laser locking technique allows an implementation with a minimal impact on other subsystems as only end tower optical benches will be impacted. On each bench, we need to install an auxiliary laser with its electro-optic, Faraday isolator and possibly a rigid cavity for laser frequency stabilization. The auxiliary beam has to be superposed to the outcoming main beam and then injected in the arm cavity. The reflected auxiliary beam will be used for the control of the cavity.

11.3.3 Full interferometer lock acquisition

The strategy foreseen for AdV is an extension of the Variable Finesse technique successfully implemented in Virgo [150]. After the two cavities are on resonance, if the signal recycling mirror is maintained mis-aligned, the system behaves as a power-recycled interferometer and it can be locked up to the dark fringe condition with a Virgo-like technique [151]. After reaching the dark fringe configuration, the signal recycling mirror can be re-aligned and its control system activated.

The key point of this strategy is the choice of suitable modulation frequencies in order to decouple as much as possible the various degrees of freedom [153, 154]. When the interferometer is in its operating point, the carrier must be resonant in the power recycling cavity as well as in the arm cavities. It must also be anti-resonant (in the Resonant Sideband Extraction regime) in the signal recycling cavity. In this condition, a first modulation frequency f_1 is chosen in order to have the corresponding pair of sidebands SB1 resonant in the power recycling cavity and close to anti-resonance in the arms. Moreover, the Schnupp asymmetry must be tuned in order to have a small transmission of SB1 to the anti-symmetric port. In this way the amplitude of carrier and SB1 inside the signal recycling cavity is small and the re-alignment of the signal recycling mirror has a small effect on these fields. If all the power-recycled-interferometric degrees of freedom are controlled using signals coming from the beating of carrier and SB1, it would be possible to maintain their control even during the re-alignment of the signal recycling

mirror [153, 154]. A second pair of sidebands SB2 must be used to extract a suitable control signal for the signal recycling cavity length.

To avoid troubles from radiation pressure effect, the lock acquisition sequence must be carried out at reduced input power and the final level should be reached only when the interferometer is already stably controlled in its final configuration.

11.4 Linear locking scheme

11.4.1 Requirements

The length sensing and control design starts with the simulation of the optical response of the system. The large circulating power inside AdV induces large radiation pressure effects, which significantly alters the shape of the opto-mechanical response of the system. Optickle, developed by our LIGO colleagues, is the only available tool capable of dealing with radiation pressure effects.

Once the interferometer has been brought to the final working point, the longitudinal control system must be tuned in order to reach low noise operations. The design of the science mode control strategy deals with the simulation of the entire system and the selection of the error signals that can give the best performance in terms of quantum-noise limited operation.

The requirements for the length sensing and control system can be stated in terms of maximum residual RMS fluctuation of all degrees of freedom around the operating point and in terms of sensing noise re-injected inside the observational bandwidth. The latter translates in the requirements that the quantum-noise-limited operations of the LSC system must not limit the detector sensitivity (at the design level) at any frequency.

The RMS fluctuations are instead clearly dominated by the very low frequency residual motions. Requirements can be set up considering the resonance width of the cavities and possible estimates of noise up-conversion [159]:

$$\begin{aligned} RMS_{DARM} &< 2 \cdot 10^{-14} \text{ m} \\ RMS_{CARM} &< 1.3 \cdot 10^{-14} \text{ m (1.3 mHz)} \\ RMS_{MICH} &< 1.1 \cdot 10^{-11} \text{ m} \\ RMS_{PRCL} &< 9 \cdot 10^{-11} \text{ m} \\ RMS_{SREC} &< 2 \cdot 10^{-10} \text{ m} \end{aligned}$$

11.4.2 Sensing and control design

The length sensing and control system for Advance Virgo is based on the use of three modulation frequencies, which corresponds to three pairs of sidebands with very different resonance conditions at the operating point:

SB1 are resonant in the power recycling cavity and very close to anti-resonant in the arm cavities. A 50 Hz detuning is assumed from the cavity anti-resonance to avoid the second harmonics to be resonant. The Schnupp asymmetry is chosen to be small enough to make the transmission of these sidebands to the east port (toward the signal recycling cavity) of the beam splitter very small. SB1 are in any case close to be anti-resonant in the SRC.

SB2 are resonant in the PRC and simultaneously in the SRC. The Schnupp asymmetry is optimized to have an optimal coupling of these sidebands inside the signal recycling cavity. In other words, it is chosen to maximize SB2 power inside the SRC.

SB3 are not resonant in the PRC and close to the arm anti-resonance. In this way this pair of sidebands are almost completely reflected by the interferometer. Although the use of such sidebands is not strictly necessary for the longitudinal control, the Virgo commissioning profited a lot from their use.

In addition, all these sidebands must be transmitted through the input mode cleaner.

All these requirements can be translated in two sets of lengths and modulation frequencies [155, 156, 158] for the two main options of having *marginally stable recycling cavities* (MSRC) or *non-degenerate recycling cavities* (NDRC) (reference). The two configurations are summarized in tab. 12 together with the parameters used in the simulations. Here the baseline solution of NS-NS-optimized sensitivity has been used for the signal recycling mirror tuning and reflectivity.

A full simulation has been developed using Optickle. Details can be found in [156]. The outcome is the full optical matrix, i.e. the set of transfer functions from any degree of freedom to any demodulated signal. Two demodulation schemes have been simulated:

Single demodulation scheme. Error signals are obtained by demodulating the output of each photodiode at single modulation frequencies. In this way the beating of the carrier field with each pair of sideband fields can be extracted. This is the same scheme used in Virgo. It is necessary to have such signals for controlling DARM and CARM, since these degrees of freedom affects mainly the carrier. However, any signal obtained in this way will have a large contamination from DARM and CARM due to the carrier field. This was also true in Virgo and the problem was faced by enforcing a gain hierarchy: DARM and CARM (frequency stabilization) loops had very high gain inside the active bandwidth of all other auxiliary loops, therefore suppressing the contamination. The situation is slightly more complex in AdV due to radiation pressure effects. These are mostly relevant inside the long arm cavities and therefore they will mainly affect the carrier field. Using single demodulation will result in having all error signal largely affected by radiation pressure effects [156].

Double demodulation scheme. Error signals are obtained by demodulation at the sum or difference of modulation frequencies. In this way the beating of two pairs of sidebands is detected, without any influence from the carrier field. The main drawback of this scheme is the fact that signals are proportional to the squared

Parameter	Symbol	MSRC	NDRC
Arm cavity length	L	3000.0812 m	
Signal recycling cavity length	l_{SRC}	11.033 m	25.143 m
Input mode cleaner length	l_{IMC}	143.431 m	144.00 m
Power recycling cavity length	l_{PRC}	11.953 m	24.001 m
Schnupp asymmetry	Δ	0.037 m	0.031 m
First modulation frequency	f_1	6270389.2 Hz	9368110.7 Hz
Second modulation frequency	f_2	81515709.5 Hz	65576775.2 Hz
Third modulation frequency	f_3	8360585.6 Hz	8327209.6 Hz
Modulation indexes	m_i	0.1	
End mirror transmission	T_{END}	$5 \cdot 10^{-6}$	
Input mirror transmission	T_{IN}	$7 \cdot 10^{-3}$	
Power recycling transmission	T_{PRM}	0.06	
Signal recycling transmission	T_{SRM}	0.11	
Losses per mirror	L	40 ppm	
Anti-reflection reflectivity	R_{AR}	100 ppm	
Mass of cavity mirrors	M	42 kg	
Input power	P_{IN}	125 W	
DC read-out DARM offset	δ_{DARM}	10^{-11} m	
Signal recycling cavity detuning	ϕ_{SRC}	0.15 rad	

Table 12: Reference parameters for AdV Length Sensing and Control baseline scheme.

value of the modulation index, instead of being linearly proportional to it. This brings a reduction of the signal amplitude. The advantages are manifold. First the contamination from DARM and CARM is much smaller, since the carrier field does not enter in the signal extraction. This also means that single demodulation must still be used to extract error signals for DARM and CARM, while double demodulation can provide much cleaner signals for MICH, PRCL and SREC. Moreover these signal will be much less affected by radiation pressure effects.

A detailed comparison of the optical transfer functions in the two schemes and a description of radiation pressure effects can be found in [156, 157].

To implement a single demodulation scheme, the input beam must be phase modulated for all three frequencies, while to use double demodulation it must be phase modulated for f_1 and amplitude modulated for f_2 and f_3. In this way SB1 can still be used for single demodulation and DARM/CARM control, while SB2 and SB3 beating with SB1 can be extracted with double demodulation [156, 157].

The Optickle simulation computes also the level of quantum noise for each output signal. This can be used together with the optical matrix to select suitable error signals to control each degree of freedom and to simulate the effect of the control loops. The list of error signals used for each degree of freedom is given in tab. 13

D.O.F.	Single demod.	Double demod.
DARM	ASY_DC	ASY_DC
CARM	SYM_SB1_P	SYM_SB1_P
PRCL	SYM_SB3_P	SYM_3P1_P
MICH	SYM_SB2_Q	SYM_2M1_Q
SREC	SYM_SB1_P	SYM_2M1_P

Table 13: Error signals used in the single and double demodulation scheme. Names containing SB1, SB2 or SB3 are given to signals obtained by single demodulation at respectively f_1, f_2, f_3. Names containing 3P1 and 2M1 are instead given to signals obtained with double demodulation at $f_3 + f_1$ and $f_2 - f_1$. P and Q refers to the two signal quadratures. SYM refers to the symmetrical port (POPR port in figure 13) and ASY to anti-symmetric port (AP port).

The accuracy of each loop has been computed using as a reference the real motion of suspended test masses of Virgo [156]. The results are compatible with the requirement computed above.

The quantum noise of each error signal has been used to compute the noise re-injected in the gravitational channel. The result for the single and double demodulation scheme in the case of marginally stable recycling cavity is shown in fig. 48. The result for non-degenerate recycling cavities is similar [158]. So far control loops have been designed to be robust and not at all optimized for low noise performance, for example introducing steep roll-off in the control filters.

In both cases the LSC system would be the limiting source of noise in a large bandwidth: in the double demodulation scheme control noise is as much as a factor 100 above the target design sensitivity. This is similar to what happened in Virgo and the solution is the implementation of noise subtraction paths [160]. To bring control noise below the design sensitivity it would be necessary to obtain roughly a factor 100 of noise suppression, which seems easily feasible given the factor 1000 obtained in Virgo. The side-effect of the use of noise subtraction path is the amplification of seismic noise coming from the auxiliary degrees of freedom [159].

11.4.3 Status of LSC design

A full simulation machinery has been set up to design the length sensing and control system given a rough set of desired lengths and modulations. Optickle simulations have been tested and can now be used to compute optical matrices taking into account also radiation pressure effects. A set of possible parameters which results in consistent LSC configuration has been computed for both the MSRC and NDRC options. The foreseen lengths and modulations has a significant impact on the vacuum system, since the displacement of some towers would be needed to met the requests in terms of distances between mirrors. However a more detailed optical design is needed to quantify these needs.

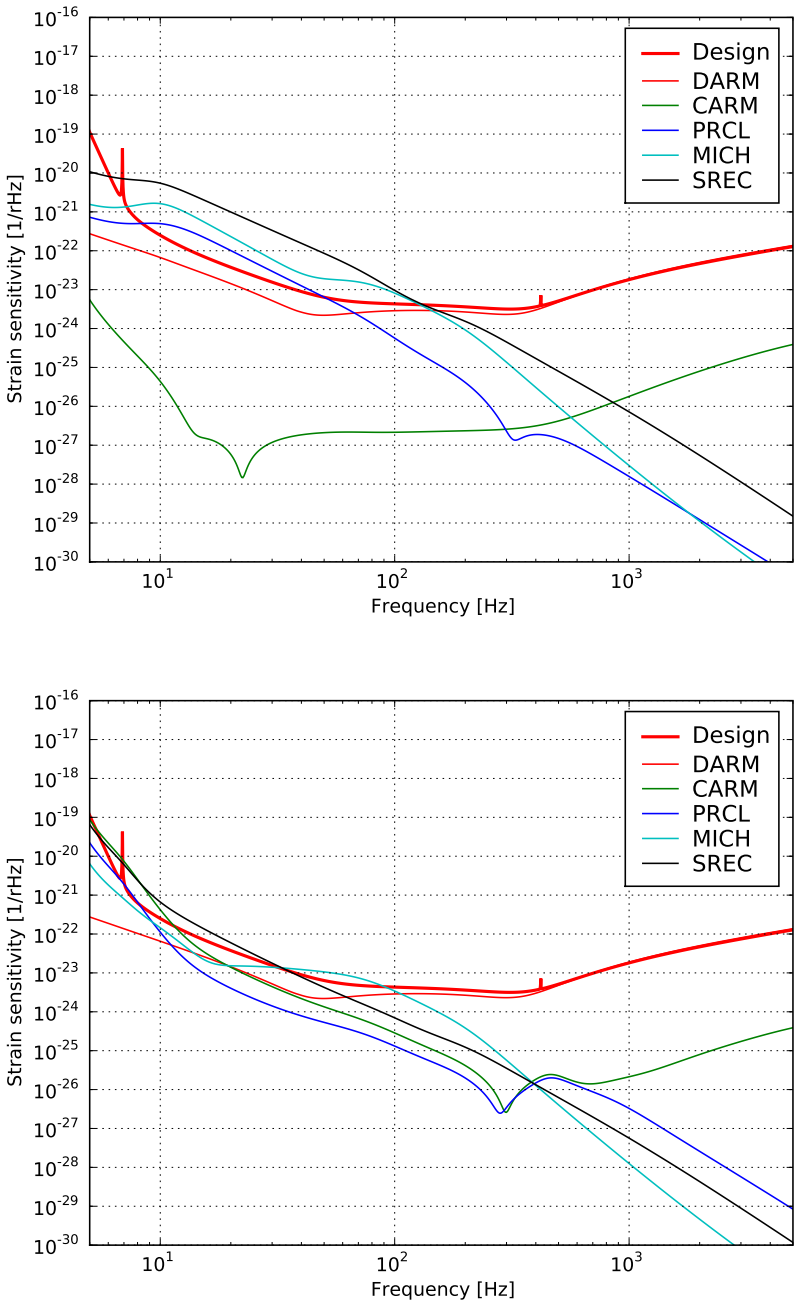

Figure 48: Noise re-introduced in the gravitational channel by the length sensing and control system, in the double (top) and single (bottom) demodulation schemes.

Two possible signal extraction schemes have been identified. In the single modulation one the amount of control noise re-injected in the dark fringe is lower, at the price of very large radiation pressure effects for all degrees of freedom. The double demodulation scheme gives radiation-pressure-independent signals for MICH, PRCL and SREC, at the price of a larger level of control noise. This is not worrying, since it can be fixed using noise subtraction paths, which are in any case needed in both schemes. The choice between the two systems has impacts on the LAS/INJ systems, since it determines if amplitude modulation is needed.

11.5 Alignment

A global angular control has to be developed to control the pitch and yaw directions for mirrors IMX, EMX, IMY, EMY, BS, PRM, SRM, and rotations and transversal translations of the suspended injection bench.

The first investigation point was about the use or not of the Anderson-Giordano technique [161], the control technique developed for the Virgo interferometer angular control system, that measures the arm alignment with respect to the laser beam in transmission. The Virgo commissioning highlighted several disadvantages: incompleteness of the sensing scheme, bad quality of the terminal error signals and an offset on error signals. For these reasons a Ward-like technique [162] for the AdV alignment control is preferable, using beam pick-offs of the light reflected on the arms for am alignment. It will use the same modulation frequencies as for the longitudinal control.

In AdV the strong presence of the radiation pressure generates a negative optical torque in one of the angular modes which might generate an unstable loop if not compensated for. This effect will prevent to control the mirror degrees of freedom separately.

Some investigations for the angular control system have been already done or started such as:

- the influence of the Etalon effect of a curved/curved terminal mirror on the automatic alignment error signals [163]
- consequences of the presence of compensation plates for the thermal compensation on the alignment error signals
- preliminary design on the automatic alignment control scheme in a steady state [164], using the frequency simulation tools Finesse [166] and Optickle [152]

In order to provide a complete angular control scheme for the AdV interferometer few steps are necessary:

- the evaluation of the accuracy specifications of the mirror local controls (PAY) in order to bring the system within the AA error signal linear regions;
- steady state control configuration development and optimization of the opto-electrical configuration for the eighteen degrees of freedom (Gouy phases, demodulation

phases, etc.)

- the evaluation of the automatic alignment specifications and the evaluation the control noise performances

- the mitigation of negative optical torque

These study will require the upgrade of optical simulation software to the simultaneous use of high order optical modes and radiation pressure. A light field with high order modes would allow the possible existence of offsets in alignment signals.

11.6 Parametric instabilities

The parametric instability (PI), which consists in the coherent ringing of a mechanical mode of a cavity mirror by the circulating optical power [167], may significantly affect the performance of high-power signal-recycling gravitational-wave interferometers [168]. The mode is indeed likely to reach a very important vibration amplitude and therefore prevent any stable operation of the interferometer, eventhough most mechanical modes are outside the detection window.

Up to now, the PI has already been demonstrated in systems such as micro-toroids [169] or silicon micromirrors [170], in which a single optical mode interacts with a single mechanical mode, with a mechanical frequency much smaller than the cavity bandwidth. The instability of interest for gravitational-wave interferometers is slightly different, as it involves a 3-mode coupling between the main optical mode, a mechanical mode and a second optical mode, the frequency mismatch between the two optical modes matching the mechanical resonance frequency. The large-scale interferometers, with their very high mechanical mode density at frequencies such as tens of kHz, unfortunately are very good candidates to display such an instability.

Such a 3-mode coupling has already been observed in the australian high-power laser facility [171]. Different experiments (Paris, Perth) are underway to demonstrate the instability in such a configuration, using almost degenerate optical cavities.

Detailed simulations of the impact of the PI have been performed by the Perth group and show that in the current Adv Ligo optical configuration, the number of unstable mechanical modes is unlikely to be below 5 for any set of optical parameters (mostly the radius of curvature of the mirrors, the resonance condition being extremely sensitive to the Gouy phase).

Possible solutions include the use of lower Q mirrors, thermal tuning of the cavities, or monitor and control of the instabilities.

Work to be performed includes an experimental demonstration of the PI in a 3-mode configuration (2 years) at LKB, a simulation of its impact over the current AdvVirgo design, and the investigation of possible solutions.

12 Parasitic noises

12.1 Introduction

As Virgo commissioning has demonstated, environmental noises can have an important impact on sensitivity and must not be neglected. Magnetic and seismic noises were contributing to limit the last Virgo sensitivity curve (May 2008) in the 10 to 100 Hz domain [173]. During Virgo commissioning we have identified the most relevant noise paths, performed preliminary measurements of noise coupling, and identified major disturbing sources. Based on this preliminary information we set some rough constraints on the maximum environmental noises levels allowed for AdV. We also propose noise mitigation actions. The case of magnetic noise in exposed in sec. 12.2 and for seismic and acoustic noise in sec. 12.3. We conclude in sec. 12.4 remarking AdV environmental needs.

12.2 Magnetic noise

One of the possible noise sources that could limit the sensitivity at low frequency is related to the magnets that are glued to the mirrors for the interferometer control, since they can directly couple any environmental magnetic noise to a displacement of the mirrors. In the past, it was already discovered that some bumps in the sensitivity around 100 Hz were caused by a power supply sitting just a few meters from the mirrors. Once understood, this problem was solved by simply moving the supply several meters away.

A number of dedicated measurements were recently performed by injecting magnetic fields with a large coil. By measuring simultaneously the magnetic field using the permanent magnetometers and the optical signal of the interferometer, a transfer function from magnetic fields to the gravitational wave signal can be calculated. Multiplying this transfer function with the background magnetic noise in quiet conditions gives an estimate of the contribution to the sensitivity, see fig. 49. The magnetic noise is currently not limiting the sensitivity, except for the 50 Hz mains frequency, some of its side-bands and a few lines below 20 Hz [174]. This is confirmed by coherence measurements between gravitational channel and the magnetometers. Some weak, broad-band coherence is sometimes observed between 10 and 20 Hz.

The measured transfer functions are about one order of magnitude larger than that based on a simple dipole model. Further bench-tests showed that the large measured coupling with environmental magnetic fields can probably be attributed to the aluminum reference mass, which distorts the local magnetic field because of induced eddy-currents. This causes strong gradients close to the location of the mirror magnets, which increase the coupling between far-field magnetic fields and mirror motion [175].

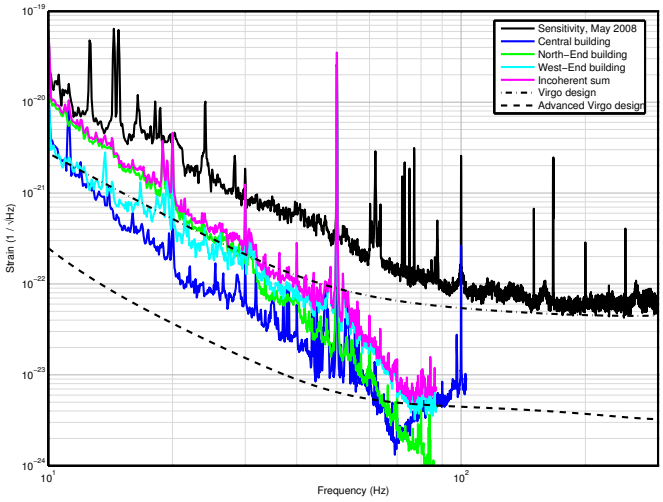

Figure 49: Magnetic noise projection, May 2008. Note that this projection is only valid for magnetic sources located far away from the mirrors and that there is a relatively large uncertainty in the measurements due the 3D nature of magnetic fields.

12.2.1 Improvements for AdV

For AdV, a reduction of the magnetic noise of about one order of magnitude is needed between 10 up to 60 Hz, and slightly less for frequencies up to 100 Hz. This can be achieved in two ways: either lowering the coupling or reducing the background magnetic noise. Both strategies should be followed.

Reducing the coupling factor The main factor that determines the coupling is the strength of the magnets. In the beginning of 2008, the magnets of the input mirrors were already reduced by a factor 5, the reduced coupling was confirmed by measurements [176]. A similar operation has been performed for the end-mirrors. It is expected that at the restart of the interferometer (end of 2008), the contribution of the end-buildings will have dropped below that of the central building. A further reduction of the magnet strength has to be studied, but this is limited by the maximum allowable current of the coils and the minimum force required to lock the arm cavities (which will be more difficult due to a higher finesse). The most radical change would be to use no magnets at all and go for electrostatic actuation of the mirrors, but this introduces a completely new set of technical challenges and is currently not foreseen for AdV.

A different way to reduce the coupling is to apply magnetic shielding of the mirrors, for example with mu-metal. This might be costly and complicated given the size of the vacuum chambers and the surrounding tubes. Some reduction in the coupling factor is expected from a new design of the reference mass, which will be constructed from a dielectric material instead of aluminum. This should lower any induced eddy currents

and the creation of local gradients in the field. Finally, the displacement of the mirror caused by a magnetic force on the magnets will decrease by increasing the weight of the mirrors, but this advantage might be lost if it requires a similar increase in magnet strength needed to lock the cavities.

Reducing the background magnetic noise A campaign to identify which racks or machines contribute the most to the background magnetic field will have to be carried out in the next few months. One resulting action that could be foreseen is to move all the digital electronics out of the central building, leaving only the analog front-ends. Another solution might be to move all the power converters away from the mirrors and distribute the power as low-voltage DC current. Rather than shielding the mirrors, it might be easier to apply local shielding to any noisy electronics. At least the racks remaining close to the mirrors should probably be constructed 'leak-tight' for magnetic fields.

12.3 Seismic and acoustic noise

Virgo commissioning evidenced that one major coupling path for seismic and acoustic noise is the back scattering of light by in-air not seismically isolated surfaces: vacuum chambers, optical windows, and optical benches [173]. Other seismic and acoustic coupling paths, which as well concern optical benches, are angular jitter of the input beam and sensing noise of photodiodes used for alignment controls [173, 179].

Noise from diffused light at external optical benches is a major issue and it is described first (sec. 12.3.1). Its reduction necessarily proceeds through: (1)the reduction of scattered light on benches (this item is just addressed in sec. 12.3.1 but not discussed here), (2) the mitigation of air conditioning noise (discussed in sec. 12.3.2), and (3) the isolation of optical tables (see sec. 12.3.3). Other identified sources are vacuum pumps (see sec. 12.3.4) and electronic racks (see sec. 12.3.5). Finally we briefly discuss the more general issues of rotating devices (sec. 12.3.6) and acoustic reverberation of experimental halls (sec. 12.3.7).

Light scattering by glass baffles in the arm tubes is another potential source of noise [**?**]. Shaking of the tubes were performed at the location of the initial, itermediate and end baffles observing no effect. An upper limit has been set which is compatible with the AdV design [177].

12.3.1 Noise coupling at optical benches

The back-scattering noise by optical benches is particularly relevant. It was one of the limitations of the last Virgo sensitivity below 100Hz, and was thoroughly studied [180, 181, 182]. The noise was found to affect all benches. Its effect in the sensitivity is a phase noise of the form (time-domain formula):

$$h_{\rm sc} = K \sin(dx\, 4\pi/\lambda), \tag{24}$$

where $dx(t)$ is the displacement of the scattering surface, and K is proportional to the fraction of beam power that gets scattered back into the ITF, and also depends on ITF optical parameters. Thus, for displacements of the scattering surface small compared to $4\pi/\lambda$, the noise is proportional to the displacement itself, while for larger values of dx up-conversion effects appear [178].

It follows from eq. 24 that the noise can be reduced in two ways: (1) reducing as much as possible the amount of back-scattered light on the bench, and (2) reducing the vibrations of the bench. The first way was pursued during the last phase of the Virgo commissioning, when the amount of diffused light was considerably reduced by several cures (replacement of scattering objects, lens cleanings, damping of spurious beams, etc.) [182]. In the following we address only the second way, assuming conservatively that the quantity of backscattered light on benches for AdV is the same as measured in Virgo after the above mentioned cures.

In reference [183] the noise model in eq. 24 is computed for AdV optical parameters and specifications are set for the benches maximum allowed displacement. Figure 50 shows the specification for the end benches compared to the benches typical displacement noise. For other benches (EDB, EIB, and new TCS) an accurate specification cannot be set at present, since more understanding is needed of the light scattering processes or other competing mechanisms of noise coupling [183]. It seems however reasonable and conservative to require for all benches a factor 10 to 50 reduction of noise in correspondence to the table resonances (50 is required for the end benches whose resonance has higher Q) and a factor 5 to 10 elsewhere in the 5 to 100 Hz band. The reduction of bench noise obviously proceeds by the synergy of two actions which are: (1) the reduction of noise from the sources, and (2) the reduction of noise coupling to benches. The air conditioning systems of the experimental halls and clean rooms are the dominant cause of bench motion in the frequency band of interest. This subject is discussed in sec. 12.3.2 below. The issue of benches isolation is discussed in sec. 12.3.3.

12.3.2 Air conditioning improvements

Seismic and acoustic noise produced by the air conditioning system (HVAC) of the experimental halls and clean rooms are the first cause of bench motion in the frequency band of interest (5-100Hz) [184, 185, 186]. Figure 51 illustrates the HVAC noise on the west end bench (WEB). Noise is originated by moving parts (amplified if unbalanced) and air turbulence, and transmitted through floor and ducts vibrations, and air flux. Also the water pumps serving these machines are source of noise if located close to experimental hall, as it is currently the case for the central hall HVAC.

The study and reduction of HVAC noise is a task of the V+ commissioning. We thus expect for the spring 2009, to have for each machine, a better understanding of the noise coupling path and implementation of simple ad-hoc mitigation solutions. For AdV we aim instead to a solution capable to reduce the HVAC noise at optical benches below the anthropic seismic background.

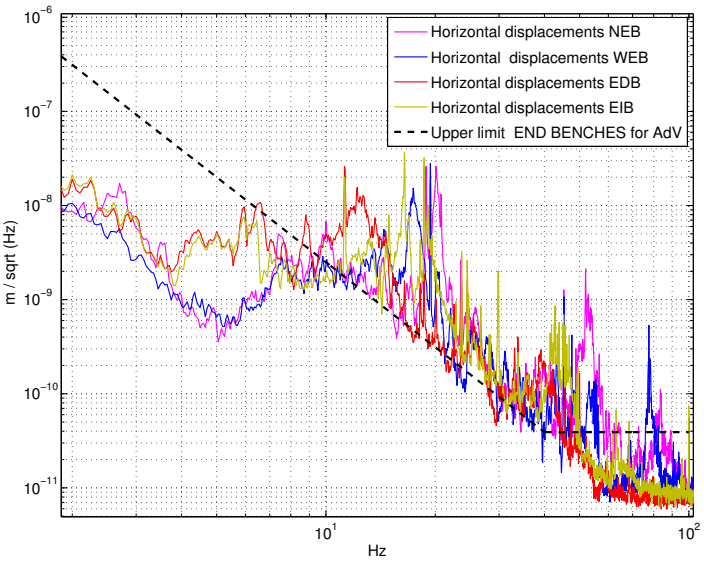

Figure 50: Displacement noise of all Virgo optical benches, compared to the upper limit set in [183] for the terminal benches (NEB and WEB).

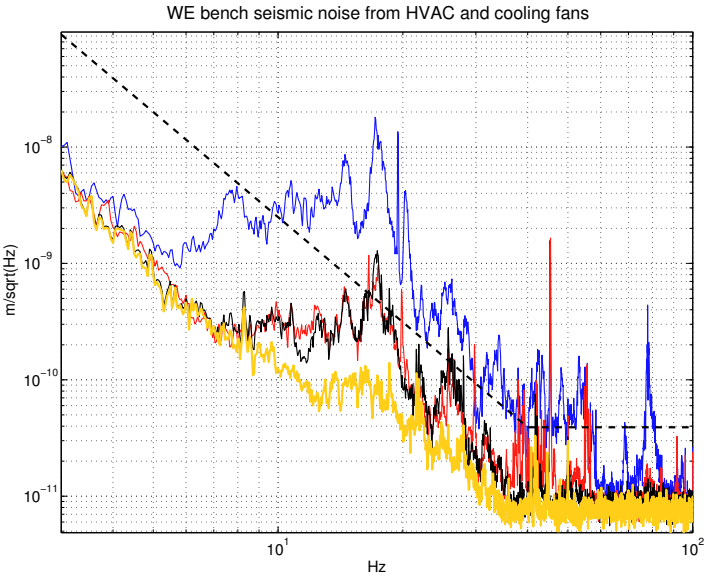

Figure 51: Contribution to WE bench seismic displacement from the air conditioning (blue to red curves), and the cooling fans of racks and vacuum pumps (red to black). Also shown is the amplification of ground seismic noise by the table mechanical transfer function (black to yellow).

Preliminary results indicate that reducing fan speed and air flux can reduce noise significantly [187]. If the thermal stabilization of suspension towers by means of heating blankets will be adopted for AdV, requirements on the temperature stability of the experimental hall will be relaxed, and it would be possible to reduce the HVAC power.

Preliminary investigations of the central hall HVAC indicate the seismic coupling is relevant. This machine shares the same foundation as the EDB and EIB benches. This is not the case for the end buildings machines for which instead we can suspect a dominant coupling through ducts vibrations and air flux.

Several not too invasive solutions which are being studied for V+ are:

1. reduce fans speed (and consequent air flux) if compatible with thermal needs;
2. take care of good balancing of rotating parts;
3. add seismic attenuation stages under the fans and the HVAC case. The frequency cut-off (few Hz) and Q (<5) of the attenuators, as well as their 3-D capability (horizontal and vertical attenuation) must be carefully evaluated;
4. as well seismically isolate ducts and water pipes from the HVAC case and from the walls by means of suspensions of anti-vibrating supports (just easy isolations from the walls are foreseen at this stage, see point 4 below).

Additional solutions proposed for AdV are:

1. a more effective seismic isolation of low frequency ground vibration can be assured by placing the machine on a separated floor (as it is not the case presently for the central building machines), which could be suspended on low frequency (<2 Hz) isolation stages, eventually laid on a layer of sand or other material with good dissipation properties;
2. displacing HVAC machines from the experimental hall (dedicated building) would guarantee a seismic attenuation of $1/\sqrt{(}r)$ that is a factor 3 at 10m. It should however be evaluated the impact on noise of the consequent increase of machine power to compensate for pressure drops on the longer ducts;
3. water pumps close to the HVAC (recycling pumps) should be avoided, instead located in far buildings (Tech Building) and properly dimensioned and isolated;
4. not the least: a thorough revision of the path of inlet and return air ducts (especially for the central building) is necessary to seismically isolate them from building walls.

Other solutions are aimed to mitigate the acoustic noise in the halls by reducing air turbulence:

1. installation of flow strengtheners at the inlet ducts;
2. carefully design ducts paths to avoid unnecessary or abrupt turns (as it is presently the case for the central hall HVAC);
3. silencers at air outlets (not effective below 100Hz);

4. isolation of HVAC rooms with phono-absorbing material;
5. not the least: reducing acoustic reverberation on experimental halls (see sec. 12.3.7).

Water cooling might be employed to condition small rooms. This is currently under investigation for the laser room. Thermoelectric plus water cooling might be considered for devices which have a small and localized thermal load.

12.3.3 Optical tables damping

Even if we can kill completely machines induced environmental noises (for example HVAC) the residual anthropic background noise coupling through the external benches is still too high [188, 189]. Thus an isolation of external benches in needed. Benches isolation is also a task of the Virgo+ commissioning whose objective, at present, is to study and test simple and not invasive solutions. We thus expect to have better defined isolation requirements and proposed solutions for spring 2009.

A sure concern is the amplification of environmental noise in correspondence of the tables horizontal mechanical resonances which happen to be at quite low frequency (around 15-20 Hz for all benches). Another possible serious concern is the effect of micro-seismic noise. This is being investigated.

We have done a preliminary evaluation of commercial solutions consisting of servoed damping legs with ultra low resonance frequency (0.7 Hz). Simulation studies indicate that the very good performance above a few Hz might be spoiled by the extra noise introduced at the proper resonance of the damping system [188, 189].

On the other hand a significant and possibly sufficient bench noise reduction might be obtained by implementing simple solutions and by improving the tables mechanical transfer function [179]. A partial solution, successfully tested, consists in applying a coupled damped oscillator whose frequency is tuned to the bench resonances [190]. A reduction of bench motion at resonances of a factor 4 or more can be obtained with this method. A more significant improvement might be obtained by increasing the bench stiffness and thus shifting resonances to higher frequencies where the force to displacement transfer function is smaller.

12.3.4 Vacuum pumps noise through output windows

Back-scattered light noise can originate also at the other optical links, as it was occurring for example at the detection Brewster window [191]. Such optical links at present are the injection Brewster window and the tower output windows towards the external benches: the first might be eliminated and replaced with a second cryogenic trap (Chapter 17), while the optical windows links to the external benches would stay. We expect these windows to couple seismic vibrations of the vacuum tower to which they are rigidly fixed. The vacuum turbo pumps are the major source of this noise. During Virgo commissioning, was evidenced a large coupling of this noise through the output window of the detection

tower. A seismic damping of the detection turbo-molecular vacuum pump was prepared and proved very effective [191]. A reduction of the seismic noise produced by continuously working vacuum pumps at towers is a necessary requirement. An isolation system similar to that implemented on detection, of most critical vacuum pumps is foreseen for Virgo+. Less noisy turbo-molecular pumps are under study and can be an option for AdV.

12.3.5 Noise from electronics racks

Cooling fans of electronics racks and crates produce acoustic and seismic noise peaks at 40-50 Hz and harmonics which were present in Virgo sensitivity. DAQ room racks were first found to couple noise through the old Brewster window link [184], then laser racks and, more recently, also racks on the platform (vacuum and suspensions) have been demonstrated to couple noise at the injection optical benches [179]. Although, a seismic coupling through floor it is also possible, we think favored the acoustic path through vacuum pipes and towers. While seismic isolation of fans frequencies is feasible (commercial anti-vibration supports for racks with 8-10 Hz cut-off would give 90% attenuation at 40-50 Hz) acoustic isolation is more challenging. Acoustic enclosures do little below 100 Hz (see isolation performance of bench acoustic enclosures, in [192]). A preferable solution is to relocate racks inside dedicated rooms of thick concrete walls or double walls (see measured isolation performance of new electronics room, in [186]). However, control issues require the suspensions and vacuum electronics to be kept in the experimental hall and in proximity of towers. We thus propose a more radical solution: (1) move racks power supplies, AC-DC converters to one dedicated conditioned and acoustically isolated room (this solution brings advantages for magnetic noise) and (2) eliminate the present air cooling system of crates and racks and adopt for AdV electronics board a conduction type of cooling, compliant to IEEE standard 1101.2,[193].

12.3.6 About motors and rotating devices

Several motors are used to drive rotating devices such pumps (for vacuum, cooling water, dirty water, drain water) or fans (cooling fans, HVAC fans). These are usually asynchronous motors with 2, 4, 6 or 8 poles. They produce seismic, acoustic and magnetic noise at their rotation speed (i.e. slightly less than 50, 25, 16.6, 12.5 Hz) and harmonics. The noise increases with the motor's power, and for seismic and acoustic noise, with the square of its rotation speed. Unbalancing of the shaft also increases acoustic and seismic noise emissions. It follows that motor vibrations should be mitigated by applying damping feet and assuring a good balancing of the shaft. No unique rule exist for the motor's speed: on one side slower rotating ones are less noisy, but faster vibrations are easier to damp. The guideline is to avoid motor frequency close critical ITF resonances, such as those of optical tables.

12.3.7 Reduction of halls reverberation

Measurements of acoustic reverberation of the experimental halls revealed reverberation times of a few seconds, comparable to that of a "concert hall". This high reverberation has negative effect for both continuous (cooling fans, vacuum pumps, air conditioning) and transient acoustic noise (such as planes, occasional alarm whistles, ...). Multiple reflections amplify the acoustic energy inside the halls and dilate acoustic bursts. Reverberation effects can be reduced with the installation of absorbing elements (panels, suspended columns) in the ceilings and walls. Commercial products exist which claim a good phono-absorption performance starting from some tens of Hz.

12.4 Concluding remarks

As demonstrated in Virgo commissioning, environmental noises can have a significative impact on sensitivity and must not be neglected. Magnetic and seismic acoustic noises were contributing to limit the last Virgo sensitivity curve in the 10 to 100 Hz domain. It has been as well demonstrated that primary issues are the reduction of noise from HVAC machines, the reduction of the coupling of ground seismic noise to optical benches, and the reduction of magnetic noise. The Virgo+ commissioning plan foresees a thorough study of environmental noise coupling and the implementation of low-impact and low-cost solutions to mitigate some noise paths. These studies should permit, by spring 2009, to better define noise requirements and noise reduction actions for AdV. We believe however that a conservative and safe approach is needed for AdV and an effective mitigation of environmental noise must be pursued. This requires the isolation of sources, and of sensitive ITF parts (like the optical benches) and whenever possible the displacing of sources from sensitive areas to properly isolated rooms. These implementations necessitate of infrastructure works that need to be planned well in advance. Two possible scenarios of necessary infrastructure works for AdV are illustrated in section 18.

Advanced Virgo Preliminary Design:

PART 3:

Test mass vibration isolation, suspension and control

13 Superattenuators

13.1 Vibration isolation and test mass suspension

The isolation performance of the Virgo suspensions is expected to be compliant with the requirements of AdV. Therefore, no major changes to the vibration isolation system are required, and the general design with the Superattenuator (SA) chain, suspending the steering marionette and the payload itself (mirror and reference mass (RM)), will be maintained. However, the experience of the Virgo commissioning has shown that some aspects of the design can be improved:

- the inverted pendulum preisolator (IP) is controlled in 4 d.o.f. only (the three translations and the rotation around the vertical axis). It has been understood that the ground tilt, especially in windy days, can spoil the performance of the inertial damping and cause low frequency noise to be transmitted to the mirror. Therefore, the SA design has to be modified to allow tilt control;
- a new design of the suspension last stage is proposed (see sec. 14), with the option of using a recoil mass for the marionette that would greatly simplify the procedure for the suspension of the payload, and allow to overcome the geometrical constraints on mirror size of the current set-up;
- the new mirror reaction mass must be compliant with the heavier test masses and with the requirements of the thermal compensation system;
- the new payload must be compliant with the mirror monolithic suspension.

13.2 IP modifications and tilt control

The present Virgo pre-isolation stage, the IP, must be upgraded to be controllable in all six d.o.f., using tiltmeters as sensors for the rotational d.o.f. (see sec. 13.3). Since the beginning the mechanical structure of the IP was designed taking into account the possibility to implement a tilt control: an elastic element was embedded within its feet (see fig. 52) and the space for inserting PZT actuators was foreseen. Each IP leg can be thus acted upon in the vertical direction to compensate the tilt effect measured on the IP top stage. In this way, the IP top stage could become an inertial platform controlled in 6 d.o.f.. Moreover, a complete revision of the leg structure, changing it in a monolithic one with an increased sectional area (higher momentum of inertia) will move to higher frequency the annoying leg resonance now at about 10 Hz.

Also the low resonance mode of the Filter Zero (F0) crossbar falls in the same region. Such structures in the IP transfer function reduce the attenuation performance and make difficult to widen the control bandwidth of the inertial damping. Therefore, it would be helpful to revise the F0 design making the crossbar more rigid. A detailed simulation of the F0 mechanical system would be implemented, to explore and optimize the various options of intervention on the wires of F0 crossbar centering system, and on the position of

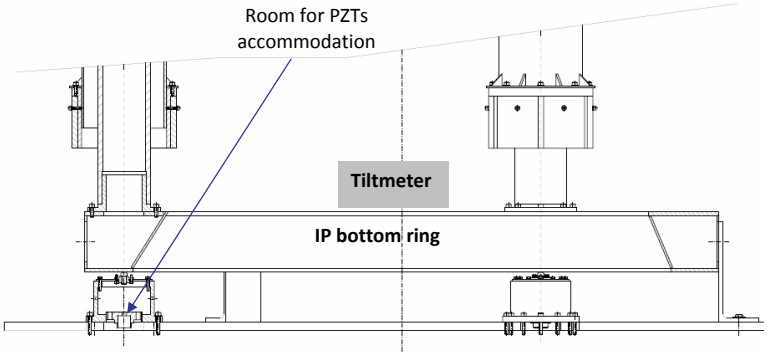

Figure 52: The IP bottom part is visible. A section of a foot supporting the IP bottom ring and the last part of IP leg is visible on left side. A schematic box representing the tilt meter accommodation is also shown.

the two vertical accelerometers accommodated over the same crossbar. An alternative or complementary solution could be the development of a more compact hoist mechanism for the wide vertical motion of the suspension point ($\pm$ 35 mm) to be accommodated within the crossbar structure. Even in this case the reduction of the total weight pushing on the crossbar structure could be relevant for the final goal. As a consequence of this intervention an alternative design for the vertical damping should be studied.

13.2.1 Status of the related R&D

The INFN Pisa group is involved in the design, development and construction of a new mechanical structure of the IP. This new system will be installed and tested on the SA facility at EGO (SAFE) [106]. This facility will host a complete SA chain operating also the tilt control and the other foreseen upgrades.

Starting from the present design, and reducing the impact of the changes at the minimum level, a new IP has been designed with stiffer monolithic legs (about 6 m tall for the long SA) and increased sectional area (see fig. 53). The first IP prototype has been already produced, and is being installed in SAFE together with piezoelectric actuators.

13.3 Tiltmeters

The operation of Virgo has shown that the inertial damping performance is partly spoiled in presence of strong wind. This has been explained as an effect of wind-induced ground tilt. The signal of the in-loop horizontal accelerometers is coupled to the tilt of the SA top stage around the horizontal axes, and this turns into low frequency noise transmitted to the mirrors. This makes the VIRGO lock acquisition more difficult with bad weather conditions and the effect will become even more relevant in AdV. An active control of tilt should then be implemented to make the detector more robust. A direct way to deal with the tilt compensation is operating a feedback control with tilt-meter sensors, requiring a

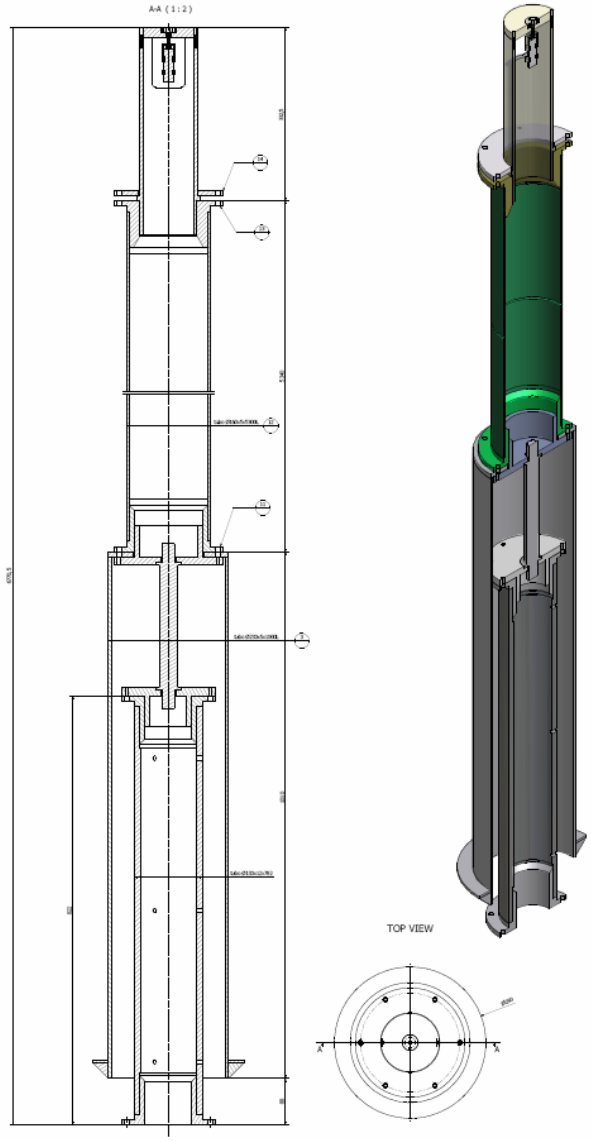

Figure 53: Technical drawing of the new IP based on monolithic legs with increased sectional area. The visible length of the leg (green) is not in scale.

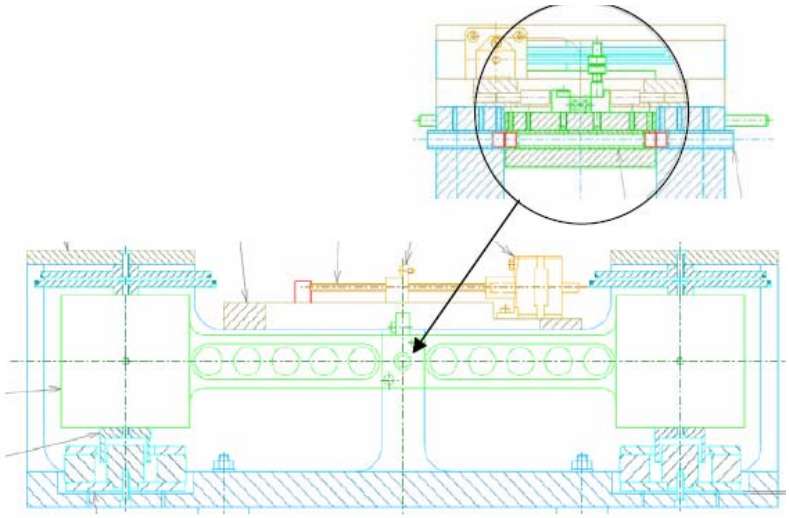

Figure 54: Technical drawing of the tilt meter prototype. Within the circle a detail of the device pivoted bar is shown.

sensitivity of about 10^{-8} rad/$\sqrt{\text{Hz}}$ at 30 mHz [107]. The activity in progress is focused on the study and the development of tiltmeter based on a device conceived around a pivoted bar with an LVDT sensor (see fig. 54). Two of these sensors, aligned along the main axis of the interferometer, will be installed within the vacuum vessel of each SA on top of the IP platform ring(see fig. 52).

13.3.1 Status of the related R&D

Two groups are involved in this activity: INFN Pisa and INFN Roma Tor Vergata.

Two identical prototypes have been build and assembled. No problem appeared in the electronics chain, while unexpected serious problems took place in the robustness of the flex joints. The prototypes have been upgraded to reduce pre-stresses in the flex-joints, but they have broken during operations. In April 2008 a new set of elastic flex pivot elements was installed with a few mechanical changes on one prototype. This device has shown setup difficulties with low reliability and reproducibility. The fine tuning system is being upgraded replacing a metric screw adjustment with a precision micrometer. New tests will follow in the next months

13.4 SR SA

A complete long SA must be assembled to suspend the SR mirror. It will be provided with all the upgraded parts (new IP legs, tilt control, new payload).

13.5 Short SA upgrade

The adoption of non-degenerate recycling cavities in AdV will require the installation of some optics of the PR and SR cavities on the IB and DB benches. This upgrade would eventually set new specifications for the anti-seismic attenuation of the IB, DB and IMC end mirror short SAs, up to requiring additional filter stages. These attenuation specifications are being investigated with optical simulations, evaluating the level of residual displacement noise in the AdV control signals. Eventually, one more filter stage could be added, maintaining the same SA height. The need of more than one extra filter stage would also imply the change of the SA height. In this last case the interventions will concern not only the upgrade of the first SA stage (F0), of the IP flexible joints and partially of cabling, but also the substitution of the whole IP, the upgrade of the safety structure and the complete cabling reshuffling.

SAT will update the plans for IB, DB and IMC SAs as soon as their vibration isolation requirements will be established.

Tilt control will also be implemented on these towers, while the IP legs, being already monolithic, will be changed only in case of SA length change.

Figure 55: Schematic picture of the new payload in the configuration with the marionette reaction mass is adopted.

14 Payload for Advanced Virgo

The payload is the last stage of the mirror suspension, located in the lower part of the tower where there is a separated vacuum chamber. The role of the last stage suspension is to compensate the residual seismic noise and to steer the optical components maintaining the relative position of the interferometer mirrors. In the current configuration, it is essentially a double stage branched system with the so called marionette as first pendulum, and as branches, the reaction mass and the mirror both suspended from it with steel wires. The position of the mirror is controlled by two sets of coil-magnet actuators. One set is between the F7 and marionette and the second one is placed between the reaction mass and the mirror.

The advanced payload must be compliant with the new mirrors having larger mass and different thickness, suspended with silica fibers. Moreover the whole payload must be compatible in shape and materials with the thermal compensation system (see sec. 9).

A further improvement that could be introduced is to move the coils from the F7 to a separate reaction mass around the marionette. This could greatly simplify the payload installation and it is crucial in case the beam splitter will have a large diameter ($\sim$ 50 cm). The study of this new element is currently in an R&D phase and a first prototype has been produced (see fig. 55).

14.1 The New Marionette

In the new marionette design the usual requirements for cleanliness, vacuum compatibility, mechanical precision, magnetic and electrical properties apply. Moreover several new aspects must be considered: the use of the fused silica fibers and the change of geometry of the mirror.

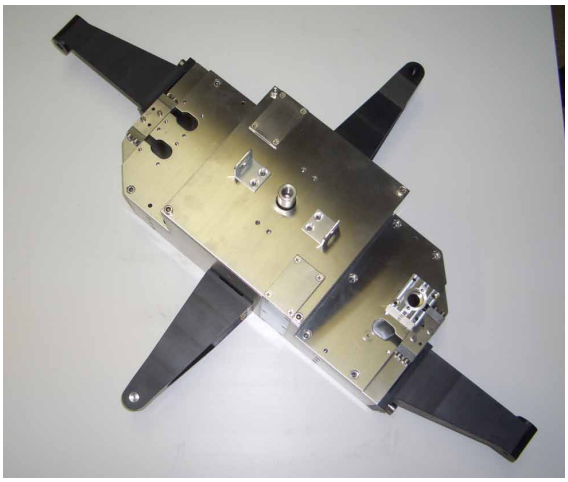

Figure 56: A picture of the new marionette designed for Virgo+ monolithic suspensions. The black dielectric arms are in Peek CF30.

In the case of the monolithic suspensions, the silica wires must be attached to the marionette by a new kind of clamps which must not introduce further mechanical losses in the interface between the silica and the marionette surface. These new clamps have to be placed in such a way the fibre bending point lays on the horizontal plane passing through the center of mass of the marionette to minimize the coupling between different degrees of freedom. As the wire bending section is different by the clamping section, because of the tapered fibre tip (see section 15.1.3), this is carefully taken into account in the new design.

The coupling between the marionetta and the fibre also influences the mounting procedure of the payload and consequently the new assembly tool design.

Moreover the change of the position of suspension wires of the new reference mass, and, in case of need, of the balancing motor, are taken into account.

Finally, the design is conceived in such a way to avoid any risk of fiber rupture, both during the assembly and the operation.

A complete FEM analysis of the new marionetta, has been very helpful to ultimate the design (see figure 56).

14.2 The New Reference Mass

In the new reference mass design the usual requirements for cleanliness, vacuum compatibility, mechanical precision and magnetic and electrical properties apply.

The new design takes into account the bigger thickness and mass of the mirrors, the implementation of the mirror control and the thermal compensation system.

The RM surrounds the mirror in order to protect it by accidents and hosts its actuators. It is equipped with safety stops that must be redesigned taking into account the different shape and increased mass of the mirrors suspended with a monolithic structure.

The design is conceived to host the ring heater and compensation plate foreseen in the thermal compensation system. To this aim, the dielectric parts of the RM must work at high temperature because of the possible contact with the heaters.

The presence of a compensation plate (see sec. 9) could deeply affect the dynamical behaviour of the last stage suspension: the centres of mass of mirror and RM must coincide to reduce the coupling among the various degrees of freedom. The structure required to carry the compensation plate will make more difficult to satisfy this requirement. This aspect must be carefully studied.

The actuators have to be dimensioned to fulfill the displacement requirements for the locking purposes and consequently are related to the optical configuration. Moreover these actuators must not introduce extra noise that can spoil the sensitivity curve.

There are two different options for the mirror actuation by the reaction mass: the coil-magnet actuators and the electrostatic actuators.

In the case of the coil-magnet actuation [108], which is currently the reference solution, it is necessary to use a dielectric material to avoid eddy current dissipation and magnetization effects. The mechanical strength of the new insulating material must allow to use the reaction mass also as a safety structure for the mirror.

The design of the RM can be similar to the one of Virgo+ which is composed by different parts (see figure 57): an inner dielectric hollow cilinder which holds the coils and is in direct contact with the mirror sides and an outer stainless steel part, far from the coils, which makes the RM structure stiffer and increases the overall mass. The dielectric material must be chosen to be UHV and cleanliness compatible. The use of a dielectric material could give rise to the problem of the mirror static electric charging by friction with the RM. A solution can be the use of dielectric materials having a finite high resistivity that avoids the formation of stray currents but reduces the presence of static charges. The market offers several kinds of high technology plastic or ceramic materials that can be useful for our purpose. A possible choice is the TecaPeek CF30, a kind of polimeric plastic, loaded by carbon and grafite particles to increase its density and have a slight electrical conductivity which is useful to avoid the static charges formation. This material will be used for the Virgo+ update and it is being tested in this frame. For an advanced configuration other hi-tech materials will be studied in order to improve the performance of the system.

14.3 The Marionette Reference Mass

A new configuration for the last stage suspension system is being studied for AdV. It will include a new element: the Marionette Reference Mass (MRM). The new design of the last stege is conceived having in mind three main objectives:

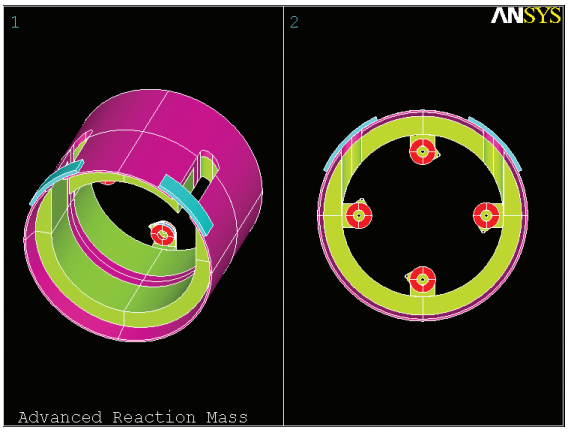

Figure 57: Schematic picture of the new mirror reaction mass. The various colours indicate the different materials used.

- to suspend a larger diameter mirror avoiding any mechanical interference between the marionette and the pots installed on the separating roof of the Ultra High Vacuum (UHV) chamber;
- to simplify the payload installation and its preliminary alignment procedure;
- to guarantee a high level of mirror cleanness without spoiling mechanical performance of the suspension system.

The vacuum chambers hosting the Superattenuators (about 10 m tall) have volume of about 30 cubic meters and they are divided in two sections: the upper part hosting the IP and the filter chain, and a lower part where the marionette, reference mass and mirror are hung. The two sections are divided by a separating roof (see fig. 58) consisting of two metallic plates (about 2 m in diameter) and forming an Intermediate Vacuum Chamber (IVC). This technical solution allows the two compartments to be kept at different vacuum level: 10^{-6} mbar of total pressure for the tower upper part and 10^{-9} mbar of total pressure for the UHV chamber where the mirrors are accommodated. Moreover the IVC structure represents a very good mechanical protection from any contaminant and pollution of the mirror environment. The separating roof structure is completed with four pots bolted on the second plate. These pots are adopted to enclose, in the low vacuum level (10^{-6} mbar) volume, the legs of the steering filter (better known as Filter7, F7) and the coils acting on the marionette magnets. The two vacuum compartments are in connection only through a conductance pipe used as a passage of the suspension wire connecting the payload to the F7 (see fig. 58). In order to simplify the assembling procedure reducing the human presence in the vacuum chamber during that phase, it is necessary to review the last stage structure and its interface connection with the F7. Changes in the suspension system structure will also have an impact on the hierarchical control strategy of the mirror. A structural change of payload and F7 will require a detailed study of the new dynamic behavior, new mode identification and a careful compensation of the recoil effect. The MRM will be installed, as an additional suspended element,

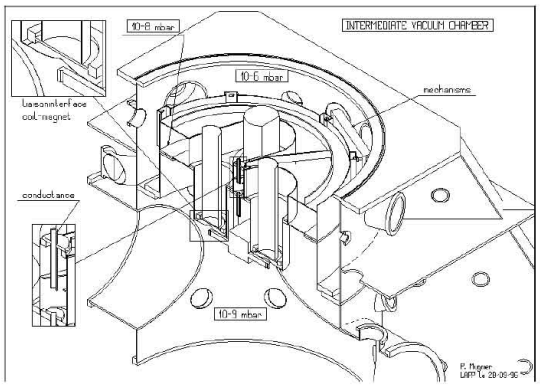

Figure 58: Sectional view of the base tower with the Intermediate Vacuum Chamber, the pots and the conductance pipe.

within the UHV chamber between F7 and marionette re-placing the F7 legs. It will host the actuator coils for steering the marionette. In this way a more compact design of the payload will be conceived and the IVC structure could be revised to accommodate a mechanical filtering system for the air flow entering within the UHV chamber. Following these project guidelines, the payload integration on the suspension system will benefit of:

- a wider clearance for the monolithic payload assembly, including the possibility to install a larger diameter mirrors;
- a more compact payload pre-aligned on bench will reduce the permanence time of two operators within the high vacuum chamber for the installation and its fine positioning;
- a quasi-laminar flow of clean air within the UHV chamber volume to be used during the assembly phase (TBC).

14.3.1 Status of the related R&D

Two groups are involved in this activity: the INFN Roma1 and the INFN Pisa. After a preliminary experience performed on a small scale MRM prototype built and assembled at INFN Roma1 laboratory, the geometry has been changed and a new full scale prototype has been conceived. The development of this second design has been done with a fundamental support of a detailed FEA [194] through which the mechanical inner modes of the structure have been identified. The prototype has been built with a shape of four petals flower having the structure inner modes at high frequency. With this choice a contamination of the control bandwidth with annoying modes should be avoided confining them in the high frequency region (higher of about 200 Hz). The MRM assembling, recently carried on, has been also very important to better define the wire suspension system to be adopted for its integration within the payload volume (installation between the F7 and the Marionette). In addition, even if the design is not the final one, it will be

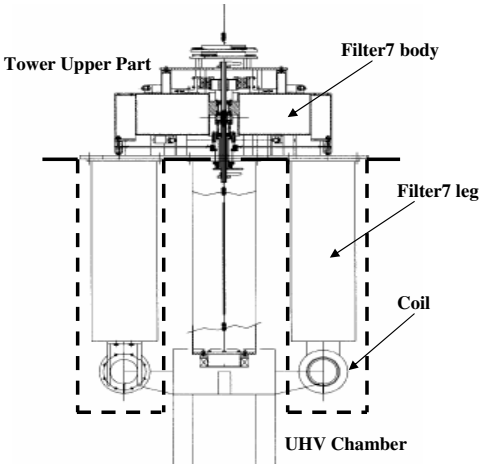

Figure 59: Technical drawing of the F7 body and legs. The dotted line in the picture represents the separation limit between the two vacuum compartments obtained bolting the pots on the second plate of IVC. The mechanical support (F7 legs) of the coil actuators faced to the marionette permanent magnets is also visible.

of great relevance in testing the feedback control strategy of the last stage suspension for AdV.

14.4 Mirror local control system

The main function of local control system is to drive the position of the mirrors in the signal and dynamical range of automatic controls even starting from very large misalignments related to the presence of a low frequency suspension. During the commissioning this system has to ensure both robustness and control low-noise in order to gradually drive the interferometer towards the delicate phases of locking and automatic alignment in various intermediate configurations. The control is limited by the ground seismic noise and acts in the range $5 \times 10^4 - 0.02\,\mu$rad. Mirror local control of AdV system will be similar to that implemented in Virgo. However, given the Virgo experience and the new design of AdV payload one can delineate few main constraints for the update of the system. They are listed below each followed by a concise motivation.

(i) Coarse mirror control The existence of further bodies attached to the mirrors should be reduced. If it will not be possible to prevent the need of dynamical re-alignment the markers will be attached to the rear face of the reaction mass. Their use through the novel CCD imaging will provide the same performance as those located on the mirror main face.

(ii) Transversal pendulum A further optical lever with incidence on the mirror reaction mass will be used to damp transversal pendulum oscillations of the payload.

(iii) Large oscillation prevention Large oscillations of the payload are normally prevented by digital control guardian, however the experience shows that they can still occur and that they are due to SA control operation or hardware failures. In long suspensions the effect is quite reduced by the presence of the conductance pipe between the payload and the marionette. Provided the use of monolithic fibre suspensions and the possible novel design of the payload (MRM) a suitable system of motorized stops, preventing misalignments and oscillations larger that $\pm$ 7 mrad would bring the system in the range of optical levers through the standard viewports using standard PSD devices, with the further advantage of simplifying the local control setup, which would make the use of CCD optional.

(iv) Remote optical diagonalization The efficiency in separating the degrees of freedom by means of optical diagonalization reachable with Virgo equipment is significant (0.2-0.5 %) but the access to the location of local control micrometric slides have occurred more frequently than expected. Motorized control would significantly improve safety conditions (it is close to viewports) speeding up the process of PSD slide readjustments after maintenance interventions.

(v Laser diodes of optical levers. The standard devices used for Virgo will not be changed, provided that a diode replacement facility is being set up at the site in order to cut the cost of factory replacement. These devices are suitably robust in case of stable loading on the electric means (3-4 y). However, new systems with LED will be studied in parallel.

14.4.1 Status of the R&D

The local control facility used to test, in air, the Virgo+ payload with monolithic suspension is very similar to the Virgo standard. It allowed to compare the payload equipped first with steel wires and then with fused silica fibres. The transfer functions of all the d.o.f. but roll, vertical and transversal pendulum (x) have been measured and the payload have been controlled using both marionette and mirror optical levers and acting from ground and reaction mass. It is foreseen to install the x damper using a further optical lever (item ii above). A set of vertical resonant frequency measurements using an accelerometer will be performed in order to close the and refine the analytical model developed and the FEM model. The main result is that the fibre suspension and the actual design of the prototype are robust with respect to tilt and translation oscillations, even sustained at the level of an excitation caused by control operation failure occurring at the payload level $20 - 50$ mrad$_{0P}$, 5 mm$_{0P}$), for several days. The slight differences with respect to the steel case can be exploited and optimized by implementing in the final design of the marionette few modifications in order not to have pitch resonant frequency in the range of microseismic disturbance (150-600 mHz).

14.4.2 The Electrostactic Actuators R&D

The reference solution for the ADV actuator is the coil-magnet. However, an interesting alternative option for the control of the suspended mirrors is the use of electrostatic actuators (EA). This solution, already proposed years ago [109], was implemented on GEO600 [110] with good performances, and other research groups are currently working on it for the implementation on Advanced LIGO. The full characterization of a typical EA can be found in [111].

The use of EA could offer several advantages with respect to the coil-magnet one. The first evidence is the possibility to use the mirrors as they are, without the necessity to glue the magnets on them. This give, of course, an immediate benefit in term of reduced contamination of the mirror surfaces during the preparation of the payload. But the main advantage is the reduced degradation of the mechanical quality factor of the test mass [112]. Another advantage is the strongly reduced coupling with external magnetic fields. A residual coupling could arise at the level of the marionetta, that is still controlled by magnet-coil pairs, but in this case the residual noise requirements are more relaxed. On the other hand, any possible coupling with variations of external electric fields, is largely reduced thanks to the high electrical conductivity of the vacuum tank.

On the other hand, also some drawbacks are expected. The most important are summarized in the following. A reduction of the quality factor both for the suspension as well as for the test mass itself is foreseen, as reported for example in [113] [114] [115]. This damping effect seems also related to the geometry of the system and to some working condition, as, for example, the frequency of the actuation signal or the electric field intensity. Another problem arises since the EA can only pull the test mass respect to the actuator, as a consequence, in order to achieve an effective displacement control of the mirror it is necessary to use a bias voltage. This can generate two different problems. The first one is related to the presence of stray electrical charges on the dielectric test mass, that can couple with the strong electric field generated by the actuator resulting in an increasing force between the mass and the actuator that produce a slow drift as final effect. The second one concerns the improved actuation noise due to the this large bias. Another possible source of noise can be the joule dissipation inside the actuator electrodes, in particular if the driving voltage is at high frequency. The heat dissipation can result in extra thermal noise for the mirror. Finally the distance between the actuator and the test mass has to be fixed taking into account the safety conditions for the monolithic suspension that will be adopted in AdV.

14.4.3 Status of the Related R&D

An R&D program is in progress at INFN Napoli to if this kind of actuation system can be effectively used in AdV, replacing the existing coil-driver system. The main topics to investigate in the R&D program are the following:

- Design of the EA pattern;

- Study of the actuator driving technique;
- Reduction of coupling noises;
- Effect of the Coulomb damping.

The action of an EA, composed by a simple array of electrodes polarized at opposite voltage is fully discussed in [111] by using a model based on the image charge. On the basis of the model, and assuming a distance between the actuator and the mirror of about 1 mm, a simple 4-patterns actuator was designed and characterized. The length of each electrode is $a = 4$ mm, the distance between each electrode is $b = 5$ mm, the height of the electrodes is $L = 4$ cm and the number of electrodes for each pattern is $N = 8$. The test mass used in this phase was a plexiglass cylinder with a diameter $d = 14$ cm and length $l = 10$ cm. As readout system, a standard optical lever was used to measure the position of the test mass.

The distance between the electrodes was chosen in order to allow a polarization as high as 2 kV, without perforating the dielectric substrates. The other dimensions, as well as the number of electrodes, derive from the space available to actuate on the test mass and from the theoretical model.

Another feature of the actuator is the influence of the electric charges that can be found on the test mass. Since the actuator generates also a static electric field, it is clear that any unbalanced charge on the test mass produce an additional force on the mass itself. This effect is very well visible on the prototype. As a driving signal is applied on the actuator, a slow drift of the test mass position takes place. This effect was removed by modulating the correction signal at high frequency. In this way the residual electric filled has no static component and the net electric charge do not produce any drift.

The sensitivity of the optical lever (about 10^{-8} m/Hz1/2 at 10 Hz) did not allow to perform measurement at higher distances, that are the more interesting one for the application in AdV. To overcome this problem a new set-up was developed. It is composed by a simple Michelson interferometer. The optical lever for reading the suspended mass position respect to the ground is still included to monitor angular displacement of the suspended mass and to reduce the natural oscillation of the suspended mass before to start the interferometric measurement. The interferometer is locked by acting on a PZT mirror and the displacement due to the electrostatic actuator can be deduced by the correction signal applied to the piezoelectric actuator.

In the first phase of this R&D step, the standard actuator designed on a vetronite substrate was used, but in the second step of this study it is necessary to move toward a more realistic set-up. In particular, since the choice for the future recoil mass of AdV, is a dielectric, vacuum grade, substrate (the tecapeek is the most promising), it will be necessary to realize an actuator on the same substrate. In this case the pattern has to be realized by metallic evaporation or sputtering as well, depending on the property of the substrate. Moreover a full scale prototype has to be used in this step, in order to perform a realistic evaluation of the system performances.

Finally a careful study will be devoted to the design of the driving electronics, as well as to the wiring of the actuator. Up to now, in fact, a commercial high voltage amplifier was used, one for each pattern of the actuator, while the AC bias was digitally performed. For the future it will be better to have a suitable home-made electronics, both for the lower cost and for the more appropriate design. Moreover an analog oscillator should be used to produce the AC bias, in this way it will be possible to increase the frequency of the bias, in order to not introduce any interference in the measurement frequency band.

15 Monolithic suspensions

Monolithic fused silica (FS) suspension of the four 42 kg Fabry-Perot cavity mirrors will be realized for AdV, exploiting the experience achieved developing the Virgo+ payload. The optimal geometry and technology is being pursued with the objectives of minimizing the pendulum thermal noise, fulfilling the requirements for an optimal control of the test mass, ensuring safety and reliability. For Virgo+ a large amount of work has been made to reduce the risk in the welding procedure. The fibers (once welded directly to the mirror) are now welded to intermediate components (called ears) silicate bonded to the lateral flats of the test mass. The former procedure induced a lot of thermal stress on the bonded surfaces that could damage the silicate bonding and eventually break it. Another problem is that the fibers pass through a dangerous manipulation procedure that can open cracks on their surface decreasing their breaking strength. To recover these problems a new technique has been developed: two lateral supports with vertical grooves are attached using silicate bonding to the mirror lateral flats. Fibers are produced apart from a fused silica bar previously welded to an upper clamp and a lower anchor. The fibers are then placed in position clamping the upper part to the marionetta and inserting the lower anchor below the lateral supports bonded to the mirror. In the end the anchor and the supports are bonded together through silicate bonding or *water glass*. Although this solution has been successfully implemented for Virgo+ it would be easier (and with lower mechanical dissipation) to avoid the lateral bonding of the supports to the mirror. For AdV it is therefore proposed to machine the lateral supports out of the test mass bulk (see sec. 15.1.2). The technical feasibility is under investigation.

15.1 Geometry and dimensions

In this section the preliminary considerations that drive the design of the monolithic suspensions are presented. Breaking strength is not the only parameter that matters.

15.1.1 Mirror geometry

The AdV test masses will weight 42 kg. They will have a diameter of 350 mm and a thickness of 200 mm. Such mirrors are twice as heavy and thick with respect to the Virgo and Virgo+ test masses. This

15.1.2 Lateral support machining

The suspension scheme tested for Virgo+ can be applied for AdV trying to reduce the most critical part induced by silicate bonding the lateral supports on the lateral mirror flats. The supports can be machined out from the mirror as in figure 60, the lower surface of the support is polished to perform a silicate bonding. This solution must be

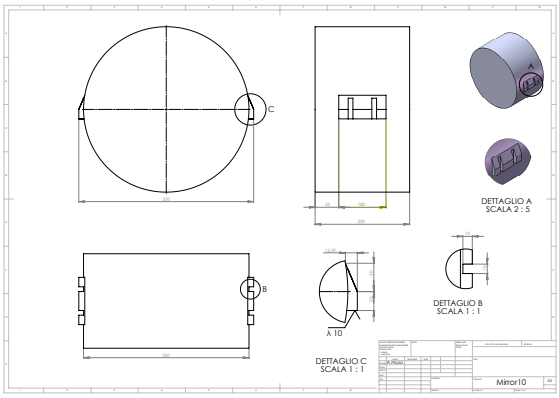

Figure 60: Scheme of a 42 kg mirror with a possible shape of the lateral supports for applying the monolithic suspension as in the Virgo+ configuration.

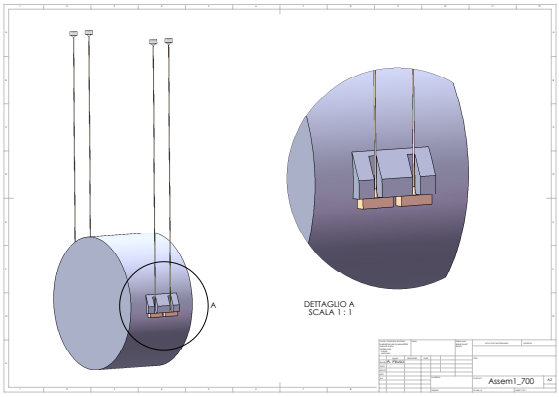

Figure 61: Sketch of a 42 kg mirror with lower clamps and fibers in position.

deeply discussed with the company which produces the mirror and with the LMA people working on the mirror substrate and coating production (see section 8) for the cost and time evaluations. In addition, it is important to evaluate the deformation caused by the mirror large mass on the mirror face when it is suspended vertically and, in case of a non-negligible result, to evaluate how much to increase the distance between the suspension wires in order to reduce it.

The suspension scheme proposed is the following: one fused silica part called "anchor" will be welded to a 1.5 mm fused silica bar and to an upper clamp. Using the CO_2 laser machine the fiber will be produced from the bar welded to the clamps, the whole clamp-fiber will be placed in position on top to the marionetta and on the bottom under the mirror support. The contacting surfaces of the two parts (both with a polishing) will be bonded onsite using the silicate bonding or *water glass* procedure as for Virgo+ see figure 61.

To this aim it is necessary to find a geometry of the lateral supports easy to machine, and

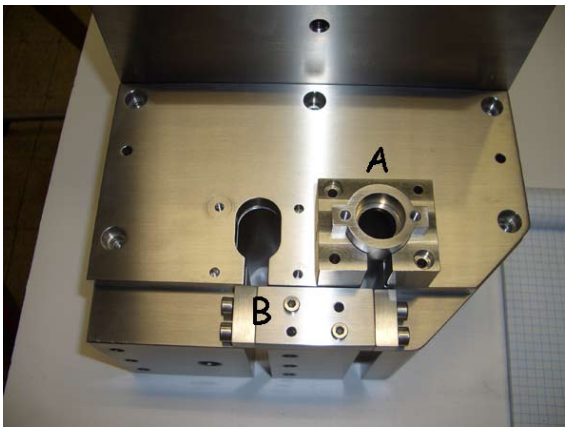

Figure 62: Photo of the wire clamps on the marionette. A. Steel box for the silica upper clamps. B. Reaction mass wires clamp.

to demonstrate that the surface quality is sufficiently good for thermal noise performances.

As anticipated in the section 14.1 the role of the upper clamps coupling with the marionette in order not introduce further frictions and recoil losses is very important. For this purpose a stainless steel box has been carefully designed with the aim to host the silica upper clamp and to attach it to the marionette without introducing further losses (see fig. 62). The steel box is formed by two pieces. An external one fastened to the marionette by four screws. An internal one in direct contact with the fused silica and fastened by lateral screws to the external one. The silica core is kept fixed in its box by an upper lid fastened by screws. The steel inner box is also designed as the support of the upper clamp during the fiber pulling (see section 15.1.3) and then is coupled to the tool used to insert the fibre on the marionette lateral side, as foreseen by the assembly procedure.

In the frame of the development of Virgo+ monolithic suspensions, optimization tests of the upper and lower clamps will be performed in the facility in Perugia. A pendulum composed by one of the fibers produced for the payload suspensions, coupled to an upper clamp and a lower clamp, and loaded with 1/4 the mirror mass, about 5 kg will be used. With this set up, the maximum Q value which could be measured in the facility will be about 6 10^7, very close to the value expected for the monolithic fibers, 7 10^7.

15.1.3 Fibres geometry and properties

Fibre length, fibre stiffness and position of bending points are driven by the room available and the choice of resonant frequency of the various modes of the suspension. This choice depends strongly on control issues and a careful investigation is being carried on. The vertical bouncing frequency of the last stage represents the lower limit of the detection band because although the vertical to horizontal coupling is small (it has been assumed 10^{-3}), the vertical oscillation does not have any dilution factor. The result is that the

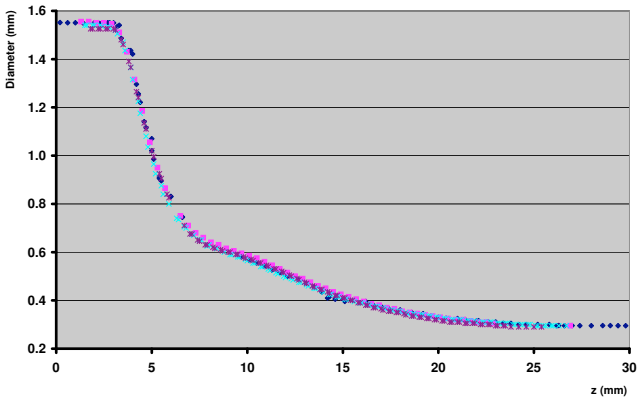

Figure 63: Profiles of the 'neck' region of several 280 μm diameter fibres: the superposition of the curves shows the good reproducibility of the fibre shape.

vertical bouncing mode is clearly visible in the thermal noise spectrum and this frequency must be kept below 10 Hz. In order to have the detection band with the smaller number of resonant modes as possible, the first violin mode should be as high as possible. The position of the violin mode depends on the fibre cross section and then ultimately on its breaking stress. A violin mode at about 430 Hz is about 100 Hz higher than what can be obtained with steel wires.

Fused silica fibres are presently produced for Virgo+ starting from high purity fused silica cylindrical bars commercially available 1.5 mm thick. A machine for pulling fused silica fibres using a CO_2 laser has been developed at the University of Glasgow [207]. A duplicate of this machine has been assembled in a dedicated laser room at the site of the Virgo experiment. After modifications of the optical path the 100 W CO_2 laser provides enough power for welding the rod to the silica parts used for realizing the monolithic suspension. The fibre is then pulled directly from this welded rod.

Due to the low thermal conductivity of silica the thermoelastic peak of 400 μm diameter fibre is at 11 Hz. At this frequency the fibres mode shape is almost straight and the only significant bending is at the upper and lower ends. Using the effect of non linear thermoelasticity it is possible to demonstrate that exists a stress at which the thermal expansion and thermal elastic compliance compensate each other and that this stress for fused silica is in the range 200 MPa to 250 MPa. All these data seem to indicate that the fused silica fibre with a dumbbell shape has the lowest thermal noise. The possibility to control the pulling velocity offered by the CO_2 pulling machine allows to realize tapered fibres with a profile that is reproducible with a precision lower than 10 μm.

When produced the fibres are tested with a 10 kg load. Fibers breaking during this first

Violin mode (Hz)	Bouncing mode (Hz)	Distance between b.p. (mm)
435±1	5.9±0.1	692.0±0.2
434±1	5.9±0.1	691.9±0.2
434±1	5.9±0.1	691.6±0.2

Table 14: First violin and bouncing modes frequencies and measured fibre lengths between bending points for some of the 280 μm diameter fused silica fibres realized for Virgo+.

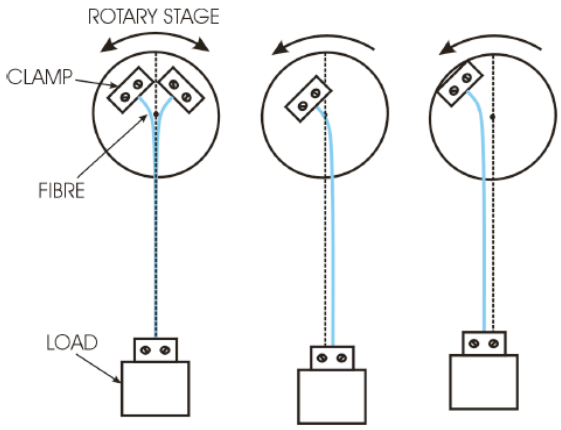

Figure 64: Sketch of the setup used for a direct measurement of the fibre bending length.

test phase are very few. Measurements of the breaking stress for several 280 μm diameter fibres were performed, showing values always greater than 4 GPa. A full caracterization of the breaking stress distribution will be performed.

The bending length λ of the suspension is the distance of the fibre bending point from the clamped end. Positioning the bending point on the center of mass plane of boththe marionette and the mirror allows minimum coupling between the different degrees of freedom; it is also possible through a simple model of the fibre based on the knowledge of λ to study its dynamical behaviour. The tapered profiles of the fibres near the heads require this quantity to be directly measured. For doing this a specific instrument was realized [208]. The fibre is clamped to a rotary stage, suspending a load as close as possible to the working conditions. If the bending point is placed exactly on the rotation axis of the stage, when the top head of the fibre is rotated, the bottom part of it actually does not move.

Acting on a micrometric sleigh moving along a diameter of the rotary stage it is possible to find a position where the fiber movements get their minimum amplitude, thus having a measurement of the bending length. This device provides also an easy way to measure the first violin and bouncing frequencies. The results obtained for some of the 280 μm diameter fibres suspended to a 5 kg load are summarized in table 14.

Advanced Virgo Preliminary Design:
PART 4:

Electronics, Vacuum, Facilities

16 Electronics, controls and data acquisition

This section describes the most important components of the DAQ, Control Electronics, Environmental Monitoring, and Software systems for AdV. The main upgrades, with respect to the Virgo or Virgo+ configurations are discussed together with the R&D programs already active, or to activate, that are necessary to achieve the AdV requirements. In fact for the advanced detector it is expected to perform more effective and less noisy controls, to increase the number of the suspended optical components to control, and, in general, to manage a larger amount of signals with respect to Virgo+.

A strong interaction with many other subsystems is foreseen to make effective the efforts on all the listed tasks .

16.1 Suspension Electronics

The main activity concerning the Suspension Electronics is the upgrade of the conditioning Electronics used to manage the sensor and the actuators placed in the suspension stage, namely the accelerometers, the LVDTs, the stepping motors, the local control sensors and the coil working at different levels of the chain. Other components, not foreseen for the Virgo interferometer, that will be likely implemented in the Advanced detector, like tilt-meters and PZT actuators, are described in dedicated sections.

Moreover, since the AdV optical scheme consists in a double recycled interferometer, a new suspension electronic, including the sensors and the actuators, have to be implemented for the control of the Signal Recycling Suspension.

16.1.1 LVDT Electronics

The LVDT sensors actually used to measure the position of the top stage of the suspended chain in the very low frequency band, did not require any particular improvement. They are, in fact (and being dominated by seismic noise), enough sensitive to be compliant with the AdV requirements. On the other hand the conditioning electronics of these sensors need to be upgraded for two main reasons. The first one is the age of the electronic components used in the driver, that are now obsolete and difficult to maintain; moreover a significant improvement in terms of performances is expected by using more recent and specific components. The second reason concerns the possibility to implement a digital output on the driver by using an onboard ADC to immediately digitize the position signal, and sending it to the processing and control electronics through a digital link. This solution has the clear advantage to greatly reduce the possible interferences and electrical pick-ups from the electromagnetic noise present in the environment. Finally it is foreseen to use such new drivers also to manage the LVDT sensors used inside the accelerometers of the top stage; this solution will avoid the development of hybrid electronic board and will make more logical and easy to maintain the full suspension electronics.

INFN Pisa is being studying a new design for LVDT electronics since a few years. A candidate ADC converter was selected and tested together with a DAC converter and a PLL circuitry capable of letting the two converters operate at different rates synchronously with VIRGO timing signal. Such studies were partially integrated in the R&D activity for the upgrade of Virgo control electronics together with new DSP design. Characterization of the developed prototype board was subject of a University Degree thesis [195]. Digital data link was studied taking advantage from a fellowship. The final report is available [196].

Nevertheless a full integration of a such system has still to be made and has to be carefully evaluated.

16.1.2 Accelerometer Design and Electronics

The upgrade of the accelerometers used to perform the inertial damping of the top stage involves both the sensor and the internal driver (sensors are force-balance accelerometers). At sensor level some adjustment in the design is needed to enhance the performances. In particular the balancing and the stability of the suspended mass, have to be improved for enhancing noise performances, especially in the low frequency range, that is the most interesting for the inertial damping application.

The main upgrade foreseen for the driving electronics, apart from the use of an external LVDT driver, and the introduction of a digital output for the acceleration signal, as already stated in the previous section, is the replacement of a digital feedback instead of the analog one currently used. The implementation of such digital system would allow the design of more effective feedback for the internal loop, resulting in a wider frequency band, in an improved robustness and in improved noise performances. Of course for this aim some suitable additional electronics has to be hosted on the driver, namely an ADC to digitize the position signal coming from the LVDT, a DSP for the digital filtering, and a DAC for the actuation on the internal coil.

In addition to the studies carried on for ADC and DAC converter mentioned above, a few different option for the digital controller implementation were investigated by INFN Pisa. Such controller could be implemented with either a devoted DSP processor or with one of the multi-DSP boards developed by INFN Pisa handling several sensors at a time or with fast FPGA.

Of course, as already quoted in the previous section, the effectiveness of such digital driving has to be carefully evaluated.

Concerning the actuation system inside the accelerometer, a few initial studies were carried on to evaluate the possibility to replace existing voice coil actuator (coil-magnet) with a coil-coil pair.

16.1.3 Coil Driver Electronics

The Coil Driver were upgraded for Virgo+ and their current performances, in terms of noise, linearity and frequency band are already compliant with the AdV requirements [197] [198].

The major upgrade is related to the introduction of a digital input, through a fast optical link connected to an onboard DAC and to a selection of a new DAC converter (the one in use is obsolete). The digital link is particularly important since the actuation signals of the coil are the most critical for the ITF sensitivity, and a connection between the control and processing electronics that is virtually unaffected by environmental interferences is strongly desirable.

The R&D related to the development of an engineered version of coil driver prototypes is now closed. What still remain to be studied is the use of high power-low noise modes with marionetta actuators. INFN Pisa will carry on some test during next commissioning phase.

16.1.4 Step Motor Driver

No changes are foreseen for the driving system of the stepper motors working on the suspension. A minor changes is related to the control logic that is currently obsolete. A standard commercial solution seems the best choice since there are no special requirement on the performances of the system.

Possible solutions are being investigated by EGO Electronics group in collaboration with INFN Pisa.

16.2 Control Electronics

The major upgrade in the architecture of the Processing and Control Electronics, namely the DSP, the real time CPU, the ADC, the DAC and the digital optical link, was already performed during the Virgo+ upgrade. In particular the new processing board [199], with its 6 DSP, allows a very high computing power with respect to the old Virgo single DSP board. Moreover the new Photodiode Readout Scheme and the new Global Control Architecture (section 16.4), both based on more recent CPUs and faster digital optical links, allow a better conditioning, more powerful control algorithms and an higher frequency band of the error signals. Thanks to these changes it is possible to perform better control strategies and to design more effective digital filters.

Some improvement is still required for the analog/digital converters, ADCs and DACs, in particular about the effective number of bits, in order to reduce the quantization noise introduced during both the sensing and the driving.

16.2.1 DSP

No major change is foreseen on the processing board. Nevertheless a daughter-board has to be developed to manage the digital signals exchanged with the suspension electronics equipped with digital input or output. The architecture should be very similar to the one already implemented for the global control signal in Virgo and in Virgo+, but in this case it refers also to local control signals.

Digital data link was studied by INFN Pisa taking advantage from a fellowship [196]. A preliminary design of the board is already available.

16.2.2 ADC and DAC

The ADC of the suspension control electronics, in the Virgo and Virgo+ configuration, are located in the same unit of the processing electronics and are used mainly to convert signals coming from the suspension electronics, located close to the respective tower. In AdV some of these converters will be placed directly in the suspension electronics (section 16.1). Despite of their location, an improvement of their performances, mainly in terms of quantization noise reduction, should be achieved.

As for the case of ADC, also the DAC performances need to be improved. The DAC noise is even more critical, since the current performances are still a limiting factor for the achievement of the Advance Virgo sensitivity in the low frequency region, due to the direct coupling with the coils actuating on the test masses. A specific R&D is dedicated to the selection of a suitable chip, with an higher number of bits with respect to now and higher sampling frequency to decrease the noise content.

A candidate ADC converter was selected and tested together with a DAC converter and a PLL circuitry capable of letting the two converters operate at different rates synchronously with VIRGO timing signal.. Such studies were partially integrated in the R&D activity for the upgrade of Virgo control electronics together with new DSP design. Characterization of the developed prototype board was subject of a University Degree thesis by M. Errante, “Caratterizzazione e realizzazione di una scheda di conversione D/A A/D per l’esperimento VIRGO”, Facoltà di Ingegneria Università di Pisa.

The ADC used for the photodiode and quadrant readout system are described elsewhere (sections 16.3.1 and 16.4).

16.3 Data Acquisition System

The most important upgrade of the Data Acquisition system was already performed during the Virgo to Virgo+ migration [200] [201]. The main changes concern the use of a new ADC board, the substitution of the RIO cpu with more performing PC running under RT-Linux OS for data collection and pre-processing, the substitution of the old digital optical link (DOL) with new fast optical link (TOLM) that can be hosted both by

the existing VME architecture and by new RT-PC architecture and the introduction of a modulation-demodulation optical card that is used to multiplex and demultiplex packets of data transmitted through optic links.

Many changes are foreseen in AdV that will produce an increase of the data flow. Some of them will be implemented on Virgo+:

- Pre-ModeCleaner (PMC) in the laser system, compensation for the thermal lensing in the Faraday isolator;
- Initial Thermal Compensation System (TCS) and Phase Cameras;

Other changes will be done on the Advanced detector:

- Enhancement of the Thermal Compensation System (TCS) and Phase Cameras;
- Introduction of the Signal Recycling (SR) system;
- Auxiliary laser and sensing system for the locking of high the finesse cavities (CALVA);
- Introduction of the marionette reference mass (MRM) equipped with sensing and actuation systems;
- Introduction of tilt sensing and control in the superattenuators (SAFE).

Nevertheless the performances of the new Data Acquisition System is already able to sustain and manage a data flow even 4 times higher with respect to the past, and it is, for this reason, already compliant with the AdV requirements.

16.3.1 ADC

The new ADC board [202] will be used both for the photodiode and quadrant readout as well as for the environmental monitoring. The new ADC have a larger number of bit (18 bit instead of 16 as in the past) and an higher sampling frequency. These changes result in a reduction of the expected quantization noise with respect to the Virgo configuration. The ADC boards are equipped with a digital output, consisting of a fast optical link, that greatly facilitate the distribution of the collected data to the other components of the Data Acquisition System.

No major change is foreseen on the ADC Board architecture. The minor upgrades, driven by the check of their performances during the Virgo+ commissioning, will be performed by the LAPP group.

16.3.2 RT-PC

This item requires no particular comment. Commercial solutions are used for the hardware and in the next future the performances of such computers are expected to increase.

In this way it become easy to increase the computing power if necessary. The other components, namely the TOLM, are independent devices and can be easily inserted in the new hardware.

16.3.3 TOLM/ MUX-DEMUX

The TOLM (Timing & Optical Links Mezzanine) [203] provides for the timing and data exchange between the transmission media, namely the fast optical link, and the hosting hardware, usually the PCI bus of a PC. Since all the systems collecting or sending data for Data Acquisition purposes are equipped with this mezzanine, it becomes very easy to distribute the signal along the chain. Of course, since the data collected by the different RT-PCs have to be sent to few main collecting computers, it necessary to introduce an intermediate system able to collect the data coming from different sources and to drive them to the selected destination. This is exactly the task of the MUX-DEMUX board [204]. With respect to the Virgo architecture, based on DOL boards on VME/VSB bus, the performances of this new DAQ scheme, allows the transmission of an higher amount of data, thus allowing for additional channels and higher sampling frequencies in the data flow.

No major change is foreseen for the MUX-DEMUX boards, while the developing of a TOLM board with a PCI-X interface, instead of the PCI one, is very opportune to face likely future upgrade in the RT-PC hardware.

16.4 Global Control Electronics and Software

A new global control system [205] will be implemented on Virgo+, but its main characteristics are expected to be compliant also with the AdV requirements. The main difference between the old architecture is the use of PT-PC (section 16.3.2) equipped with TOLM board [203] that allow better performances in terms of computing power and data flow rate with respect to the system based on RIO cpu and DOL. The signals used by the global control to compute error signal come from the photodiode and quadrant readout, that will be also changed for Virgo+. It will be based on the same architecture used by the data acquisition system (section 16.3) and global control systems: RT-PC and TOLM, with MAX-DEMX board for data routing.

A significant change in AdV, from the global control point of view, is the insertion of the Signal Recycling mirror. In fact the new global control has to manage the generation of SREC error signal both for locking and alignment. Moreover for the locking and alignment purposes, AdV will use at least three modulation frequency, up to 80 MHz. Due to this change, the electronics devoted to perform the modulation and the demodulation need some upgrade.

16.4.1 Modulation Frequency Generation

The oscillator and the frequency synthesizer have to be selected in order to ensure a low noise, highly stable modulation. A survey of the existing devices has to be done to understand in advance any possible constraint on the modulation frequency.

The R&D on this task will be performed inside the ARTEMIS group.

Moreover the electromagnetic compatibility of the high modulation frequencies with the environment, especially for possible effects on other electronic devices has to be verified.

A study about possible unwanted interferences will be performed within the EGO electronic group.

16.4.2 Global Control software

The software architecture of the global control, as it is foreseen for Virgo+, should be compliant with the AdV requirements. Nevertheless it is necessary to verify if major software upgrades in the global control architecture are necessary to face new requirements that could come from the ISC design.

The work on this item will be performed inside the LAPP group.

16.5 Environmental Monitoring System

The high expected sensitivity of AdV requires a very carefully designed environmental monitoring system, since the coupling of ambient noises will be more challenging with respect to Virgo or Virgo+. Anyway the experience gained during the Virgo functioning is a fundamental guide in this task, both in sensors choice and placement in the most critical part of the interferometer.

Nevertheless a general improvement of the system performances has to be achieved, mainly in terms of probe sensitivity, both for a fruitful noise hunting during the commissioning phase and for an effective vetoing system during the scientific runs. The general upgrade of the environmental monitoring has also to take into account the presence of the new SR tower, that needs to be equipped with all the standard sensor.

As usual the environmental monitoring system is divided in two part: the slow monitoring and the fast monitoring, depending on the nature of the parameter to monitor.

16.5.1 Slow Monitoring

There are several step to perform to enhance the effectiveness of the slow monitoring system. The most useful probes of this set, temperature and humidity probe, need to be upgraded with more effective sensors, with higher accuracy with respect to the present

situation, reducing the need of periodic sensor calibration. Also the conditioning electronics of the probes need to be upgraded to better fit the dynamic range of the digital converter user to collect the data, allowing a full exploitation of the probe performances.

Related to this point, an important step is the selection of a new modular acquisition system to substitute the existing one, that is now obsolete and difficult to maintain. Moreover the actual system generates, in some conditions, a significant RF noise that produces some noise on other subsystems that use any modulation/demodulation electronics, like photodiode readout or LVDT position sensors. During the Virgo commissioning this problem was partly removed, but a more robust solution has to be found.

Another minor upgrade consists in the addition of weather and lightning sensors also in the terminal building.

The R&D activity, carried out at INFN Napoli, on this task, has started with the selection of a new modular acquisition system, equipped with 32 ADC channels with 16 bit resolution. There are two main improvements with respect to the old module. The first is the number of bits: the old module was only 12 bits. The second is related to the simpler architecture of the DAQ chain. In fact the new architecture needs no master collector, while each module can be independently managed through the standard network, using a ModBus protocol. The next step is the evaluation of the ADC characteristics and the measurement of RF immunity of the module.

16.5.2 Fast Monitoring

The fast environmental probes, and related conditioning electronics, have to be upgraded to increase the monitoring system sensitivity in the case where the disturbance dynamic range is significantly smaller with respect to the converter range. Most of the actual sensors can be upgraded simply by modifying the conditioning electronics, also taking into account that the increased dynamic range of the new ADC (section 16.3.1) will allow an enhancements of the sensitivity for the sensors that are currently not limited by the electronic noise. Moreover the new ADC will integrate also shaping filters that could relax the requirements for the signal conditioning.

For some sensors a major upgrade is required:

- Episensors: the sensitivity of these probes is not at limit, but due to the slow drift of the DC content, it is difficult to increase their response without saturating the conditioning electronic. In particular it is necessary to filter out the low frequency part of the signal before the amplifier. Since these sensor are limited, in the low frequency range, at about 100 mHz, this change will not compromises the effectiveness.
- PZT Accelerometers: the current probes have limited sensitivity and the conditioning electronics is too noisy to allow further gain. It is necessary to change the sensors to gain sensitivity.

- Magnetometers: the high sensitivity produces, in some conditions, a saturation of the probe due to the 50 Hz contamination in the environment. To overcome this problem the conditioning electronics was modified to reduce the sensitivity, but the likely lower electromagnetic background foreseen in the buildings for AdV should allow the reverting to the original sensitivity.

Finally, due to the larger number of system to monitor in AdV, with respect to Virgo+, the total number of fast sensors should grow by a small amount: at least 2 low frequency seismometers and 2 microphones for the end buildings and 3 PZT accelerometers for the SR tower and for the TCS benches.

The R&D on these arguments is in progress at INFN Napoli. The selection of the new PZT accelerometers was already done, while the reshuffling of the episensors conditioning electronics is just started.

16.6 Local Control Electronics

The Local Control System, is composed by the CCD cameras and the optical levers, together with the respective drivers, amplifiers, and related software. All these equipments need to be upgraded to fulfill the AdV requirements, for different reasons.

16.6.1 Cameras

The major reason for changing the CCD cameras is due to their obsolescence. Limited spare parts are now available, while it is not too difficult to provide for new and more performing components based on the same technology. Of course, since these sensors have to be used for the generation of error signals for the local control system,as well as for the beam imaging, it is necessary to provide also for a suitable driving hardware that can be easily inserted in the AdV DAQ architecture.

An R&D program is starting to face this task. It will be performed by the LAPP group that already developed the current system, both for hardware and software. Some of the cameras used for the beam imaging will be changed during the Virgo+ commissioning.

16.6.2 Optical Levers

In the Virgo configuration the optical levers use a laser diode as light source. The experience done on the system, during the ITF functioning showed that the high noise level of the laser diode output power produce a spoiling of the local control performances. Moreover the interference fringe formation on refractive surfaces, like the photodiode window, produce unwanted bias on the position signals, slowly varying with environmental condition, that greatly reduces the performances of the system at low frequencies. Finally, the

actual limited dynamic of the ADC used to sample the signals from the position sensitive diode, strongly limits the sensitivity of the sensor; for AdV this contribution should decrease thanks to the lower quantization noise of the new ADC.

A partial upgrade was already obtained by modifying the PSD amplifier. In fact by performing some simple operations directly in the amplifiers, it was possible to increase the gain of the amplifier to better fit the ADC input range.

Nevertheless, due to the higher arm finesse of AdV, there are stronger requirements on the pre-alignment of the far mirrors that result in an higher required sensitivity from the local control sensors. To this aim is also desirable to use a sensitive optical lever to monitor at least the marionetta's displacements, for all six degrees of freedom, being the actual system limited to the θ_x, θ_x, and z displacements.

An R&D activity on this topic is already carried out at INFN Napoli. As source for the optical lever an ultra luminescent LED emitting at 830 nm, pigtailed with a single mode optical fiber, was selected. Due to the incoherency of the emitted light, no interference fringes are produced on any surface. Also an improvement in the driving electronics was performed to allow an optimal match with the ADC dynamic range. The next step is the definition of a suitable set-up to implement a sensing system, at marionetta level, for all six degrees of freedom.

16.7 Software Framework

The control of large experiment like AdV constitute classical examples of a heterogeneous Distributed Control System (DCS). When looking at the software part of these systems there are several functionalities that can be found in all of them, which constitute their fundamental services:

- Communication: allows that the components (control servers and clients) of the distributed system communicate among them
- Online database: refers to the possibility to access online any data point of the DCS
- Configuration database: keeps and manages the configuration data
- Logging: collects the logs from all over the system and presents it to the operator

At the beginning of the Virgo Project the choice made at that time was developing a complete custom software framework in which the majority of the mentioned services and functionalities are implemented. Over the years, this framework has been made more robust and has demonstrated to be able to satisfactorily support the experiment operational phase like during VSR1. Within the scope of the upgrades to be done for AdV is reasonable to bring the question if the existing custom framework is still a viable choice. If the current framework has to be maintained the software maintenance could become a relevant issue especially in case of major Hardware or Operating System upgrades.

Since different solutions are available and largely supported, a change of the existing one has to be considered. A first survey about possible different software frameworks was already started [206].

The EGO software group will be the leading investigator about a possible change of the software framework, while its opportunity will be verified inside the whole collaboration.

17 Vacuum system modifications

17.1 Requirements

17.1.1 Vacuum level

The improvement of the Virgo sensitivity by a factor 10 needs an improvement of the present vacuum level to lower the phase noise due to pressure statistical fluctuations. At present the system operates at about $2\,10^{-7}$ mbar (dominated by water). Originally it has been designed and tested to reach a base pressure below 10^{-9} mbar (dominated by hydrogen) and in principle this would be still possible after an overall bake-out. The formula used to evaluate the noise corresponds to the one also proposed by LIGO, which has been experimentally validated (see the appendix). The lowest point of the AdV sensitivity curve: $3\,10^{-24}/\sqrt{\mathrm{Hz}}$ at 200-400 Hz is not compatible with the residual gas noise at a pressure of $2\,10^{-7}$ mbar in the 3 km arm tubes, as shown by fig. 65, with the foreseen beam geometry.

Table 15 shows that, taking into account all the main species composing the residual gas in the arm tubes at the presently attained pressure of $2\,10^{-7}$ mbar, the corresponding noise is at the level of $10^{-23}/\sqrt{\mathrm{Hz}}$. In order to make this noise not dominant in AdV it has to be reduced by at least a factor of 10, hence the residual pressure in the tubes has to be reduced by a factor of 100.

Species	**Pressure (mbar)**	**Noise ($Hz^{-1/2}$**
H_2	2.0e-8	1.0e-24
H_2O	1.5e-7	8.2e-24
air+others	2.0e-8	3.8e-24
HC	1.0e-11	3.5e-24
TOTAL	1.9e-7	9.7e-24

Table 15: Phase noise given by actual residual gases for AdV beam geometry. It decreases as the square root of the pressure. HC contribution evaluated conventionally, less relevant in the high frequency range due to the high molecular weight.

The originally planned method of improvement consists in baking the whole system at 150C, the 3km tubes plus the 7 mirror towers. The result is presented in table 16: the resulting noise is estimated to be a factor 10 below the reference sensitivity value for AdV.

With the experience gained during the Virgo commissioning phase, when frequent interventions inside towers were needed, we have realized that the baking choice as foreseen is not convenient. After each intervention inside a tower it would be necessary to re-bake it before opening the valves toward the rest of the vacuum system, in order not to spoil the effect of the overall bake-out. The 'Brewster windows', recently removed at the Detection tower, shall be needed to separate UHV mirror towers from bench towers. This procedure

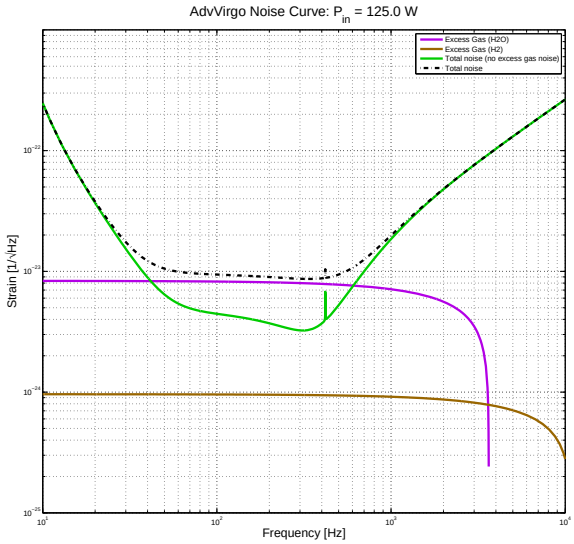

Figure 65: AdV sensitivity curve, taking into account the phase noise given by water at a partial pressure of $1.5\,10^{-7}$ mbar. The sensitivity would be limited to $8.5\,10^{-24}/\sqrt{\mathrm{Hz}}$. Including all the other residual gases as in table 15 the limit would raise to about $10^{-23}/\sqrt{\mathrm{Hz}}$

would require a minimum of two weeks for the warm-up, baking, cool-down.

Moreover baking a tower would imply further time consuming activities:

- to dismount and reinstall all 'local controls' devices and other not bakeable parts present inside the ovens, and do the tuning again once reinstalled;
- to dismount/remount links between ovens and optical benches and acoustic enclosures at input and end towers.

The overall ITF interruption shall be of the order of 1 month (to be compared to the present two days), affecting very much the commissioning plan, since several interventions inside the towers can be needed every year.

Finally baking a tower could produce unpredictable effects:

- warm-up of the lower stages of the anti-seismic suspension at 50C or more, involving movements/stresses, could be difficult to recover
- baking a tower with a real mirror has never been tried; recondensation of contaminants on mirrors and detaching of glued or silicate bonded parts are risks to be considered.

To improve the vacuum level by two orders of magnitude, it is also to be considered to reduce as much as possible other sources of water and air. Without 'Brewster windows' a significant gas load will come from bench towers upper parts, released from polymeric materials, charged up during each venting, and also through the Viton o-rings, due to

Species	**Pressure (mbar)**	**Noise ($Hz^{-1/2}$**
H_2	1.0e-9	2.1e-25
H_2O	5.0e-11	1.5e-25
air+others	5.0e-11	1.9e-25
HC	<1.0e-13	3.5e-25
TOTAL	1.1e-9	4.7e-25

Table 16: Phase noise for baked tubes and towers. The AdV reference limit is $3\,10-24/\sqrt{\mathrm{Hz}}$. The effect of the various gases is shown: the improvement is also due to gas composition change; hydrogen has a lower polarizability with respect to water.

permeation (water and air). We have to evaluate if an even very simplified IVC could be adopted on bench towers (DT/IB/MC) while permeation shall be avoided using metallic gaskets.

17.1.2 Further requirements

Other requirements are the need of displacing central area towers and of enlarging the tubes linking the towers to allow for different optical schemes. Different positions of the 'mirror towers' of the central are envisaged to allow for optimal strategies of interferometer control. The feasibility of towers displacement needs to be evaluated with respect to the existing constraints. In AdV the waist of the gaussian beams will be set in the center of the cavities; the average radius of the beam impinging on the central and terminal mirrors is assumed to be 60 mm. This requires larger diameter link tubes (four) between the central towers, larger Brewster links (Input/PR and SR/Detection). The correct aperture is to be determined, for each case, depending on the selected optical scheme. Diameters up to 1m are under evaluation, including the case of not having vacuum valves on the links.

17.2 Vacuum upgrade

17.2.1 Present status

The vacuum system consists of the two 3 km long straight tubes, 1.2 m in diameter, and 10 towers: vacuum chambers 2 m in diameter and up to 11 m high, containing the optical elements suspended to the antiseismic attenuators. Each tower can be separated from the other ones and from the tubes by vacuum valves, with up to 1 m aperture. Fig. 66 shows the lay-out of the vacuum system. Along each tube there are 6 pumping stations, 4 of them are presently in use and are equipped with a 1000 l/s turbomolecular pump. Furthermore, in each pumping station there is an Ion pump (70 l/s to 250 l/s) and a Titanium sublimation pump, conceived to be used once the tube is baked, to pump hydrogen at a total pressure of 10^{-9} mbar. They are not in use now. Presently a 1600 l/s turbomolecular pump installed in SR tower contributes to pump the central area,

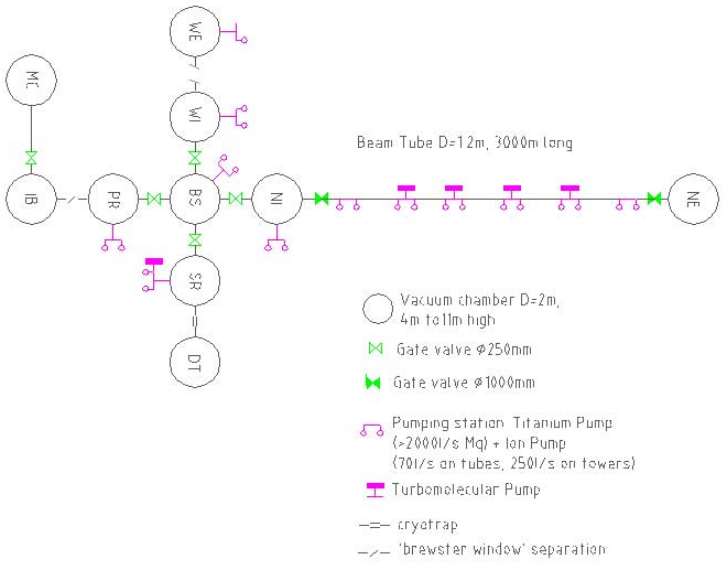

Figure 66: A scheme of the vacuum system.

constituted by the lower parts of the towers containing the payloads. Towers comprehend also an upper vacuum compartment, containing the 'super-attenuator' at a lower vacuum level (10^{-6} mbar), separated by a small 'conductance' pipe from the lower compartment. Figure 67 shows the evolution of the total pressure measured in the arm tubes during nine months of service, including the last three months of VSR1.

Fig. 68 shows the residual gas compositions on West arm taken recently during service. As usual for an unbaked chamber, water is the dominant gas.

In the present situation, towers are mainly pumped by tubes, due to their enormous conductance. The outgassing load from materials inside tower lower compartments such

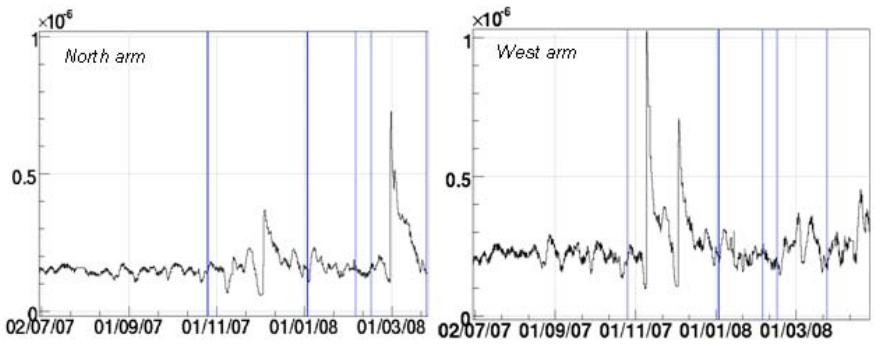

Figure 67: Total pressure in both tubes, during some months of service. Pressure peaks are due to opening towers. In some cases the peaks are cut because the sensor was temporarily offline.

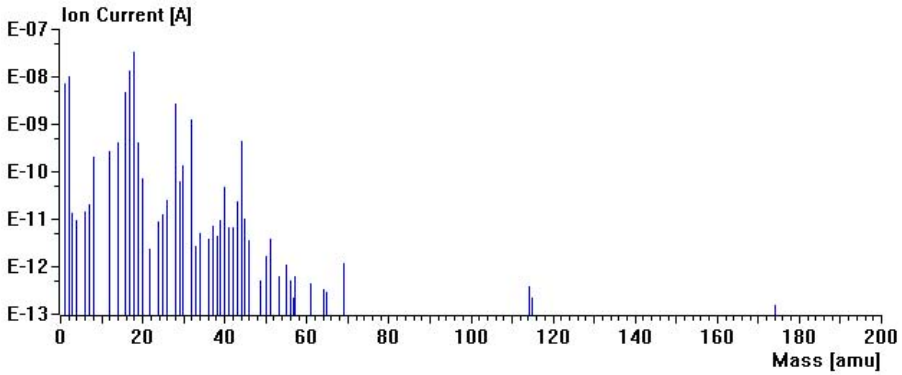

Figure 68: A recent measurement of residual gas composition at the middle of W arm. Horizontal axis reports the ratio mass/charge of the ions and the vertical axis the corresponding current, proportional to the pressure. The dominant peak corresponds to mass 18, water.

as stainless steel walls, payloads, magnets, coils, reference mass and marionette, glass baffles, TCS components, stepping motors, viton oring and cables is released inside the tubes. For AdV large parts made out of a polymer (peek) shall be added in the tower lower compartments, likely increasing the outgassing load with respect to the present. During each venting (e.g. every two months) these materials will be recharged of water vapor that will be released once in vacuum. In any case the vacuum compatibility of samples of all new payload materials will be tested. Fig. 69 reports the total pressure measured along the tubes when connecting to the towers: the amount of gas coming from towers is considerable; RGA analysis shows that the main component is water.

During the transition from the present to AdV, the vacuum system will continue its evolution, mainly to deal with the environmental noise aspects. In particular it is possible that some evolutions shall concern the 'Brewster sections', separating the DT and IB bench towers from the mirror towers. Presently the DT one has been already substituted with a liquid nitrogen cryogenic pump (cryotrap), and a similar evolution is possible also for the IB one. The gas load coming from bench towers will increase, if also the cryotrap diameter will be increased together with the links diameter.

17.3 Possible evolutions of the vacuum system

The get a vacuum level of 10^{-9} mbar in the 3 km tubes there are three main solutions:

- increasing by 100 times the pumping speed all along the tubes
- performing an overall bake-out, as foreseen in the Virgo design
- baking only the tubes adding a very large pumping speed on the towers.

The hypothesis of increasing pumping speed on the tubes was already discarded during the first design of Virgo, selecting the bake-out option, being not practically feasible

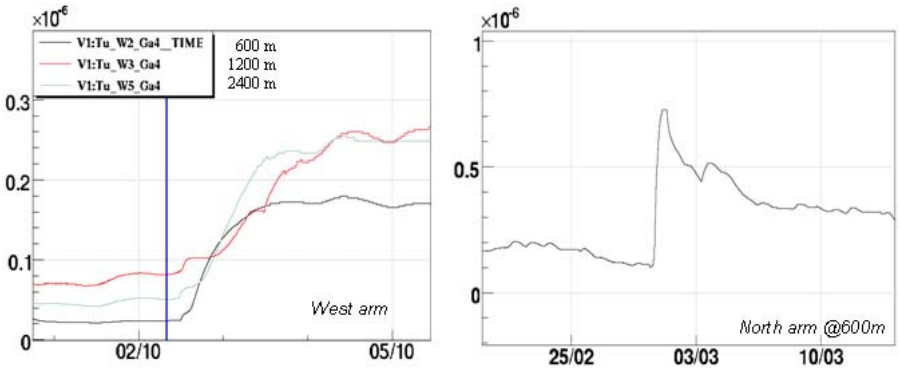

Figure 69: Pressure (mbar) versus time (day/month). Left: W tube isolated and pumped some weeks during a recent stop reached in average $5\,10^{-8}$ mbar, and went back to around $2\,10^{-7}$ mbar when reconnected to the towers (WE, WI here pumped since several days). Gas load (water) from towers is considerable. Gauges at 600 m, 1200 m, 2400 m from WI tower. Right: NI tower, vented then pumped for 2 days is connected back to the N tube (gauge at 600 m). Pressure inside tubes can reach temporarily 10^{-6} mbar.

and economical the achievement of the necessary pumping speed. In practice the pumping speed can be increased in a straightforward way adding complete pumping stations (pumps+valves+control command racks) on the available spare ports existing along the tubes (positions at 300, 900, 1500, 2100, 2700 m), each one with three suitable vacuum pumps and large vacuum valves. The gain in pumping speed could be about a factor 10, and even less on the average pressure, not getting a reasonable reduction on phase noise. Moreover the overall cost shall be high and also the maintenance duty shall be significant. In this scenario the towers would be still in the present situation, mainly pumped by tubes.

The hypothesis of an overall bake-out is ruled out by the difficulty of baking the towers, as extensively explained in the first chapter.

Remains the third solution consisting in baking only the tubes and installing a very large pumping speed for towers. This has the additional advantages to allow a fast recovery of a good vacuum level after tower venting and to keep tube residual pressure less affected by gases released from towers. The *very large* pumping speed cannot be installed directly on the towers because:

- there is not sufficient space around the central towers
- in case of mechanical pumps, their vibrations cannot be tolerated
- in case of cryopumps, large cold surfaces cannot be installed in sight of the mirrors.

17.4 The proposed solution

We propose to install large cryogenic pumps (or cryotraps) at the ends of each arm tube to keep their residual pressure at Advanced Virgo compatible levels, after bake-out. Initially the cryotraps shall allow the improvement of the vacuum in the tube, in the range of 10^{-8} mbar, thanks to the 'isolation' from towers and to their high pumping speed for water (10^5 l/s) without any moving part and thus with very limited environmental noise. For planning or budget reasons, tube baking could be postponed to a later time, when strictly required by the attained sensitivity.

Facing similar issues, the LIGO choice was to bake tubes and not the mirror vacuum chambers. In order to maintain the required low pressure in the tubes also the LIGO vacuum system comprehends these large cryogenic traps.

According to different models reported in literature, the pressure vs. time behavior of a typical unbaked vacuum system will depend on both the inherent adsorption-desorption and diffusion behavior of the gases present in the system. It will also depend on system configuration, in particular the extent of the surface area of the system relative to the system pumping speed. In Virgo the surface area is much larger than the size of the orifice through which gas must be pumped, and a gas molecule released inside the tubes has a long residence time, being more likely re-adsorbed by the surfaces than removed by the pumps.

LIGO established how much water can be put back into the tubes after the bake-out without compromising the phase noise of the interferometer. For the LIGO case this number is about 400 torr·liters into each 2km module, intended for the whole interferometer life. It is a quantity of water equivalent to less than 1 g, and corresponding to about 40 mbar·liters/year . In the Virgo case a similar quantity of water vapor is presently released into the tubes in about one day at the restart after a tower venting,and the amount of water released every year can be about two orders of magnitude larger . Installing devices like large cryotraps would decrease the flux released in the tubes by more than two orders of magnitude, preserving the vacuum level and avoiding multiple bakeouts. Baking the tubes is a complex, long and expensive operation, which cannot be repeated every year or even every few years.

A remarkable issue is about mirror cleanliness. In Virgo the HC partial pressure, as conventionally estimated by RGA measurements, is well above the figure considered originally in the Final Design as the final goal for mirror vacuum environment (10^{-13} mbar) which was intended after baking. The cryotraps, with their very large pumping speed, will reduce the HC pressure by about two orders of magnitude, at a similar level of what obtained during the baking tests of a complete tower (10^{-12} mbar). Moreover the large pumping speed provided by cryogenic traps shall allow to eliminate the brewster windows handling the additional load of water and contaminants coming from bench towers . Small cryotraps, as that recently installed between SR and DET tower, will not be any more effective due to the larger diameter required by the increased beam dimensions.

17.5 Evaluation criteria for the cryotraps

Evaluations criteria for the cryotraps choice are, in general:

1. cost
2. performances
3. easyness of operation from the vacuum point of view
4. maintenance needs (cost, manpower and time) and interferometer duty cycle during science runs
5. duty cycle during commissioning = required times for venting/putting in service towers during commissioning activity.

Cost is probably one of the principal issues for cryotraps, the cost breakdown includes: design, raw material and fabrication in workshop, installation, LN2 plant setup, maintenance and running costs. It has also to be remarked that normally, there will be the need of another large vacuum valve per each cryotrap, to isolate it during regenerations. Savings can be made on different parts, at first making use of available tube modules (length of 40m available). The additional large valve shall be a very simplified valve allowing only reducing the conductance without the need of standing to the vacuum pressure. We can also consider that repeating a bake out of the tubes is probably not much cheaper than cryotraps. Being already used in LIGO, the need of prototypes and long design phase is also reduced. Moreover, a small scale cryotrap, has been already installed and successfully operated between SR and DET towers. Along with vacuum and optical constraints on traps geometry and positioning, the design process will be lead by the accurate study of the thermal effects on the optics . Finally a cryogenic plant based on 77K liquid nitrogen coming from external cryo-condensers will be studied, as an option with respect to the traditional LN2 reservoir which needs periodical refillings.

17.6 Larger link tubes

The *links* (vacuum tubes) connecting the various towers in the Central Building have to be replaced for different reasons:

- the positions of the towers will be changed by up to one meter along the beam direction
- the clear apertures of the links have to be increased since:
    1. the average radius of the beam in the central zone will be 60 mm, instead of the present 21 mm
    2. the optical lay-out of the interferometer may require a clear passage for multiple beams between the towers, needed to have not degenerate recycling cavities and widely separated pick-off beams, as produced by large wedge angles in the mirrors.

The length of the various links will range between 2 and 4 m, including bellows to allow thermal expansion and, possibly, valves to separate the towers. A final decision on point 2 has not yet been taken, hence we will consider here two extreme options: links of 600 mm with valves of 500 mm and links of 1 m without valves. A strong effort shall be done to find a suitable tradeoff among optical constraints and flexibility in towers operation. A careful inspection in the Central Building confirmed that both options are affordable, dismantling parts of the ovens and of the platforms, as it is anyway required to displace the towers. For both options the gaskets will be metallic (Helicoflex, by Cefilac, or equivalent) and all the new parts will have to be fired at 400 °C, as it has been done for all the UHV components. Suitable tools, like chariots and movable beam cranes, will have to be developed and built for handling and accurate positioning of the links.

17.6.1 600 mm links

This is the minimum aperture to be chosen in order to have a free diameter about 5 times larger than the average beam diameter, as requested for non suspended obstacles on the beam path. The valves will have a diameter of 500 mm in order to limit their dimensions and easy the installation in the reduced space between two towers. Also the 1 m tower flanges with the 250 mm or 400 mm ports for link connection will have to be replaced or modified with 500 mm or 600 mm ports. No particular difficulty is expected in designing, manufacturing and installing 600 mm links. The option to build each link in one or more pieces is being studied. With an aperture of 500-600 mm, it will be not more possible the use of cryogenic traps between the bench towers and the interferometer for two reasons:

- the efficiency of a trap with a 600 mm diameter and a length of less than 1 m will be reduced to about 90%, with respect to the present 99%, compensated only in part by a larger pumping speed due to the higher exposed surface
- such a large aperture will expose benches and mirrors to large cold solid angles, with uncontrolled thermal effects.

If this will be confirmed by a suitable modeling, it will be necessary to provide suitable solutions to reduce hydrocarbon partial pressure in the mirror towers, as explained in the vacuum improvement paragraph. In order to cover completely the link tube walls and the valve, as seen by scattered light produced from the beam spot on each mirror, suitable baffles will be installed. They will be made out of absorbing glass with antireflection coating, as in Virgo; the inner diameter will be about 490 mm and the outer diameter will be 590 mm to fit the link inner wall. There will be about 5 baffles per link.

17.6.2 1 m links

This is the largest possible option, given the 1 m diameter of the main ports on the tower bases. Also in this case no particular difficulty is expected in designing and manufacturing; similar links already exist between towers and Large Valves. Installation would be more challenging, given dimensions and weights. Different options are being considered, like

one or more pieces per link, to be joined by flanges and gaskets or by lip welding on site. Glass baffles will not be installed, since the large diameter would imply more than ten fragile narrow baffles per link; stainless steel baffles could be used instead, as in the arm tubes, while parasitic beams will have to be caught by suitable glass traps. Also in this case it will be not more possible the use of cryogenic traps between the bench towers and the interferometer for the same, stronger, reasons. One advantage of 1 m links is that the tower 1 m flanges will be no more necessary, bolting the links directly to the tower main ports. With this choice it will be impossible to fit 1 m aperture valves between each tower pair; also the cost would be too high. This will have several heavy drawbacks from the vacuum point of view. All the mirror and bench towers of the central zone will become one single volume, to be vented and evacuated at the same time. Care will be needed to avoid pressure difference and gas flow (moving dust) from one tower to another. All the bottom flanges will have to be opened/closed in a fast sequence, and starting and stopping of the clean air flow in all the towers shall be "simultaneous". The clean air supply will have to be at least doubled, in order to allow a sufficient flow in all the towers contemporarily. All this will require an upgrade of the vacuum control system hardware and software, introducing suitable interlocks. Finally the number of tower openings will have to be limited to keep mirror pollution and water load in the tubes to acceptable levels.

17.7 UHV chambers improvement for AdV

The contamination reduction during the payload integration phase within the Ultra High Vacuum chamber is a crucial item. The surface mirror pollution, indeed, is responsible of the light absorption. Moreover, the non-perfect cleanliness conditions of the mirror create additional difficulties in the interferometer locking procedure and, as AdV is based on larger light power stored in the optical cavities, the interferometer may become uncontrollable.

During the integration phase, the long tuning procedure of the suspension system could be avoided introducing the Marionette Reference Mass installed within the UHV chamber. This element is tunable on bench minimizing the human intervention when it is hung to the filters chain (see sec. 14). In addition a better system to direct a quasi-laminar air flow within the vacuum chamber will have a positive impact on the mirror contamination, as requested by specialists since years. A system feeding laminar flow can be realized only locally, because the presence of other payload components (probably marionette) constrains the space and shade the mirror. Also personnel operating inside towers would be disturbing the flux of the clean air if it would come from peripheral zones. Suitable metallic diffusers installed inside towers near mirror will achieve this purpose.

The circuit will use the present clean air apparatus, with the addition of two metallic channels, to be installed inside towers, feeding the air from the actual port to the mentioned filters.

The detailed design of the system depends on marionette one, a suitable integration shall

be studied.

17.8 SR tower

To support the SR mirror, it is necessary a long SA .The tower has to grow by 3 vertical rings (viroles), and by the technical ring. Also the separating roof has to be built together with all its accessories. All this will be a simple replica of existing objects.

17.8.1 Towers displacement

As described in other sections of this document, the interferometer optical configuration and the control strategies require changes of up to about 1m in the position of the principal mirrors. The displacement of the towers involves a considerable work and is submitted to infrastructural constraints, affecting the final choice of the optical scheme, which is not yet finalized. The main limitation to the possible displacements comes from the structure of the Central building. In order to install the payloads from below, the towers have bottom flanges that can be opened and under each tower there is a rectangular aperture in the building floor, allowing to connecting the tower inner volume to the basement clean room. Each tower (fig. 70) has one bottom flange with the same 2 m diameter as the whole tower, with a smaller 1 m diameter lid in the center. It is only the 1 m lid that is opened to install the payload. The large 2 m flange has been conceived for exceptional needs that did never happen up to now. It has a Helicoflex metallic gasket, being chosen for safe bake-out. . Different configurations have been examined , in all cases the concerned towers are essentially NI, WI, SR, PR. The respective distances from the BS tower will change by up to 1m. (see sec. 5,11). The 2 m flanges of largely displaced towers will not remain completely inside the corresponding rectangular aperture in the floor, hence they will not be demountable any more. This is considered acceptable since there are no plans for introducing payloads larger than 1 m. Also the appearance of leaks is considered very unlikely, since bake-out is not considered any more an option for the towers. The advantageous option among the various possibility, for what concern the vacuum system, is moving WI and NI towards BS, because the 1 m diameter tube links between the large valves and the towers don't need to be replaced, but just extended by adding a short piece of tube of the same diameter.

Complex preparatory works will be necessary before the real tower displacement:

- geometry survey
- removing parts of scaffoldings and stiffening beams
- removing oven walls
- removing the air tight connections between tower bottom and basement clean room
- removing clean air ducts
- removing cables and cable trays

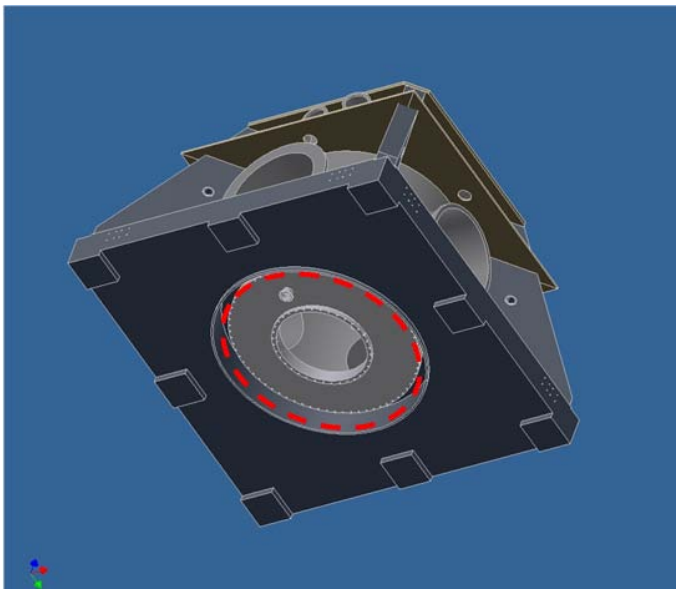

Figure 70: The 2m diameter flange: it would be no more accessible after the displacement of the tower.

- displacement of electrical cabinets and electronics racks
- displacement of vacuum control racks
- removing the platform

The real displacement could be done by moving the entire tower on special sliders or rollers, once removed links and payloads and having blocked the Superattenuators. A similar operation has been already performed successfully in the past, displacing the MC tower by about 800 mm. In a preliminary hypothesis, scaffoldings could be moved along with the respective towers, using contemporarily sliders and bridge cranes.

The matter of cabling could be one of the principal issues. The possibility of avoiding a large cabling removal-reinstallation has to be studied in detail. In a more recent hypothesis, also BS should be displaced by about 40mm; in this case the flanges of the new links will have to be slightly eccentric.

All the preparatory works will have to be recovered at the end in the opposite sequence.

The working schedule will have to be very carefully planned because of the large interference with almost all other activities: new links, Superattenuators upgrade, new payloads, etc.

17.9 Vacuum control system

The vacuum control system comprises 22 main control stations, and several others components installed along the whole vacuum system. It includes also the supervisor software

which is used to drive the vacuum system. While being effective for today's needs, it requires to be revised, since it has been designed more than 10 years ago, based on the OS-9 standard, using components no more available on the market. This procedure has already been started and will have to be strongly boosted for sake of AdV. Besides the new hardware, it will be necessary to upgrade also the control logic, both hardware and software, for more versatility and to include new coming devices, like new pumping stations and pump types. For instance also the time limited operation of scroll pumps should be better controlled and automatized, and suitable interlocks and loops shall be added to actively control the improved vacuum conditions . Different options shall be studied once finalized the vacuum design, taking in consideration the environmental noise aspects, now emerging.

17.10 Appendix

The formula employed to evaluate the noise corresponds to the one also reported by LIGO, which has been experimentally validated.

$$S_h(f) = \frac{1}{L}\sum_A \frac{8P_A\,(2\pi\alpha_A)^2}{k_B T\,V_{p,A}} \int_0^L \frac{1}{w(z)} \exp\left[-2\pi f \frac{w(z)}{V_{p,A}}\right] dz \tag{25}$$

where the sum is over all the molecular species present inside the beam pipe, the integration is over all the beam axis and the parameters are defined as follows:

$w(z)$ Beam radius. For a gaussian beam it is given by

$$w(z) = w_0\sqrt{1+\frac{(z-z_0)^2}{z_R^2}}$$

where w_0 is the waist, z_R the Rayleigh's range and z_0 the waist position along the axis.

$V_{p,A}$ Most probable speed of the A specie. It is given by

$$V_{p,A} = \sqrt{\frac{2k_B T}{m_A}}$$

where m_A is the molecular mass.

α_A Molecular polarizability of the A specie.

P_A Average partial pressure of the A specie in the beam pipe. Pressure gradients along the tube are low, and it will be possible to take them into account simply by carrying the pressure inside the integral eq. 25.

The main assumptions which lead to Eq. 25 are the following:

- collisions between molecules are not important.
- a molecule emerges after a collision with the beam pipe with a Boltzmann distribution of velocity.

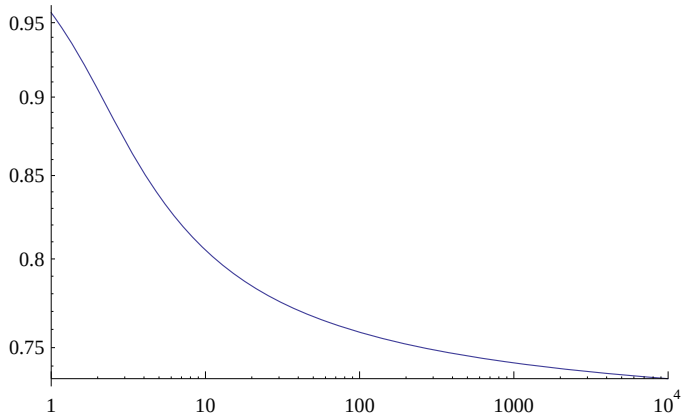

Figure 71: *The improvement factor in the strain noise amplitude $\sqrt{S_h}$ for a configuration with the waist on one of the two mirrors, compared with a configuration with the waist at the center of the cavity. The independent variable is L/z_R.*

- only forward scattering of light is take into account.

The exponential cut in the integral is effective for frequencies greater than the inverse of the typucal time requested by a molecule of the given specie to travel a distance $2\pi w(z)$. The cut off frequency is typically in the kHz region.

Expanding the exponential we find

$$S_h(f) = \frac{1}{L}\sum_A \frac{8P_A\left(2\pi\alpha_A\right)^2}{k_B T w_0 V_{p,A}} \sum_{n=0}^{\infty} \frac{1}{n!}\left(-\frac{2\pi w_0 f}{V_{p,A}}\right)^n Q_n \tag{26}$$

where

$$Q_n = {}_2F_1\left(\frac{1}{2}, \frac{1-n}{2}; \frac{3}{2}, -\frac{\ell_1^2}{z_R^2}\right)\ell_1 + {}_2F_1\left(\frac{1}{2}, \frac{1-n}{2}; \frac{3}{2}, -\frac{\ell_2^2}{z_R^2}\right)\ell_2 \tag{27}$$

has an analytic expression for each value of n, and ℓ_1, ℓ_2 are the distences of the two mirrors from the waist.

Explicitly we get in the low frequency region, retaining only the $n = 0$ term,

$$S_h = \frac{1}{L}\frac{\pi w_0}{\lambda}\left(\sinh^{-1}\frac{\ell_1}{z_R} + \sinh^{-1}\frac{\ell_2}{z_R}\right)\sum \frac{8P_A\left(2\pi\alpha_A\right)^2}{k_B T V_{p,A}}\,. \tag{28}$$

The geometry factor show that the worse configuration for given partial pressures and waist size is the one with the waist on the center of the cavity. The best configuration is the one with the waist on one of the two mirrors. The improvement factor in the noise amplitude between these two extreme cases is plotted in the Figure 71 as a function of L/z_R and apparently it is never very relevant.

On the other hand the noise increases roughly as the square root of the waist.

The previous expressions for the noise power spectrum can be used also to find the hoghest partial pressure which is compatible, for a given specie, with a desired noise level. It is convenient to write

$$P_A < (k_B T)^{3/2} \frac{\sqrt{2}}{32\pi^2 \alpha_A^2 \sqrt{m_A}} \frac{L \frac{\lambda}{\pi w_0}}{\left(\sinh^{-1} \frac{\ell_1}{z_R} + \sinh^{-1} \frac{\ell_2}{z_R}\right)} S_h^{max} \tag{29}$$

where the dependences on temperature, molecular parameters and beam geometry are clearly seen.

If we choose a particular specie (for instance water) as a reference we get the simple expression

$$P_A = P_{H_2O} \left(\frac{\alpha_{H_2O}}{\alpha_A}\right)^2 \left(\frac{m_{H_2O}}{m_A}\right) \tag{30}$$

which can be used to obtain easily other estimates in the low frequency region.

18 Infrastructure modifications for environmental noise reduction

18.1 The work done so far

The operation of Virgo has shown that some noise-inducing machines can spoil the Virgo sensitivity (see section 12). The machines producing the more significant *environmental* mechanical noise are:

- the HVAC (Heating Venting Air Conditioning) machines, particularly the air handler machines located near the experimental halls;
- the water pumps;
- the racks for the electronics (suspensions, vacuum, laser, detection, DAQ, etc.);
- the harmonic compensator for the UPS (Uninterrupted Power Supply) electrical systems.

More machines are source of noise: the chillers, the UPS machines, the power generators, the heat generators, the air compressors, the electric transformers. However, these are located far enough from the experimental halls that their noise can be considered a secondary issue with respect the previous ones.

In order to limit the environmental acoustic/seismic noise there are two possible lines of action:

- **mitigation of the sources:**
  - modification/improvement of parts of the machines;
  - proper damping systems;
  - replacement of some machines with more silent ones;
- **isolation of the rooms hosting the machines:**
  - improvement of the acoustic performances of the internal structures;
  - realization of acoustic enclosures;
  - realization of structural joints.

Several improvements have already been performed both during the Virgo commissioning and the installation of Virgo+, with the purpose of mitigating the noises transmitted from the present facilities to the sensitive parts of the interferometer (particularly the external optical benches). Such works concerned the realization of acoustic enclosures for the optical benches and the acoustic isolation of the rooms where some of the machines are located. Further actions are already in progress such as the improvement of the acoustic isolation of the air flow distribution. More works are under investigation such as the improvement of the damping systems of the machines and of the water pipelines.

The analysis of the results obtained from the above mentioned improvements is the starting point for defining the AdV environmental noise requirements. However, such analysis can only represent a projection of the present noises on the AdV sensitivity and gives qualitative indications for the new facilities.

The requirements and the specifications for the HVAC machines and the electronics' racks displacement will be determined soon. The basic requirements needed to proceed with the IME (Infrastructure Modifications for Environmental noise reduction) detailed design are: minimum distance from the experimental halls of HVAC machines, electronics racks, maximum level of acoustic noise, maximum proper frequency of damping systems.

18.2 Possible solutions for the infrastructure upgrades

At present we have considered several interventions for each experimental building, summarized in the following as two solutions named *reference solution* and *further upgrades*. The difference between these two scenarios concerns only the End Buildings.

18.2.1 Reference solution

This scenario concerns the infrastructure upgrades to be realized for each experimental building and described in the following.

- The optimization of the HVAC equipments, both for the acoustic and the seismic performances (see fig. 72), through:
  - the realization of independent platforms for the machines to mitigate noise transmission;
  - the suspension of the machines on adequate anti-vibrating supports;
  - the installation of damping joints for the water pipes;
  - the seismic isolation of the air ducts from the walls and from the HVAC machines by flexible joints, the installation of proper air ducts acoustic isolation and silencers;
  - the improvement of the air flow distribution by optimization of the air conditioning machines (air fans balancing, installation of more noiseless machines).
- The installation of proper phono-absorbing elements in the ceiling and the walls to reduce the high value of the reverberation time of each experimental hall.
- The displacement of the electronics racks in *ad hoc* spaces (Electronics Equipments Room - EE Room). Such action concerns the realization of dedicated acoustic enclosures or the improvement of the acoustic isolation of the existing structures. These spaces are necessary, even though they may be reduced, in case the electronics racks are kept in the current positions and their cooling systems are modified. In

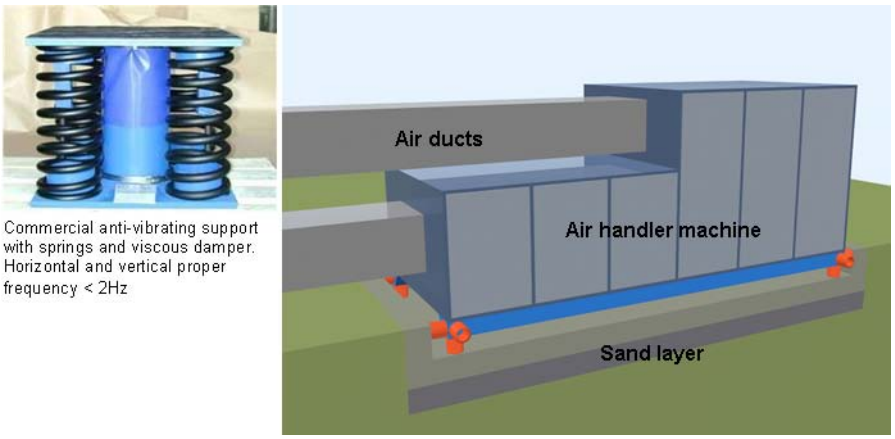

Figure 72: Suspension of HVAC machines on adequate anti-vibrating supports.

such case the enclosures can be used to accommodate only the power supplies and the AC/DC converters.

The above described interventions are detailed for each building in the following.

Central Building It is foreseen the realization of a new external technical area of about 150 m^2, on the east side of the Central Building (CB), to install the air handler machines (for the CB hall, the Clean Rooms and the EE Rooms) and the relevant equipments (manifolds, water pumps). The foundation supporting the machines will be ground isolated by an appropriate damping system or a sand layer, while the machines will be set on damping pads. New water pipelines to link the machines to the Technical Building will be realized (fig. 73). Other improvements concern the separation of the Laser Lab HVAC system from the Clean Rooms one. Finally it has been considered the realization of an EE Room hosting the electronics racks (suspensions and vacuum). This new EE Room can be realized in two unused offices (CB - level 2). For this scope we need to improve the acoustic isolation of the concrete-floors and the walls; moreover we have to realize a dedicated HVAC system.

Mode Cleaner Building For this building we considered the realization of an external technical area of about 25 m^2, on the west side of the building, with the same characteristics of the CB, to install the chillers (heat pumps) and the air handler machine. Moreover it has been foreseen the realization of an appropriate acoustic enclosure hosting the electronics racks (suspensions and vacuum). For the electronics the same recovery actions as for the CB can be applied.

End Buildings In this case the air handler machine might be kept in the current position. In fact the floor of the technical building and the foundation of the tower are already independent by structural joints. Anyway, we considered the realization of a further

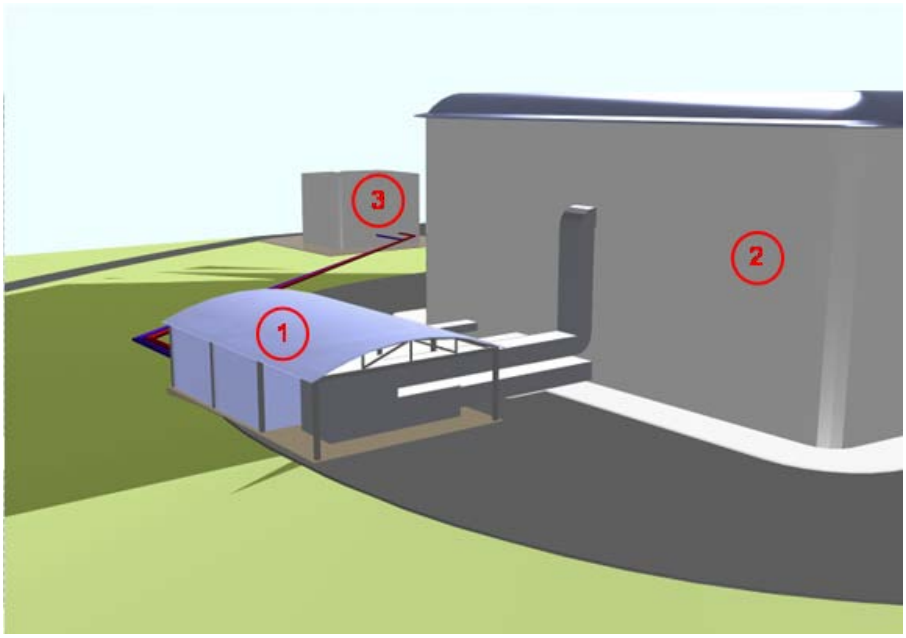

Figure 73: Perspective view of the Central Area: 1) New external technical area, 2) Central Building, 3) Technical Building.

structural joint between the foundation supporting the machine and the remaining part of the room. The machine will be set on damping pads and, if needed, the foundation might be rebuilt and ground isolated by a specific damping system or an appropriate sand layer. All the other machines (the heat generator, the air compressor and the electric machines) will remain in their current position, considering that as a sufficient distance. Even for these buildings the realization of an acoustic enclosure hosting the electronics racks (suspensions and vacuum) has been considered.

18.2.2 Further upgrades

A further grade of intervention has been developed based on the hypothesis of realizing a new separated technical area also for the End Buildings, as already described as reference solution for the other experimental buildings. These facilities will have the same technical solutions and characteristics of the CB's one. The estimated surface could be of about 150 m^2, in order to accommodate both the air handler machine and the relevant equipments (tanks, water pumps) as well as the other potential noisy machines (the heat generator, the air compressor, the electric power generator, the transformer and the UPS machine). However in this case various intermediate solutions are possible, such as displacing only a part of the machines in the new area and moving the remaining part in the existing technical building.

References

[1] R.Flaminio, A.Freise, A.Gennai, P.Hello, P.La Penna, G.Losurdo, H.Lueck, N.Man, A.Masserot, B.Mours, M.Punturo, A.Spallicci, A.Viceré, *Advanced Virgo White Paper*, Virgo Internal report VIR-NOT-DIR-1390-304 (2005). 3

[2] The Virgo Collaboration, *Advanced Virgo Conceptual Design*, Virgo Internal report VIR-042A-07 (2007). 3, 73, 75

[3] The Virgo Collaboration, *Advanced Virgo Preliminary Project Execution Plan*, Virgo Internal report VIR-043A-07 (2007). 3

[4] Advanced LIGO team, *Advanced LIGO Reference Design*, LIGO-M060056-06-M (2006). 3

[5] http://lhocds.ligo-wa.caltech.edu:8000/advligo/GWINC . 10

[6] S. Hild and G. Losurdo: *Advanced Virgo design: Comparison of the Advanced Virgo sensitivity from Bench 4 and GWINC (v1)*, Virgo note, VIR-055A-08 (2008). 10, 47, 54

[7] A.Buonanno, Y.Chen, gr-qc/0102012 (2001).

[8] G.Losurdo, Virgo Note VIR-024A-07 (2007).

[9] C.Comtet et al., *Proceedings of the 42th Rencontres de Moriond*, 2007. 91

[10] A.Heptonsthall, talk at the LSC-Virgo meeting (G080227-00), Caltech, March 2008

[11] M.Beccaria, *et al.*, *Class. Quantum Grav.*, **15**, 3339 (1998).

[12] Y. Gürsel, M. Tinto, *Near optimal solution to the inverse problem for gravitational wave bursts*, Phys.Rev.D**40**:3884-3938,1989. 32

[13] C.Kim, V.Kalogera and D.Lorimer, *Effect of PSRJ0737-3039 on theDNS Merger Rate and Implications for GW Detection*, astro-ph:0608280 http://it.arxiv.org/abs/astro-ph/0608280, to appear in proceedings of "A life with stars", a conference in honour of Ed van den Heuvel (Amsterdam, August 2005). 16

[14] K.Belczynski, R.E.Taam, V.Kalogera, F.A.Rasio, T.Bulik, *On the rarity of double black hole binaries: consequences for gravitational-wave detection,* astro-ph:0612032 http://it.arxiv.org/pdf/astro-ph/0612032, The Astrophysical Journal 662:1 (2007) 504-511. 17, 18, 20, 21, 22

[15] T.Bulik, K.Belczynski, A.Prestwich, *IC10 X-1: the immediate progenitor of a double black hole* astro-ph:0803.3516 http://it.arxiv.org/pdf/0803.3516, submitted to Astrophysical Journal. 21, 22, 23

[16] F.Pretorius, *Evolution of binary black hole spacetimes.*, Phys.Rev.Lett.**95**:121101,2005. 20

[17] F.Pretorius *Simulation of binary black hole spacetimes with a harmonic evolution scheme*, Class.Quant.Grav.**23**:S529-S552,2006. 20

[18] A.Buonanno, G.B.Cook, F.Pretorius *Inspiral, merger and ring-down of equal-mass black-hole binaries*, Phys.Rev.D**75**:124018,2007. 20

[19] M.Vallisneri *Prospects for gravitational wave observations of neutron star tidal disruption in neutron star / black hole binaries.*, Phys.Rev.Lett.**84**:3519,2000. 20

[20] R.Narayan, Ap.J.**319** (1987), 162. 25

[21] The LIGO Scientific Collaboration *All-sky LIGO Search for Periodic Gravitational Waves in the Early S5 Data*, LIGO-P080024, http://arxiv.org/abs/0810.0283 25

[22] R.Diehl et al (INTEGRAL) *Radioactive ^{26}Al from massive stars in the Galaxy*, Nature **439** (2006), 45-47 27

[23] C.Ott *The gravitational wave signature of core collapse supernovae*, astro-ph:0809.0695v1 http://arxiv.org/abs/0809.0695v1 27

[24] W.H.Lee, E.Ramirez-Ruiz *The Progenitors of Short Gamma-Ray Bursts*, astro-ph/0701874v3, New J.Phys **9** (2007) 17. 28, 36

[25] S.E.Woosley and J.S.Bloom *The Supernova - Gamma-Ray Burst Connection*, astro-ph/0609142v1, Ann.Rev.Astron.Astrophys.**44** (2006) 507-556. 28

[26] The LIGO Scientific Collaboration, *Search for gravitational wave radiation associated with the pulsating tail of the SGR 1806-20 hyperflare of December 27, 2004 using LIGO*, astro-ph:0703419, http://arxiv.org/abs/astro-ph/0703419, Phys.Rev.D**76** (2007) 062003 28

[27] F.Acernese et al. (The Virgo Collaboration) *Search for gravitational waves associated with GRB 050915a using the Virgo detector*, to appear in Class.Quant.Gravity (2008). 29

[28] N.Arnaud, M.Barsuglia, M.A.Bizouard, F.Cavalier, M.Davier, P.Hello, T.Pradier *Gravity wave and neutrino bursts from stellar collapse: A Sensitive test of neutrino masses.* Phys.Rev.D**65**:033010,2002 27

[29] N.Arnaud, M.Barsuglia, M.A.Bizouard, V.Brisson, F.Cavalier, M.Davier, P.Hello, S.Kreckelbergh, E.K.Porter *Coincidence and coherent data analysis methods for gravitational wave bursts in a network of interferometric detectors.*, Phys.Rev.D**68**:102001,2003. 32, 33

[30] A.Viceré, *Network analysis for coalescing binaries: Coherent versus coincidence based strategies.*, Class.Quant.Grav.**21**:S1793-S1800,2004. 32, 33

[31] C.Rover, R.Meyer, G.M.Guidi, A.Vicere, N.Christensen, *Coherent Bayesian analysis of inspiral signals.*, Class.Quant.Grav.**24**:S607-S616,2007. 33

[32] F.Beauville et al. (The joint LIGO-Virgo working group) *Detailed comparison of LIGO and Virgo inspiral pipelines in preparation for a joint search* Class.Quant.Grav.**25** (2008) 045001. 33

[33] F.Beauville et al. (The joint LIGO-Virgo working group) *A comparison of methods for gravitational wave burst searches from LIGO and Virgo.* Class.Quant.Grav.**25** (2008) 045002. 33

[34] F.Cavalier, M.Barsuglia, M.A. Bizouard, V.Brisson, A.C.Clapson, M.Davier, P.Hello, S.Kreckelbergh, N.Leroy, M.Varvella, *Reconstruction of source location in a network of gravitational wave interferometric detectors.*, Phys.Rev.D**74**:082004,2006. 33

[35] S.Birindelli, *Coherent algorithm for reconstructing the location of a coalescing binary system using a network of three gravitational interferometers*, Ph.D. thesis, University of Pisa, 2008, http://www.infn.it/thesis/PDF/getfile.php?filename=2427-Birindelli-dottorato.pdf 33

[36] Chandra http://chandra.harvard.edu 34

[37] X-MM Newton http://xmm.esac.esa.int 34

[38] XEUS http://sci.esa.int/xeus 34

[39] SWIFT http://www.nasa.gov/mission_pages/swift/bursts/index.html 35

[40] GLAST http://www.nasa.gov/mission_pages/GLAST/team/index.html 35

[41] S.Fukuda et al. *The Super-Kamiokande detector*, N.I.M. A **501** (2003), 418-462. 35

[42] The LVD Collaboration *The 1 kton LVD neutrino observatory*, Proc. 27th ICRC,Hamburg, 1, 1093, 2001. 35

[43] SuperNova Early Warning System http://snews.bnl.gov 35

[44] Sudbury Neutrino Observatory http://www.sno.phy.queensu.ca 35

[45] SNO+ http://snoplus.phy.queensu.ca 35

[46] S.R.Klein for the IceCube Collaboration *IceCube: A Cubic Kilometer Radiation Detector* http://www.icecube.wisc.edu/science/publications/update2008/update.pdf 35

[47] http://amanda.uci.edu 36

[48] The KM3NeT Consortium, *KM3NeT: Conceptual Design for a DeepâĂŘSea Research Infrastructure Incorporating a Very Large Volume Neutrino Telescope in the Mediterranean Sea*, http://www.km3net.org/CDR/CDR-KM3NeT.pdf 36

[49] ANTARES Collaboration *A Deep Sea Telescope for High Energy Neutrinos*, astro-ph/9907432v1 http://lanl.arxiv.org/abs/astro-ph/9907432v1 36

[50] NEMO http://nemoweb.lns.infn.it 36

[51] NESTOR http://www.nestor.noa.gr 36

[52] J.D. Mansell et al, Appl.Opt., 40, 366-374 (2001) 79

[53] LIGO T-060267-00-D (2006). 79

[54] LIGO G-07011700-00-R (2007). 79

[55] G.Mueller, LIGO T020021-00-D (2002). 79

[56] P.Fritschel, LIGO T010075-00-D (2001). 79

[57] *Input Optics Subsystem Preliminary Design Document*, LIGO-T060269-01-D 79

[58] *Complex modulation*, LIGO-T070197-00-R 79

[59] B.Willke, *Status of Adv Ligo PSL*, talk at the LSC-Virgo meeting, March 08, Caltech 69

[60] D.Shaddock et al, *Opt Lett*, **24**, 1499, (1999). 68

[61] E. Khazanov et al, *IEEE Journ. Quant. Electr.*, **35** (8), (1999) 81, 86

[62] E. Khazanov et al, *IEEE Journ. Quant. Electr.*, **40** (10), (2004) 81, 85

[63] D.Tanner et al, *The LIGO input optics*, LIGO-G070296-00-R 81

[64] The Virgo collaboration, "In-vacuum optical isolation changes by heating in a Faraday isolator" *Appl. Opt.*, accepted for publication, (2008) 80

[65] F.Acernese, *et al.* (The Virgo Collaboration), *Class. Quantum Grav.*, **21**, S395-S402 (2004). 74

[66] N.Man, talk at the *Advanced Virgo workshop*, June 14th, 2007. 74

[67] S.Hebri, Virgo Note VIR-NOT-EGO-1390-331 (2006). 75

[68] The VIRGO Collaboration, *The Virgo Physics Book*, vol. II, Chap. 6 (2006). 75

[69] S.Avino et al, *Class. Quant. Grav.*, **23**, 5919-5925 (2006)

[70] S. Avino et al, *Phys. Lett. A*, **355**, 258-261 (2006)

[71] B. Canuel, E. Genin, *R&D project : High power input optical components for Advanced Virgo April 2008 status report*, Virgo Internal Document VIR-082A-08 (2008) 83

[72] E. Khazanov et al, *Appl. Opt.*, **41** (15), (2002) 86

[73] http://www.virgo.optique.espci.fr/Virgo_Mirrors/ 90

[74] A.Brillet, *et al.*, Phys. Rev. D, **67**(10), 102006 (2003) 90

[75] Z. Yan, Li Ju, *et al.*, Applied Optics 45 (2006) 2631-2637 89

[76] M. Smith, P. Willems, Auxiliary Optics Support System Conceptual Design Document, Vol. 1 Thermal Compensation System, LIGO-T060083-01-D 97

[77] A. Rocchi, talk at the LSC-Virgo Meeting, Cascina May 24, 2007. 97

[78] V. Fafone, talk at the Virgo Meeting, Cascina July 16, 2008. 98

[79] P. Willems, LIGO-T060224-00D (2006). 98, 105

[80] J. Degallaix, Ph.D. thesis, UWA, 2006. 99, 105

[81] F. Bondu, private communications. 100

[82] R.C. Lawrence, Ph.D. thesis, MIT, 2003, LIGO-P030001-00-R. 105

[83] T.L. Kelly, *et al.*, *Appl. Opt.*, **46**(6), 861-866 (2007) 105

[84] Virgo Collaboration, *R&D for Advanced Virgo*, VIR-042A-08 (2008) 105

[85] INFN Roma Tor Vergata, presentation to the Advanced Virgo R&D Review, Cascina April 22, 2008. 105

[86] J.C. Kamp, H. Kawamura, R. Passaquieti, R. DeSalvo, LIGO-G080414-00-R (2008). 106, 108

[87] R. Passaquieti, talk at the LSC-Virgo Meeting, Amsterdam September 24, 2008. 106

[88] V. Fafone, Y. Minenkov, I. Modena, A. Rocchi, talk at the Advanced Virgo Meeting, Cascina September 18, 2008. 106

[89] E. Tournefier, *Technical noises for Virgo+: DC and AC readout cases*, VIR-NOT-LAP-1390-338 110

[90] A. Buonanno, Y. Chen, Phys.Rev. D **64,** 042006 (2001)

[91] D.E. McClelland et al., Phys Rev D**48,** 5475 (1993)

[92] R. NMavaddat et al., J. Optics (Paris) **26,** 145 (1995)

[93] E. D'Ambrosio, R. O'Shaughnessy, S. Strigin, K.S. Thorne and S. Vyatchani, gr-qc/0409075 (Sept. 2004) 55

[94] Y. Pan gr-qc/0608128 (Aug. 2006) 55

[95] G. Müller and S. Wise, LIGO document Number T020026-00-D, http://www.ligo.caltech.edu/docs/T/T020026-00.pdf

[96] J. Mizuno, Ph.D. thesis Max Planck Institute für Quantenoptik, Garching 1995

[97] A.E.Siegmann, *Lasers*, Oxford Univ. Press (1989)

[98] Y.Levin, *Phys. Rev. D*, **57**, 659 (1998)

[99] F.Bondu, *et al.*, *Phys. Lett. A*, **246**, 227 (1998)

[100] J.Y.Vinet, *Class. Quant. Grav.*, **24**, 3897 (2007)

[101] E.D'Ambrosio, *Phys. Rev. D*, **67**, 102004 (2003)

[102] J.Y.Vinet, to be published in *Living reviews* 62

[103] B.Mours, *et al.*, *Class. Quant. Grav.*, **?**, 5777 (2006)

[104] V.Braginskij, *et al.*, *Phys. Lett. A*, **264**, 1 (1999)

[105] CALVA Conceptual Design, https://edms.in2p3.fr/file/I-010870/2/Conceptual_Design.pdf

[106] *SAFE: Superattenuator Facility at EGO*, VIR-048A-07 (2007). 138

[107] G. Losurdo, D. Passuello, P. Ruggi, VIR-NOT-FIR-1390-318 (2006). 140

[108] P.Puppo and P.Rapagnani, VIR-NOT-ROM-1390-311 144

[109] P. S. Linsay, D. H. Shoemaker, Rev. Scient. Instrum. **53** (1982) 1014. 149

[110] H. Luck *et al.*,*Status of the GEO600 detector*, Class. Quant. Grav. **23** (2006) S71. 149

[111] S. Grasso, C. Altucci, F. Barone, V. Ragozzino, S. Solimeno, T. Pham, J. Y. Vinet, R. Abbate, Phys. Lett. A **244** (1998) 360. 149, 150

[112] P. Amico, L. Bosi, L. Carbone, L. Gammaitoni, M. Punturo, F. Travasso, and H. Vocca, Class. Quant. Grav. **19** (2002) 1663-1668. 149

[113] V. P. Mitrofanov, N. A. Styazhkina and K. V. Tokmakov, Class. Quant. Grav. **19** (2002) 2039-2043. 149

[114] S. Rowan, S. Twyford, R. Hutchins and J. Hough., Class. Quant. Grav. **14** (1997) 15371541. 149

[115] M. J. Mortonson, C. C. Vassiliou, D. J. Ottaway, D. H. Shoemaker, and G. M. Harry, Rev. Scient. Instrum. **74** (2003) 4840-4845. 149

[116] V. P. Mitrofanov, L. G. Prokhorov and K. V. Tokmakov, Phys. Lett. A **300** (2002) 370.

[117] Virgo Collaboration, *Virgo Final Design* (1997).

[118] M. Mantovani, A. Freise, *Initial set of optical parameters for numerical simulations towards Advanced Virgo*, Virgo note VIR-002B-07 (2007). 40, 43

[119] J. Marque, *AdV optical layout: macroscopic wedge on Input Mirrors and BS issue*, talk at Advanced Virgo meeting (2008). 49

[120] S. Hild and A. Freise: *Advanced Virgo Design: Differential Arm Length Noise from Vertical Movement of Wedged Input Mirrors*, Virgo note VIR-037A-08 (2008). 49

[121] S. Hild, R. Schilling, J. Degallaix, M. Mantovani, S. Chelkowski and A. Freise: *Using the etalon effect for in-situ balancing of the Advanced Virgo arm cavities*, submitted to Classical and Quantum Gravity, available at arXiv:0807.2045 (2008). 48, 50

[122] S. Hild and A. Freise: *Advanced Virgo design: Optical phase noise originating from the etalon effect driven by thermo-refractive noise*, Virgo note VIR-058A-08 (2008). 51

[123] Somiya K and Chen Y et al *Frequency noise and intensity noise of next-generation gravitational-wave detectors with RF/DC readout schemes Phys. Rev. D* **73** (2006). 50

[124] Somiya K and Chen Y et al *Erratum: Frequency noise and intensity noise of next-generation gravitational-wave detectors with RF/DC readout schemes Phys. Rev. D* **75** (2007). 50

[125] M. Mantovani, A.Freise, S.Hild: *The consequences of using the etalon effect to tune the arm cavity finesse on the alignment signals for Advanced Virgo*, Virgo note VIR-027A-08 (2008). 51

[126] G. M. Harry et al *Thermal noise in interferometric gravitational wave detectors due to dielectric optical coatings Classical and Quantum Gravity* **19** (2002). 45

[127] S. Hild, A. Freise: *Advanced Virgo Design: Preliminary Revision of the Beam Size and the Test Mass Curvatures*, Virgo note VIR-038B-08 (2008). 45

[128] S. Hild, M. Mantovani, A. Perreca and A. Freise: *Advanced Virgo design: The Advanced LIGO approach for choosing modulation frequencies*, Virgo note VIR-066A-08 (2008). 44, 47, 54

[129] S. Hild and A. Freise: *Near-symmetric arm cavity design for Advanced Virgo*, Virgo note VIR-066A-08 (2008). 48

[130] S. Hild, G. Losurdo and A. Freise: *Optimising the Advanced Virgo sensitivity for astrophysical sources*. Presentation at Virgo week July 2008. Available at http://wwwcascina.virgo.infn.it/collmeetings/presentations/2008/2008-07/AdV/hild_160708.ppt 10, 47, 54

[131] S. Hild and A. Freise: *Why use FinesseTools for Advanced Virgo simulations*. Presentation at AdV biweekly meeting, June 2008. Available at http://wwwcascina.virgo.infn.it/advirgo/biweekly/2008/2008-06/hild_190608.ppt 54

[132] P.Fritschel et al., *Stable recycling cavities for advanced LIGO*, LIGO internal note LIGO-T080208-0-D (2008).

[133] Gretarsson et al. , *Effects of mode degeneracy in the LIGO Livingston Observatory recycling cavity*, arXiv:0708.3470 (2008). 54

[134] M.A. Arain and G. Mueller, *Design of the Advanced LIGO recycling cavities*, Optics Express Vol. 16, Issue 14 (2008). 56

[135] A. Freise and S. Hild: *Advanced Virgo: A draft design for a non-degenerate power recycling cavity*, Virgo note VIR-081A-08 (2008). 43, 57

[136] Hild S and Grote H et al *Demonstration and comparison of tuned and detuned signal recycling in a large-scale gravitational wave detector*, *Classical and Quantum Gravity* **24** (2007). 51

[137] Freise A and Heinzel G et al *Demonstration of detuned dual recycling at the Garching 30 m laser interferometer*, *Physics Letters A* **277** (2000). 51

[138] Meers B. J *Recycling in laser-interferometric gravitational-wave detectors*, *Phys. Rev. D* **38** (1988). 51

[139] Mours B and Tournefier E et al *Thermal noise reduction in interferometric gravitational wave antennas: using high order TEM modes Classical and Quantum Gravity* **23** (2006). 60

[140] Bondarescu M and Thorne K. S *New family of light beams and mirror shapes for future LIGO interferometers Physical Review D (Particles, Fields, Gravitation, and Cosmology)* **74** (2006). 60

[141] S. Chelkowski *Higher order Laguerre-Gauss modes in future gravitational wave detectors* LIGO-G080522-00 (2008). 60, 61

[142] S. Chelkowski *Higher order Laguerre-Gauss modes in future gravitational-wave detectors* Talk at GWADW (2008), paper in preparation. 60

[143] Arlt J and Dholakia K et al *The production of multiringed Laguerre-Gaussian modes by computer-generated holograms Journal of Modern Optics* **45** (1998). 62

[144] Kennedy S. A and Szabo M. J et al *Creation of Laguerre-Gaussian laser modes using diffractive optics Phys. Rev. A* **66** (2002). 62

[145] Courtial J and Padgett M. J *Performance of a cylindrical lens mode converter for producing Laguerre-Gaussian laser modes Optics Communications* **159** (1999). 62

[146] E. Tournefier, *Back-scattering by the optical benches: results from Virgo and constraints for AdV Technical noises for Virgo+: DC and AC readout cases*,VIR-NOT-070A-08 111

[147] E. Tournefier, *Advanced Virgo output mode cleaner: specifications"*,VIR-NOT-071-08 113

[148] F. Bondu, *"Advanced Virgo ISC Work Breakdown Structure"*, Virgo Internal Document VIR-071A-08 (2008) 116

[149] E. Tournefier, *"Advanced Virgo output mode cleaner: specifications"*, Virgo Internal Document VIR-071A-08 (2008) 117

[150] F. Acernese et al. [Virgo collaboration], *"The variable finesse locking technique"*, Class. Quant. Grav. **23** (2006) S63 118

[151] F. Acernese et al. [Virgo collaboration], *"Lock acquisition of the Virgo gravitational wave detector"*, Astropart. Phys. **30** (2008) 29 118

[152] Optickle web-page `http://ilog.ligo-wa.caltech.edu:7285/advligo/ISC_Modeling_Software` 99, 124

[153] G. Vajente, *"Note on signal recycling I: Field equations"*, Virgo Internal Document VIR-030B-08 (2008) 117, 118, 119

[154] G. Vajente, *"Note on signal recycling II: Lengths and modulations"*, Virgo Internal Document VIR-032A-08 (2008) 118, 119

[155] G. Vajente, *"Possible sets of lengths and modulation frequencies for Advanced Virgo"*, Virgo Internal Document VIR-049A-08 (2008) 120

[156] G. Vajente, *"Simulation of Advanced Virgo Length Sensing and Control system"*, Virgo Internal Document VIR-068B-08 (2008) 120, 121, 122

[157] G. Vajente, *"Advanced Virgo Length Sensing and control: Double demodulation vs Single demodulation"*, Virgo Internal Document VIR-069B-08 (2008) 121

[158] G. Vajente, *"Advanced Virgo Length Sensing and Control System: parameters for Non-Degenerate Recycling Cavities"*, Virgo Internal Document VIR-080A-08 (2008) 111, 120, 122

[159] G. Vajente, *"Requirements for the Advanced Virgo Length Sensing and Control system"*, Virgo Internal Document VIR-083A-08 (2008) 111, 119, 122

[160] B. Swinkels, E. Campagna, G. Vajente, L. Barsotti and M. Evans, *"Longitudinal noise subtraction: the alpha-, beta- and gamma-technique"*, Virgo Internal Document VIR-050A-08 (2008) 122

[161] D. Babusci, H. Fang, G. Giordano, G. Matone, L. Matone, V. Sannibale, "Alignment procedure for the VIRGO interferometer: experimental results from the Frascati prototype", *Phys. Lett. A* **226**, 31–40 (1997). 124

[162] E. Morrison, *Appl. Opt.* **33** (1994), 5041. 124

[163] M. Mantovani, A. Freise, S. Hild "The consequences of using the etalon effect to tune the arm cavity finesse on the alignment signals for Advanced Virgo" Virgo note VIR-027A-08 124

[164] M. Mantovani, "Initial thinking on the advanced Virgo Automatic Alignment control scheme design" 124

[165] G. Vajente, "Simulation of Advanced Virgo Length Sensing and Control system" Virgo note VIR-068A-08

[166] A. Freise, G. Heinzel, H. Luck, R. Schilling, B. Willke and K. Danzmann, "Frequency domain interferometer simulation with higher-order spatial modes", Class. Quant. Grav. **21** (2004) S1067 [arXiv:gr-qc/0309012]. 124

[167] V B Braginsky, S E Strigin, and S P Vyatchanin, *Phys. Lett. A* **287**, 331 (2001) 125

[168] C. Zhao *et al.*, *Phys. Rev. Lett.* **94**, 121102 (2005) 97, 104, 125

[169] T. Carmon *et al.*, *P*hys. Rev. Lett. **95**, 223902 (2005) 125

[170] O Arcizet *et al.*, *Nature* **444**, 71 (2006) 125

[171] C Zhao *et al.*, *P*hys. Rev. A **78**, 023807 (2008) 125

[172] CALVA web-page `http://calva.lal.in2p3.fr/` 118

[173] Virgo commissioning progress report, VIR-043A-08 126, 128

[174] B. Swinkels, presentation at Virgo Week, July 2008 126

[175] B. Swinkels, presentation at Virgo Week, April 2008 126

[176] Virgo Logbook entries 20563 and 20567 127

[177] S.Braccini, presentation at ILIAS WP1 Meeting, Cascina, March 2008 128

[178] S.Braccini, presentation at Detector Meeting, February 2006 129

[179] I.Fiori, presentation at Virgo Week, July 2008 128, 132, 133

[180] J.Marque, presentation at Weekly Meeting, April 2008 128

[181] I.Fiori and A.Gennai, presentation at Virgo Week, April 2008 128

[182] B.Canuel, presentation at Virgo Week, July 2008 128, 129

[183] E.Tournefier, VIR-NOT-070A-08 129, 130

[184] I.Fiori, presentation at Virgo Week, November 2007 129, 133

[185] I.Fiori, VIR-022A-08 129

[186] I. Fiori, presentation at Ligo-Virgo Week, Amsterdam, September 2008 129, 133

[187] I. Fiori, presentation at Weekly Meeting, October 2008 131

[188] B.Canuel, ILIAS WP1 Meeting, Birmingham, July 2008 132

[189] I.Fiori, Simulations of bench upconversion noise, AdV-INJ working area 132

[190] Paolo R. and F.Frasconi, Virgo e-log enty 20540 132

[191] J.Marque, ILIAS WP1 Meeting, Birmingham, July 2008 132, 133

[192] I.Fiori, presentation at Ligo-Virgo Meeting, Cascina, May 2007 133

[193] IEEE 1101.2 Standard for Mechanical Core Specifications for Conduction-Cooled Eurocards 133

[194] F.Frasconi et al., Virgo Note VIR-024A-08 (2008). 146

[195] M. Ferrante, *"Caratterizzazione e realizzazione di una scheda di conversione D/A A/D per l'esperimento VIRGO"*, University Degree thesis, Facoltà di Ingegneria Università di Pisa. 160

[196] G. Scandurra, *"Sviluppo di una scheda di I/O dotata di interfacce PCI e IEEE1394b per il rivelatore Virgo"*, fellowship paid by Fondazione Bonino-Pulejo. 160, 162

[197] The Virgo Collaboration, *Commissioning progress report for the STAC and EGO council*, VIR-043A-08 (2008). 161

[198] A. Gennai, *DAC Contribution to Virgo Sensitivity*, VIR-072A-08 (2008). 161

[199] A. Gennai, *New DSP board installation*, http://wwwcascina.virgo.infn.it/collmeetings/DMwebpages/Virgo+/2ndReviewDocuments/DSP.pdf. 161

[200] T. Bouedo, S. Cap, N. Letendre, A. Masserot, B. Mours, J.M. Nappa, E. Pacaud, S. Vilalte, *Virgo+ Control and DAQ Electronic Deployment*, VIR-022C-07 (2007). 162

[201] N. Letendre, A. Masserot, B. Mours, *Virgo+ Timing Deployment*, VIR-073A-08 (2008). 162

[202] LAPP Group, *ADC Board Specifications*, VIR-NOT-LAP (2007). 163

[203] O. Chautemps, C. Drancourt, N. Letendre, A. Masserot, B. Mours, J. Prast, *Proposal for the Timing & Optical Links Mezzanine (TOLM)*, VIR-NOT-LAP-1390-279 (2004). 164

[204] LAPP Group, *MUX/DEMUX optical card specifications*, VIR-NOT-LAP-1390-321 (2006). 164

[205] T. Bouedo, F. Carbognani, N. Letendre, A. Masserot, B. Mours, E. Pacaud, D. Sentenac, *New Global Control*, VIR-056A-o8 (2008). 164

[206] EGO Software Group, *Non Commercial Framework for Distributed Control Systems*, EGO-NOT-OPE-92 (2006).

[207] A. Heptonstall, I. Martin, A. Cumming, C.A. Cantley, G. Cagnoli, R. Jones and D.R.M. Crooks, ŞProduction and characterization of synthetic fused silica ribbons for advanced ligo suspensions,T̃ 2005. LIGO technical note, LIGO-T050206-00-K. 169

[208] For details see M.Lorenzini, "Suspension thermal noise issues for advanced GW interferometric detectors", thesis for Dottorato di Ricerca in Astronomia, University of Florence (http://www.infn.it/thesis/). 155

156